SMART INTERPRETATION OF TRANSFORMER FREQUENCY RESPONSE SIGNATURE

by

Venera NURMANOVA

In Fulfillment of the Requirement for the Degree of Doctor of Philosophy
in Science, Engineering and Technology

School of Engineering and Digital Sciences

Supervisor: Prof. Mehdi BAGHERI
Co-supervisor: Prof. Amin ZOLLANVARI

Nazarbayev University
[September 2022]

ACKNOWLEDGMENT

First of all, I want to thank my supervisor, Dr. Mehdi BAGHERI, for his support and guidance throughout my PhD study. His unquenchable energy and devotion to a cause has been both inspiration and motivation for me, and his constructive comments and feedbacks has helped to keep the right track in pursuing the quality work.

I also would like to express my sincere appreciation to my co-supervisor, Dr. Amin ZOLLANVARI. His invaluable experience and knowledge has helped me keep my research at the highest level. His insightful ideas and keen reviews enabled the progress of the work.

Special thanks to my external advisor Dr. Toan PHUNG for his valuable support throughout these years. His vast experience in the field of high voltage engineering and power systems equipment testing made his feedback and advice extremely helpful.

I am also immensely grateful to my family and friends for their endless motivation and emotional support during this journey.

DECLARATION

I hereby declare that the research presented in this thesis, unless it is otherwise formally indicated within the text, is the author's original work. The thesis has not been previously submitted to this or any other university for a degree and does not incorporate any material already submitted for a degree.

Signature(s): 

Date: 05 September 2022

ABSTRACT

Distribution and power transformers are essential components of any electricity network, hence electrical and mechanical safety of the transformer unit is among the highest concerns of electricity providers. Over the course of their operation, transformers face with a wide range of internal and external disturbances which may lead to a partial or full malfunction of the equipment. The service life and condition requirements for distribution and power transformers are now changed and utilities altered their maintenance policy from time-based to condition-based approach. In fact, the priority has been shifted towards fast and informative assessments with minimum risk to equipment and personnel. Transformers inevitably face with occasional fault and consequent deterioration of the overall performance. Therefore, to maintain the optimal working mode and intermittency of the power supply, transformers undergo a scheduled maintenance works, overhaul, visual inspection, cooling and insulating system tests, and even internal components inspection. Within the past several decades, a wide range of different transformer condition monitoring techniques have been developed.

Among existing diagnostic techniques, the Frequency Response Analysis (FRA) is a well-established testing method known as one of the most accurate and the least invasive evaluation technique. Conventionally, the FRA test results are interpreted via visual comparison of the reference and new measurement, which requires a certain level of experience and credibility from the maintenance personnel. Therefore, for the progress of the FRA interpretation process the application of different approaches have been widely discussed including statistical analysis, machine learning, image processing, to name a few. In this thesis, the proposed smart interpretation of the FRA data entails an automated classification of the transformer working condition along with estimation of the confidence level associated with reported classification results.

A new introduced interpretation technique is applied, formulated, examined, and evaluated in several practical case studies where different scenarios of the winding short circuit and mechanical deformation are emulated on a diverse set of test objects, from a single-phase 1 kVA distribution transformer up to a three-phase 40 MVA power

ABSTRACT

transformer. A new strategy for classification of given test observations is devised and implemented for green, yellow and red operating zones corresponding to healthy, suspicious and critical working conditions, respectively. This strategy is conducted based on the predefined green-to-yellow (healthy-to-suspicious) and yellow-to-red (suspicious-to-critical) decision boundaries represented by critical values of the 12 utilized Statistical Indicators (SIs). Moreover, the classification uncertainty in the form of the confidence level is studied for the first time, and is estimated using bolstered error estimation and bootstrap sampling technique borrowed from the pattern recognition and machine learning. The reported data is of great practical importance since it facilitates a more qualified decision regarding further diagnosis and maintenance of transformer under the test. In summary, this thesis provides a new smart approach to analyze transformer frequency response measurement data, to classify them into normal, suspicious, and critical working conditions, and assign an uncertainty level for each corresponding classification. Having the outcome of this thesis in place, the industrial operators and utility managers would be able to make a more accurate decision on transformer condition.

TABLE OF CONTENTS

TABLE OF CONTENTS

TABLE OF CONTENTS

LIST OF TABLES

LIST OF FIGURES

LIST OF FIGURES

LIST OF ABBREVIATIONS

FRA	Frequency Response Analysis
ITIC	Information Technology Intelligence Consulting
RLC	Resistor (*R*), Inductor (*L*), and Capacitor (*C*)
LV	Low voltage
HV	High voltage
SCI	Short circuit impedance
MAPD	Mean absolute phase distance
MAMD	Mean absolute magnitude distance
CDC	Current deviation coefficient
DGA	Dissolved Gas Analysis
PD	Partial discharge
ppm	Parts per million
IFRA	Impulse Frequency Response Analysis
SFRA	Sweep Frequency Response Analysis
FFT	Fast Fourier Transformer
IEC	International Electrotechnical Commission
IEEE	Institute of Electrical and Electronics Engineers
AI	Artificial Intelligence
SVM	Support Vector Machine
DNN	Deep Neural Network
CNN	Convolutional Neural Network
MLP	Multilayer Perceptron
DIP	Digital Image Processing
SML	Supervised Machine Learning
RFV	Resonant Frequency Variation
MSE	Mean Square Error
CC	Correlation Coefficient
ASLE	Absolute Sum of Logarithmic Error

LIST OF ABBREVIATIONS

SD	Standard Deviation
SSE	Sum Squared Error
CCF	Cross-correlation Factor
RF	Relative Factor
ED	Euclidean Distance
SDA	Standardized Difference Area
IFD	Index of Frequency Deviation
IAD	Index of Amplitude Deviation
DABS	Absolute Difference
RMSE	Root Mean Square Error
CSD	Comparative Standard Deviation
MM	Minimum-maximum Ratio
SSRE	Sum Squared Ratio Error
SSMMRE	Sum Squared Max-min Ratio Error
SI	Statistical Indicator
LF	Low Frequency
MF	Middle Frequency
HF	High Frequency
CIGRE	International Council on Large Electric Systems
SPICE	Simulation Program with Integrated Circuit Emphasis
DSV	Disk Space Variation
VCVS	Voltage Controlled Voltage Source
SCADA	Supervisory Control and Data Acquisition
LVQ	Learning Vector Quantization
NN	Neural Network
ANN	Artificial Neural Network
SI	Statistical Indicator
CL	Confidence Level
LDA	Linear Discriminant Analysis

CHAPTER 1. INTRODUCTION

1.1 Problem statement

An intermittent and safe electrical energy has become an essential part of the modern life. For instance, medical facilities, telecommunication and transportation networks, financial institutions, national security agencies, and water supply stations are electricity dependent objects and long-term power outage will inevitably entail serious issues in economic, social and even political situation. For instance, the power network of certain utility might not be engineered properly enough to overcome blackout or surge. Based on the survey conducted by Information Technology Intelligence Consulting (ITIC) in 2020 [1] , about 91% of the respondents reported that one hour of the power outage will cost them approximately $100,000 on average, while 40% of large industrial consumers claimed an hourly cost of the power blackout to even exceed $1 million.

Transformers perform a vital role in the power grid by stepping voltages up for transmission and down for distribution purposes. The reliability of the electricity network is highly related to electrical and mechanical condition of the transformer unit [2], [3]. However, in-service transformers are subjected to different external and internal disturbances during their operation, which eventually will jeopardize the integrity of the transformer's structure [4]. Therefore, despite the regular maintenance, after typically 20-25 years of operation, transformer needs to be repaired or even refurbished [5]. In case if a power outage is the result of transformer failure, the power supply can be restored by replacement of the transformer unit by a new transformer which may take about an hour or two in distribution level, and over several days or a month in transmission level. However, if there is no backup transformer available, the diagnostic and repair will be significantly longer depending on the severity of the damage. According to [6], the replacement of a large power transformer (75-750 MVA) varies in range between $ 1 million to $ 7.5 million and the process of repair and replacement mechanism may take up to 16 months. In this regard, it is quite important to conduct timely inspection and diagnostic tests of the transformer, which will in turn directly influence the reduction of expenses for complex repair procedures or elimination of the power blackout consequences [7].

Among the number of transformer condition assessment methods, the FRA is widely used due to its least complexity and non-invasive nature of the measurement setup [8], [9]. The FRA test basically implies measuring the response of the system to a sinusoidal input swept in a certain frequency spectrum. It is expected that any deviations in mechanical and electrical characteristics of the transformer will inevitably affect the frequency response signature [10]. Having that said, this method can detect a wide range of transformer faults including mechanical deformation and displacement of the winding and core structure, weakening and oxidation of lead connections and tap changers, core grounding fault, open windings, and turn short-circuit [11]-[13]. However, despite the fact that FRA is well-established and standardized as a diagnostic technique, successive interpretation of its results is still a quite challenging procedure [14], [15].

1.2 Motivation

Conventional methods mostly contain visual comparison, where condition of the test object is evaluated based on magnitude of the new measurement's deviation from the fingerprint (reference) spectrum and the affected frequency range [14], [16]. This, in turn, raises further issues such as biased diagnostics and human error due to lack of the background knowledge and experience on the operator side [17]. The commercialized and widely used FRA analyzers provide software built-in interpretation tools, which may classify the obtained frequency response. The classification is conducted among different levels of the winding mechanical deformation and is based on estimation of the numerical index from the FRA data [18], [19]. The disadvantages of this approach lie in limitations in terms of other fault types, utilization of a single Statistical Indicator (SI), lack of applicability to different transformer types and sizes, and absence of suitable classification criteria [20]. Therefore, it is highly desired to develop a comprehensive interpretation technique which will facilitate an automated interpretation of the FRA test data and also provide uncertainty level associated with given classification results [9], [21]. This confidence level will facilitate a more precise communication of the obtained results and observations. Moreover, it is important that the introduced interpretation codes and criteria is not bounded by the size of the test object and type of the fault.

1.3 Research objectives

Despite FRA is a well standardized transformer diagnosis technique, the automated interpretation codes are not yet available. The effectiveness and accuracy of the FRA test and adequacy of its interpretation are extremely dependent on the experience of the on-site personnel. Besides visual comparison of the obtained FRA signatures, different methods are being widely utilized to improve the FRA data interpretation process. Therefore, it is suggested that the combined application of statistical analysis and machine learning tools will facilitate automated interpretation of FRA results and classification of the transformer working condition. The reported confidence levels of classification will enable utility operators to effectively interpret FRA results and significantly improve the decision-making process. Hence, the aim of this research thesis work is to apply statistical analysis and machine learning tools to automatically interpret the FRA data and classify the transformer working condition. For that, the following objectives should be fulfilled:

- Design an experimental setup to emulate the reversible transformer winding short circuit faults;
- Develop a physical and software RLC models of the transformer winding;
- Validate the winding software model via comparison of theoretical and practical FRA signatures;
- Apply different mechanical deformations (axial, radial, axial and radial combined) over the developed winding physical and software models;
- Apply different severity levels of the winding short circuit fault over the distribution and power transformers;
- Conduct the FRA measurements of faulty scenarios and collect data for supervised machine learning and statistical analysis;
- Transformer working condition classification using predefined decision boundaries;
- Estimate the confidence level for the classification results utilizing bolstered error estimation and bootstrap sampling techniques;
- Modernize existing standards and setup configurations to enable smart and automated FRA results interpretation;

- Preparation of automated interpretation pipeline and software with effective user interface for automated on-site FRA data interpretation.

1.4 Thesis outline

The background information on various transformer fault types followed by extended discussion on their causing factors are covered in Chapter 2. The interconnection between mechanical, electrical, and chemical/thermal faults is explained and nature of the winding mechanical deformations is discussed in detail. Moreover, a review of existing different diagnostic techniques to evaluate the working condition of the transformer is conducted in Chapter 2.

In Chapter 3, the fundamental theory on Frequency Response Analysis (FRA) is discussed along with presentation of available measurement setups. Furthermore, the state-of-the-art of transformer FRA results interpretation is covered in Chapter 3, followed by detailed explanation of the currently utilized FRA standards.

The detailed description of the developed transformer winding physical and software models is covered in Chapter 4. Moreover, the methodology of the software based RLC model is explained and validation of the models is provided via comparison of the practical and theoretical FRA signatures. After validation of the developed winding models, Chapter 6 presents the methodology applied for emulation of mostly occurring transformer winding faults. It includes winding mechanical deformation (axial, radial, axial and radial combined) applied to developed winding models and simulation of the winding partial and full short circuit of the distribution and power transformers.

The proposed transformer working condition classes (zones) and classification criteria are explained in Chapter 5. It also contains the detailed presentation of the methodology and procedure to define the decision boundaries. The review of utilized statistical indicators (SIs) and machine learning tools engaged into transformer condition classification are also discussed in Chapter 5.

The classification results of different winding fault scenarios are covered in Chapter 6. It presents several practical case studies, where the proposed FRA interpretation technique is utilized to classify the transformer working condition under the presence of different levels of mechanical deformation and winding short circuit. The physical meaning

and practical application of the reported classification confidence level is also explained in Chapter 6.

Chapter 7 includes the conclusion of the thesis and discussion on further research perspectives.

1.5 Publications during candidature

1.5.1 Journal papers

[1] **V. Nurmanova**, Y. Akhmetov, M. Bagheri, A. Zollanvari, B. T. Phung and G. B. Gharehpetian, "Confidence Level Estimation for Advanced Decision-Making in Transformer Short-circuit Fault Diagnosis," in *IEEE Transactions on Industry Applications*, vol. 58, no. 1, pp. 233-241, Jan.-Feb. 2022, doi: 10.1109/TIA.2021.3118661.

[2] **V. Nurmanova**, M. Bagheri, A. Zollanvari, K. Aliakhmet, Y. Akhmetov and G. B. Gharehpetian, "A New Transformer FRA Measurement Technique to Reach Smart Interpretation for Inter-Disk Faults," in *IEEE Transactions on Power Delivery*, vol. 34, no. 4, pp. 1508-1519, Aug. 2019, doi: 10.1109/TPWRD.2019.2909144.

[3] Y. Akhmetov, **V. Nurmanova**, M. Bagheri, A. Zollanvari and G. B. Gharehpetian, "A New Diagnostic Technique for Reliable Decision-Making on Transformer FRA Data in Interturn Short-Circuit Condition," in *IEEE Transactions on Industrial Informatics*, vol. 17, no. 5, pp. 3020-3031, May 2021, doi: 10.1109/TII.2020.3007607.

[4] Y. Akhmetov, **V. Nurmanova**, M. Bagheri, A. Zollanvari and G. B. Gharehpetian, "A Bootstrapping Solution for Effective Interpretation of Transformer Winding Frequency Response," in *IEEE Transactions on Instrumentation and Measurement*, vol. 71, pp. 1-11, 2022, Art no. 3508811, doi: 10.1109/TIM.2022.3159012.

[5] **V. Nurmanova**, Y. Akhmetov, M. Bagheri, A. Zollanvari and B. T. Phung, "A Confidence Level Estimation Technique for Reliable Data-Driven FRA

Interpretation in Transformer Active Part Faults", in *IEEE Systems Journal* (submitted).

1.5.2 Conference papers

[1] **V. Nurmanova**, Y. Akhmetov, M. Lu, M. Bagheri and T. Phung, "Transformer Winding Modelling to Study the Effect of Inter-disk Faults on Frequency Response Signature," *2019 8th International Conference on Renewable Energy Research and Applications (ICRERA)*, 2019, pp. 540-544, doi: 10.1109/ICRERA47325.2019.8997076.

[2] **V. Nurmanova** et al., "Simulation and Analysis of Transformer Winding Inter-disk and Inter-turn Faults for Online Diagnosis," *2019 IEEE International Conference on Environment and Electrical Engineering and 2019 IEEE Industrial and Commercial Power Systems Europe (EEEIC/I&CPS Europe)*, 2019, pp. 1-5, doi: 10.1109/EEEIC.2019.8783743.

[3] **V. Nurmanova** et al., "Distribution Transformer Frequency Response Analysis: Behavior of Different Statistical Indices During Inter-disk Fault," *2019 IEEE International Conference on Environment and Electrical Engineering and 2019 IEEE Industrial and Commercial Power Systems Europe (EEEIC/I&CPS Europe)*, 2019, pp. 1-6, doi: 10.1109/EEEIC.2019.8783252.

[4] **V. Nurmanova**, Y. Akhmetov, M. Bagheri, A. Zollanvari, G. B. Gharehpetian and T. Phung, "A New Transformer FRA Test Setup for Advanced Interpretation and Winding Short-circuit Prediction," *2020 IEEE International Conference on Environment and Electrical Engineering and 2020 IEEE Industrial and Commercial Power Systems Europe (EEEIC / I&CPS Europe)*, 2020, pp. 1-6, doi: 10.1109/EEEIC/ICPSEurope49358.2020.9160545.

[5] **V. Nurmanova**, A. Khassenov, M. Bagheri, T. Phung and G. B. Gharehpetian, "The Influence of External Parameters on Transformer Frequency Response Signature and Numerical Indices," *2019 IEEE International Conference on Environment and Electrical Engineering and 2019 IEEE Industrial and*

Commercial Power Systems Europe (EEEIC / I&CPS Europe), 2019, pp. 1-4, doi: 10.1109/EEEIC.2019.8783609.

[6] **V. Nurmanova**, Y. Akhmetov, M. Bagheri, A. Zollanvari, G. B. Gharehpetian and T. Phung, "A New Transformer Winding RLC model to Study the Effect of the Disk Space Variation on FRA Signature," *2021 IEEE International Conference on Environment and Electrical Engineering and 2021 IEEE Industrial and Commercial Power Systems Europe (EEEIC / I&CPS Europe)*, 2021, pp. 1-6, doi: 10.1109/EEEIC/ICPSEurope51590.2021.9584786.

[7] M. Bagheri, **V. Nurmanova**, A. Zollanvari, S. Nezhivenko and B. T. Phung, "IoT Application in Transformer Fault Prognosis Using Vibration Signal," *2018 IEEE International Conference on High Voltage Engineering and Application (ICHVE)*, 2018, pp. 1-5, doi: 10.1109/ICHVE.2018.8641873.

1.5.3 Complementary journal papers

[1] M. Bagheri, **V. Nurmanova**, O. Abedinia and M. Salay Naderi, "Enhancing Power Quality in Microgrids With a New Online Control Strategy for DSTATCOM Using Reinforcement Learning Algorithm," in *IEEE Access*, vol. 6, pp. 38986-38996, 2018, doi: 10.1109/ACCESS.2018.2852941.

[2] R. Asghari, B. Mozafari, M. Salay Naderi, T. Amraee, **V. Nurmanova** and M. Bagheri, "A Novel Method to Design Delay-Scheduled Controllers for Damping Inter-Area Oscillations," in *IEEE Access*, vol. 6, pp. 71932-71946, 2018, doi: 10.1109/ACCESS.2018.2878038.

CHAPTER 2. TRANSFORMER FAULTS AND DIAGNOSTIC TECHNIQUES

2.1 Introduction

This Chapter is structured in the following manner: Section 2.2 discusses different types of the transformer faults. Detailed investigation of the fault causing factors and their frequency is conducted. In Section 2.3, the conventional transformer diagnostic techniques and literature are reviewed.

2.2 Transformer fault types and factors

During the operation of power and distribution transformers, various damages will inevitably occur, which can disrupt the optimal operation of the equipment. However, with some defects, some of the units can still continue to function, while others may lead to critical disorders or complete shutdown. In any case, it is extremely necessary to promptly carry out maintenance, which will avoid a serious accident and catastrophic damage. Therefore, it is essential not only to determine the nature of the defect, but also the reasons for its appearance [22]-[24].

Based on the origin, transformer faults can be classified as internal and external failure. Mechanical and electrical faults correspond to the internal category and occur in the transformer tank. Specifically, mechanical faults are usually expressed by deformation or displacement of the winding structure (turns and disks), conductors looping or break off, cooling system fault (extreme temperatures in transformer tank, fire and explosion), tap changer failure caused by high currents, and dielectric breakdown in the result of the high voltage stress force [25]-[27]. Internal electrical faults are overload leading to insulation deterioration, aging and rupture of the connections, inter-phase or phase faults due to short-circuit current stress, and occurrence of arcs between winding terminals. Transformer's mechanical, electrical, and chemical faults are interrelated, Figure 2.1 illustrates mutual causality between electrical, mechanical and thermal/chemical damages [28].

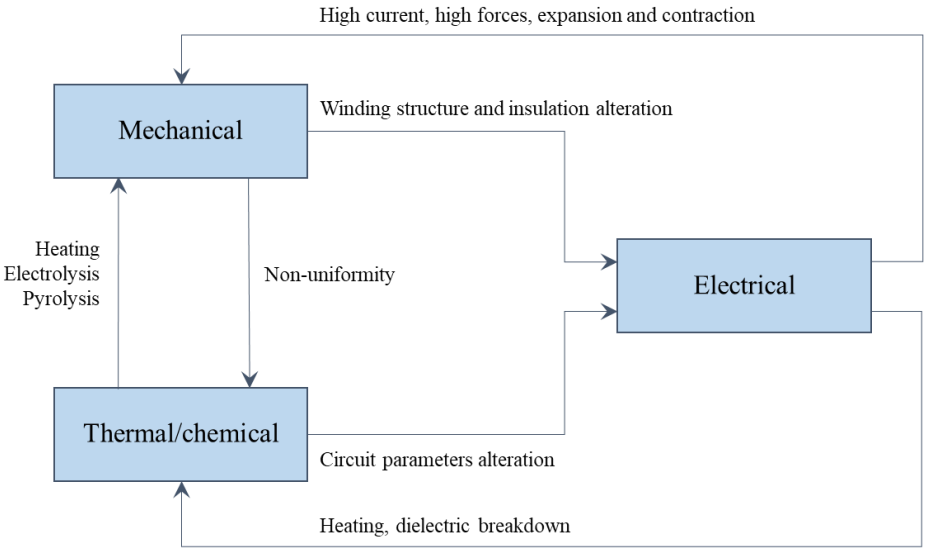

Figure 2.1. Transformer faults interconnection

External (through) faults are basically eliminated by overload protection systems. However, high severity faults might outstep the protection network and lead to equipment overload, which in turn may induce severe internal faults such as extreme high currents through primary and secondary winding terminals and insulation damage [12], [29]. As reported by [30], almost 70-80% of transformer damages are initiated by winding inter-turn short-circuit fault. A study by [31] claims that electrical disturbances and lightning are the major factors of transformer failure. Particularly, the transformer protection system, bushing, and tap changer faults have the highest frequency compared to windings, core, tank, and cooling failure [32].

The integrity of the transformer unit can be damaged due to the following internal and external factors [31], [33]:

- factory and installation defects;
- low quality repair works;
- short-circuit forces resulting from secondary failures;
- safety and rules negligence during transportation;
- effect of dynamic forces, such as vibration during operation or earthquake;
- internal damages that develop due to long-term operation under the influence of internal and external disturbances;
- insulation deterioration and moisture;

- electrical disturbances, overload, and lightning;
- weakening of the clamping force as a result of ageing, which hence mitigates the ability to oppose the abovementioned challenges.

Nevertheless, transformer failure should be considered from two perspectives – (*i*) frequency of occurrence, and (*ii*) the severity of the damage [31]. For instance, electrical disturbances appear to have both highest fault risk and severity (see Figure 2.2). Although, lightning induced damages are about twice frequent than insulation deterioration failures, they trigger less severe damage to the equipment. It is notable to highlight that the faults due to overload and sabotage have similar frequency rate and severity, whereas transformer faults triggered by poor maintenance and service procedures occur twice as often as overload or sabotage [34].

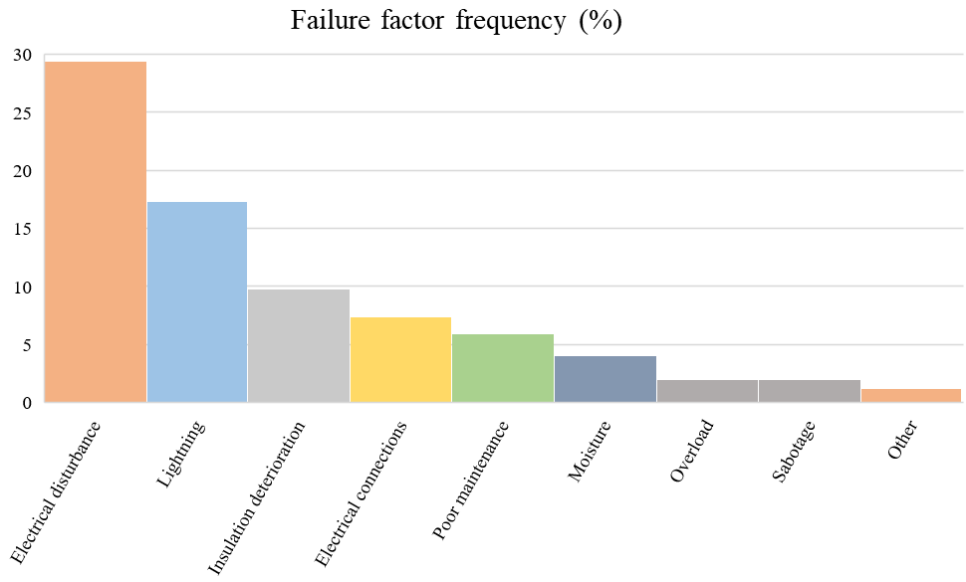

Figure 2.2. Transformer failure factor frequency [34]

Over the course of the normal working process, transformer active part is subjected to mechanical stresses in the result of the magnetic forces [5]; however, in the event of the failure, where a fault current flows through transformer, the magnitude of these mechanical forces may increase significantly, imposing a severe mechanical damage to the structure of the core or the windings. Since the short-circuit current magnitude may sometimes reach up to 8-10 times the nominal current and the force exerted on the active part is proportional to the square if the current, the force induced by fault current may exceed the system's

tolerable force by the factor of one hundred. The electromagnetic forces are then the product of the winding current and the leakage flux as illustrated in Figure 2.3.

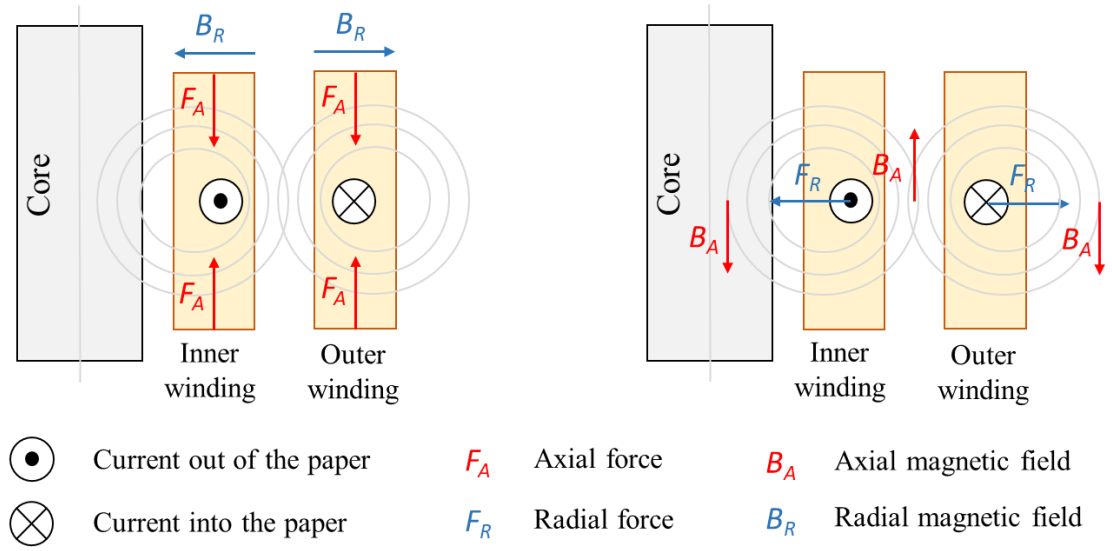

Figure 2.3. Axial and radial forces induced by interaction of the winding current and leakage flux

These short-circuit currents have axial and radial component fluxes which interact with the winding current and initiate, radial and axial mechanical forces, respectively. The axial force has a compression effect, where the tension is directed from the ends of the winding towards the center of the winding structure. The radial force has a complex effect on concentric low voltage (LV) and high voltage (HV) windings; the outer HV winding undergoes an outward force, whereas the inner LV winding is compressed towards the limb.

Deformation of transformer winding (see Figure 2.4(a)-(e)) caused by radial, axial, and twisting forces can be categorized as [35]-[40]:

- radial buckling;
- conductor tilting (cable-wise tilting, strand-wise tilting);
- conductor bending between supporting spacers;
- telescoping due to windings insufficient radial thickness;
- spiraling and twisting;
- fatigue and collapse of the winding end supports.

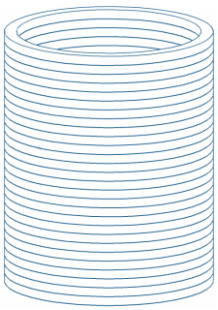


(a) normal winding [44], [109]

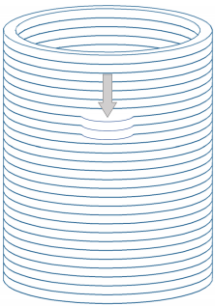


(b) bending [41]

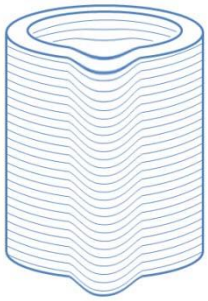


(c) buckling [43], [109]

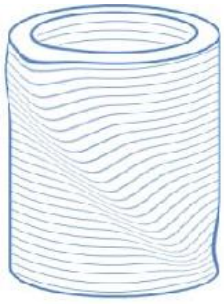


(d) spiraling [42], [109]

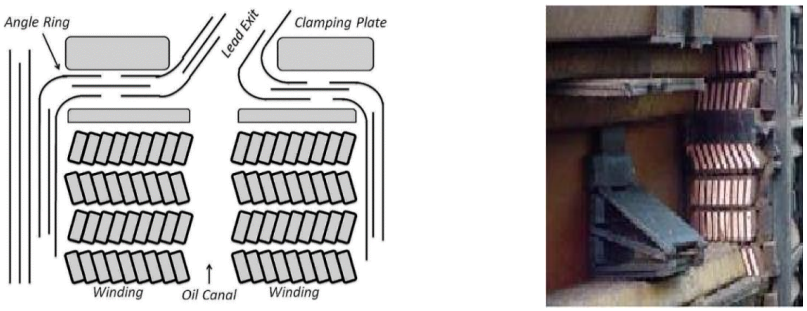

(e) tilting [8], [41]

Figure 2.4. Illustration of different mechanical conditions of transformer winding structure, taken from [8], [41]-[44], [109]

2.3 Transformer condition diagnostic techniques

In the past several decades, a numerous diagnostic techniques have been established to assess the working condition of the power and distribution transformers. These techniques can be classified as electrical, mechanical, chemical, thermal, and optical methods [45]. Particularly, frequently applied electrical methods include signal analysis, partial discharge evaluation and location, insulation resistance, etc. Mechanical analysis usually includes pressure and flow rate in the insulating oil and mechanical stresses produced in the result of the excessive noise in the transformer tank. Chemical testing techniques are majorly focused on the contamination of the oil insulation by moisture, gases, etc. Thermal methods are based on the thermal characteristics of the transformer active part evaluated via thermography test. Optical analysis is conducted using endoscopy and fiber optics, where acoustic signals due to internal disturbances in transformer (for example, partial discharge) are detected [46]. Some of the aforementioned methods are incorporated into international standards and currently are in commercial practice, while others are still under development or at final validation phases.

2.3.1 Short circuit impedance (SCI) method

The given method is used to detect transformer's internal electrical and mechanical faults. SCI value has resistive and reactive components, the latter is represented by leakage inductance, which is directly relevant to transformer winding configuration. The LV

winding is usually shorted, letting a full-load current to flow in the HV side. Since the magnitude of the full-load short circuit current is lower on HV side as opposed to LV side, all measurements are reasonably conducted on the HV side [36], [47]. Measured SCI value is then compared to one given in the nameplate or obtained during factory acceptance tests [36]. According to [48], more than ±1% change from expected value should be considered as a serious deformation. However, [49] and [50] claim, that changes only exceeding ±3% are indicators of the winding deformation.

2.3.2 Vibration method

Forces occurring during transformer operation induce vibrations in transformer core and windings [51]. Core vibrations can be explained by magnetostriction, when dimensions of the material undergo alterations when exposed to magnetic field. Winding vibrations are initiated by interaction of the current flowing through the winding with the leakage flux. As a result, windings will be compressed or expanded in horizontal and/or vertical directions. The intensity of magnetic and electrodynamic forces inducing vibrations is directly proportional to the square of the voltage and current, respectively [52]-[56].

Sensors are installed on the transformer and collect vibrational signals, then spectrum of this signal is processed by means of microprocessor. The displacement of the transformer's inner structure from the predefined fingerprint position is investigated [51], [56]-[60]. Deviation magnitude, harmonic components, and direction of dislocation are used to analyze the severity of the fault and determine the working condition of the transformer winding [61]-[63].

2.3.3 Communication method

Similar to FRA, the fingerprint of the transformer is used in communication method. In this case, the magnitude and phase values of scattering parameters obtained by several antennas are taken as a basis for identification of any mechanical changes in windings [64]. Antennas are installed either in our outside the transformer tank. According to [65] and [66], the key terms indicating the windings deformation are the mean absolute phase

distance (*MAPD*) and mean absolute magnitude distance (*MAMD*) and are estimated as (1) and (2):

$$MAPD = \frac{\sum_{i=1}^{n} \left| \angle S_i - \angle S_{ref} \right|}{n} \tag{1}$$

$$MAMD = \frac{\sum_{i=1}^{n} \left\| S_i \right| - \left| S_{ref} \right\|}{n} \tag{2}$$

where S_{ref} is the reference (fingerprint) scattering parameters and S_i represents the measured scattering parameters [66].

2.3.4 Current deviation coefficient (CDC) method

In this method the deviation of terminal currents at selected high frequency is estimated and compared to fingerprint values [67]. In particular, line-end and neutral end high frequency currents are continuously measured and any changes in mechanical condition of transformer windings will result in change of these currents, since capacitive inductance value will alter as well. The current deviation coefficient claimed by [67] is calculated as the ratio of terminal currents in (3) and is able to detect the location of winding deformation, as well as the severity of the damage.

$$CDC = \log_{10} \frac{I_{ref1} - I_{m1}}{I_{ref2} - I_{m2}} \tag{3}$$

where I_{ref1} and I_{ref2} are initial current measurements at high frequency terminals and I_{m1} and I_{m2} are measured current measurements, respectively.

2.3.5 Ultrasonic method

This technique suggests detecting the transformer winding deformation using an ultrasonic reflection phenomena [68]. Basically, the injected pulse ultrasonic wave is reflected from the transformer winding surface. The resulting wave is then converted into

the electrical signal and is amplified in order to conduct analysis of the windings condition. Changes in the mechanical integrity of the windings will alter the reflected waveform.

On the other hand, in [69], the electric-ultrasonic sensor is installed on transformer tank to detect a spherical wave penetrating the insulation oil. This ultrasonic signal occurs as the result of the partial discharge. The proposed method can effectively detect the number of the partial discharge, as well as the location of the insulation damage.

2.3.6 Short circuit impedance and winding stray reactance method

The on-line SCI method implies comparison of initially measured short circuit impedance with the one taken after certain period of transformer operation. As it has been mentioned in off-line transformer diagnosis methods, short circuit impedance value depends on the winding configuration [70]-[76]. Nevertheless, since on-line test implies that the transformer will be energized, it is no longer possible to apply the secondary winding short circuit topology on operating transformer. Therefore, transformer is now reviewed as a two-port network system as illustrated in Figure 2.5 [77].

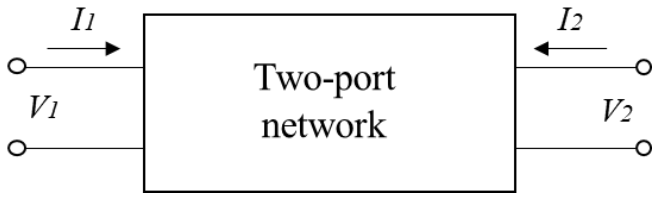

Figure 2.5. Model of the two-port network

Given the input and output currents, the following impedance model can be used to estimate voltages:

$$\begin{bmatrix} V_1 \\ V_2 \end{bmatrix} = \begin{bmatrix} Z_{11} & Z_{12} \\ Z_{21} & Z_{22} \end{bmatrix} \begin{bmatrix} I_1 \\ I_2 \end{bmatrix} \tag{4}$$

$$\begin{aligned} V_1 &= Z_{11} I_1 + Z_{12} I_2 \\ V_2 &= Z_{21} I_1 + Z_{22} I_2 \end{aligned} \tag{5}$$

where Z_{11} and Z_{22} are open circuit input and output impedances, respectively, and Z_{12} and Z_{21} are open circuit transfer impedances. Shorting the secondary side (V_2=0), the short circuit impedance can be expressed as (6):

$$Z_{SC}=Z_{11}+\frac{Z_{12}Z_{21}}{Z_{22}} \quad (6)$$

Recalling, that short circuit impedance has resistive and inductive components, and inductive reactance is dependent on winding configuration, any changes in mechanical integrity of the transformer winding will be resulting in deviation of Z_{SC}.

2.3.7 Voltage-current (V-I) locus diagram method

This method was primarily introduced by [79], implies plotting the current-voltage characteristic curve of a certain phase of the transformer. Specifically, continuous measurements of injected current and primary and secondary voltages are conducted. Hence the locus diagram is basically input current against difference of voltages, which is illustrated as an ellipse in Cartesian coordinate system. It is suggested to inject a low voltage signal at 50 Hz to the terminal of transformer winding and conduct measurements with the period of 10 μs [80]. Similar to other comparison based techniques, the initial locus diagram is considered as the reference. Changes in transformer winding configuration leads to alteration of impedance values, thus will be reflected on V-I locus diagram (see Figure 2.6). Practical implementation of the mentioned technique validated that ellipse feature indicators as major and minor axes lengths and angle between major axis and x-axis are influenced by transformer winding condition [81], [82].

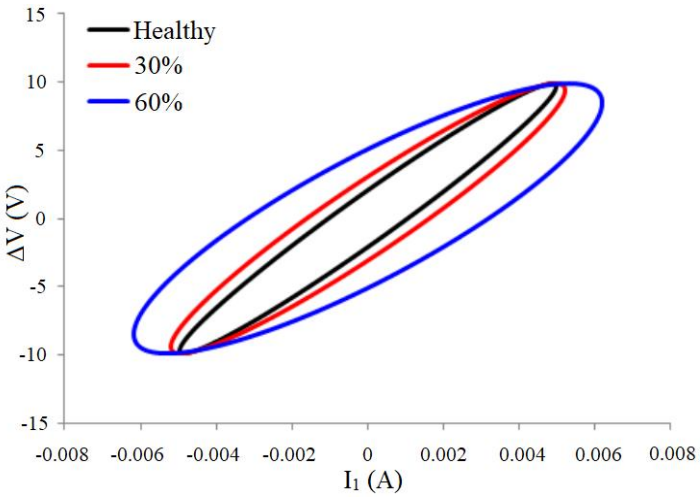

Figure 2.6. Impact of different levels of the buckling on V-I locus diagram [80]

2.3.8 Dissolved Gas Analysis (DGA) method

The Dissolved Gas Analysis (DGA) is among widely used techniques to diagnose the condition of the oil-immersed transformers without the requirement of de-energizing the test object [83]. Internal disturbances and deviations in transformer active part may lead to contamination of the oil insulation by gases such as acetylene, ethane, hydrogen, carbon monoxide, carbon dioxide, methane, and ethylene [84], [85]. The type of dissolved gas and its content facilitates to define the partial discharge (PD), paper insulation ageing, overheating, overloading, surge, and other electrical, chemical and thermal faults [86]. The conventional DGA measurement and interpretation methods are covered in IEEE Standard C57.104-2008 [87] and [88]. The test results interpretation is based on the concentration of the specific gases in ppm (parts per million) in the oil content or the ratio of the different gases (for example, ethane/methane) [89].

2.3.9 Transfer function method

The transfer function method, also referred as Frequency Response Analysis (FRA) has been extensively discussed in the literature [90]-[94]. FRA is sensitive to a wide range transformer faults including mechanical deformation and displacement of the core and winding, turn-to-turn and disk-to-disk short circuit, aging, oxidation, and rupture of the tap and lead connections, and grounding faults. FRA implies injecting a sweep signal into one

end of the winding, and measuring the response from the other end of the winding for single-phase transformer and from neutral or either phase for three-phase transformer [95]-[97]. Essentially, the transfer function represents the magnitude ratio and phase angle between the output signal and the input signal in a wide bandwidth.

$$H(j\omega)=\frac{V_2(j\omega)}{V_1(j\omega)} \tag{7}$$

where $H(j\omega)$ is the transfer function, $V_2(j\omega)$ is output (response) and $V_1(j\omega)$ is input (excitation) signal.

Based on the type of the injected signal, FRA can be categorized into: (i) Impulse Frequency Response Analysis (IFRA) and (ii) Sweep Frequency Response Analysis (SFRA). As mentioned above, in IFRA, a high voltage (hundreds of volts) impulse signal is injected into one end of the winding and response is measured from the other end in time domain. The measured signal is converted into frequency domain via Fast Fourier Transform (FFT) for evaluation of the transfer function and further analysis [98]-[100]. In SFRA, the input signal is a low amplitude sinusoidal signal swept across 20 Hz – 2 MHz and the response is also obtained in frequency domain [101]-[103]. The conceptual difference between IFRA and SFRA can be observed in Figure 2.7(a) and (b).

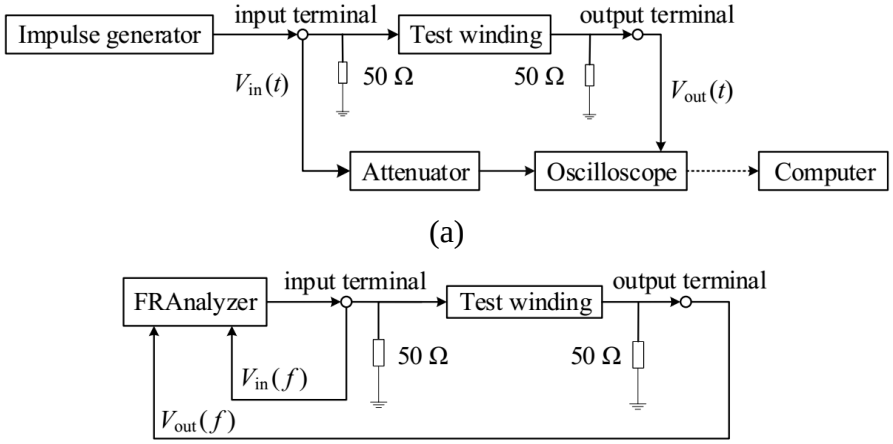

Figure 2.7. FRA measurement conceptual circuit: (a) IFRA method and (b) SFRA method

Each of abovementioned diagnosis methods have been successively implemented in practice; yet, it is vital to distinguish their drawbacks and define the most effective and viable method. As an example, the vibration method test results can be deteriorated by ever occurring external forces. The telecommunication method can be no longer effective to be applied on operating transformer, since access to active part is restrained by grounded transformer tank. Similarly, in on-line application short circuit impedance method suffers significant degradation of test results, as the voltage on the secondary part is no longer zero. On the other hand, this method is unable to define the axial displacement such as tilting and bending. Similar to SCI, transfer function is a comparison based technique, where the reference (fingerprint) response and new measurement are compared. This, in turn, will give information about transformer mechanical state since winding structure deformation will inevitably result in deviation of the transfer function, yet SCI is unable to distinguish axial deformations such as tilting and bending [104]. Exciting current method is not sensitive to winding mechanical deformations and is highly influenced by core's residual magnetic field. Frequency response of stray losses is capable to detect short circuit fault, yet does not have a standardized measurement and interpretation instructions. Although the leakage reactance and winding capacitance methods have the standardized interpretation criteria and measurement setup, they are limited to radial deformation detection. In this regard, the transfer function method is considered as the most effective and least invasive diagnostic technique capable to detect a wide range transformer faults. This method has no practical limitations in terms of the transformer size and type and has well-established standards widely used in the industry.

CHAPTER 3. FREQUENCY RESPONSE ANALYSIS (FRA)

3.1 Introduction

This Chapter is structured in the following manner: in Section 3.2 the conceptual information on Frequency Response Analysis (FRA) theory and measurement configurations is presented. Section 3.3 discusses conventional techniques for the FRA data interpretation and Section 3.3 covers the existing standards for the FRA measurement and results analysis.

3.2 FRA concept

FRA is a well-established, industrialized method [12] which is performed by injecting a reference swept signal to the transformer input terminal and measures the winding response from other side of the winding if the test object is single-phase and from the neutral bushing tap is transformer has three-phases [105], [106]. The input signal is usually low-amplitude (20 V peak-to-peak) sinusoidal waveform.

In the know, the FRA measurements are conducted on a de-energized transformer unit which has been taken out of service, referred as the off-line FRA which is illustrated in Figure 3.1(a). The on-line FRA test configuration on the energized transformer depicted in Figure 3.1(b) implies injection of the sine wave to bushing tap terminal and measuring the response signal from the lateral bushing terminal [106]-[108]. Depending on the transformer vector group, the response is measured from the neutral bushing (wye configuration) or between two phases (delta configuration) [8], [109]. However, in accordance with [14], the outcome of the on-line and off-line FRA tests usually differ in low-frequency band (up to 1 kHz) [109].

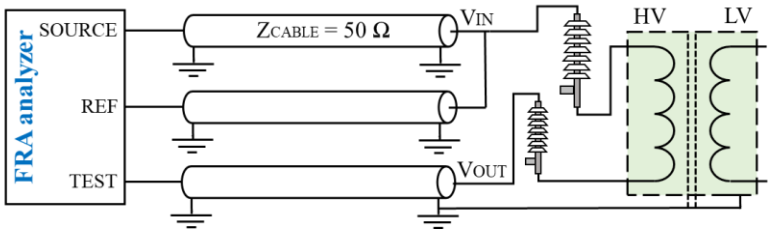

(a)

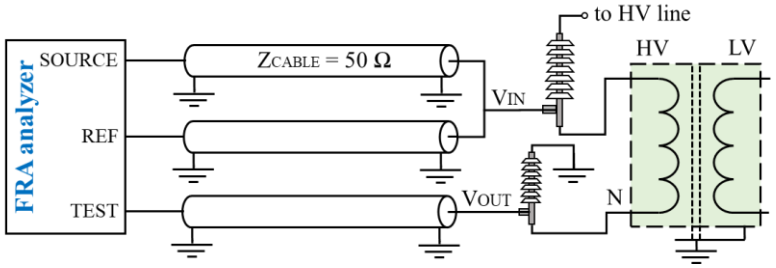

(b)

Figure 3.1. FRA test setup: (a) off-line mode and (b) online mode, taken from [110] and [146]

Transformer frequency response signatures are usually reported between 20 Hz and 2 MHz. This frequency band is able to provide significant information regarding the transformer mechanical integrity and is agreed upon in literature and standards [101]-[103], [111], [112]. It is well-known that the low-frequency band is primarily influenced by the core, clamping structure, and yoke. Mid-frequencies mainly depend on the transformer winding structure and interaction between windings, and high-frequency band represents leads and connections in FRA spectrum [113]-[115]. Nevertheless, according to [8], it is unlikely to obtain similar frequency response over a whole band during off-line and on-line tests. Particularly, discrepancies occur at frequencies below 1 kHz. The reason for this discrepancy is already discussed in [109]. The FRA signature is illustrated as Bode plot and results are plotted in logarithmic scale (see Figure 3.2), giving an opportunity to investigate a whole frequency spectrum [115], [116].

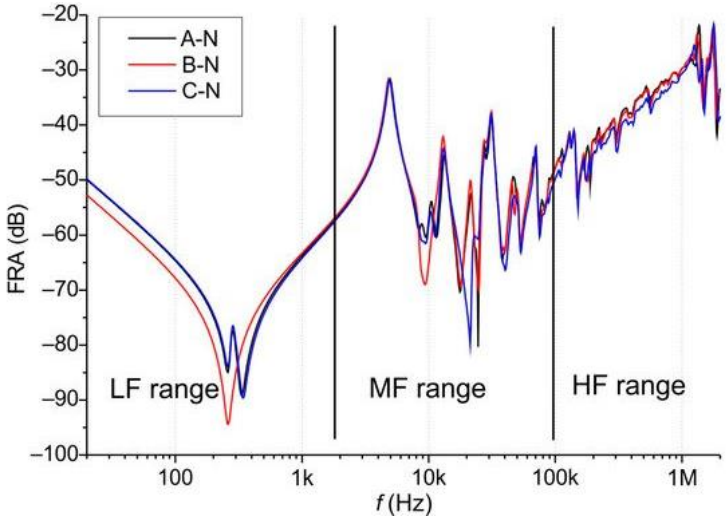

Figure 3.2. Example of FRA signature of the three-phase transformer with frequency sub-bands indicated, taken from [117]

$$H(f) = 20\log\frac{|V_2(f)|}{|V_1(f)|} \tag{8}$$

$$\varphi = \tan^{-1}(\angle V_2 - \angle V_1) \tag{9}$$

where $H(f)$ is the magnitude of the transfer function, $|V_2(f)|$ is the magnitude of the output (response) and $|V_1(f)|$ is the magnitude of the input (excitation) signal, and φ is the phase angle of the signal.

According to the international standards IEC 60076-18, section 2 and page 8 [48], IEEE Guide C57.149-2012 [50], and National standard of China DL/T 911–2004 [19], the FRA test setups are introduced and recommended as:

- End-to-end open-circuit test,
- End-to-end short-circuit test,
- Capacitive inter-winding test,
- Inductive inter-winding test.

Each and every test setup has its own advantages. All the standard FRA test setups are provided in Figure 3.3 [110] ©2019 IEEE. The end-to-end open-circuit FRA measurement setup provides broad information on conditions of transformer core and windings — it is mostly conducted in the transformer manufacturer factory. In this test, the test signal is injected into one terminal of the winding, and response signal is collected

from the other end of the winding, while rest of the terminals are left open. The end-to-end short-circuit FRA test is mainly conducted on customer site and assists in evaluating the integrity of transformer windings, and ignores transformer core effect. Its measurement setup is similar to previous setup, except for the second winding of the measured limb, which is shorted. Capacitive inter-winding test configuration implies injection of the test signal into one terminal of the winding and collecting the response from one of the terminals of the same phase secondary winding while other terminals are left open, whereas in inductive inter-winding test second terminals are grounded [118]. Other than that, inter-winding measurements provide comprehensive information regarding radial deformations (capacitive test) and transfer admittance (inductive test) of the transformer unit. Among all, the end-to-end open-circuit measurement has been widely used by industry and discussed by researchers. This measurement setup provides information on conditions of transformer core and windings [119]. It is also mostly conducted as the baseline measurement in the factory during the transformer acceptance and insulation tests along with type or special transformer tests. The baseline test is usually conducted to obtain a reference trace (signature) for upcoming diagnosis of the same unit or sister-transformer [49], [120].

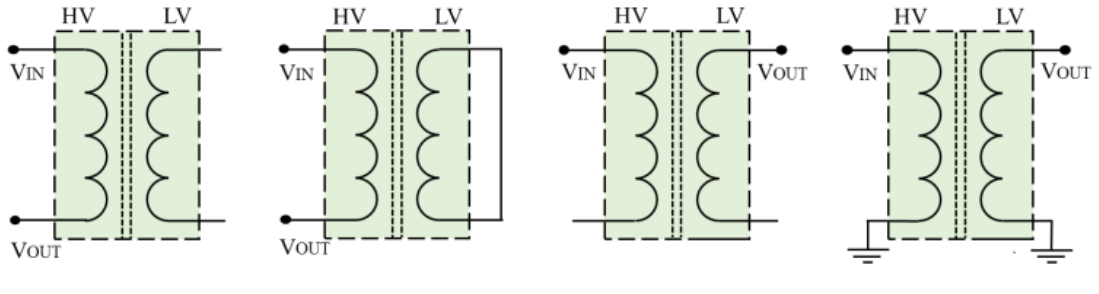

Figure 3.3. FRA test setups: (a) end-to-end open-circuit test, (b) end-to-end short-circuit test, (c) capacitive inter-winding test, (d) inductive inter-winding test [110]

3.3 FRA interpretation techniques

The FRA is a well-established and widely used monitoring technique with standardized measurement setup. However, till now the interpretation guidelines of the test

results are quite general and non-informative, since the fault type and its severity level has become essential information for qualified maintenance procedure [121], [122]. Over the past decades, different techniques have been applied for the progress of the FRA interpretation [3], [123]. These techniques mainly include simulation models, statistical analysis, artificial intelligence (AI), and digital image processing [18], [112], [122]-[129]. The simulation model is usually used to emulate different winding mechanical faults and investigate their influence on the distributed parameters of the winding, such as resistance, inductance, and capacitance [130]. Afterwards, the database of the faulty scenario FRA signatures is applied to classify the given frequency response.

3.3.1 Visual inspection

Conventionally, the measured FRA signatures are interpreted through a visual comparison of the reference spectrum with the current measurement. Commonly, this type of the inspection is carried out in the field by maintenance personnel and requires a solid background and expertise in FRA testing [131], [132]. Depending on the magnitude of the deviation and affected frequency range, an on-site operator can report which part of the transformer is undergoing a certain fault and to what extent. The lower frequencies are usually influenced by the core structure, the mid-frequencies are affected by winding internal faults, and the higher frequencies are the function of lead connections and clamping [133]. Having this at hand, it is observed that the accuracy and quality of the FRA diagnostic test highly rely on the experience of operator and, thus, it is prone to a human error and biased decision [134], [135].

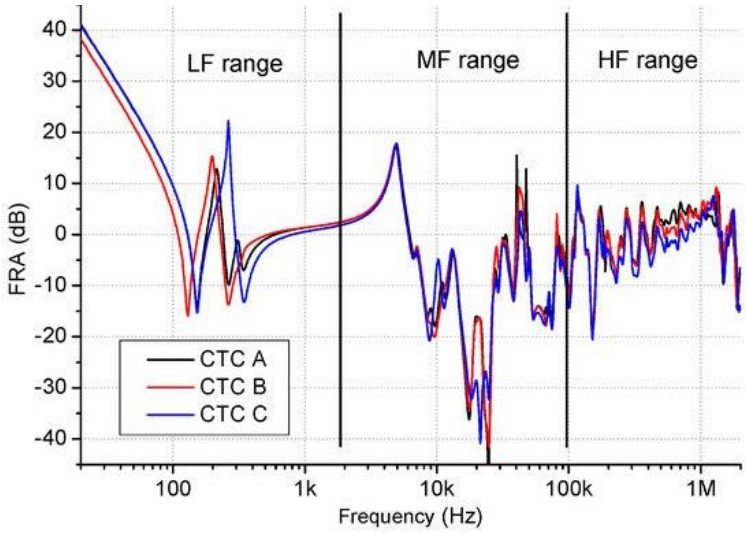

Figure 3.4. FRA signatures of phases A, B, and C with frequency sub-bands illustrated, taken from [133]

3.3.2 Machine learning tools

One of the challenges of accurate prognosis algorithm and fault localization technique is interpretation of FRA output data. In this regard, a number of researchers have been working on application of computing techniques that train and improve a neural network (back propagation, radial basis function, and self-organizing feature map) in analysis of FRA data. Other than that, various AI techniques, such as machine learning (neural networks (NN), support vector machines (SVM), regression, etc.) and fuzzy logic have been extensively used on FRA data to detect, classify, and localize the fault in a test object. In particular, SVM, deep neural networks (DNN), convolutional neural networks (CNN), multilayer perceptron (MLP), etc. are among mostly applied techniques borrowed from AI [136]-[139]. The transfer function magnitude and phase response are used as an input for the image recognition algorithm where digital image processing (DIP) techniques are used to process the raw frequency response spectra and compare reference and recent FRA signatures based on their geometric properties and features, and define the fault level [122]-[129].

Ma and Ren [140] applied SVM classification algorithm for transformer winding deformation detection and prognosis. A training data set for supervised machine learning

(SML) was collected from the off-line Impulse Frequency Response Analysis (IFRA) results [140]. The detection system demonstrated a sufficient level of accuracy during industrial tests. However, it is designed for analysis on an isolated and grounded transformer, hence further studies should be conducted to adjust the approach for on-line diagnosis. Zhao et al. [141] claimed feasibility of IFRA data based SVM classification algorithm on energized transformer. Two statistical indicators as resonant frequency variation (*RFV*) and mean square error (*MSE*) are extracted from IFRA data and used for further training and testing set to diagnose radial deformation, short circuit and disk space variation. The diagnostic results of ten groups show the average accuracy of 78.1% and 83.3% for *RFV* and *MSE,* respectively [141].

Moreover, Bigdeli et al. [142] utilized measurements taken in time domain and employed FFT for SVM classification algorithm. Additionally, along with SVM indices of frequency and amplitude ratio and vector fitting have been applied for detection of transformer winding fault, such as radial and axial deformation, disc displacement. It has been stated that SVM method is more accurate compared to artificial neural network for identification of winding fault type.

In [143], the learning vector quantization (LVQ) borrowed from artificial neural networks (ANN) is used for classification of the transformer insulation damage. The minor and major axis parameters from voltage-current (V-I) characteristic diagram are utilized for the feature extraction of the classification model. The proposed classification algorithm resulted in 98.2% accuracy of identifying different levels of the insulation fault.

3.3.3 Statistical analysis

In contrast to conventional visual interpretation, the method of statistical analysis reports the numerical difference between fingerprint and new FRA spectra, and the magnitude of the calculated Statistical Indicator (SI) basically defines the severity of the transformer fault. For instance, various statistical methods were applied to localize the partial discharge inside the transformer winding. The studies by [144]-[147] provided a thorough review on different numerical indices used for interpretation of FRA results. For instance, in [144], a detailed review on statistical indices discussed in literature is provided. Moreover, according to Samimi and Tenbohlen [144], SIs can be categorized into three

groups based on whether retrieved from FRA signatures, from resonance and anti-resonance peaks, or from rational functions. The first group proposes SIs to be expressed in linear or logarithmic scale, yet there is no standard or methodology agreed upon between researchers and industry. The second group of indices are usually expressed in logarithmic scale and demonstrate the behavior of the resonating peaks in case of any internal fault. However, it is claimed that this method requires additional noise mitigation and standardization. The third group, also referred to as the vector or rational function fitting, is the most challenging among all three methods. This approach implies estimation of the SIs from the pre-defined rational functions fitted into the original FRA signature. The order of the rational function determines the amount functions fitted into the spectrum, which, in turn, might lead to different results. The study conducted by Banaszak and Szoka [145] proposed SI grouping and used 14 indices widely used in literature. The grouping approach implies diving the SIs into four main groups depending on the behavior of each index towards mechanical deformation fault. Hence, via considering at least one index from each group, this method facilitates to distinguish frequency sub-bands more sensitive to mechanical deformation and mitigate the possibility of the information loss. The study by Nurmanova et al. [146] analyzed the behavior of several SIs, namely, Correlation Coefficient (*CC*), Root Mean Square Error (*RMSE*), Absolute Sum of Logarithmic Error (*ASLE*), and Euclidean distance (*ED*) when distribution transformers are exposed to different external resistive and capacitive impedances. According to [147], where statistical analysis was applied to evaluate the numerical difference of frequency response for intact and faulty conditions (short-circuit and mechanical displacement), all five used indices were able to detect FRA signature deviations, however Comparative Standard Deviation (*CSD*) reported highest sensitivity to fault and linear relationship towards the severity of the fault. Jeyabalan and Usa [148] implemented the correlation of winding response for reference partial discharge impulse across transformer sections with response for impulse of different width. Since time domain method was unsuccessful to distinguish the location of partial discharge when the width of excitation pulse is different form reference pulse, it was suggested to conduct correlation of winding response in frequency domain.

Although IEEE Standard [49], [50] suggests to use *CC* for FRA results interpretation, in [149] alternative indices such as *ASLE*, *SSE*, and *SD* are utilized to distinguish among

different fault types, namely, clamping and bushing tap fault, disk-to-disk fault, mechanical deformation of the winding structure, and short circuit fault. Moreover, in [149] the statistical indices are calculated for three sub-bands individually, since frequency response may be deviated differently according to the type of the fault. According to numerical comparison of the response spectra, *SD* reported higher sensitivity towards bushing and short circuit fault, *SSE* is mostly affected by disk-to-disk and short circuit fault, whereas *ASLE* reported sensitivity towards all three of the mentioned fault types.

In addition, in [106] and [150] the decision boundaries for cross-correlation factor (*CCF*) and relative factor (*RF*) for classification of the transformer condition has been determined. Specifically, as per Kennedy et al. [150] the critical *CCF* values were used to classify between good, marginal, and need-to-investigate working conditions. Other than that, in DL/T911-2004 Standard [19] critical values for *RF* have been established to distinguish amongst normal condition, slight, obvious, and severe winding deformations. According to practical results in [151] and [152], *CCF* and *RF* demonstrated significantly low sensitivity to define the transformer's faulty condition.

On the contrary, Kim et al. [153] stated that *ASLE* and *SSE* proved quite effective in defining the mechanical deformation of the transformer winding. It should be noted, that in some studies a collaborative decision of several indices were also taken into account. For example, in study by Samimi et al. [154] the collective result of both *CC* and *ED* were reported, since *CC* was insensitive to mechanical deformation of the winding structure. Moreover, in [155] a standardized difference area (*SDA*), correlation factor (ρ), index of frequency deviation (*IFD*), index of amplitude deviation (*IAD*), frequency weight function (*Wf*), and the amplitude weight function (*Wa*) were applied to classify the type of the winding deformation and also to define its severity.

3.3.4 Digital image processing

The transfer function magnitude and phase response are used as an input for the image recognition algorithm where DIP techniques are used to process the frequency response spectra and compare the reference and the recent measured FRA signatures based on their geometric properties and features, and define the fault level [7].

The study conducted by Aljohani and Abu-Siada [112] proposed a consideration of both transfer function magnitude and phase plot in one combined 2-D image for successive detection and classification of transformer fault. After elimination of the noise and background from the pictorial data, it was further used for extraction of the features for oil and bushing fault classification.

Zhou et al. [156] proposed an innovative approach to determine transformer winding faults from FRA signature. Frequency response magnitude plot is transformed into a binary image and went through the data erosion in order to reduce some minor disturbances. Afterwards, features extracted from the processed images were used to determine the deviation between reference (fingerprint) and new FRA measurement, which helped to diagnose any occurring faults in the winding structure. Furthermore, the SVM based classification model was utilized to classify the results of practical case studies among axial deformation, series capacitance deviation, and short circuit fault.

Zhau et al. [157] applied DIP technique to magnitude and phase plot of the transfer function and estimated similarity indicator for two dimensional images representing intact condition and mechanical deformation; and observations reported higher sensitivity of the proposed method compared to conventional statistical analysis engaged into standards.

The study by [158] introduced a new FRA results interpretation technique, where the phase response of the transformer winding is converted into 2D image with real and imaginary parts. Comparison of the FRA spectra is conducted via calculation of the Sum square max-min ratio error (*ISSMMRE*) and further used to define condition of the winding under the test. However, the practical results revealed that the proposed method is insufficient to define both type and severity of the applied mechanical fault.

3.4 FRA Standards

3.4.1 DL/T911-2004

The Standard of the People's Republic of China DL/T911-2004 [19] proposed the interpretation method based on the estimation of the relative factor for separate frequency sub-bands. The standard is used to define the mechanical condition of the transformer

winding among severe, obvious, slight deformation and normal winding condition. Classification criteria for relative factor is presented in Table 1 [19].

Table 1 – Relative factor and the deformation degree

Degree of winding deformation	Relative factor, R
Severe deformation	$R_{LF} < 0.6$
Obvious deformation	$1.0 > R_{LF} \geq 0.6$ OR $R_{MF} < 0.6$
Slight deformation	$2.0 > R_{LF} \geq 1.0$ OR $0.6 \leq R_{MF} < 1.0$
Normal winding	$R_{LF} \geq 2.0$, $R_{MF} \geq 1.0$ AND $R_{MF} \geq 0.6$

The relative factor is calculated using:

$$R_{XY} = \begin{cases} 10 & 1\text{-}\sigma < 10^{-1} \\ -\log_{10}(1\text{-}\sigma) & \text{otherwise} \end{cases} \tag{10}$$

where R_{XY} represents the relative factor R_{LF}, R_{MF} and R_{HF} for low (1 kHz – 100 kHz), medium (100 kHz – 600 kHz) and high (600 kHz – 1000 kHz) frequency sub-bands, respectively, and σ is the normalization covariance factor estimated as:

$$\sigma(X,Y)=\frac{C_{XY}}{\sqrt{D_X \cdot D_Y}} \tag{11}$$

where the variables C_{XY}, D_X and D_Y are evaluated using:

$$C_{XY}=\frac{1}{N}\sum_{i=0}^{N-1}\left[\left(X(i)-\frac{1}{N}\sum_{i=0}^{N-1}X(i)\right)^2 \times \left(Y(i)-\frac{1}{\mathrm{N}}\sum_{i=0}^{N-1}Y(i)\right)^2\right] \tag{12}$$

$$D_X=\frac{1}{N}\sum_{i=0}^{N-1}\left(X(i)-\frac{1}{N}\sum_{i=0}^{N-1}\mathrm{X}(i)\right)^2 \tag{13}$$

$$D_Y=\frac{1}{N}\sum_{i=0}^{N-1}\left(Y(i)-\frac{1}{N}\sum_{i=0}^{N-1}Y(i)\right)^2 \tag{14}$$

It should be noted, that this approach considers only the effect of the winding fault on FRA spectrum, as it estimates relative factor for the range from 1 kHz to 1 MHz; hence, the low- and high-frequency deviations are left uninvestigated [19].

3.4.2 CIGRE Working Group A2.26

The International Council on Large Electric Systems (CIGRE) standard undertaken by Working Group A2.26 [159] provided the recommendations on effective FRA measurement configurations, results interpretation and frequency response behavior affected by transformer winding movements. Along with those, the standard suggested three concepts to conduct comparative FRA data analysis depending on the availability of the fingerprint signature:

- time-based comparison: comparison of FRA spectra for exact similar measurement setup, when fingerprint is available;
- type-based comparison: comparison of FRA spectra of two identical (sister) transformer units, in case the fingerprint is not available;
- design-based comparison: comparison of FRA spectra of adjacent phases of the same transformer unit, if fingerprint is not available (only applicable to three-phase units) [159].

The technical brochure proposed a methodology to interpret FRA results via statistical analysis, namely, the estimation of *CC*. However, a successful classification of transformer working condition becomes challenging, since the guide do not provide enough information regarding definition of the critical *CC* values separating “normal” and “abnormal” conditions.

3.4.3 IEC 60076-18:2012

The standard released by the International Electrotechnical Commission (IEC) [48] has provided a comprehensive information on FRA measuring equipment and setup configurations. It is capable to be applied to power and distribution transformers, reactors and shifting transformer units. More than that, in the standard the frequency spectrum was divided into four sub-bands and different affecting factors affecting each sub-band were differentiated. In particular, low-frequency range (up to 2 kHz) is mostly influenced by core structure, mid-frequency range (from 2 kHz to 20 kHz) represents the interaction between windings, high-frequency range (from 20 kHz to 1 MHz) is affected by winding structure, and very high-frequency range is influenced by deviations in setup configuration,

lead and earthing connections. The very high-frequency sub-band varies depending on the size of the transformer under the test. The upper limit is 1 MHz for units less than 72.5 kV and 2 MHz for units rated greater than 72.5 kV, respectively. However, these frequency sub-bands may vary depending on transformer type and construction. Beside major factors influencing FRA signature, the standard discusses other issues such as effect of the tertiary winding, insulation type, and temperature.

3.4.4 IEEE C57.149

The standard developed by the Institute of Electrical and Electronics Engineers (IEEE) of Power and Energy Society [50] is applicable to the oil-immersed power transformers. The guide provides information about FRA instrumentation, measurement setups, results interpretation guidelines, and data storage. More than that, the IEEE C57.149 guide has recommendations regarding the minimum and maximum number of FRA test configurations for six different transformer types as listed in Table 2 [46]. For instance, consider the three-phase two-winding transformer under the test. It is recommended to conduct six open-circuit end-to-end FRA tests on both LV and HV sides of each phase and three short-circuit end-to-end FRA tests on HV sides with shorted LV sides, adding up to nine minimum required FRA test configurations.

The practical part of the standard provided actual FRA signatures of the transformers undergoing frequently occurred faults. This gives on-site personnel a good perspective in terms of the FRA behavior towards different fault types.

Table 2 – The number of the recommended tests based on transformer types

Transformer type	Minimum	Maximum
Two-winding transformer	9	15
Autotransformer without tertiary winding	9	12
Autotransformer with tertiary winding	18	33
Autotransformer with buried tertiary winding	9	18
Three-winding transformer Part 1	18	36
Three-winding transformer Part 2	18	36

3.4.5 NCEPRI

The North China Electric Power Research Institute (NCEPRI) [160] proposed the algorithm to define the short circuit fault of the transformer winding based on the numerical comparison of the reference and the new measurement of the frequency response transfer function based on estimated value of the effective deviation *ED* or assessment factor E_{12} using the following expression [160]:

$$E_{12}=\frac{1}{N}\sum_{i=1}^{N}(TF_{1i}-TF_{2i})^2 \tag{15}$$

where TF_{1i} and TF_{2i} represent transfer function of the fingerprint and the new measurement, respectively, and i is the corresponding measurement point from 1 to N, where N is the maximum number of the data points.

Table 3 – Assessment factor criteria for different distortion levels

Winding distortion level	E_{12} (dB)
Normal condition	$E_{12} < 3.5$
Slight distortion	$3.5 > E_{12} \geq 7.0$
Serious distortion	$E_{12} > 7.0$

NCEPRI suggested specific frequency ranges for high-voltage (HV), low-voltage (LV), and tertiary voltage (TV) sides starting from 10 kHz up to 515 kHz, 600 kHz, and 700 kHz, respectively [160].

CHAPTER 4. WINDING MODELING

4.1 Introduction

This Chapter is structured in the following manner: in Section 4.2 the comprehensive RLC model of the air-core winding is presented. Section 4.3 discusses the winding software model simulated in SPICE environment and validation of the proposed model and Section 4.4 covers the emulation of the axial and radial deformation over the validated winding model.

4.2 Winding RLC model

A comprehensive SPICE-based RLC model of the winding is discussed. The proposed modeling technique estimates distributed parameters (resistance *R*, inductance *L*, and capacitance *C*) for every turn of the transformer winding based on the geometrical characteristics and generates a SPICE netlist that describes the entire winding and setup. The model enables to emulate axial and radial displacements, DSV, and inter-turn and inter-disk short-circuit faults with excessive details. The proposed model is validated via practical fabricated model.

A properly designed, examined, and validated winding model will facilitate the detailed simulation and realization of the different winding deformations. Since the iron core has a significant influence on the mutual and self-inductance parameters, in this work, an air-core winding is utilized, where the lumped parameters exclusively depend on the geometric characteristics of the conductors. Hence, alteration in geometry of the winding structure, i.e., axial and radial deformation, will have a traceable effect on the distributed parameters.

The winding proposed in this study consists of ten disks with six turns per each disk continuously wounded around the cylindrical air core, as illustrated in Figure 4.1 [182] Wire and conductor have a circular cross-section and the distance between adjacent disks is taken as zero. It is a simple model that could be fabricated in the laboratory for the practical study and model validation. In this work, the distance between adjacent

disks are assumed to be zero and Table 4 presents the information about the wire and conducting material, including insulating material, conductor type, geometric characteristics, etc.

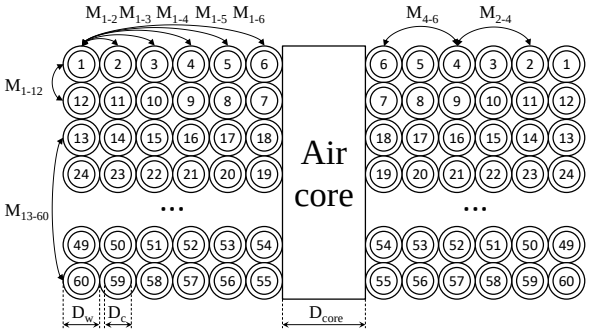

Figure 4.1. Air-core winding with continuously wounded disks

Table 4 – Physical parameters of the proposed winding

Parameter	Value
Conducting material	Copper
Conductor diameter, D_c	2.36 mm
Insulation material	Silicon rubber
Insulation thickness	1.14 mm
Relative permittivity	4
Wire diameter, D_w	4.64 mm
Core diameter, D_{core}	89 mm

As discussed earlier, the winding detailed model in this work is based on the estimation of the lumped parameters, namely, turn's self-inductance, mutual inductance between two wires, capacitances between two turns and two disks, and turn resistance.

The self-inductances L and mutual inductances between individual turns $M_{a\text{-}b}$ are estimated using equations provided for circular wires [161]:

$$L = 4\cdot 10^{-3}\pi R\left(\ln\left(\frac{8R}{r_c}\right)\text{-}1.75\right) \qquad \mu\text{H} \tag{16}$$

$$M_{a\text{-}b} = f\sqrt{R_a R_b} \qquad \mu\text{H} \tag{17}$$

where variables R_a and R_b are the turns' radii given in cm and f is the specific parameter retrieved from the lookup tables [161]. The winding total inductance matrix L_{eq} is expressed as following:

$$\boldsymbol{L_{eq}} = \begin{bmatrix} L_1 & M_{1-2} & \cdots & M_{1-60} \\ & L_2 & \cdots & M_{2-60} \\ & & \ddots & \vdots \\ & & & L_{60} \end{bmatrix}_{60\times 60} \tag{18}$$

The turn-to-turn capacitances C_{tt} for the circular wires are estimated using:

$$C_{tt} = \frac{\varepsilon_r \varepsilon_0 l_t \theta^*}{\ln\left(r_w / r_c\right)} + \varepsilon_0 l_t \left[\cot\left(\frac{\theta^*}{2}\right) - \cot\left(\frac{\pi}{12}\right) \right] \tag{19}$$

where ε_r is the relative permittivity of the insulating material, l_t depicts the turn length, r_w is the wire radius, r_c is the conductor radius, and θ^* is the angle at the crossing point estimated as:

$$\theta^* = \arccos(1-\ln(\frac{D_w}{D_c})/\varepsilon_r) \tag{20}$$

The disk-to-disk capacitances C_{dd} between the turns of neighboring disks are estimated similar to C_{tt}. The details of the winding and fault modeling are elaborated further.

The calculation of winding lumped parameters, such as self-inductances L, mutual inductances $M_{a\text{-}b}$, turn-to-turn capacitances C_{tt} and disk-to-disk capacitances C_{dd}, and turn resistances R, is necessary for building of a full RLC model of the winding. Since the winding is continuously laid around air-core as illustrated in Figure 4.1, these distributed parameters are dependent on the geometrical parameters and location of the filaments.

1) Self-inductance

In general, a magnitude of the self-inductance is influenced by the geometric features of the conductor [161]-[163]. In particular, the self-inductance L of the turn with a circular cross section is estimated via [161]:

$$L = 4\times10^{-3}\pi R\left(\ln\left(\frac{8R}{r_c}\right)-1.75\right) \tag{21}$$

where R is the radius of the circular ring in cm and r_c is the radius of the circular cross-section in cm.

2) Mutual inductance

The mutual inductance between two wires is based on the expression of the $M_{a\text{-}b}$ for two circular filaments:

$$M_{a\text{-}b} = f\sqrt{R_a R_b} \qquad \mu H \tag{22}$$

where R_a and R_b are the turns' radii in cm and parameter f is retrieved from the lookup tables using the value of k'^2:

$$k'^2 = \frac{\left(R_a - R_b\right)^2 + d^2}{\left(R_a + R_b\right)^2 + d^2} \tag{23}$$

In the above equation, d is the distance between two turns (see Figure 4.2 [182] ©2021 IEEE). When two filaments are considerably close to each other and $k'^2 \leq 0.1$, the f factor is calculated as follows:

$$f = 0.014468(\log(1/k'^2) - 0.53307) \tag{24}$$

In this work, the f factor is accurately determined from the lookup tables in [161] for $k'^2 > 0.1$ and Eq. (24) for $k'^2 \leq 0.1$.

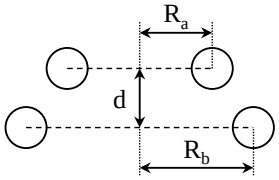

Figure 4.2. Two circular filaments separated by distance *d*

The inductance matrix L_{eq} of the proposed winding is as follows:

$$\boldsymbol{L}_{eq}=\begin{bmatrix} L_1 & M_{1-2} & \cdots & M_{1-60} \\ & L_2 & \cdots & M_{2-60} \\ & & \ddots & \vdots \\ & & & L_{60} \end{bmatrix}_{60\times 60} \tag{25}$$

Based on Figure 4.1, L_1 denotes the self-inductance of the first turn, whereas $M_{1\text{-}2}$ denotes the mutual inductance of first and second turns.

3) Turn-to-turn capacitance

A winding series capacitance has two components: 1) turn-to-turn capacitance C_{tt} between consecutive turns of the single disk and 2) disk-to-disk capacitance C_{dd} between turns of the neighboring disks as depicted Figure 4.3 [182] ©2021 IEEE.

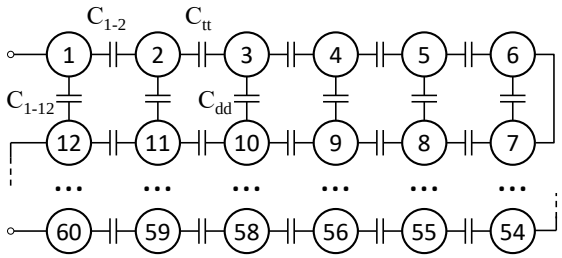

Figure 4.3. Inter-turn and inter-disk capacitances

The turn-to-turn capacitance C_{tt} is influenced by conductor geometry, in particular, the distance between conductors, and type and thickness of the insulation layer [164]. As displayed in Figure 4.4 [182] ©2021 IEEE, the turn-to-turn capacitance C_{tt} of two neighboring circular can be determined as a series combination of the air gap capacitance C_g and the insulation coating capacitance C_c [163]. In particularly, C_{tt} is calculated as [163]:

$$C_{tt}=C_{ttc}+C_{ttg} \tag{26}$$

The equivalent turn-to-turn capacitance of the insulation layer C_{ttc} and equivalent turn-to-turn capacitance of the air gap C_{ttg} are computed as following [163]:

$$C_{ttc}=\frac{\varepsilon_r\varepsilon_0 l_t\theta^*}{\ln\left(r_w/r_c\right)} \tag{27}$$

$$C_{ttg} = \varepsilon_0 l_t \left[\cot\left(\frac{\theta^*}{2}\right) - \cot\left(\frac{\pi}{12}\right) \right] \tag{28}$$

In the above, l_t represents a length of the turn, r_w is a total radius of the wire including insulation layer, r_c is the conductor radius, ε_r is the relative permittivity of the coating material, and θ^* the angle at the crossing point estimated as:

$$\theta^* = \arccos(1\text{-}\ln(\frac{D_w}{D_c})/\varepsilon_r) \tag{29}$$

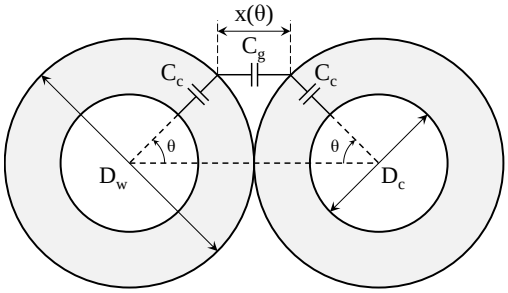

Figure 4.4. Inter-turn capacitance between two adjacent circular filaments

Disk-to-disk capacitances C_{dd} among turns of the neighboring disks are obtained similar to turn-to-turn capacitances C_{tt} for the proposed winding using (26)-(29).

4) Resistance

Since at higher frequencies the possibility of proximity and skin effects at the surface of the conductor increases, the conductor resistance in ac mode is often substantially greater than in dc operation mode [164]. The ac resistance R_{ac} of the conductors operating at frequencies higher than 50 Hz are estimated as [164]:

$$R_{ac}=\rho_{dc} l_t X \tag{30}$$

$$X = 0.027678 \sqrt{f / \rho_{dc}} \tag{31}$$

where ρ_{dc} is the conductor dc resistance expressed in mΩ/ft, l_t represents the length of the turn in ft, X is the correction factor, and f is the current frequency in Hz.

4.3 SPICE modeling and validation

An analytical model of the proposed winding is constructed in open-source SPICE simulation environment, since it facilitates an accurate simulation of large analog circuits. Since, the focus of this is the system frequency response, the SPICE simulation is configured to the ac mode.

A robust SPICE-level emulation of mutual inductance between two inductors is presented by [165]. As demonstrated in Figure 4.5 [182] ©2021 IEEE, the coupling between inductors in this model is accomplished by two inductors and voltage controlled voltage sources (VCVSs). The inductors have self-inductances of $1/K_{i\text{-}i}$ and $1/K_{j\text{-}j}$, while the VCVSs have gains of α and β. In this method, self-reluctances ($K_{i\text{-}i}$ and $K_{j\text{-}j}$) and mutual reluctances ($K_{i\text{-}j}$ and $K_{j\text{-}i}$) are obtained from the reluctance matrix K, where $K = L_{eq}^{-1}$.

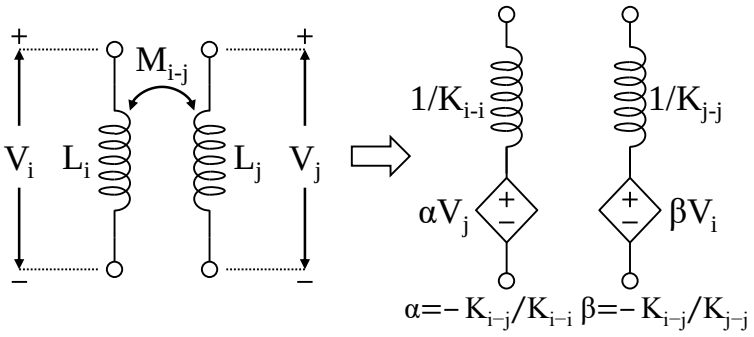

Figure 4.5. SPICE simulation of the mutual coupling between two inductors

The entire winding model is depicted in Figure 4.6. In this Figure, the injected sweep sinusoidal signal, input and output impedances of the FRA equipment are presented as V_{in}, R_{in}, and R_{out}, respectively. Each winding turn has a series resistance of R_i, an equivalent inductance of $1/K_{i\text{-}I}$, and 59 VCVSs, which simulate the effect of the magnetic coupling with other turns. As an example, the second VCVS of the turn-2 with $\alpha_{2\text{-}3}V_{34}$ output voltage emulates the voltage induced in turn-2 in the result of the voltage V_{34} at turn-3. The turn-to-turn capacitances, such as $C_{2\text{-}3}$ and $C_{12\text{-}13}$, are computed using (26)-(29). The capacitances that are connected across the turns of different disks, such as $C_{1\text{-}12}$ and $C_{2\text{-}11}$, are the disk-to-disk capacitances C_{dd}. For example, the disk-to-disk capacitance between the outermost turns of the first and second disks is presented as $C_{1\text{-}12}$. In SPICE

environment, the turn resistance R_i is simulated via frequency dependent resistor model based on the Laplace command to simulate skin and proximity effects [166]:

$$R = 1\ \text{Laplace} = 1/\{K\}/(-S*S/4/PI^2)^{0.25} \tag{32}$$

where S represents the Laplace transform's operator variable and K is the coefficient calculated using (30) and (31):

$$K = R_{ac}/\sqrt{f} \tag{33}$$

The total model shown in Figure 4.6 [182] ©2021 IEEE contains approximately 3500 circuit elements, which makes a manual setup of all circuit elements extremely challenging. Thus, winding model is configured in SPICE netlist utilizing the Python coding (see Appendices A-F).

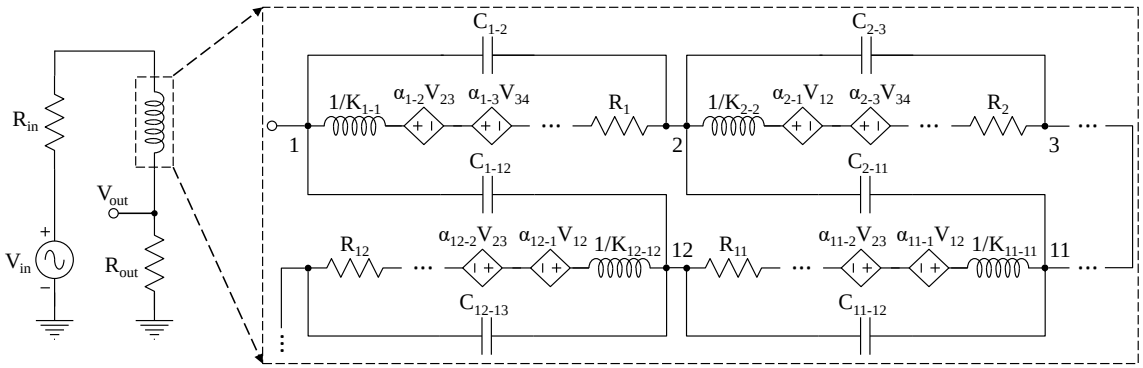

Figure 4.6. Overall RLC model of the fabricated air-core winding and FRA setup

For further application of the winding mechanical deformation, it is vital to validate the developed software model based on the physical winding prototype. To do that, the frequency response of both models are obtained and compared with each other. The circuit in Figure 4.6 [182] ©2021 IEEE demonstrates the theoretical FRA measurement of the proposed winding, where the excitation signal is the sinusoidal waveform swept from 20 Hz up to 10 MHz. Figure 4.7(a) illustrates the fabricated winding composed of ten disks with six turns per each wrapped around the air core. Figure 4.7(b) demonstrates the practical frequency response measurement setup using a well-commercialized FRA

analyzing equipment. Similarly, in physical FRA measurement the sinusoidal signal swept from 20 Hz up to 10 MHz is injected to winding terminal.

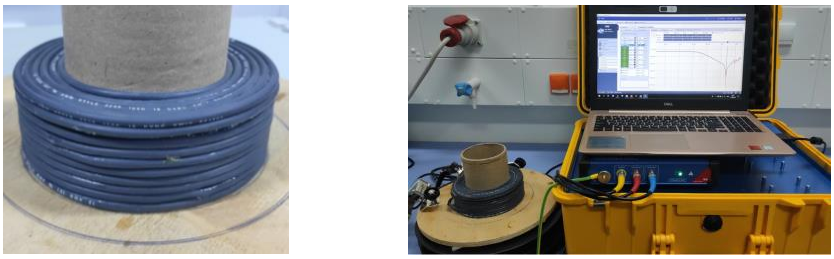

(a) (b)

Figure 4.7. Test equipment: (a) fabricated winding; (b) winding FRA measurement

The FRA spectra of fabricated and simulated winding are demonstrated in Figure 4.8 [182] ©2021 IEEE. It is observed that the overall signature shape and magnitude of the transfer function are identical. Moreover, the matching of the primary anti-resonant points at nearly 3 MHz is noted. Nevertheless, despite the location overlap of the resonant and anti-resonant peaks at higher frequency band is reported, the minor disturbances are detected at 5 MHz and onwards, which might be the result of the external noise. Having this considered, the developed software model of the air-core winding can be further considered for emulation of the axial and radial deformation and its effect on the distributed parameters and overall frequency response of the system. The discussion of the winding fault modelling is conducted in the next Section of this thesis.

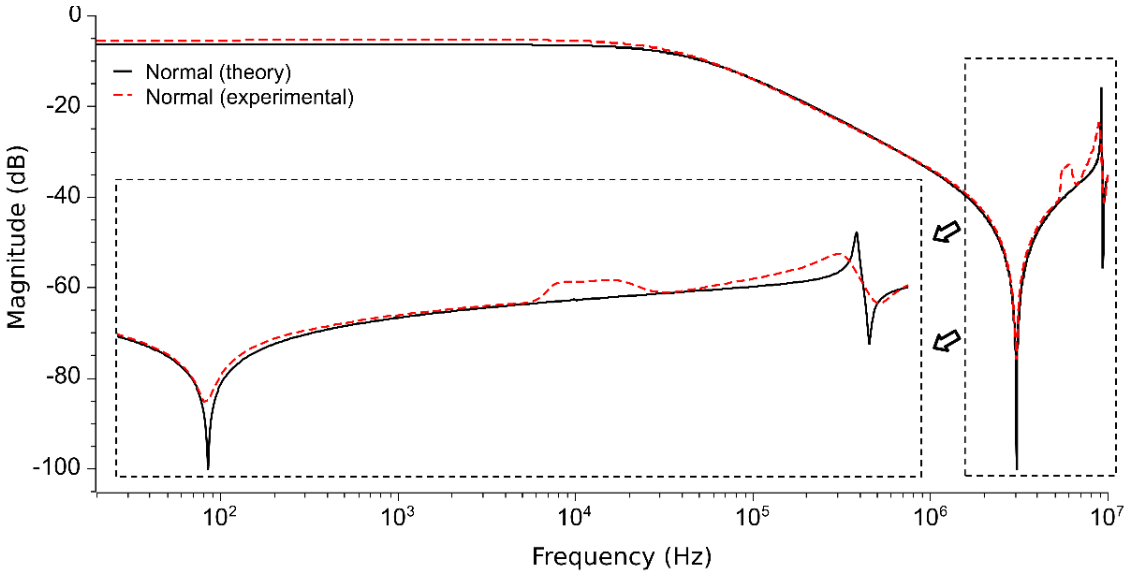

Figure 4.8. Theoretical and experimental FRA spectra of the proposed winding

4.4 Winding mechanical deformation modelling

4.4.1 Disk space variation (DSV)

The disk space variation (DSV) is among the most frequent winding axial deformations usually triggered by short circuit forces in the result of insulation deterioration, external disturbances such as earthquakes and improper transportation [162]. The DSV represents the axial displacement of the whole disk or disks from the winding structure as demonstrated in Figure 4.9 [182] ©2021 IEEE. As discussed previously, the air-core winding's lumped parameters solely depend on the geometry of the winding, the DSV fault will inevitably deviate the mutual inductance and the disk-to-disk capacitance.

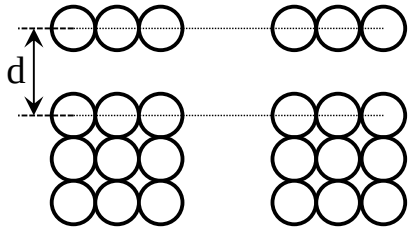

Figure 4.9. Transformer winding disk space variation (DSV)

The mutual inductance between previously adjacent, but now separated turns is now estimated using the separation distance in (22)-(24). The disk-to-disk capacitance C_{dd} is majorly expressed via the air gap C_g between separated disks [163]:

$$\frac{dC_g(\theta)}{d\theta} = \varepsilon_0 \frac{l_t D_w}{2x(\theta)} = \varepsilon_0 \frac{l_t D_w}{2(d - D_w \cos\theta)} \tag{34}$$

where l_t is the turn length, $x(\theta)$ is the air gap in terms of θ, d is the turn separation distance (measured between centers), D_w w is the diameter of the wire. Hence, integrating (34) over interval $[-\pi/2; \pi/2]$ we get the disk-to-disk capacitance:

$$C_{dd} = C_g = \frac{2\varepsilon_0 l_t}{\sqrt{a^2 - 1}} \left[\tan^{-1}\left(\sqrt{\frac{a+1}{a-1}} \tan\left(\frac{\pi}{4}\right)\right)\right] \tag{35}$$

where variable a is found via d/D_w.

4.4.2 Radial displacement

Another type of the mechanical deformation frequently occurring in transformer winding is the radial deformation, namely, displacement of the winding disk in the direction of the winding radius, as depicted in Figure 4.10. Similar to axial displacement, the mutual inductance and disk-to-disk capacitance are also affected [162].

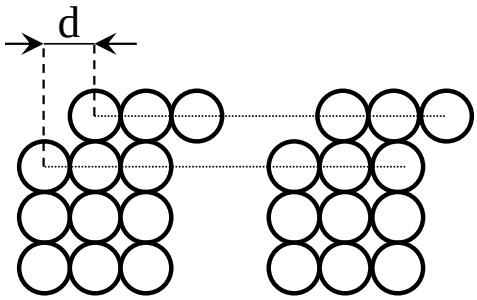

Figure 4.10. Transformer winding radial deformation

Although, these parameters are re-evaluated using a different approach. The parameter $M_{i\text{-}j}$ for intact filaments is estimated using the expression for undeformed condition; whereas, according to [161], the mutual inductance between two circular wires located on neighboring parallel disk planes and separated by distance d (see Figure 4.11) can be estimated using:

$$M = M_0 F \tag{36}$$

$$M_0 = f\sqrt{R_a R_b} \tag{37}$$

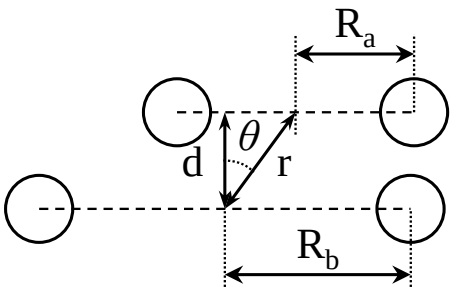

Figure 4.11. Two circular turns with parallel axes separated by distance *d*

In (36) and (37), M_0 is the mutual inductance of two circular filaments at $\theta = 0$, F is the correction factor retrieved from the table in [161] based on the value of $\mu = \cos\theta$ and, and factor f is obtained from the previously mentioned table based on the value of k'^2:

$$k'^2 = \frac{\left(R_a - R_b\right)^2 + r^2}{\left(R_a + R_b\right)^2 + r^2} \tag{38}$$

According to Figure 4.12, the disk-to-disk capacitance between 1st turn of the dislocated disk and the intact disk can be expressed in terms of parameters $C_{1\text{-}12}$ and $C_{1\text{-}11}$.

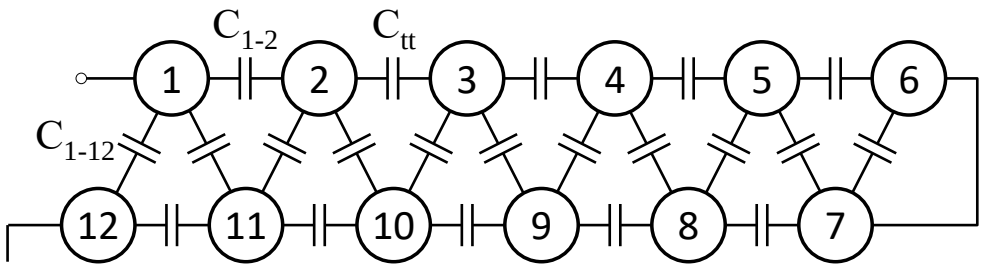

Figure 4.12. Disk-to-disk capacitances between turns of the normal and displaced disks during radial deformation fault

Since turns 1 and 12 have similar lengths, the distance between them during any homogeneous radial displacement will be constant (depicted as blue two headed arrows in Figure 4.13 below), therefore the capacitance between them can be calculated using (35) where the value of *d* will be replaced with a separation distance of turns. However, it is observed from Figure 4.13 that the distance between turns 1 and 11 is not constant (red two headed arrows), hence each turn is divided into four equal segments, and the total disk-to-disk capacitance between turns 1 and 11 will be the sum of four capacitances evaluated for each segment using (35).

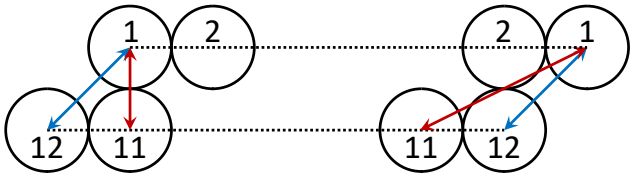

Figure 4.13. Distance between turns of the normal and displaced disks during radial deformation fault

Unaffected parameters such as the capacitance and inductance between turns of the displaced disk, turns' self-inductance and ac resistances are estimated based on intact scenario approach.

4.4.3 Disk tilting

The disk tilting is illustrated in Figure 4.14, where the disk or several disks are inclined away from the winding plane by a certain angle θ. It can be noted, that disk-to-

disk capacitance and mutual inductance between dislocated turns and intact turns are affected.

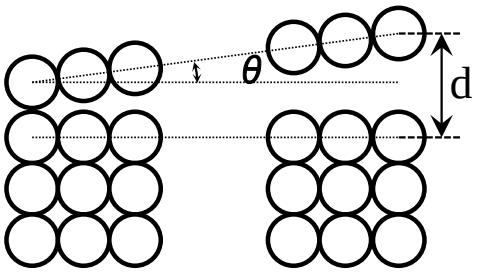

Figure 4.14. Transformer winding disk tilting

To be specific, the inter-turn mutual inductance between intact and inclined disks with circulars conductors is calculated using the following [161]:

$$M = RM_0 \cos\theta \tag{39}$$

where the equivalent mutual inductance M_0 is estimated using (22)-(24), angle θ is the tilt or inclination angle, and factor R is derived from [161] corresponding to $\mu = \cos\theta$, separation distance d, and turns radii R_a and R_b.

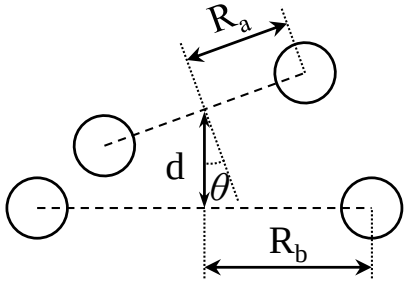

Figure 4.15. Distance between turns of the normal and inclined disks during disk tilting fault

On the other hand, the disk-to-disk capacitance between tilted and normal disks can be estimated using the approach applied for the radial deformation discussed earlier. Similarly, the distance between corresponding turns is not homogeneous throughout the

length of the turns, therefore, the total disk-to-disk capacitance between turns of two previously adjacent disks is the sum of four segments as illustrated in Figure 4.16 below.

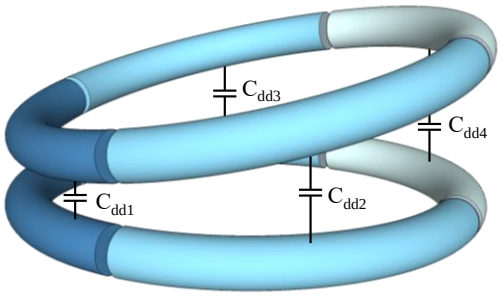

Figure 4.16. The proposed segmentation of the turns for an estimation of the distributed disk-to-disk capacitances during disk tilting fault

CHAPTER 5. TRANSFORMER CONDITION CLASSIFICATION METHODOLOGY

5.1 Introduction

This Chapter is structured in the following manner: in Section 5.2 the detailed discussion on the utilized Statistical Indicators is conducted. Section 5.3 introduces the proposed transformer working zones and explains the procedure for identification of their decision boundaries. In Section 5.4 the methodology of transformer operating condition classification via bolstered and bootstrapping methods is presented.

5.2 Statistical analysis

5.2.1 Statistical Indicators (SIs)

In this study, the numerical analysis is based on estimation of the statistical indicators (SIs) that have been widely used in the literature. The list of SIs applied for interpretation of the transformer FRA results is quite extensive and studies show that the sensitivity of the SIs towards the type, extent and location of the fault is diverse. Therefore, in this work, 12 SIs, in particular, correlation coefficient (*CC*), standard deviation (*SD*), sum squared error (*SSE*), absolute sum of logarithmic error (*ASLE*), absolute difference (*DABS*), root mean square error (*RMSE*), Euclidian distance (ED), comparative standard deviation (*CSD*), minimum-maximum ratio (*MM*), sum squared ratio error (*SSRE*), sum squared max-min ratio error (*SSMMRE*), and normalized correlation coefficient (ρ) will be utilized [167]-[174] as presented in Table 5 [180] ©2021 IEEE.

Table 5 – Statistical Indicators (SIs) used for FRA interpretation

SI	Equation	Limits
CC	$CC = \sum_{i=1}^{N} X(i)Y(i) \Big/ \sqrt{\sum_{i=1}^{N}\left[X(i)\right]^2 \sum_{i=1}^{N}\left[Y(i)\right]^2}$	[-1; 1]
SD	$SD = \sqrt{\sum_{i-1}^{N}\left[Y(i)-X(i)\right]^2 \Big/ (N-1)}$	[0; +∞)

SSE	$SSE = \sum_{i=1}^{N} \left(Y(i) - X(i)\right)^2 / N$	$[0; +\infty)$
ASLE	$ASLE = \sum_{i=1}^{N} \left\lvert 20\log_{10} Y(i) - 20\log_{10} X(i) \right\rvert / N$	$[0; +\infty)$
DABS	$DABS = \sum_{i-1}^{N} \left\lvert Y(i) - X(i) \right\rvert / N$	$[0; +\infty)$
RMSE	$RMSE = \sqrt{\frac{1}{N}\sum_{i=1}^{N}\left[\left(\lvert Y(i)\rvert - \lvert X(i)\rvert \right) \Big/ \left(\frac{1}{N}\sum_{i=1}^{N} \lvert X(i)\rvert \right) \right]^2}$	$[0; +\infty)$
ED	$ED = \lVert X - Y \rVert = \sqrt{\sum_{i=1}^{N} \left(Y(i) - X(i)\right)^2}$	$[0; +\infty)$
CSD	$CSD = \sqrt{\sum_{i-1}^{N} \left[\left(Y(i) - \mu_Y\right) - \left(X(i) - \mu_X\right) \right]^2 / (N-1)}$	$[0; +\infty)$
MM	$MM = \sum_{i=1}^{N} \min\left(Y(i), X(i)\right) \Big/ \sum_{i=1}^{N} \max\left(Y(i), X(i)\right)$	$(-\infty; +\infty)$
SSRE	$SSRE = \sum_{i=1}^{N} \left[Y(i)/X(i) - 1 \right]^2 / N$	$[0; +\infty)$
SSMMRE	$SSMMRE = \frac{1}{N}\sum_{i=1}^{N} \left[\frac{\max(Y(i), X(i))}{\min(Y(i), X(i))} - 1 \right]^2$	$[0; +\infty)$
ρ	$\rho = \sum_{i=1}^{N} X^*(i) Y^*(i) \Big/ \sqrt{\sum_{i=1}^{N} \left[X^*(i) \right]^2 \sum_{i=1}^{N} \left[Y^*(i) \right]^2}$ $X^*(i) = \lvert X(i) \rvert - \sum_{i=1}^{N} X(i) / N$ $Y^*(i) = \lvert Y(i) \rvert - \sum_{i=1}^{N} Y(i) / N$	$[-1; 1]$

In equations below, *X(i)* and *Y(i)* denote the magnitude of the transfer function *X* (fingerprint) and *Y* (recent measurement) at the *i*-th frequency point, respectively [167]-[174].

1) Correlation Coefficient (*CC*)

The extent of the similarity between fingerprint and new FRA measurements can be defined via Correlation Coefficient (*CC*). It is extremely responsive to the shift of the resonant peaks, although constant alterations of the transfer function magnitude do not have observable effect on this indicator [167]. The CC value changes between -1 and 1, corresponding to perfect negative and perfect positive correlation. In case if two signatures overlap, the *CC* value reaches 1. The magnitude of the CC represents the extent of the correlation, whereas the sign (positive/negative) represents the direction of the correlation between two data sets:

$$CC = \frac{\sum_{i=1}^{N} X(i) Y(i)}{\sqrt{\sum_{i=1}^{N} \left(X(i)\right)^2 \sum_{i=1}^{N} \left(Y(i)\right)^2}} \tag{40}$$

2) Euclidean Distance (*ED*)

Euclidean Distance (*ED*) is a statistical index that illustrates the numerical distance between two sets of data, represented via reference and new frequency response spectra. The transformer intact case corresponds to the *ED* equal to 0, while upper limit has no boundary, as its value demonstrates the deviation between two traces. The index *ED* and axial deformation have a linear relationship [167], [173]. *ED* is estimated using the following expression:

$$ED = \sqrt{\sum_{i=1}^{N} \left(Y(i) - X(i)\right)^2} \tag{41}$$

3) Root Mean Square Error (*RMSE*)

Root Mean Square Error (*RMSE*) is the estimate of the numerical difference between respective data points of two data sets. *RMSE* follows the same behavioral trend as *CSD* [168]. Similar to *ED*, *RMSE* can report values in the range from 0 to +∞, where 0 represents the total overlap of two data sets. The larger is the distance between corresponding points of two FRA spectra, the higher is the *RMSE* value.

$$RMSE = \sqrt{\frac{1}{N}\sum_{i=1}^{N}\left(\frac{|Y(i)| - |X(i)|}{\frac{1}{N}\sqrt{\sum_{i=1}^{N}|X(i)|}}\right)^2} \tag{42}$$

4) Absolute Sum of Logarithmic Error (*ASLE*)

Absolute Sum of Logarithmic Error (*ASLE*) represents the comparison of the two given sets of variables in logarithmic scale [169]. *ASLE* is sensitive to short-circuit fault and clamping structure deviation over the whole spectrum, and to mechanical deformation and displacement after 20 kHz [169]. The best-case scenario, where two data sets overlap is represented by *ASLE* value equal to 0, whereas the upper limit for *ASLE* tends to +∞, indicating the level of the difference between two sets:

$$ASLE = \frac{1}{N}\sum_{i=1}^{N}\left|20\log_{10} Y(i) - 20\log_{10} X(i)\right| \tag{43}$$

5) Absolute Difference (*DABS*)

Absolute Difference (*DABS*) demonstrates low sensitivity towards deviation of the magnitude of the transfer function [170], however the behavior of the resonance and anti-resonance peaks have a considerable effect on the value of *DABS*. The *DABS* will result in 0 if fingerprint and new trace overlap, while the upper limit tends toward +∞:

$$DABS = \frac{1}{N}\sum_{i=1}^{N}\left|Y(i) - X(i)\right| \tag{44}$$

6) Sum Squared Error (*SSE*)

Sum Squared Error (*SSE*) is highly representative of the fault's severity level, as it compresses minor errors and magnifies the errors larger than 1. However, [171] claims that *SSE* becomes less sensitive after a certain level of the fault severity is reached. The *SSE* value represents the deviation between fingerprint and new FRA spectra, where zero corresponds to the total overlap of the two datasets. *SSE* is calculated using the following expression:

$$SSE = \frac{1}{N}\sqrt{\sum_{i=1}^{N}\left(Y(i) - X(i)\right)^2} \tag{45}$$

7) Standard Deviation (*SD*)

SD is the statistical index that indicates the level of dispersion of the given data with respect to its mean. In [172] it is claimed that *SD* is capable to detect the axial dislocation of the winding structure even less than 1% severity. Although, *SD* is not sufficient indicator to be used to determine the temperature and moisture content increase. The *SD* equal to zero corresponds to the minimum deviation from the mean value, while maximum possible variability can take values up to +∞.

$$SD = \sqrt{\frac{\sum_{i=1}^{N}\left(Y(i) - X(i)\right)^2}{N-1}} \tag{46}$$

8) Comparative standard deviation (*CSD*)

The *CSD* is an extension of the abovementioned *SD*, where the deviation of each sample regarding its mean value is estimated and used to define the difference between two data sets. The *CSD* equal to 0 represents the intact case, where there are no deviations among two spectra, whereas the upper limit has no definite boundary, as it depends on the deviation level [173].

$$CSD = \sqrt{\frac{\sum_{i=1}^{N}\left[\left(Y(i)-\mu_Y\right)-\left(X(i)-\mu_X\right)\right]^2}{N-1}} \tag{47}$$

9) Minimum-maximum ratio (*MM*)

MM is the ratio between the sums of the minimum and maximum values. In other words, for each frequency point, the lowest and highest values of the transfer function magnitude within the reference and new FRA spectrum are taken into consideration. The intact case corresponds to *MM* equal to 1. *MM* is sensitive to spectral shape changes caused by amplitude variations and shifts of resonant frequencies [173].

$$MM = \frac{\sum_{i=1}^{N}\min\left(Y(i),X(i)\right)}{\sum_{i=1}^{N}\max\left(Y(i),X(i)\right)} \tag{48}$$

10) Sum squared ratio error (*SSRE*)

Basically, *SSRE* is the normalization of the *SSE* mentioned above. The value of 0 represents the absolute similarity of the two FRA data sets [174].

$$SSRE = \sum_{i=1}^{N}\frac{\left(Y(i)/X(i)-1\right)^2}{N} \tag{49}$$

11) Sum squared max-min ratio error (*SSMMRE*)

Sum squared max-min ratio error (*SSMMRE*) is the combination of the *MM* and *SSRE* and expresses a high sensitivity to the deviation of the FRA signature in higher frequencies [173], [174]. *SSMMRE* has mathematical limits from 0 to +∞ for minimum and maximum deviation between two data sets, respectively:

$$SSMMRE = \frac{1}{N}\sum_{i=1}^{N}\left(\frac{\max(Y(i), X(i))}{\min(Y(i), X(i))} - 1\right)^2 \tag{50}$$

12) Normalized correlation coefficient (ρ)

As the name stands, Normalized correlation coefficient (ρ) is the normalization of the *CC* mentioned above and is bound by limit of [-1; 1]. Nevertheless, it is stated by [173] that ρ is less sensitive with respect to mechanical fault, unlike *CC*. The relationship between ρ and radial and mechanical displacement is monotonic. The value of ρ is estimated via:

$$\rho = \sum_{i=1}^{N} \frac{X^*(i)Y^*(i)}{\sqrt{\sum_{i=1}^{N}\left(X^*(i)\right)^2 \sum_{i=1}^{N}\left(Y^*(i)\right)^2}} \tag{51}$$

where $X^*(i) = |X(i)| - \sum_{i=1}^{N}\frac{X(i)}{N}$ and $Y^*(i) = |Y(i)| - \sum_{i=1}^{N}\frac{Y(i)}{N}$

5.2.2 Coherence of SIs

It is realized, that when applied to the FRA data of the given fault condition, individually SIs may have conflicting decisions. Therefore, in this work, the level of coherence H_{uv} between the pair of SIs is estimated using:

$$H_{uv} = \left(1 - \frac{1}{n}\sum_{i=1}^{n}\left|y_i^u - y_i^v\right|\right) \times 100\% \tag{52}$$

where y_i^u and y_i^v are classification labels of the given observation *i* defined using indices *u* and *v*, respectively, and *n* is the total number of observations. The y_i^u values are evaluated via:

$$y_i^u = \begin{cases} 0 & \text{for } x_i^u \in R_{green}^u \\ 0.5 & \text{for } x_i^u \in R_{yellow}^u \\ 1 & \text{for } x_i^u \in R_{red}^u \end{cases} \tag{53}$$

where x_i^u represents index *u* for the given observation *i*, R^u_{green}, R^u_{yellow}, and R^u_{red} are the green, yellow, and red zones of index *u*. The coherence value varies from 0 to 1, where 0 corresponds to the minimum coherence (the SI pairs classify each observation as the green and red zone, respectively), and maximum coherence corresponds to identical

classification of the given scenario by all SI pairs. For example, if indices *CC* and *SD* assign all samples to the green and yellow (neighboring zones), respectively, hence H_{uv} = 50%, while if the same scenario is classified by *SD* as red zone, then coherence H_{uv} (here $u = CC$ and $v = SD$) is zero. Different fault configurations representing various short-circuit severity levels are utilized to estimate the degree of coherence between all proposed SIs. Figure 5.1 [180] ©2022 IEEE illustrates the visualized coherence between indices, where × depicts the corresponding coherence between given indicator and the remaining SIs, and blue dots represent the mean of the coherences. It is observed, that the coherence between all SIs pairs vary in the range from 0.9 to 1.0, which demonstrates the overall high coherence between proposed 12 indicators. The detailed coherence report is provided in Appendix G.

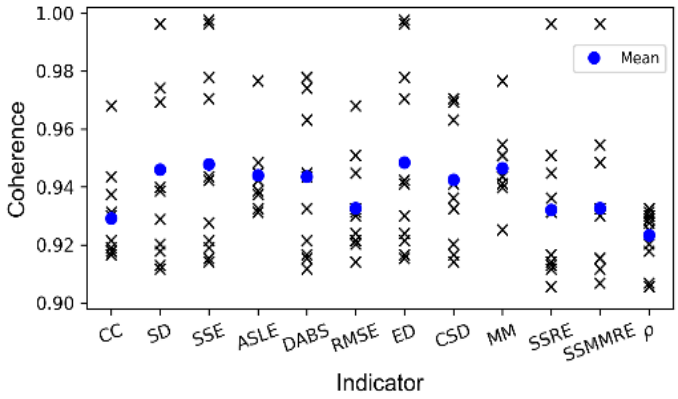

Figure 5.1. Coherence of statistical indicators

5.3 Identification of decision boundaries

In order to classify the working condition of the transformer under the test, the decision boundaries should be established first. In this work, three operating zones, in particular, green, yellow, and red zones, which correspond to healthy, suspicious, and critical transformer condition, respectively, are proposed. Therefore, two boundaries, namely, green-to-yellow and yellow-to-red decision boundaries will be practically defined.

5.3.1 Winding short-circuit emulation

The transformer winding short-circuit scenario is emulated via installation of the variable resistance rheostat in parallel to winding terminals. The maximum value of the rheostat represents the open circuit scenario, since it significantly exceeds the winding impedance and all the current coming from the source will flow the structure of the winding (see Figure 5.2(a) [110] ©2019 IEEE). The open circuit scenario corresponds to the healthy working mode of the transformer. In this work, the maximum value of the rheostat is 5 kΩ and 5 MΩ for distribution and power transformers, respectively, and both values are high enough to be compatible with windings' total impedance. The worst-case scenario corresponds to the full short-circuit of the transformer winding, where all the current coming from the source flows through the rheostat as illustrated in Figure 5.2(b) [110] ©2019 IEEE.

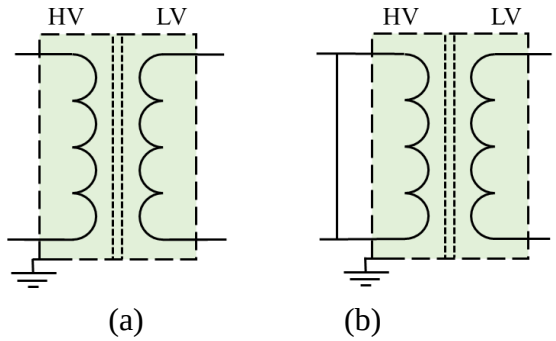

Figure 5.2. Equivalent circuit of the (a) best- and (b) worst-case scenarios

Therefore, by changing the paralleled resistance value (see Figure 5.3 [110] ©2019 IEEE) it is possible to alter the amount of the current flowing through rheostat and winding. Hence, while decreasing step-by-step the rheostat value at a certain point, the rheostat value becomes low enough so that a small amount of short-circuit current will start flowing through it.

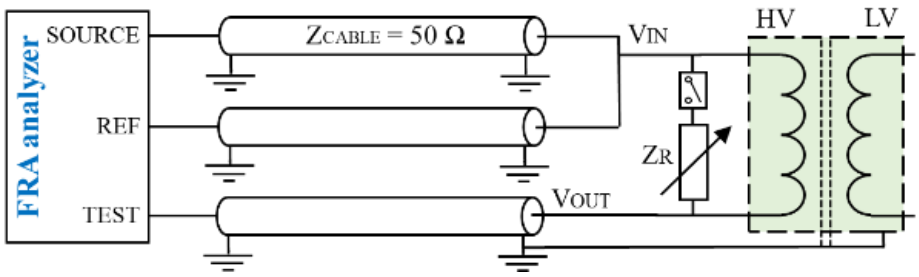

Figure 5.3. Circuit representation of the winding short-circuit emulation

The paralleled resistance is decreased with 500 Ω from highest (either 5 kΩ or 5 MΩ) to lowest (~Zero Ω) resistance. Generally, the relationship between input and output signal can be expressed in terms of the impedances as following:

$$V_{out}/V_{in} = Z_{out}/(Z_w + Z_{out}) \tag{54}$$

$$V_{out}/V_{in} = Z_{out}/(Z_w \parallel Z_R + Z_{out}) \tag{55}$$

where V_{in} and V_{out} represent the input and output voltages, correspondingly, Z_{out} is the cable impedance, Z_R is the rheostat's value, and Z_w represents the winding impedance. Therefore, it is observed that the transfer function becomes the function of the new equivalent impedance.

Figure 5.4 illustrates the behavior of the frequency response signature towards the different short-circuit scenarios, where 5 kΩ parallel resistance corresponds to the 0% short-circuit (healthy state) and 1 Ω corresponds to 100% short-circuit (critical). One of the major observations is that the magnitude of the transfer function increases along with severity of the winding short-circuit, which results in flattening of the signature around the first anti-resonance point (depicted by blue vertical line in Figure 5.4 [110] ©2019 IEEE). The first anti-resonant peak corresponds to the frequency at which the winding self-inductance L resonates with the equivalent capacitance C, represented via following expression [175]:

$$f_{\text{anti-resonance}} = 1/2\pi\sqrt{LC} \tag{56}$$

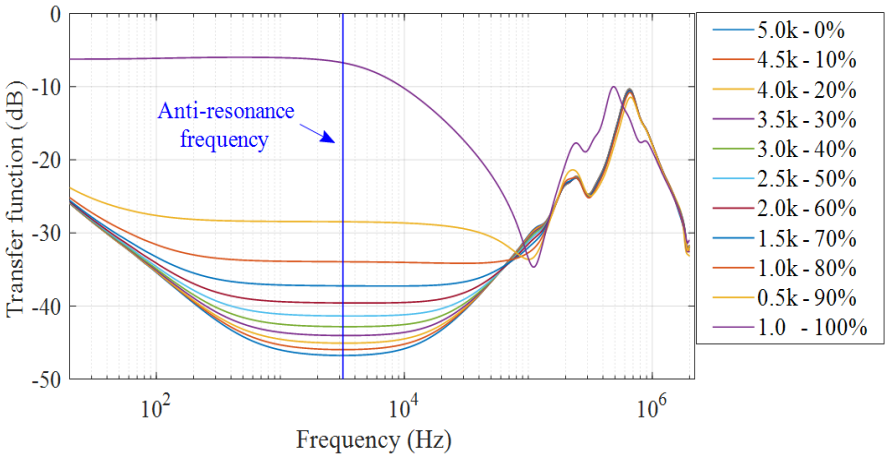

Figure 5.4. FRA signatures for different short-circuit severities

5.3.2 Green-to-yellow decision boundary

The green-to-yellow decision boundary $B_{G|Y}$ corresponds to the transition point from healthy (green) to suspicious (yellow) working mode. In this work, the boundary $B_{G|Y}$ represents the case where the short circuit current starts to flow in the system and is expressed in terms of the SIs values estimated from the corresponding FRA measurement. For each iteration step, short-circuit monitoring and FRA signature measurement is conducted via experimental setup depicted in Figure 5.5(a)-(b), respectively [20] ©2022 IEEE.

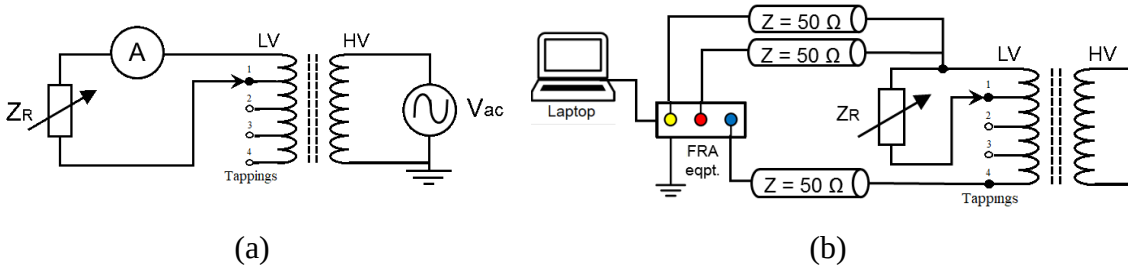

(a) (b)

Figure 5.5. Practical setup for: (a) short-circuit current monitoring and (b) FRA test

The short circuit current monitoring results given in Table 6 [181] ©2022 IEEE demonstrate the transition point (green colored) from green to yellow working mode. In the next short-circuit scenario the current flowing through the rheostat becomes measurable by the ammeter. Hence the following observations, in particular, T1-12V at 500 Ω, T1-

24V at 1.5 kΩ, T2-22V at 500 Ω, T2-42V at 1.5 kΩ, T3-24V at 500 Ω, and T3-36V at 1 kΩ, are considered as the green-to-yellow boundary $B_{G|Y}$. It was mentioned above, that for each fault scenario the FRA measurements are conducted to calculate 12 statistical indicators.

Table 7 [181] ©2022 IEEE illustrates the corresponding *CC* values for the scenarios presented in Table 6. Similarly, the green colored observations represent the critical *CC* value, i.e. the green-to-yellow $B_{G|Y}$ decision boundary. All collected $B_{G|Y}$ sample points expressed by other statistical indicators are also estimated from the obtained FRA signatures and presented in the Appendix H.

Table 6 – Short-circuit current monitoring results for different fault scenarios

Rating	Taps	Winding %	5 kΩ	4.5 kΩ	4 kΩ	3.5 kΩ	3 kΩ	2.5 kΩ	2 kΩ	1.5 kΩ	1 kΩ	500 Ω	200 Ω	0 Ω
400 VA	T1 12V	33.33%	0	0	0	0	0	0	0	0	0	0	0.034	-
	T1 24V	66.67%	0	0	0	0	0	0	0	0	0.024	0.031	0.054	-
630 VA	T2 22V	10.00%	0	0	0	0	0	0	0	0	0	0	0.022	-
	T2 42V	19.10%	0	0	0	0	0	0	0	0	0.027	0.041	0.218	-
1 kVA	T3 24V	10.90%	0	0	0	0	0	0	0	0	0	0	0.022	-
	T3 36V	16.36%	0	0	0	0	0	0	0	0	0	0.027	0.215	-

Table 7 – Estimated *CC* values for the emulated fault scenarios

Rating	Taps	Winding %	5 kΩ	4.5 kΩ	4 kΩ	3.5 kΩ	3 kΩ	2.5 kΩ	2 kΩ	1.5 kΩ	1 kΩ	500 Ω	200 Ω	0 Ω
400 VA	T1 12V	33.33%	0.9997	0.9997	0.9997	0.9998	0.9999	0.9997	0.9998	0.9997	0.9998	0.9997	0.9992	0.8983
	T1 24V	66.67%	0.9999	0.9999	0.9999	0.9999	0.9999	0.9999	0.9998	0.9998	0.9995	0.9985	0.9939	0.8985
630 VA	T2 22V	10.00%	1.0000	1.0000	0.9999	1.0000	1.0000	1.0000	1.0000	1.0000	1.0000	0.9998	0.9992	0.8296
	T2 42V	19.10%	1.0000	1.0000	0.9997	0.9999	0.9999	0.9999	0.9999	0.9998	0.9996	0.9987	0.9953	0.7701
1 kVA	T3 24V	10.90%	1.0000	1.0000	1.0000	1.0000	1.0000	1.0000	1.0000	1.0000	1.0000	0.9999	0.9996	0.8472
	T3 36V	16.36%	1.0000	1.0000	0.9999	0.9999	0.9999	0.9999	0.9999	0.9999	0.9997	0.9992	0.9966	0.7446

In this work, the list of statistical indicators used to estimate the numerical difference between reference and new frequency response includes 12 indices mostly used in the literature. The comprehensive details regarding utilized indices is presented in the next section of this thesis.

5.3.3 Yellow-to-red decision boundary

The yellow-to-red decision boundary $B_{Y|R}$ corresponds to the transition point from suspicious (yellow) to critical (red) working mode. In this work, the boundary $B_{Y|R}$ represents the maximum tolerable short-circuit current in the system and is also expressed in terms of the statistical indicators values estimated from the respective FRA

measurements. Basically, the differential relay system of the transformer under the test is set to 0.5% of the nominal current [176]. The rheostat value corresponding to this short-circuit current is found via decreasing the resistance from the highest to the lowest and measuring the current through the rheostat. Once the measured current value matches the desired value (0.5% of the nominal), the paralleled resistance is recorded and FRA signature of the given configuration is obtained. Similarly, decision boundary $B_{Y|R}$ is expressed in terms of the critical values of 12 statistical indicators calculated from the FRA data.

Table 8 [180] ©2021 IEEE provides the rheostat values corresponding to yellow-to-red decision boundary and the *CC* value of that given short-circuit condition. $B_{Y|R}$ sample points expressed by other statistical indicators are also estimated from the obtained FRA signatures. Table 9 [181] ©2022 IEEE illustrates the summary of the decision boundary identification, where 6 observations of $B_{G|Y}$ and 3 observations of $B_{Y|R}$ are collected for the index *CC* and Table 10 summarizes the calculated critical values for all SIs indicating two decision boundaries [20] ©2022 IEEE.

Table 8 – Current and paralleled rheostat values of $B_{Y|R}$ boundary

Transformer under test	T1-0.4 kVA	T2-0.63 kVA	T3-1 kVA
Nominal current (A)	11.00	2.86	4.54
Critical current (A)	0.055	0.0143	0.0227
Rheostat (kΩ)	4.6	15.4	10.5
CC	0.9990	0.9991	0.9989

Table 9 – Collected critical *CC* values for $B_{G|Y}$ and $B_{Y|R}$ boundaries

Green-to-yellow boundary, $B_{G\|Y}$		Yellow-to-red boundary, $B_{Y\|R}$
0.9997	0.9998	0.9990
0.9998	0.9999	0.9991
0.9998	0.9997	0.9989

Table 10 – Critical values of statistical indicators

SI	Green <---------->	Yellow <---------->	Red <---------->
CC	0.99978	0.9990	
SD	0.7276	2.1	
SSE	0.5727	4.4	

ASLE	0.09895	0.245
DABS	0.394	1.12
RMSE	0.02867	0.07
ED	22.71	67
CSD	0.6403	1.3
MM	1.0153	1.0354
SSRE	0.00035	0.0009
SSMMRE	0.00035	0.0009
ρ	0.99993	0.9995

5.4 Classification and Confidence level estimation

Reporting the confidence level along with classification labels is the essential part of the proposed interpretation technique. In other words, the confidence of the test object being in healthy, suspicious, and critical working condition will facilitate a more efficient decision-making process. Since transformer shut-down implies either temporary power outage or requirement of re-routing the power flow through other units, the industry is commonly reluctant to retrieve the transformer from the service unless it is inevitable and justified with sufficient test data.

5.4.1 Bolstered error estimation

As it was mentioned above, the introduced method provided the confidence level (CL) corresponding to each operating mode. The evaluation of the CL is based on the bolstered error estimation technique borrowed from pattern recognition [177]. This approach was initially proposed by Braga-Neto and Dougherty [177] as a tradeoff among variance, bias, and computational cost in small size datasets; and performed effective compared with conventional error estimation methods. The conceptual illustration of the bolstered resubstitution for linear discriminant analysis (LDA) is presented in Figure 5.6. The bolstering kernels are expressed with uniform circles and the ratio of the shaded region to the respective circle represents the error by the test observation. The total bolstered error estimated using ratio of the sum of all errors to the total number of test observation points.

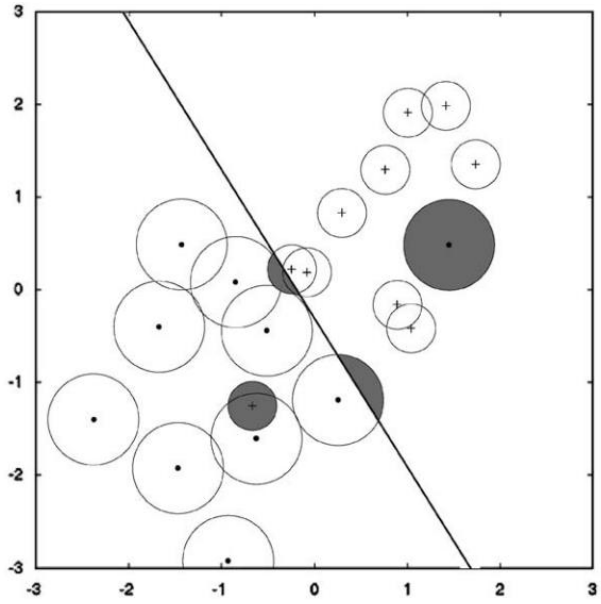

Figure 5.6. Example of the bolstered resubstitution for linear discriminant analysis, where kernels are expressed with uniform circles, taken from [177]

The bolstered error estimation method is usually used to calculate the error rate of the utilized classifier, where the feature-label practical distribution is replaced by the bolstered practical distribution. This distribution is defined through weighting each point over the true distribution using the *pdf* called bolstering kernel [177]. This *pdf* is usually the multivariate Gaussian density function which has a zero mean and the diagonal covariance matrix [177]. Following the principle of the bolstered error estimator, the bolstering kernel function is centered at each observation and for each working zone the area under the kernel *pdf* is estimated. Thus, the calculated area under the bolstering kernel for the given zone represents the confidence level of the test observation belonging to this zone. Naturally, test observations located closer to decision boundaries (either green-to-yellow or yellow-to-red) have the lower confidence of being assigned to a specific region (the algorithm for application of the bolstered error estimation method is presented in Appendix I).

Consider an example of utilizing the bolstering kernels for the classification of the obtained FRA signature. The visual illustration of the introduced method is depicted in Figure 5.7 [180] ©2021 IEEE. The given observation is represented by yellow circle, the estimated SI value is 0.5, and the Gaussian kernel is centered at this observation point. Two

solid vertical lines represent the pre-defined decision boundaries, specifically, green-to-yellow $B_{G/Y}$ boundary is 0.3 and yellow-to-red boundary $B_{Y/R}$ is 0.55. It is observed, that the bolstering kernel is divided into three parts by boundaries, hence, the area under the kernel corresponding each of these three zones yields the respective classification confidence percentages (calculation of the area under the kernel is given in Appendix J).

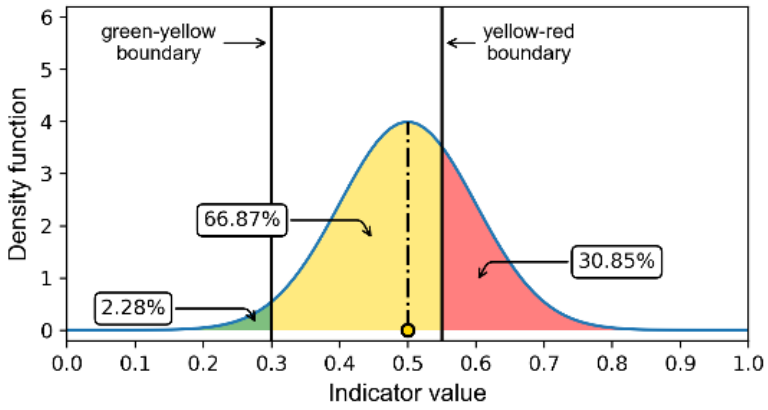

Figure 5.7. Visual representation of the confidence levels

For instance, the area under the kernel is equal to 0.0228 in the range from 0 to 0.3 (green zone), which implies the 2.28% confidence that this scenario belongs to healthy state; similarly, 0.6687 is the area under the Gaussian distribution between 0.3 and 0.55 (yellow zone), leading to 66.87% confidence of suspicious working condition. Generally, the confidence level retrieved from the area under the kernel is estimated using:

$$C_j(x) = C_j(x) \Big/ \sum_j S_j(x) \tag{57}$$

where $C_j(x)$ is the confidence level and $S_j(x)$ is the area under the bolstering kernel in the given range R_j, defined via:

$$S_j(x) = \int_{R_j} \frac{1}{\sigma_j \sqrt{2\pi}} \exp\left(-(t-x)^2 / 2\sigma_j^2\right) dt \tag{58}$$

where σ_j denotes the standard deviation of the Gaussian distribution used for the zone j (implied to be the same for observations under a similar class). The total area under the kernel is 1, which is ensured through normalization (see (57)). It should be noted, that each

SI has its unique mathematical range, whereas the utilized Gaussian kernel is non-zero at $(-\infty, +\infty)$. The index *MM* varies between $(-\infty, +\infty)$, too, whereas ρ and *CC* have the range of [-1; 1], and remaining indices take values between $[0; +\infty)$ (refer to Table 5).

The standard deviation σ_j in (58) is based on the empirical distribution of observation points belonging to a specific category (zone) [177]. It is shown in Figure 5.8 [180] ©2021 IEEE that more scattered observation points result in a wider bolstering kernel (meaning larger σ_j). For example, samples corresponding to green zone are distributed denser compared to red zone samples, which is reflected in a narrower kernel for green zone.

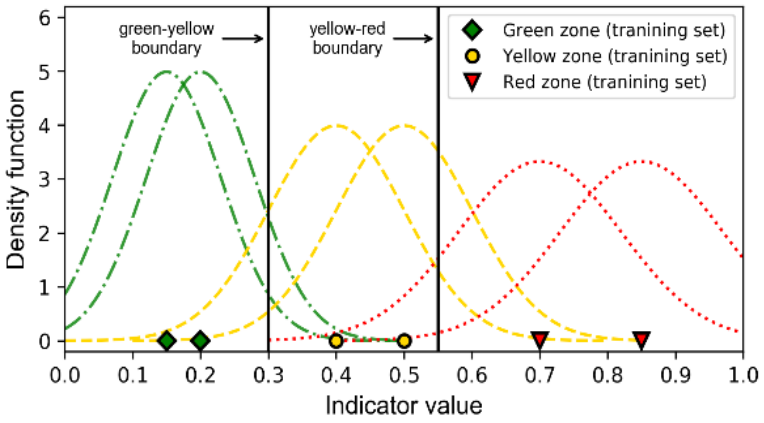

Figure 5.8. Various sample distributions and the corresponding kernels

Therefore, the standard deviation σ_j (the width of the distribution for each class), should be estimated. To do that, 15 test objects (14 distribution transformers and one power transformer) were examined. The detailed information regarding the number of phases, power rate, and accessible voltage tap positions are given in Table 11 [180] ©2021 IEEE.

Table 11 – Test objects utilized for the confidence level estimation

Transformer	Phases	Power rate	Voltage taps
T1	1	0.4 kVA	220/5/12/24/36 V
T2	1	0.4 kVA	230/24 V
T3	1	0.4 kVA	230/24 V
T4	1	0.63 kVA	220/5/12/22/42/110/220 V
T5	1	0.63 kVA	230/230 V
T6	1	0.63 kVA	230/220 V
T7	1	0.75 kVA	230/53/200/400 V, tertiary 230/115/230 V
T8	1	1 kVA	230/5/12/24/36/110/220 V

T9	3	0.35 kVA	230/400-230 V
T10	3	1.2 kVA	220-24/42 V
T11	3	5 kVA	230/380-42 V
T12	3	20 kVA	10 kV/400 V
T13	3	40 kVA	10 kV/400 V
T14	3	40 MVA	132 kV/33 kV

The FRA measurements are conducted on the abovementioned transformers using the standardized offline setup configuration. The collected data is used to estimate the bolstering kernel width σ_j and true mean distance $\hat{d}_j$. The frequency response is measured for different levels of the winding short-circuit emulated through changing the value of the paralleled rheostat. Specifically, for distribution transformers, the rheostat value is changed from 5 kΩ down to 0 Ω with 500 Ω steps; whereas for power transformer the rheostat value was varied from 5 MΩ to 5 kΩ so that the highest parallel resistance is compatible with winding impedance. Along with faulty conditions, the reference FRA signature was also collected according to the standard end-to-end open circuit measurement setup. Essentially, each fault configuration has its corresponding SI value estimated with respect to the intact condition. Hence, every scenario is classified according to the pre-defined decision boundaries and σ_j and $\hat{d}_j$ are estimated (see Table 12 [180] ©2021 IEEE). The respective classification confidence levels are calculated by applying σ_j and $\hat{d}_j$ into (57) and (58).

Table 12 – True mean distance and kernel standard deviation

Statistical indicator	True mean distance, $\hat{d}_j$ (10^{-3})			Standard deviation, σ_j (10^{-3})		
	Green	**Yellow**	**Red**	**Green**	**Yellow**	**Red**
CC	0.10	0.11	0.95	0.15	0.16	1.41
SD	2.39	12.55	55.98	3.55	18.62	83.05
SSE	2.38	35.97	1684.20	3.54	53.37	2498.80
ASLE	0.49	1.26	28.53	0.73	1.86	42.34
DABS	1.34	6.79	64.31	1.99	10.08	95.42
RMSE	0.17	0.26	1.97	0.24	0.39	2.93
ED	75.05	422.29	1740.90	111.34	626.54	2582.90
CSD	2.24	5.04	39.07	3.32	7.49	57.97
MM	0.12	0.23	6.00	0.17	0.34	8.91
SSRE	0.10	0.10	1.09	0.15	0.15	1.62
SSMMRE	0.10	0.10	0.99	0.15	0.15	1.47
ρ	0.10	0.10	0.39	0.15	0.15	0.59

5.4.2 Bootstrap sampling

The bootstrap sampling is another technique borrowed from the pattern recognition and statistical analysis. Application of the bootstrapping method for standard deviation estimation was introduced by Efron and Tibshirani [178] and its schematic conceptualization is depicted in Figure 5.9. According to [178], given a sample, bootstrapping method implies generating *B* bootstrap sample of the same size where each bootstrap sample is created by resampling (with replacement) the original set. The standard error of statistic $s(\mathbf{X})$ is replicated for every bootstrap sample as presented in Figure 5.9. The main aim in utilizing bootstrapping in this thesis is to simulate sufficient amount of experimental scenarios represented by bootstrap samples in situations where experiments are limited by various experimental restrictions.

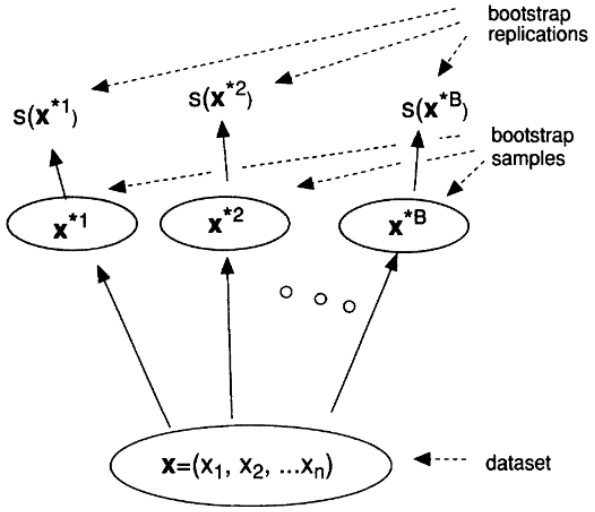

Figure 5.9. Bootstrap sampling scheme taken from [178]

Consider a dataset consisting two red balls, two yellow balls, and three green balls. The illustration of generating numerous samples from the original batch, where the elements of the original distribution are replaced and/or removed in the new sample is depicted in Figure 5.10.

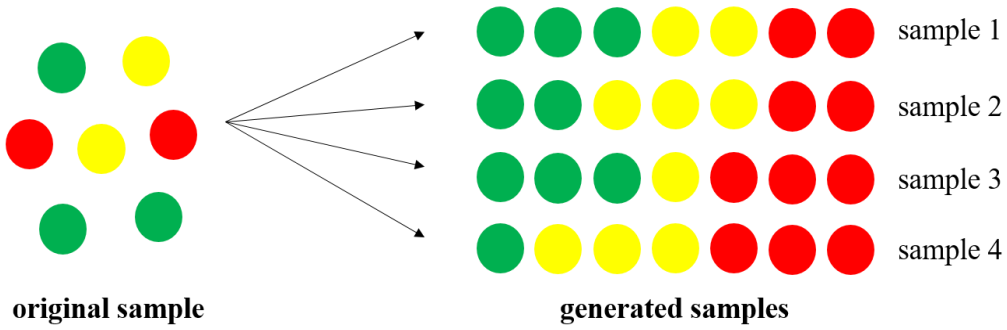

Figure 5.10. Visual illustration of the bootstrap sampling

Unlike the conventional bootstrap approach, where the generation of the bootstrap samples is conducted in a random manner, in this work all possible bootstrap samples generated from an available data is considered. This is feasible in our experiments due to the limited size of available sample generated from a limited number of experiments. For example, a previously defined three critical *CC* values representing the yellow-to-red boundary are 0.999, 0.9991, and 0.9989. Thus, by bootstrap sampling the given data set we will get 10 combinations of similar size samples as following:

1.	0.9990	0.9991	0.9989
2.	0.9990	0.9990	0.9990
3.	0.9990	0.9990	0.9991
4.	0.9990	0.9990	0.9989
5.	0.9990	0.9991	0.9991
6.	0.9990	0.9989	0.9989
7.	0.9991	0.9991	0.9991
8.	0.9991	0.9991	0.9989
9.	0.9991	0.9989	0.9989
10.	0.9989	0.9989	0.9989

Consider the application of the bootstrap sampling technique to the FRA data interpretation and classification of the transformer working condition. The pre-defined observations for two decision boundaries can be denoted as $n_{G|Y}$ (six green-to-yellow decision boundaries $B^{(k)}_{G|Y,l}$) and $n_{Y|R}$ (three yellow-to-red decision boundaries $B^{(k)}_{Y|R,l}$). Let $S^{(k)}_{G|Y}$ and $S^{(k)}_{Y|R}$ denote the sets of decision boundary observations for $B^{(k)}_{G|Y,l}$ and $B^{(k)}_{Y|R,l}$, accordingly:

$$S_{G|Y}^{(k)}=\left\{B_{G|Y,\,1}^{(k)},B_{G|Y,\,2}^{(k)},\ldots,\;\;B_{G|Y,\,n_{G|Y}}^{(k)}\right\} \tag{59}$$

$$S_{Y|R}^{(k)}=\left\{B_{Y|R,\,1}^{(k)},B_{Y|R,\,2}^{(k)},\ldots,\;\;B_{Y|R,\,n_{Y|R}}^{(k)}\right\} \tag{60}$$

where superscript k denotes the utilized statistical index, thus $k = 1, \ldots, N_{SI}$ and in this work N_{SI} =12. The mean of the decision boundaries is obtained as:

$$\overline{B}_{G|Y}^{(k)}=\frac{1}{n_{G|Y}}\sum_{l=1}^{n_{G|Y}}B_{G|Y,\,l}^{(k)} \tag{61}$$

$$\overline{B}_{Y|R}^{(k)}=\frac{1}{n_{Y|R}}\sum_{l=1}^{n_{G|Y}}B_{Y|R,\,l}^{(k)} \tag{62}$$

Bootstrap sampling the original set of the defined decision boundaries yields:

$$S_{G|Y}^{(k),\,i}=\left\{B_{G|Y,\,1}^{(k),\,i},B_{G|Y,\,2}^{(k),\,i},\ldots,\;\;B_{G|Y,\,n_{G|Y}}^{(k),\,i}\right\} \tag{63}$$

$$S_{Y|R}^{(k),\,j}=\left\{B_{Y|R,\,1}^{(k),\,j},B_{Y|R,\,2}^{(k),\,j},\ldots,B_{Y|R,\,n_{Y|R}}^{(k),\,j}\right\} \tag{64}$$

where $i = 1, \ldots, M_{G|Y}$ and $j = 1, \ldots, M_{Y|R}$. The values for $M_{G|Y}$ and $M_{Y|R}$ sets of generated green-to-yellow and yellow-to-red decision boundaries are estimated via:

$$M_{G|Y}=\binom{2n_{G|Y}\text{-}1}{n_{G|Y}}=\frac{(2n_{G|Y}\text{-}1)!}{(n_{G|Y}\text{-}1)!n_{G|Y}!} \tag{65}$$

$$M_{Y|R}=\binom{2n_{Y|R}\text{-}1}{n_{Y|R}} \tag{66}$$

In this research work, six values for green-to-yellow and three values for yellow-to-green decision boundaries are defined for 12 SIs, resulting in 6×3 = 18 pairs of decision boundaries. Therefore, having the original values for $n_{G|Y}$ = 6 (six green-to-yellow decision boundaries $B_{G|Y,l}^{(k)}$) and $n_{Y|R}$ = 3 (three yellow-to-red decision boundaries $B_{Y|R,l}^{(k)}$) applied to (65) and (66), $M_{G|Y}$ = 462 and $M_{Y|R}$ = 10 sets of bootstrap samples are obtained. The illustration of the generated decision boundaries is provided in Figure 5.11 [181] ©2022 IEEE. Hence, after applying the bootstrap sampling, 4620 boundary pairs are generated instead of original 18 pairs, justifying that this approach will be effective in case of the limited experimental measurements.

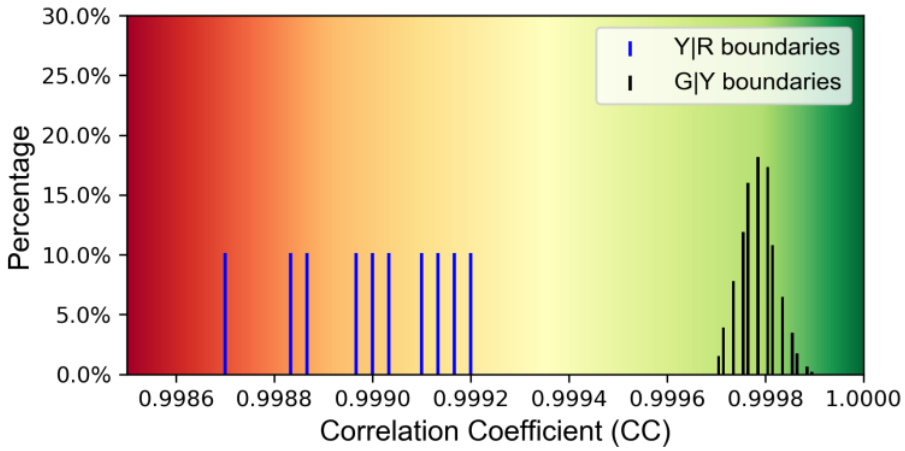

Figure 5.11. Decision boundaries for *CC* obtained with bootstrap sampling

Similar to (61) and (62) the averages of the decision boundary observations for each indicator can be obtained for extended set as:

$$\overline{B}_{G|Y}^{(k),\,i} = \frac{1}{n_{G|Y}} \sum_{l=1}^{n_{G|Y}} B_{G|Y,\,l}^{(k),\,i}, \text{ where } i = 1, \ldots, 462 \tag{67}$$

$$\overline{B}_{Y|R}^{(k),\,j} = \frac{1}{n_{Y|R}} \sum_{l=1}^{n_{G|Y}} B_{Y|R,\,l}^{(k),\,j}, \text{ where } j = 1, \ldots, 10 \tag{68}$$

Thus, the overall set of decision boundaries for all 12 SIs can be represented in the following matrix forms:

$$\overline{\boldsymbol{B}}_{\boldsymbol{G|Y}} = \begin{bmatrix} \overline{B}_{G|Y}^{(1),\,1} & \overline{B}_{G|Y}^{(1),\,2} & \cdots & \overline{B}_{G|Y}^{(1),\,M_{G|Y}} \\ \overline{B}_{G|Y}^{(2),\,1} & \overline{B}_{G|Y}^{(2),\,2} & \cdots & \overline{B}_{G|Y}^{(2),\,M_{G|Y}} \\ \vdots & \vdots & \ddots & \vdots \\ \overline{B}_{G|Y}^{(N_{SI}),\,1} & \overline{B}_{G|Y}^{(N_{SI}),2} & \cdots & \overline{B}_{G|Y}^{(N_{SI}),\,M_{G|Y}} \end{bmatrix}_{N_{SI} \times M_{G|Y}} \tag{69}$$

$$\overline{\boldsymbol{B}}_{\boldsymbol{Y|R}} = \begin{bmatrix} \overline{B}_{Y|R}^{(1),\,1} & \overline{B}_{Y|R}^{(1),\,2} & \cdots & \overline{B}_{Y|R}^{(1),\,M_{Y|R}} \\ \overline{B}_{Y|R}^{(2),\,1} & \overline{B}_{Y|R}^{(2),\,2} & \cdots & \overline{B}_{Y|R}^{(2),\,M_{Y|R}} \\ \vdots & \vdots & \ddots & \vdots \\ \overline{B}_{Y|R}^{(N_{SI}),\,1} & \overline{B}_{Y|R}^{(N_{SI}),2} & \cdots & \overline{B}_{Y|R}^{(N_{SI}),\,M_{Y|R}} \end{bmatrix}_{N_{SI} \times M_{Y|R}} \tag{70}$$

Finally, the generated set of boundaries and 4620 decision pairs are further applied to classification and confidence level estimation. This process is identical to bolstered method discussed in Sub-section 5.4.1, where the given test observation is compared

towards the defined decision pairs. In this case, the obtained 4620 decision pairs are employed to calculate the confidence level of a specific label (green, yellow, and red zone) corresponding to each SI. The probability of the test observation belonging to label l is denoted as $C_l^{(k)}$ (where k indicates the specific SI) is defined as the ratio of this label l to all labels for the given index k. As an example, consider that for the index $k = CC$, 3000 out of 4620 decision pairs report the red (critical) class. Hence, the probability (confidence level) of this test observation belonging to yellow zone is $C_{red}^{(CC)} = (3000/4620)\times 100\% = 65\%$. It should be taken into account, that in this work, the collective decision of 12 SIs is estimated and the final decision regarding the condition of the test object is based on the label with the highest cumulative confidence of all indices. The overall confidence level denoted C_l is estimated via summing the $C_l^{(k)}$ (confidence of indices $k = 1, \ldots, N_{SI}$ to belong to certain class l) and normalizing it. To sum up, the interpretation and classification procedure can be summarized into the following steps which are implemented in the algorithm provided further:

1. The FRA measurement of the given scenario is conducted
2. The 12 SIs are estimated based on the acquired frequency response and the fingerprint signature
3. The decision boundaries are generated using (63)-(70)
4. SI-based probabilities $C_l^{(k)}$ for each label l are estimated using boundaries defined in (69) and (70)
5. The cumulative decision for each label l is defined via summation of the SI-based confidences and normalization
6. The working condition of the test object is classified according to the label l with the highest confidence C_l.

---

for $j = 1$ to N_{SI} **do** N_{SI} – number of all SIs ($N_{SI} = 12$)
  select SI-specific test observation, $x^{(j)}$
  initialize counters, $Q_l = 0$ $l \in$ {green, yellow, red}
  for $i = 1$ to $M_{Y|R}$ **do** $M_{Y|R} = 10$
    select yellow-to-red boundary, $\overline{B}_{Y|R}^{(j),i}$
    for $k = 1$ to $M_{G|Y}$ $M_{G|Y} = 462$
    do

select green-to-yellow boundary, $\overline{B}_{G|Y}^{(j),k}$

if ($j = CC$ **or** $j = \rho$) **and** ($\overline{B}_{G|Y}^{(j),k} > \overline{B}_{Y|R}^{(j),i}$) **then**

classify $x^{(j)}$ based on $\overline{B}_{G|Y}^{(j),k}$ and $\overline{B}_{Y|R}^{(j),i}$, $\hat{y}(x^{(j)})$

if $\hat{y}(x^{(j)}) = l$ **then**

increment Q_l

end if

end if

elseif (j != CC **and** j != ρ) **and** ($\overline{B}_{G|Y}^{(j),k} < \overline{B}_{Y|R}^{(j),i}$) **then**

classify $x^{(j)}$ based on $\overline{B}_{G|Y}^{(j),k}$ and $\overline{B}_{Y|R}^{(j),i}$, $\hat{y}(x^{(j)})$

if $\hat{y}(x^{(j)}) = l$ **then**

increment Q_l

end if

end elseif

end for

end for

$C_l^{(j)} = (Q_l / (M_{Y|R} \times M_{G|Y})) \times 100\%$

end for

$C_l = \sum_j C_l^{(j)} / N_{SI}$

assign label, $\hat{l} = \underset{l}{argmax}\ \{C_l\}$

Notations:

N_{SI}	– number of all SIs (N_{SI} = 12)
$x^{(j)}$	– SI-specific test observation for indicator j
l	– label, $l \in$ {green, yellow, red}
$M_{Y\|R}$	– all combinations of yellow-to-red boundaries ($M_{Y\|R}$ = 10)
$M_{G\|Y}$	– all combinations of green-to-yellow boundaries ($M_{G\|Y}$ = 462)
$\overline{B}_{G\|Y}^{(j),k}$	– k-th SI-specific observation of $\overline{\boldsymbol{B}}_{\boldsymbol{G\|Y}}$ for indicator j
$\overline{B}_{Y\|R}^{(j),i}$	– i-th SI-specific observation of $\overline{\boldsymbol{B}}_{\boldsymbol{Y\|R}}$ for indicator j
$\hat{y}(x^{(j)})$	– estimated label of $x^{(j)}$ for indicator j
$C_l^{(j)}$	– SI-specific CL of indicator j for class l
C_l	– cumulative CL for class l

CHAPTER 6. SIMULATION AND PRACTICAL RESULTS, ANALYSIS AND DISCUSSION

6.1 Introduction

This Chapter presents the practical results of the introduced FRA results interpretation method and it is structured in the following manner: in Section 6.2 three cases with different predefined levels of the winding short-circuit are investigated using the proposed FRA interpretation and classification technique. In Section 6.3 the introduced method is applied to define and classify the working condition of the winding undergoing different types of the winding mechanical deformation and displacement.

For all fault types (short-circuit, deformation and displacement) the test setup is classified among the green, yellow, and red operating zones and the corresponding confidence levels are identified. The discussion of the obtained results and comparison with conventional methods are conducted in Section 6.4.

6.2 Case studies: Winding short-circuit

In this section, the classification of the transformer working condition and its confidence level are reported using the bootstrap resampling method discussed in Sub-section 5.4.2. In this regard, two dry-type distribution transformers (see Figure 6.1(a)-(b) [20] ©2021 IEEE) and one oil-filled power transformer (see Figure 6.1(c)) are exposed to the short-circuit fault via parallel placing the rheostat to winding terminals. Transformers are exposed to different levels of the winding short-circuit fault by varying the rheostat value in accordance to the size of the test object and its total winding impedance.

(a) (b) (c)

Figure 6.1. Equipment and test objects: (a) FRA analyzer and 1 kVA open-wounded transformer; (b) 20 kVA dry-type transformer; (c) 40 MVA oil-filled transformer

6.2.1 Case 1: 1 kVA distribution transformer

In the first practical case study, a single-phase 1 kVA distribution transformer is utilized. The 110 V tap changer terminals of the transformer are paralleled with 3 kΩ rheostat. The FRA signatures of healthy condition and short-circuit scenario are presented in Figure 6.2. It is observed, that around first anti-resonant peak at 10 kHz the frequency response expectedly flattens, which is the result of the winding short-circuit. Transfer function magnitude is increased by nearly 7 dB at first anti-resonance point. In compliance with IEC 60076-18 Standard [38], the mid-frequency band (2 kHz – 20 kHz) is mostly influenced, which corresponds to the inter-winding fault. Moreover, higher frequencies (20 kHz – 1 MHz) are not influenced by short-circuit fault according to the FRA signatures presented in Figure 6.2 [181] ©2022 IEEE.

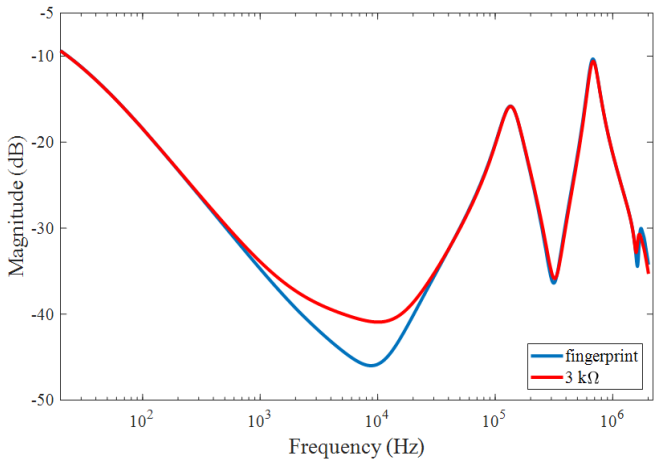

Figure 6.2. FRA signatures for intact case and short-circuit scenario of 110 V tap in parallel with 3 kΩ rheostat

The obtained FRA signatures were used to estimate the corresponding SIs and results were used to classify the given scenario based on pre-defined decision boundaries. Figure 6.3 [181] ©2022 IEEE demonstrates the pre-defined boundaries and the value of *CC* estimated for the given scenario, which is equal to 0.9990. It is observed that the current test observation lies on the distribution of the yellow-to-red boundaries, where 40% confidence corresponds to the yellow zone, whereas remaining 60% is in the red zone.

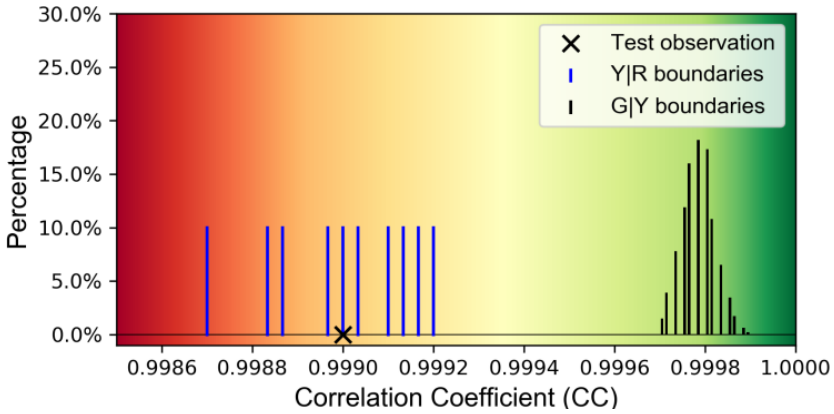

Figure 6.3. *CC*-specific decision boundaries and given test observation for Case Study 1

The SI-based confidence levels are estimated for each operating zone and are presented in Table 13 [181] ©2022 IEEE. It is remarkable, that the cumulative decision of

12 SIs is 0%, 52.5%, and 47.5% for the test object to be in green, yellow, and red working conditions, respectively. Hence, a 1 kVA transformer with 3 kΩ resistance in parallel to 110 V tap terminals is ultimately classified to belong to the yellow (suspicious) zone.

Table 13 – Classification results and SI-based CLs for Case study 1

SI	Value	Confidence Levels (%)		
		Green	Yellow	Red
CC	0.9990	0	40	60
SD	1.8647	0	90	10
SSE	3.4736	0	80	20
ASLE	0.2460	0	50	50
DABS	1.0829	0	60	40
RMSE	0.0619	0	100	0
ED	58.196	0	80	20
CSD	1.6068	0	0	100
MM	1.0372	0	40	60
SSRE	0.0019	0	0	100
SSMMRE	0.0019	0	0	100
p	0.9997	0	90	10
Cumulative		**0**	**52.5**	**47.5**
Assigned Label			**Yellow**	

6.2.2 Case 2: 20 kVA distribution transformer

The second case study examines the 20 kVA three-phase dry-type distribution transformer. The 400 V tap terminals are paralleled with 5 kΩ resistance. The FRA reference signature and this fault scenario are depicted in Figure 6.4 [181] ©2022 IEEE, where it is noted, that similar to previous case study, the frequency response flattens around the first anti-resonance at 4 kHz–80 kHz band, resulting in magnitude increase by 3 dB. Moreover, it is observed that around 130 kHz (second anti-resonant point) the magnitude of the transfer function slightly increased by 1 dB.

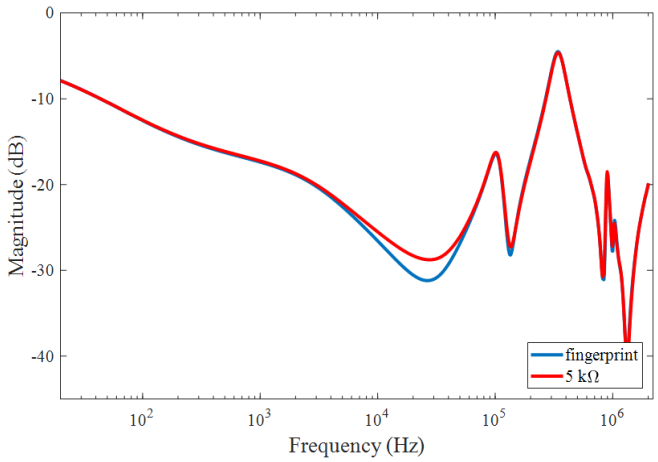

Figure 6.4. FRA signatures for intact case and short-circuit scenario of 4000 V tap in parallel with 5 kΩ rheostat

The visual representation of the pre-defined boundaries in Figure 6.5 [181] ©2022 IEEE and the estimated *CC* value (0.9996) demonstrate that the given short-circuit scenario does not belong to any boundary, neither green-to-yellow, nor yellow-to-red zone, but rather mostly corresponds to the yellow (suspicious) zone.

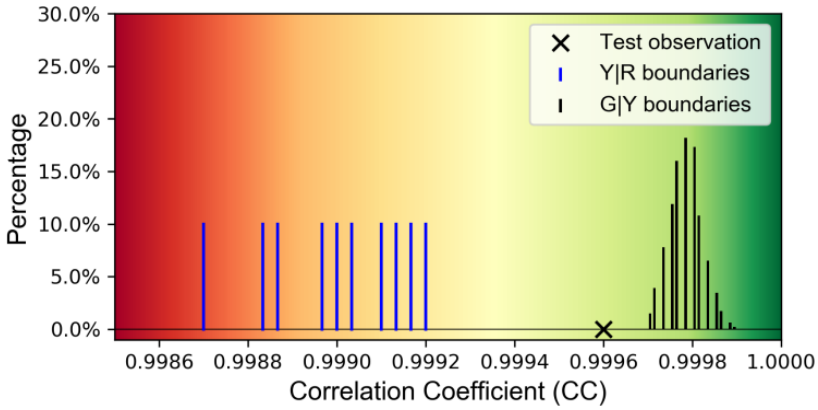

Figure 6.5. *CC*-specific boundaries and given test observation for Case Study 2

The classification results and confidence levels associated with them are also estimated for other indicators and are provided in Table 14 below [181] ©2022 IEEE. The collective decision of 12 indicators reports 18.8%, 75.4%, and 5.8% confidence that this scenario corresponds to the green, yellow, and red working zones, respectively. Therefore, a scenario of 20 kVA transformer with 5 kΩ resistance in parallel to 400 V tap terminals is

ultimately classified to belong to the yellow zone, which is the suspicious working condition.

Table 14 – Classification results and SI-based CLs for Case study 2

SI	Value	Confidence Levels (%)		
		Green	Yellow	Red
CC	0.9996	0	100	0
SD	0.5629	92.21	7.79	0
SSE	0.6191	39.18	60.82	0
ASLE	0.1642	0	100	0
DABS	0.4616	18.40	81.60	0
RMSE	0.0386	0	100	0
ED	24.570	31.17	68.83	0
CSD	0.6875	31.60	68.40	0
MM	1.0231	0	100	0
SSRE	0.0008	0	60	40
SSMMRE	0.0008	0	70.02	29.98
p	0.9999	13.20	86.80	0
Cumulative		**18.8**	**75.4**	**5.8**
Assigned Label		**Yellow**		

6.2.3 Case 3: 40 MVA power transformer

In the third case study, a three-phase oil-filled power distribution transformer with 40 MVA power rating is used. The short-circuit fault is emulated via connecting 500 kΩ rheostat in parallel with 33 kV tap terminals. The corresponding FRA measurements of the given setup and fingerprint spectra are presented in Figure 6.6 and the effect of the fault is observed in terms of the significant flattening of the spectrum in the frequency range of 20 Hz – 3 kHz. Similarly, frequency response magnitude is increased by 40 dB at first anti-resonance point, which occurred at 500 Hz (see Figure 6.6 [181] ©2022 IEEE).

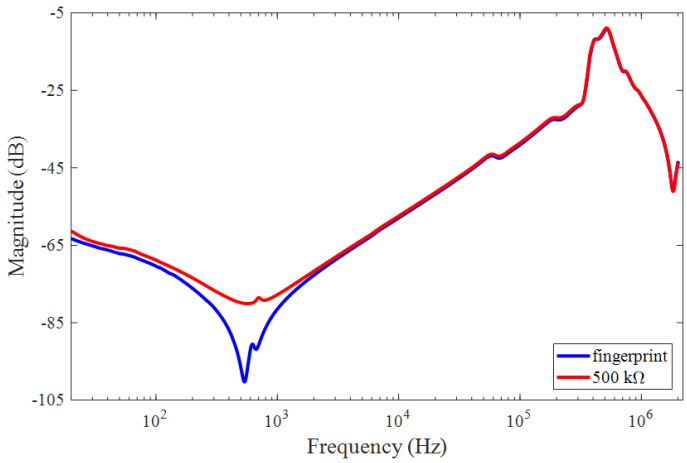

Figure 6.6. FRA signatures for intact case and short-circuit scenario of 33 kV tap in parallel with 500 kΩ rheostat

The SIs values for the given short-circuit scenario were estimated from the FRA measurements and compared towards the pre-defined critical SI values, representing each boundary. In Figure 6.7 [181] ©2022 IEEE the allocation of the computed *CC* value (0.9987) over the distribution of the boundary values is presented. It is observed that the given *CC* value lies in the upper limit of the yellow-to-red boundary, which is numerically reported in 100% confidence level of the given observation being in the red zone.

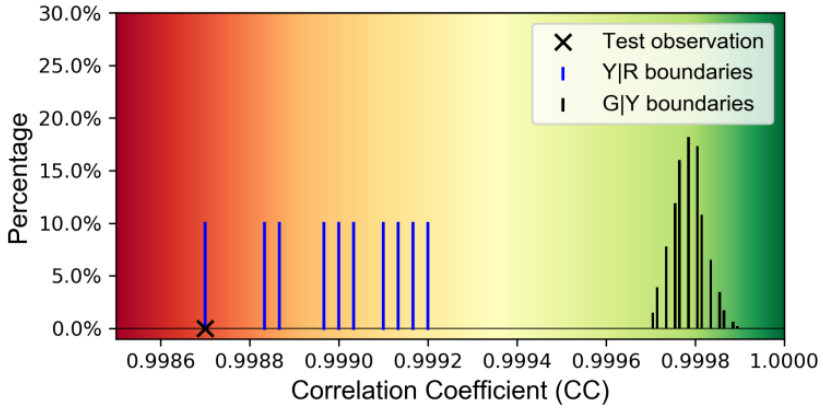

Figure 6.7. *CC*-specific decision boundaries and given test observation for Case Study 3

The SI-based confidence levels are estimated for each operating zone and are presented in Table 15 [181] ©2022 IEEE. The results report 0%, 15.0%, and 85.0%

collective confidence levels for green, yellow, and red zones, respectively. Therefore, a 40 MVA transformer with 500 kΩ resistance in parallel to 33 kV tap terminals is ultimately classified to belong to the red (critical) working zone.

Table 15 – Classification results and SI-based CLs for Case study 3

SI	Value	Confidence Levels (%)		
		Green	Yellow	Red
CC	0.9987	0	0	100
SD	3.7794	0	0	100
SSE	14.269	0	0	100
ASLE	0.2224	0	70	30
DABS	1.8247	0	0	100
RMSE	0.0686	0	50	50
ED	117.95	0	0	100
CSD	3.3138	0	0	100
MM	1.0870	0	0	100
SSRE	0.0018	0	0	100
SSMMRE	0.0018	0	0	100
p	0.9996	0	60	40
Cumulative		**0**	**15.0**	**85.0**
Assigned Label			**Red**	

It is noteworthy, that the FRA test report comprised of transformer working mode classification and corresponding confidence levels reported to the technical maintenance personnel will significantly improve the conventional diagnostic and decision making process.

6.3 Case studies: Mechanical deformation

In this section, the classification of the transformer working condition and its confidence level is reported using the bolstered error estimation method discussed in Section 5.4. For that, the winding software model developed and validated in Section 4.3 is used. The configuration of the FRA measurement is based on the standardized end-to-end open-circuit test with 20 $V_{p\text{-}p}$ sinusoidal input signal swept from 20 Hz to 10 MHz as illustrated in Figure 6.8 [182] ©2021 IEEE. Since the size of the test object is considerably small, the upper boundary of the frequency is increased as per recommendation by FRA standard.

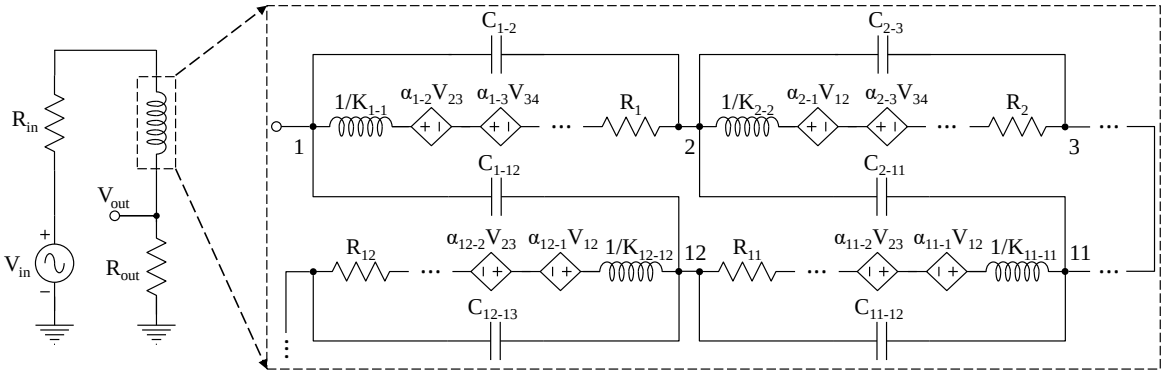

Figure 6.8. Illustration of the FRA measurement over the winding software model

6.3.1 Case 1: Disk space variation (DSV) fault

The winding axial deformation, namely, the disk space variation (DSV) is analyzed in the first practical study, during which the upper disk of the winding structure is displaced upwards along the main winding axis, so that the separation distance between intact and the displaced disks is ¼ of the wire diameter D_w. The altered lumped parameters of the winding RLC model are estimated based on the approach discussed in Chapter 4, Section 4.4, and Sub-section 4.4.1. The frequency responses of the intact and fault condition are illustrated in Figure 6.9. Unlike short-circuit fault which led to flattening of the curve at first ant-resonance frequency and deviation of the transfer function magnitude, mechanical deformation is mostly observed in terms of anti-resonant and resonant peaks' shift along the spectrum towards high frequency range. To be specific, in the result of the DSV fault, the first anti-resonance frequency displaced from 3.041 MHz to 3.048 MHz, which is influenced by decrease of the winding equivalent self-inductance. The frequency shift is not quite significant; however, the relatively low extent of the axial displacement should also be taken into consideration. Nevertheless, Figure 6.9 clearly displays the response of the FRA signature to the introduced fault.

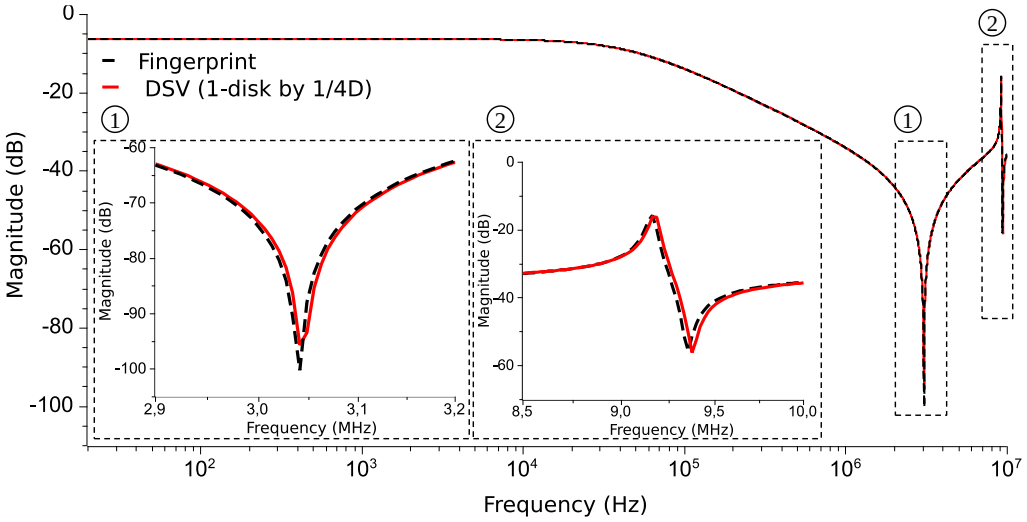

Figure 6.9. The FRA signatures of intact and DSV fault scenario

Figure 6.10 displays the Gaussian kernel and corresponding CLs for the *CC* value estimated from the obtained FRA data. It is clear, that the kernel mass of the current observation where *CC* = 0.99945 mostly lies in the yellow (suspicious) zone with 99.83% confidence; whereas remaining 0.17% confidence corresponds to the green (healthy) zone.

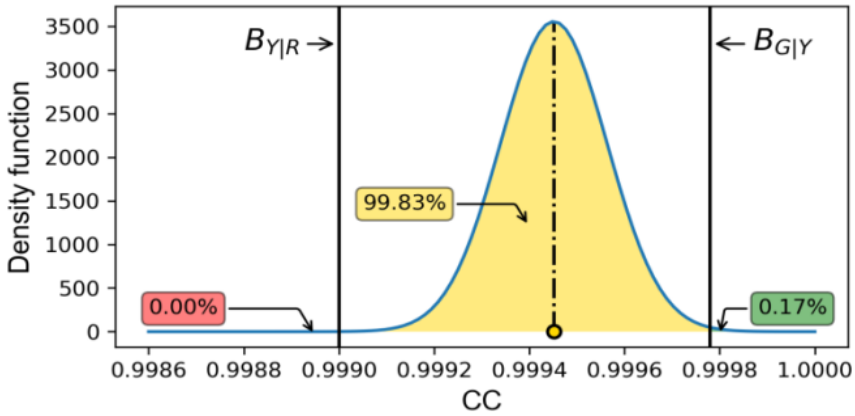

Figure 6.10. The *CC*-specific confidence levels for Case Study 1 (*CC* = 0.99945)

The collective decision of all 12 indicators should be taken into consideration. The SIs estimated for the given scenario, their respective classification results and confidence levels are summarized in Table 16. In particular, the green, yellow, and red zones are allocated with 50.82%, 47.11%, and 2.06% overall confidence, accordingly. Thus, the ultimate assigned label for the given fault condition is the green (healthy) working mode.

The class label is given based on majority vote of SIs, whereas the confidence percentage is estimated via averaging the reported CLs.

Table 16 – Classification results for Case study 1

SI	SI value	Classification result	Confidence (%)		
			Green	Yellow	Red
CC	0.99945	yellow	0.17	99.83	0
SD	0.67043	green	65.68	34.32	0
SSE	0.44940	green	91.73	8.27	0
ASLE	0.01944	green	100	0	0
DABS	0.09012	green	100	0	0
RMSE	0.04586	yellow	1.22	98.70	0.08
ED	50.6122	yellow	0	99.79	0.21
CSD	0.67021	yellow	23.57	76.43	0.00
MM	1.02585	yellow	22.31	53.24	24.45
SSRE	0.00007	green	100	0	0
SSMMRE	0.00006	green	100	0	0
ρ	0.99979	yellow	5.22	94.78	0
Overall		**green**	**50.82**	47.11	2.06

6.3.2 Case 2: Radial displacement fault

Winding radial deformation is investigated in this study. To be specific, the upper disk of the winding is shifted along the radius of the winding structure by the distance equivalent to one wire diameter D_w. The affected lumped parameters of the winding RLC model are re-evaluated based on the methodology discussed in Sub-section 4.4.2. The frequency responses of the intact and fault condition are illustrated in Figure 6.11 below. It is noted, that the first anti-resonant peak is shifted towards lower frequencies from 3.02 MHz to 2.92 MHz. On the contrary, high frequency resonance and anti-resonance peaks shifted to higher frequencies from 9 MHz up to 9.5 MHz. Moreover, the radial displacement triggered new resonating peaks at approximately 6.5 MHz.

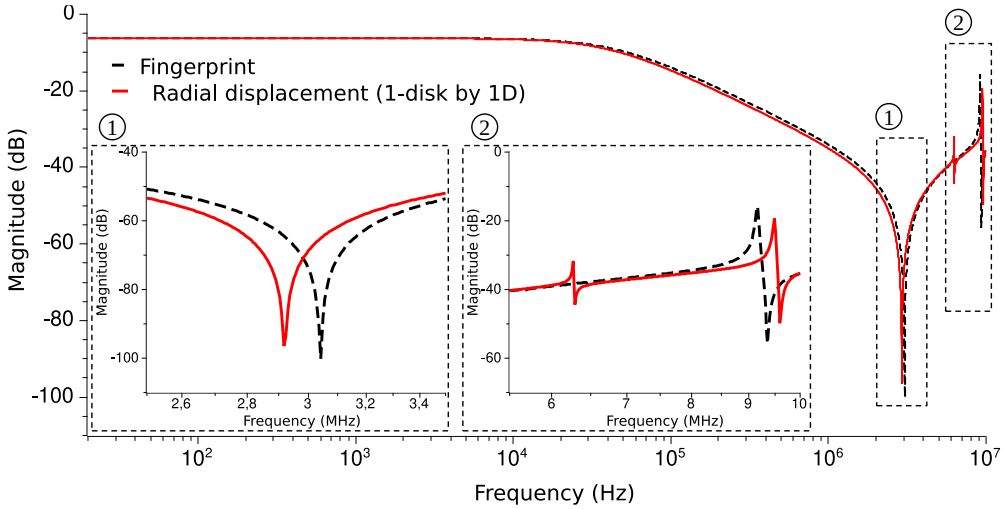

Figure 6.11. The FRA signatures of intact and radial displacement scenario

Figure 6.12 displays the Gaussian kernel and corresponding CLs for the *CC* value estimated from the obtained FRA data. It is clear, that the kernel mass of the current observation where *CC* = 0.99745 lies in the red zone, hence *CC* reports 100% confidence of belonging to the critical working mode.

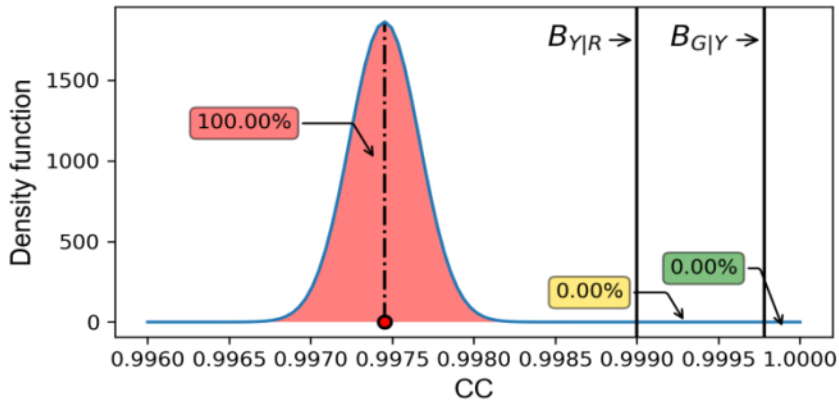

Figure 6.12. The *CC*-specific confidence levels for Case Study 2 (*CC* = 0.99745)

The estimated SIs and their respective classification results are reported in Table 17, demonstrating overall 37.07% and 63.93% confidence of belonging to yellow (suspicious) and red (critical) operating modes, accordingly. Thus, based on the majority vote of the statistical indices' results, the given radial displacement scenario is considered to relate to the critical working condition.

Table 17 – Classification results for Case study 2

SI	SI value	Classification result	Confidence (%)		
			Green	Yellow	Red
CC	0.99745	red	0	0	100
SD	1.52106	yellow	0	100	0
SSE	2.31321	yellow	0	100	0
ASLE	0.18216	yellow	0	100	0
DABS	0.51154	yellow	0	100	0
RMSE	0.10404	red	0	0	100
ED	114.8273	red	0	0	100
CSD	1.48460	red	0	0	100
MM	1.10207	red	0	0	100
SSRE	0.00111	red	0.01	14.18	85.81
SSMMRE	0.00096	red	0	30.70	69.30
ρ	0.99901	red	0	0	100
Overall		**red**	0.00	37.07	**62.93**

6.3.3 Case 3: Disk tilting fault

In this practical study, winding disk tilting is emulated and proposed classification method is examined. In particular, the upper disk of the winding is tilted upwards so that the angle between tilted and intact disks planes is 1.16º. This angle corresponds to the scenario where one end of the upper disk is still touching the lower disk, whereas the other end of the disk is separated from the lower disk by 1 wire distance D_w. The affected lumped parameters of the winding RLC model are evaluated based on the methodology discussed in Sub-section 4.4.3. The frequency responses of the intact and fault condition are illustrated in Figure 6.13. Unlike radial deformation, in the result of the tilting fault, the first anti-resonant peak is slightly shifted towards higher frequencies from 3.02 MHz to 3.08 MHz. In addition, high frequency resonance and anti-resonance peaks also dislocated towards higher frequencies at around 9 MHz.

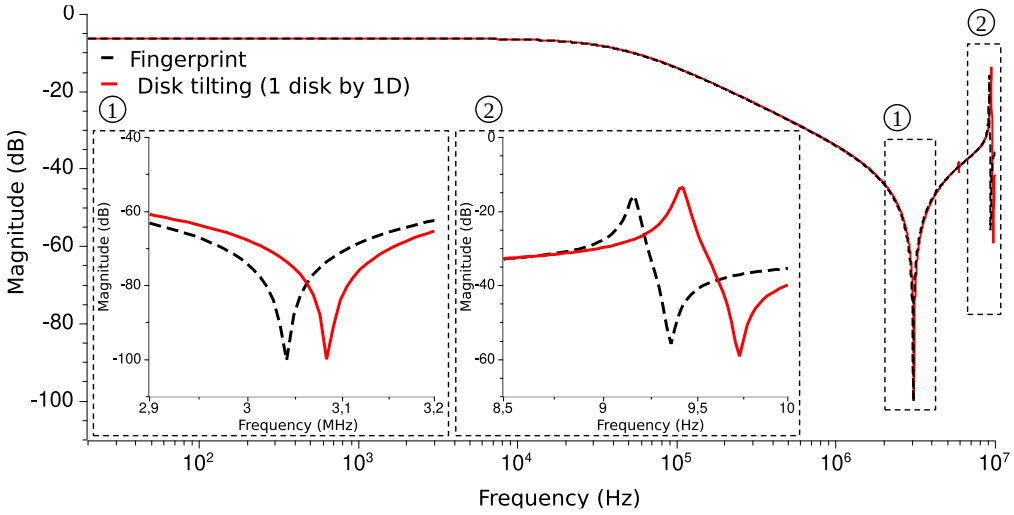

Figure 6.13. The FRA signatures of intact and disk tilting scenario

Figure 6.14 depicts the Gaussian kernel and the current observation of *CC* value. It is observed that the kernel of *CC* = 0.99915 covers both yellow and red zones, with majority of the mass belonging to yellow zone (90.86%).

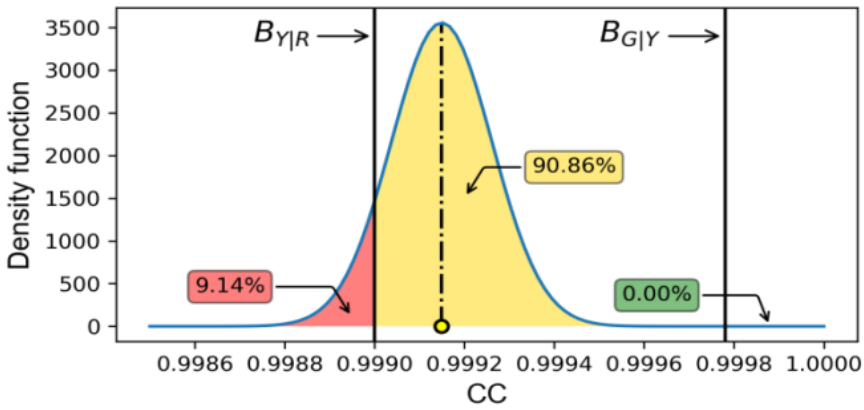

Figure 6.14. The *CC*-specific confidence levels for Case Study 3 (*CC* = 0.99915)

Table 18 presents the classification results of all SIs retrieved from the frequency response spectra. It is noted, that four out of 12 SIs report healthy mode with overall 34.23% confidence, seven SIs report suspicious condition with 57.72% gross confidence, and single SI reports the critical condition leading to 8.05% confidence. Hence, the final decision regarding the examined tilted winding will be yellow zone. Although it is vital, that all three confidence levels are

reported to the operator, so that the issue of whether to return the test object back to service or send it for further diagnosis is resolved based on full data.

Table 18 – Classification results for Case study 3

SI	SI value	Classification result	Confidence (%)		
			Green	Yellow	Red
CC	0.99915	yellow	0	90.86	9.14
SD	0.83514	yellow	0.05	99.95	0
SSE	0.69734	yellow	10.67	89.33	0
ASLE	0.03310	green	100	0	0
DABS	0.13488	green	100	0	0
RMSE	0.05712	yellow	0.01	95.41	4.58
ED	63.04624	yellow	0	75.5	24.5
CSD	0.83426	yellow	0	100	0
MM	1.03622	red	0	42.47	57.53
SSRE	0.00013	green	100	0	0
SSMMRE	0.00011	green	100	0	0
ρ	0.99967	yellow	0.05	99.09	0.86
Overall		**yellow**	34.23	**57.72**	8.05

6.4 Discussion

In this work, conventional and advanced methodologies for transformer condition monitoring and diagnosis were investigated. Specifically, basic concept of the transfer function method (FRA), up-to-date standards and interpretation techniques were discussed emphasizing their advantages and challenges. In this regard, a new approach based on statistical analysis and machine learning tools (bolstered error estimation and bootstrap sampling) for automated and quantitative interpretation of the FRA data was introduced in this thesis. The proposed method was examined on different test objects such as fabricated winding, distribution and power transformers with different power rating and type.

To estimate the efficiency of the introduced method, here its performance with other methods proposed in literature and standards is compared. Four alternative techniques utilizing statistical analysis for FRA interpretation were applied to three case studies with pre-defined short-circuit scenario. The summary of the results is presented in Table 19 [181]

Simulation and Practical Results, Analysis and Discussion

It is observed, that Nirgude et al. [168] employed three SIs to classify the test observation (*CC*, *SD*, and *ASLE*) and their results contradict among all case studies. On the other hand, Tahir et al. [179] used *CCF* and reported "good" condition for all scenarios. Similarly, the NCEPRI [160] method using the relative factor E_{XY} classified all cases as "normal". The Chinese Standard DL/T911-2004 [19] which applies statistical analysis to three sub-bands separately reported "gentle deformation" for the Case Study 1, and "normal winding" for Case Studies 2 and 3.

Table 19 – Comparison of the introduced technique with FRA interpretation state-of-the-art

Case study		Proposed method	Nirgude et al. [168]			Tahir et al. [179]	DL/T911-2004 [19]	NCEPRI [160]
№1	**Label**	Suspicious	Critical CC = 0.9990	Critical SD = 1.8647	Normal $ASLE$ = 0.2460	Good CCF = 0.9934	Gentle deformation R_{LF} = 1.94, R_{MF} = 2.21, R_{HF} = 1.20	Normal E_{XY} = 1.57
	CLs	52.5% yellow 47.5% red	–	–	–	–	–	–
№2	**Label**	Suspicious	Critical CC = 0.9996	Normal SD = 0.5269	Normal $ASLE$ = 0.1642	Good CCF = 0.9964	Normal R_{LF} = 2.61, R_{MF} = 3.04, R_{HF} = 2.37	Normal E_{XY} = 1.21
	CLs	75.4% yellow 18.8% green 5.8% red	-	-	-	-	-	-
№3	**Label**	Critical	Critical CC = 0.9987	Critical SD = 3.7794	Normal $ASLE$ = 0.2460	Good CCF = 0.2224	Normal R_{LF} = 3.16, R_{MF} = 4.01, R_{HF} = 4.23	Normal E_{XY} = 0.44
	CLs	85.0% red 15.0% yellow	–	–	–	–	–	–

However, it should be noted, that each of these methods have its certain limitations in terms of the transformer power rating and frequency spectrum of the injected signal. For example, the DL/T911-2004 Standard [19] measures the system frequency response between 1 kHz and 1 MHz and NCEPRI [160] analyzes the transfer function from 10 kHz up to 700 kHz range, thus overlooking the lower and higher frequencies. Although the abovementioned techniques propose a quantitative interpretation of the FRA data, they have practical limitations that might result in significant data loss. Moreover, since SI-based decisions for the same condition may contradict, the necessity of the confidence level reporting proves its validity and importance. The results of any maintenance and diagnostic test are quite important and should facilitate the effective decision-making process

Simulation and Practical Results, Analysis and Discussion

The overall concept of the introduced method is to classify the test object among three operating zones (green-healthy, yellow-suspicious, and red-critical) and report the confidence levels corresponding to all three zones. The proposed method was applied to test objects undergoing winding short-circuit fault and mechanical deformation, which are some of the most frequent fault types occurring in transformer active part. Moreover, practical case studies were conducted both in laboratory and simulation medium. The short-circuit fault was emulated via installing rheostat in parallel to winding terminals, thus provided the opportunity to control the severity of the fault. Winding RLC model in SPICE environment is developed over the fabricated winding and facilitated emulation of the three types of winding deformation, namely, axial, radial, and tilting (combination of axial and radial forces).

The obtained results reported classification of the transformer and winding prototype exposed to different faults along with decision confidence levels. This sort of comprehensive report, in turn, has a significant practical advantage because it can potentially facilitate well-informed decisions regarding transformer under the test for on-site technicians.

CHAPTER 7. CONCLUSIONS AND FUTURE WORK

7.1 Conclusions

Qualified transformer diagnostic works to maintain its electrical and mechanical integrity are among the highest priorities for utility stakeholders. Over the past decades, different transformer condition testing techniques have been developed, among which a transfer function method, namely, the Frequency Response Analysis (FRA), is known as the most accurate, widely accepted and the least invasive method. Other than that, FRA is capable of detecting a wide range of transformer internal faults, such as core problems, connection failure, winding structure deviations, etc. Despite the fact that FRA is quite a mature method with well-developed standards and solid background, understanding and interpretation of the FRA results requires further research and improvement. Therefore, different advanced techniques borrowed from machine learning, statistical analysis, image processing, and system modelling are being actively integrated with FRA results interpretation.

Transformer diagnostic state-of-the-art techniques, major internal and external fault triggering factors, FRA concept, measurement setup configurations, standards and interpretation techniques were discussed. Advantages and challenges of conventional and advanced interpretation methods were emphasized. A new approach combining machine learning tools and statistical analysis was introduced in this research. In particular, bolstered error estimation and bootstrap sampling techniques were used to classify the working condition of the transformer under the test, while 12 statistical indicators were utilized as the classification criteria. The critical values of indices representing decision boundaries were obtained via emulation of the winding short-circuit fault, where the variable resistance rheostat was installed in parallel with winding terminals. The established green-to-yellow (healthy-to-suspicious) and yellow-to-red (suspicious-to-critical) decision boundaries were applied to different severity levels of the winding short-circuit and mechanical deformation. Other than that, proposed interpretation method was assessed on the winding software RLC model based on the fabricated air-core winding.

The obtained classification results were compared with the conventional methods available in the literature and standards.

Machine learning and statistical-based real-life diagnosis and forecasting will, in turn, facilitate isolation of the transformer unit from the grid before it damages other equipment, ignites or even causes major power outages. Hence, expenses for repair works, component replacement, and work injury compensation will be significantly reduced. On the other hand, determination of the residual service lifespan and severity of the damage of the transformer is vital for planning maintenance and repair budget. This in turn will decrease an inexpedient use of financial resources and a cash outflow.

7.2 Future work

Based on the theoretical study and practical results, there are several topics that can be studied in the future.

7.2.1 On-line FRA

It is obviously beneficial to implement a continuous on-line diagnosis system, which will alert the grid operator about the changes in the transformer structure. This will, in turn, prevent the emergency situation on the power network and severe damage of components, which might lead to severe economic and environmental losses. The on-line FRA test will also eliminate the necessity to de-energize transformer from the grid. Nevertheless, implementation of the on-line FRA requires further research to resolve a number of challenges such as injection of the sweep signal, measuring the response signal, compensation circuit, mitigating the impact of external equipment and high voltage grid lines, etc. Stability of the power grid and loading should also be taken into consideration during on-line FRA measurements.

On the other hand, the merger of the real-time on-line FRA with the Supervisory Control and Data Acquisition (SCADA) network of the grid will give the opportunity to remotely isolate faulty transformer or reroute the power flow, hence reducing the necessity for direct operational and maintenance activities, which in turn will raise the safety of personnel and equipment. However, since electricity network is one of the most

strategically important facilities, the demand for cyber security of smart grid will most likely increase.

7.2.2 Three-phase winding RLC model

In this research work, a single-phase air-core winding was fabricated and its software model was created in SPICE environment. The detailed RLC model was, as the name suggest, based on the distributed parameters of the winding – resistance, inductance, and capacitance. The mutual coupling between turns and adjacent disks were taken into account by an analytical model. The winding software model was validated via practical FRA measurements of the physical winding and further used for axial and radial winding deformation. As the next step, it is reasonable to extend the created RLC model up to three-phase winding with the magnetic core. Obviously, the model will become significantly complicated in this case because the number of the distributed elements will dramatically increase and additional element in terms of the mutual coupling between core and the winding structure should be taken into consideration. Nevertheless, a comprehensive model of the two-winding single-phase or three-phase transformer will facilitate a detailed investigation of the winding mechanical deformation and displacement without having to physically implement the irreversible fault.

REFERENCES

[1] Laura DiDio, "The 2020 ITIC Global Reliability Survey shows the value of POWER9," 2020. Accessed on Nov. 20, 2021. [Online]. Available: https://techchannel.com/IT-Strategy/09/2020/increased-uptime-tco.

[2] J. Dai, H. Song, G. Sheng and X. Jiang, "Dissolved gas analysis of insulating oil for power transformer fault diagnosis with deep belief network," in *IEEE Transactions on Dielectrics and Electrical Insulation*, vol. 24, no. 5, pp. 2828-2835, Oct. 2017, doi: 10.1109/TDEI.2017.006727.

[3] J. Liu, Z. Zhao, C. Tang, C. Yao, C. Li and S. Islam, "Classifying Transformer Winding Deformation Fault Types and Degrees Using FRA Based on Support Vector Machine," in *IEEE Access*, vol. 7, pp. 112494-112504, 2019, doi: 10.1109/ACCESS.2019.2932497.

[4] M. Fischer, S. Tenbohlen, M. Schäfer and R. Haug, "Determining power transformers' sequence of maintenance and repair in power grids," *2010 IEEE International Symposium on Electrical Insulation*, 2010, pp. 1-6, doi: 10.1109/ELINSL.2010.5549785.

[5] U.S. Department of the Interior Bureau of Reclamation, "Transformers: Basics, Maintenance, and Diagnostics,", 2005. Accessed on Nov. 25, 2021. [Online]. Available: https://www.google.com/url?sa=t&rct=j&q=&esrc=s&source=web&cd=&ved=2ahUKEwiom-iOot70AhXNpIsKHTtaAdsQFnoECAIQAQ&url=https%3A%2F%2Fwww.usbr.gov%2Ftsc%2Ftechreferences%2Fmands%2Fmands-pdfs%2FTrnsfrmr.pdf&usg=AOvVaw216tJ2Sp3u96ncV0gWVYul.

[6] Office of Electricity Delivery and Energy Reliability, "Large Power Transformers and the U.S. Electric Grid, "U.S. Department of Energy, 2014. Accessed on Feb. 15, 2018. [Online]. Available: https://energy.gov/sites/prod/files/2014/04/f15/LPTStudyUpdate-040914.pdf.

[7] Jong-Wook Kim, ByungKoo Park, Seung Cheol Jeong, Sang Woo Kim and PooGyeon Park, "Fault diagnosis of a power transformer using an improved frequency-response analysis," in *IEEE Transactions on Power Delivery*, vol. 20, no. 1, pp. 169-178, Jan. 2005, doi: 10.1109/TPWRD.2004.835428.

[8] M. Bagheri, M. S. Naderi and T. Blackburn, "Advanced transformer winding deformation diagnosis: moving from off-line to on-line," in IEEE Transactions on Dielectrics and Electrical Insulation, vol. 19, no. 6, pp. 1860-1870, December 2012.

[9] N. Hashemnia, A. Abu-Siada and S. Islam, "Improved power transformer winding fault detection using FRA diagnostics – part 1: axial displacement simulation," in *IEEE Transactions on Dielectrics and Electrical Insulation*, vol. 22, no. 1, pp. 556-563, Feb. 2015, doi: 10.1109/TDEI.2014.004591.

[10] B. Cheng, Z. Wang and P. Crossley, "Using Lumped Element Equivalent Network Model to Derive Analytical Equations for Interpretation of Transformer Frequency

REFERENCES

Responses," in *IEEE Access*, vol. 8, pp. 179486-179496, 2020, doi: 10.1109/ACCESS.2020.3027798.

[11] J. C. Gonzales Arispe and E. E. Mombello, "Detection of Failures Within Transformers by FRA Using Multiresolution Decomposition," in *IEEE Transactions on Power Delivery*, vol. 29, no. 3, pp. 1127-1137, June 2014, doi: 10.1109/TPWRD.2014.2306674.

[12] E. P. Dick and C. C. Erven, "Transformer diagnostic testing by frequency response analysis", IEEE Trans. Power App. Syst., Vol. PAS-97, No. 6, pp. 2144–2153, 1978.

[13] A. Moradzadeh, K. Pourhossein, B. Mohammadi-Ivatloo and F. Mohammadi, "Locating Inter-Turn Faults in Transformer Windings Using Isometric Feature Mapping of Frequency Response Traces," in *IEEE Transactions on Industrial Informatics*, vol. 17, no. 10, pp. 6962-6970, Oct. 2021, doi: 10.1109/TII.2020.3016966.

[14] S. Wang, S. Wang, H. Feng, Z. Guo, S. Wang and H. Li, "A New Interpretation of FRA Results by Sensitivity Analysis Method of Two FRA Measurement Connection Ways," in *IEEE Transactions on Magnetics*, vol. 54, no. 3, pp. 1-4, March 2018, Art no. 8400204, doi: 10.1109/TMAG.2017.2743986.

[15] A. Abu-Siada, M. I. Mosaad, D. Kim and M. F. El-Naggar, "Estimating Power Transformer High Frequency Model Parameters Using Frequency Response Analysis," in *IEEE Transactions on Power Delivery*, vol. 35, no. 3, pp. 1267-1277, June 2020, doi: 10.1109/TPWRD.2019.2938020.

[16] N. Hashemnia, A. Abu-Siada, M. Masoum, A.S. Mohammad, and S.M. Islam, "Characterization of transformer FRA signature under various winding faults," in *Proceedings of the 2012 International Conference on Condition Monitoring and Diagnosis*, Sep. 23-27 2012, pp. 446-449.

[17] P. Picher, S. Tenbohlen, M. Lachman, A. Scardazzi, and P. Patel, Current state of transformer FRA interpretation," in *Procedia Engineering*, vol. 202, pp. 3-12, Dec. 217, doi: 10.1016/j.proeng.2017.09.689.

[18] Z. Zhao, C. Yao, C. Tang, C. Li, F. Yan and S. Islam, "Diagnosing Transformer Winding Deformation Faults Based on the Analysis of Binary Image Obtained From FRA Signature," in *IEEE Access*, vol. 7, pp. 40463-40474, 2019, doi: 10.1109/ACCESS.2019.2907648.

[19] Professional standard of the People's Republic of China - Frequency Response Analysis on Winding Deformation of Power Transformers - DL/T911-2004, 14 December 2004.

[20] V. Nurmanova, Y. Akhmetov, M. Bagheri, A. Zollanvari, B. T. Phung and G. B. Gharehpetian, "Confidence Level Estimation for Advanced Decision-Making in Transformer Short-circuit Fault Diagnosis," in *IEEE Transactions on Industry*

Applications, vol. 58, no. 1, pp. 233-241, Jan.-Feb. 2022, doi: 10.1109/TIA.2021.3118661.

[21] M. Tahir and S. Tenbohlen, "Comprehensive Analysis of Windings Electrical and Mechanical Faults Using a High-Frequency Model," in *Energies*, vol. 13, no. 1, pp. 105-129, 2020, doi: https://doi.org/10.3390/en13010105.

[22] Yann-Chang Huang, Hong-Tzer Yang and Ching-Lien Huang, "Developing a new transformer fault diagnosis system through evolutionary fuzzy logic," in *IEEE Transactions on Power Delivery*, vol. 12, no. 2, pp. 761-767, April 1997, doi: 10.1109/61.584363.

[23] P. Rajamani, D. Dey, B. Chatterjee and S. Chakravorti, "Classification of Impulse Fault Patterns in Transformers Using Wavelet Network," *2008 Joint International Conference on Power System Technology and IEEE Power India Conference*, 2008, pp. 1-6, doi: 10.1109/ICPST.2008.4745287.

[24] H. Ma, C. Ekanayake and T. K. Saha, "Power transformer fault diagnosis under measurement originated uncertainties," in *IEEE Transactions on Dielectrics and Electrical Insulation*, vol. 19, no. 6, pp. 1982-1990, December 2012, doi: 10.1109/TDEI.2012.6396956.

[25] A. A. Etumi and F. Anayi, "The Application of Correlation Technique in Detecting Internal and External Faults in Three-Phase Transformer and Saturation of Current Transformer," in *IEEE Transactions on Power Delivery*, vol. 31, no. 5, pp. 2131-2139, Oct. 2016, doi: 10.1109/TPWRD.2016.2572608.

[26] C. Jettanasen, J. Klomjit, C. Positharn, S. Bunjongjit and A. Ngaopitakkul, "Differential protection schemes for classification of fault detection between external fault and internal winding fault in transformer using probabilistic neural network," *2012 International conference on Fuzzy Theory and Its Applications (iFUZZY2012)*, 2012, pp. 150-153, doi: 10.1109/iFUZZY.2012.6409691.

[27] C. Jettanasen, C. Pothisarn, J. Klomjit and A. Ngaopitakkul, "Discriminating among inrush current, external fault and internal fault in power transformer using low frequency components comparison of DWT," *2012 15th International Conference on Electrical Machines and Systems (ICEMS)*, 2012, pp. 1-6.

[28] M. Jablonski and E. Napieralska-Juszczak, “Internal faults in power transformers,” in IET Electric Power Applications, vol. 1, no. 1, pp. 105–111, 2007.

[29] C. d. J. Ribeiro, A. P. Marques, C. H. B. Azevedo, D. C. P. Souza, B. P. Alvarenga and R. G. Nogueira, "Faults and defects in power transformers - a case study," *2009 IEEE Electrical Insulation Conference*, Montreal, QC, 2009, pp. 142-145.

[30] A. C. Franklin and D. P. Franklin, *The J & P Transformer Book. A Practical Technology of the Power Transformer*, 11th edition, Butterworth-Heinemann, Jan. 1983.

[31] H. William and P. E. Bartley, "Analysis of Transformer Failures," in *International Association of Engineering Insurers 36th Annual Conference – Stockholm*, 2003.

REFERENCES

[32] Transformer Failures, Causes & Impact, Shayan Tariq Jan, Raheel Afzal, and Akif Zia Khan.

[33] E. Bjerkan. "High Frequency modelling of power transformers,"Ph.D. dissertation, Norwegian University of Science and Technology, Trondheim, Norway, 2005.

[34] W. H. Bartley and H. S. Boiler, "An Analysis of Transformer Failures, Part 2: Causes, Prevention, and Maximum Service Life," The Hartford Steam Boiler Inspection and Insurance Company. [Online]. Available: https://www.hsb.com/TheLocomotive/AnAnalysisOfTransformersPart2.aspx.

[35] A. Bakshi and S. V. Kulkarni, "Analysis of Buckling Strength of Inner Windings in Transformers Under Radial Short-Circuit Forces," in *IEEE Transactions on Power Delivery*, vol. 29, no. 1, pp. 241-245, Feb. 2014, doi: 10.1109/TPWRD.2013.2272102.

[36] M. Bagheri, M. S. Naderi, T. Blackburn and T. Phung, "Frequency response analysis and short-circuit impedance measurement in detection of winding deformation within power transformers," in *IEEE Electrical Insulation Magazine*, vol. 29, no. 3, pp. 33-40, May-June 2013.

[37] CIGRE, International council on large electric systems, "Mechanical condition assessment of Transformer windings using Frequency Response Analysis (FRA)," Canada, 2008. Accessed on: Jan., 31, 2017. [Online]. Available: http://a2.cigre.org/content/download/65340/3094814/version/1/file/A2.26+FRA+Tutorial.pdf

[38] A. Bakshi and S. V. Kulkarni, "Coupled Electromagnetic-Structural Analysis of the Spiraling Phenomenon in a Helical Winding of a Power Transformer," in *IEEE Transactions on Power Delivery*, vol. 29, no. 1, pp. 235-240, Feb. 2014, doi: 10.1109/TPWRD.2013.2276047.

[39] M. F. M. Yousof, C. Ekanayake and T. K. Saha, "Frequency response analysis to investigate deformation of transformer winding," in *IEEE Transactions on Dielectrics and Electrical Insulation*, vol. 22, no. 4, pp. 2359-2367, August 2015, doi: 10.1109/TDEI.2015.004750.

[40] X. Zhao, C. Yao, Z. Zhao and A. Abu-Siada, "Performance evaluation of online transformer internal fault detection based on transient overvoltage signals," in *IEEE Transactions on Dielectrics and Electrical Insulation*, vol. 24, no. 6, pp. 3906-3915, Dec. 2017, doi: 10.1109/TDEI.2017.006772.

[41] A. J. P. Rosentino Jr., E. Saraiva, A. C. Delaiba, R. Guimarães, M. Lynce, J. C. De Oliveira, D. Fernandes Jr., W. Neves, "Modelling and Analysis of Electromechanical Stress in Transformers Caused by Short-Circuits," in *Renewable Energies and Power Quality Journal*, vol. 1, no. 9, pp. 717-722, May 2011, doi: https://doi.org/10.24084/repqj09.432.

[42] I. Lazariev, "Torsion of Transformer Windings Under Short Circuit," in *2019 CIGRE Canada Conference*, Montréal, Québec, September 16-19, 2019.

REFERENCES

[43] M. Bagheri, M. S. Naderi, T. R. Blackburn, T. Phung, "A case study on FRA capability in detection of mechanical defects within a 400MVA transformer," in *44th International Conference on Large High Voltage Electric Systems 2012*, pp. 1-8, Paris, France, Aug. 26-31 2012.

[44] S. Mortazavian, M. M. Shabestary, Y. A. -R. I. Mohamed and G. B. Gharehpetian, "Experimental Studies on Monitoring and Metering of Radial Deformations on Transformer HV Winding Using Image Processing and UWB Transceivers," in *IEEE Transactions on Industrial Informatics*, vol. 11, no. 6, pp. 1334-1345, Dec. 2015, doi: 10.1109/TII.2015.2479582.

[45] I. Fofana and Y. Hadjadj, "Electrical-Based Diagnostic Techniques for Assessing Insulation Condition in Aged Transformers," in *Energies*, vol. 9, no. 9, pp. 679-704, Aug. 2016, doi: 10.3390/en9090679.

[46] J. S. N'cho and I. Fofana, "Review of Fiber Optic Diagnostic Techniques for Power Transformers," in *Energies*, vol. 13, no. 7, pp. 1789-, Apr. 2020, 1789-1812, doi: 10.3390/en13071789.

[47] Y. Liu et al., "A study of the sweep frequency impedance method and its application in the detection of internal winding short circuit faults in power transformers," in *IEEE Transactions on Dielectrics and Electrical Insulation*, vol. 22, no. 4, pp. 2046-2056, August 2015.

[48] Power Transformer: Ability to Withstand Short Circuit, IEC 60076-5, Ed. 3.0, 2006.

[49] IEEE Guide for Diagnostic Field Testing of Electric Power Apparatus, Part 1: Oil Filled Power Transformers, Regulators, and Reactors, IEEE Std.62-1995.

[50] "IEEE standard test code for liquid-immersed distribution, power, and regulating transformers", IEEE Std. C57.12.90-2010.

[51] M. Nafar, B. Bahmanifirouzi, and M. Jabbari, "Transformer Monitoring by using Vibration Analysis," in *Australian Journal of Basic and Applied Sciences*, vol. 5, no. 11, pp. 984-990, 2011.

[52] M. R. Patel, 1973, "Dynamic response of power transformers under axial short circuit forces, part I windings and clamp as individual components," in *Proceedings of IEEE PES Winter Meeting*, New York, pp: 1558-1566.

[53] K. Hiraishi, Y. Hori, and S. Shida, 1971, "Mechanical strength of transformer windings under short circuit conditions," in *Proceedings of IEEE Winter Power Meeting*, New York, pp: 2381-2390.

[54] R. D. Holm, D. A. Hoecker, D. W. Allen, and T. E. Alverson, "The short circuit radial response of core-form transformer coils," in *IEEE Trans. Power Appar. Sys. PAS*, 104(2): 469-476, 1985.

[55] J. Shengchang, S. Ping, L. Yanming, X. Dake, and C. Junling, 2001, "The vibration measuring system for monitoring core and winding condition of power transformer," in *Proc. Int. Symp. on Electr. Insulating Mater, ISEIM*.

REFERENCES

[56] P. Kang and D. Birtwhistle, 2001. "Condition assessment of power transformer on-load tap-changers using wavelet analysis," in *IEEE Transactions on Power Delivery*, 16(2001): 394-400.

[57] X. Li, X. Huang, Z. Zhou, Y. Zhao, Y. Chen, and X. Song, "Analysis of the measuring points selection of power transformer winding deformation though vibration test", *China International Conference on Electricity Distribution (CICED)*, pp. 1-3, 2016.

[58] H. Zhou, K. Hong, H. Huang, and J. Zhou, "Transformer winding fault detection by vibration analysis methods," in *Applied Acoustics*, vol. 114, pp. 136-146, 2016.

[59] S. Nezhivenko, M. Bagheri, and T. Phung, "Three-dimensional vibration analysis of single-phase transformer winding under inter-disc fault," *2017 International Symposium on Electrical Insulating Materials (ISEIM)*, Toyohashi, pp. 512-515, 2017.

[60] T. He, J-Di. Wang, J. Guo, H. Huang, X.-X. Chen and J. Pan, "A vibration based condition monitoring system for power transformers," in *Asia-Pacific Power and Energy Eng. Conf. (APPEEC)*, pp. 1-4, 2009.

[61] B. García, J.C. Burgos and A.M. Alonso, "Transformer tank vibration modeling as a method of detecting winding deformations part I: theoretical foundation," in *IEEE Transactions on Power Delivery*, vol. 21, pp. 157-163, 2006.

[62] B. García, J.C. Burgos and A.M. Alonso, "Transformer tank vibration modeling as a method of detecting winding deformations part II: experimental verification," in *IEEE Transactions on Power Delivery*, vol. 21, pp. 164-169, 2006.

[63] Kornatowski E., Banaszak S., “Diagnostics of a transformer's active part with complementary FRA and VM measurements," in *IEEE Transactions on Power Delivery*, vol. 29, Issue: 3, 2014, pp. 1398 – 1406.

[64] M. Akhavanhejazi, G.B. Gharehpetian, R. Faraji-Dana, G.R. Moradi, M. Mohammadi and H.A. Alehoseini, "A new on-line monitoring method of transformer winding axial displacement based on measurement of scattering parameters and decision tree," in *Expert Syst. Applications*, vol. 38, pp. 8886-8893, 2011.

[65] M.A. Hejazi, M. Choopani, M. Dabir, and G.B. Gharehpetian, "Effect of antenna position on on-line monitoring of transformer winding axial displacement using electromagnetic waves," *IEEE 2nd Int'l. Power Energy Conf. (PECon)*, pp. 44-49, 2008.

[66] M. A. Hejazi, G. B. Gharehpetian, G. Moradi, H. A. Alehosseini, and M. Mohammadi, "Online monitoring of transformer winding axial displacement and its extent using scattering parameters and nearest neighbour method," in *IET Proc. Generation, Transmission Distribution*, vol. 5, pp. 824-832, 2011.

REFERENCES

[67] P. M. Joshi and S. V. Kulkarni, "A novel approach for online deformation diagnostics of transformer windings," in *IEEE Power and Energy Society, General Meeting*, pp. 1-6, 2010.

[68] N. Shu, C. Zhou, F. Hu, Q. Liu and L. Zheng, "Study on ultrasonic measurement device for transformer winding deformation", IEEE Int'l. Conf. Power Syst. Techn., (POWERCON), Vol.3, pp. 1401-1404, 2002.

[69] W. Jiang, F. Liu, Z. Wang and X. Zhang, "Transformer Partial Discharge Detection Using Electrical-Ultrasonic Technology," *2012 Asia-Pacific Power and Energy Engineering Conference*, 2012, pp. 1-4, doi: 10.1109/APPEEC.2012.6307325.

[70] S.-b. Gao and G. Wang, "Study on on-line monitoring of windings deformation of power transformer", IE*EE 8th Int'l. Conf. Developments in Power System Protection*, pp. 335-338 Vol.1, 2004.

[71] A. Palani, S. Santhi, S. Gopalakrishna and V. Jayashankar, "Real-time techniques to measure winding displacement in transformers during short-circuit tests," in *IEEE Trans. Power Del.*, Vol. 23, pp. 726-732, 2008.

[72] D. K. Xu and Y. M. Li, "A simulating research on monitoring of winding deformation of power transformer by on-line measurement of short-circuit reactance," in *IEEE Int'l. Conf. Power System Technology (POWERCON)*, vol.1, pp. 167-171, 1998.

[73] Z. Berler, P. Butyrin, and M. Alpatov,"On-line diagnostics of mechanical deformations of winding," in *Proceedings of TechCon'05*, pp. 1-4, 2005.

[74] E. Arri, A. Carta, F. Mocci, and M. Tosi, "Diagnosis of the state of power transformer windings by on-line measurement of stray reactance," in *IEEE Trans. Instrum. Meas*., vol. 42, pp. 372-378, 1993.

[75] P. Li, B. G. Zhang, Z.G. Hao, X.J. Hu, and Y.L. Chu, "Research on monitoring of winding deformation of power transformer by on-line parameter estimation about leakage inductance," in *IEEE Int'l. Conf. Power Syst. Techn. (POWERCON)*, pp. 1-6, 2006.

[76] Z. G. Hao, B. H. Zhang, C. G. Yan, B. R. Shao, X. F. Bo and Z. Q., "Research on integration of transformer protection and winding deformation detecting," in *IEEE Int'l. Conf. Power Syst. Techn. (POWERCON)*, pp. 1-8, 2010.

[77] G. Hu, L. Zhang, X. Wu, D. Correia, and W. He, "Detecting the Capacity of Distribution Transformer Based on an On-Line Method," in *Asia-Pacific Power and Energy Eng. Conf. (APPEEC)*, pp. 1-4, 2011.

REFERENCES

[78] M. S. Noah and A. A. Shaltout, "Fault discrimination and protection of power transformers using voltage and current signals," *2014 IEEE International Energy Conference (ENERGYCON)*, Cavtat, 2014, pp. 254-261.

[79] A. Abu-Siada and S. Islam, "A Novel Online Technique to Detect Power Transformer Winding Faults," in *IEEE Transactions on Power Delivery*, vol. 27, no. 2, pp. 849-857, April 2012, doi: 10.1109/TPWRD.2011.2180932.

[80] A. Abu-Siada and S. Islam, "Image processing-based on-line technique to detect power transformer winding faults," *IECON 2013 - 39th Annual Conference of the IEEE Industrial Electronics Society*, 2013, pp. 5549-5554, doi: 10.1109/IECON.2013.6700042.

[81] A. Smagulova, A. Borasheva, N. Moldiyar, N. Bazarbek, M. Bagheri and B. T. Phung, "Real-time Transformer Diagnosis using Voltage-Current Signal over Cloud Environment," *2018 Condition Monitoring and Diagnosis (CMD)*, 2018, pp. 1-7, doi: 10.1109/CMD.2018.8535876.

[82] X. Zhao et al., "Experimental Evaluation of Transformer Internal Fault Detection Based on V–I Characteristics," in *IEEE Transactions on Industrial Electronics*, vol. 67, no. 5, pp. 4108-4119, May 2020, doi: 10.1109/TIE.2019.2917368.

[83] Huo-Ching Sun, Yann-Chang Huang, and Chao-Ming Huang, "A Review of Dissolved Gas Analysis in Power Transformers," in *Energy Procedia*, vol. 14, pp. 1220-1225, Mar. 2012, doi: 10.1016/j.egypro.2011.12.1079.

[84] E. Wannapring, C. Suwanasri and T. Suwanasri, "Dissolved Gas Analysis methods for distribution transformers," *2016 13th International Conference on Electrical Engineering/Electronics, Computer, Telecommunications and Information Technology (ECTI-CON)*, 2016, pp. 1-6, doi: 10.1109/ECTICon.2016.7561320.

[85] J. Golarz, "Guest Editorial | Understanding Dissolved Gas Analysis (DGA) Techniques and Interpretations," in *Electric Energy T&D Magazine*, vol. 19, no 6., Art. No. 31, Nov.-Dec. 2015.

[86] P. Mirowski and Y. LeCun, "Statistical Machine Learning and Dissolved Gas Analysis: A Review," in *IEEE Transactions on Power Delivery*, vol. 27, no. 4, pp. 1791-1799, Oct. 2012, doi: 10.1109/TPWRD.2012.2197868.

[87] "IEEE Guide for the Interpretation of Gases Generated in Mineral Oil-Immersed Transformers - Redline," in IEEE Std C57.104-2019 (Revision of IEEE Std C57.104-2008) - Redline , vol., no., pp.1-179, 1 Nov. 2019.

[88] Mineral Oil-Impregnated Equipment in Service—Guide to the Interpretation of Dissolved and Free Gases Analysis, IEC Standard 60599, 2007.

[89] R. R. Rogers, "IEEE and IEC Codes to Interpret Incipient Faults in Transformers, Using Gas in Oil Analysis," in *IEEE Transactions on Electrical Insulation*, vol. EI-13, no. 5, pp. 349-354, Oct. 1978, doi: 10.1109/TEI.1978.298141.

[90] T. De Rybel, A. Singh, J. A. Vandermaar, M. Wang, J. R. Marti and K. D. Srivastava, "Apparatus for Online Power Transformer Winding Monitoring Using

Bushing Tap Injection," in *IEEE Transactions on Power Delivery*, vol. 24, pp. 996-1003, 2009.

[91] M. Florkowski and J. Furgal, "Transformer winding defects identification based on a high frequency method," in *Measurement Sci. Techn.*, doi:10.1088/0957-0233/18/9/012, 2007.

[92] A. Setayeshmehr, H. Borsi, E. Gockenbach1, and I. Fofana, "On-line monitoring of transformer via transfer function," in *Proc IEEE Elect. Insul. Conf., Montreal*, QC, Canada, May/Jun. 2009, pp. 278–282.

[93] J. Christian and K. Feser, "Procedures for detecting winding displacements in power transformers by the transfer function method," in *IEEE Transactions on Power Delivery*, vol. 19, no. 1, pp. 214–219, Jan. 2004.

[94] P. T. M. Vaessen and E. Hanique, "A new frequency response analysis method for power transformers," in *IEEE Transactions on Power Delivery*, vol. 7, no. 1, pp. 384–391, Jan. 1992.

[95] N. Abeywickrama, Y. V. Serdyuk and S. M. Gubanski, "High-Frequency Modeling of Power Transformers for Use in Frequency Response Analysis (FRA)," *in IEEE Transactions on Power Delivery*, vol. 23, no. 4, pp. 2042-2049, Oct. 2008, doi: 10.1109/TPWRD.2008.917896.

[96] M. I. Samesima, J. C. de Oliveira and E. M. Dias, "Frequency response analysis and modeling of measurement transformers under distorted current and voltage supply," in *IEEE Transactions on Power Delivery*, vol. 6, no. 4, pp. 1762-1768, Oct. 1991, doi: 10.1109/61.97718.

[97] J. C. Gonzales and E. E. Mombello, "Fault Interpretation Algorithm Using Frequency-Response Analysis of Power Transformers," *in IEEE Transactions on Power Delivery*, vol. 31, no. 3, pp. 1034-1042, June 2016, doi: 10.1109/TPWRD.2015.2448524.

[98] Y. Q. Sun et al., "Using impulse with appropriate repetition frequency in IFRA test to diagnosis winding deformation in transformer," *2016 IEEE International Conference on High Voltage Engineering and Application (ICHVE)*, 2016, pp. 1-4, doi: 10.1109/ICHVE.2016.7800884.

[99] B. Mohseni, N. Hashemnia and S. Islam, "Online detection of partial discharge inside power transformer winding through IFRA," *2017 IEEE Power & Energy Society General Meeting, 2017*, pp. 1-5, doi: 10.1109/PESGM.2017.8273725.

[100] Y. Q. Sun et al., "Using impulse with appropriate repetition frequency in IFRA test to diagnosis winding deformation in transformer," *2016 IEEE International Conference on High Voltage Engineering and Application (ICHVE)*, 2016, pp. 1-4, doi: 10.1109/ICHVE.2016.7800884.

[101] G. A. T. N. Aravinda, K. Bandara, G. A. Jayantha, J. R. S. S. Kumara and M. A. R. M. Fernando, "Application of SFRA techniques to discriminate short circuit faults

of transformer winding," *2017 IEEE International Conference on Industrial and Information Systems (ICIIS)*, 2017, pp. 1-5, doi: 10.1109/ICIINFS.2017.8300409.

[102] G. A. T. N. Aravinda, K. Bandara, G. A. Jayantha, J. R. S. S. Kumara and M. A. R. M. Fernando, "Application of SFRA techniques to discriminate short circuit faults of transformer winding," *2017 IEEE International Conference on Industrial and Information Systems (ICIIS)*, 2017, pp. 1-5, doi: 10.1109/ICIINFS.2017.8300409.

[103] P. Werelius, M. Ohlen, L. Adeen and E. Brynjebo, "Measurement considerations using SFRA for condition assessment of Power Transformers," *2008 International Conference on Condition Monitoring and Diagnosis*, 2008, pp. 898-901, doi: 10.1109/CMD.2008.4580428.

[104] M. Bagheri, M. S. Naderi, T. Blackburn and T. Phung, "FRA vs. short circuit impedance measurement in detection of mechanical defects within large power transformer," *2012 IEEE International Symposium on Electrical Insulation*, 2012, pp. 301-305, doi: 10.1109/ELINSL.2012.6251477.

[105] N. Shanmugam, B. Madanmohan and R. Rajamani, "Influence of the Load on the Impulse Frequency Response Approach Based Diagnosis of Transformer's Inter-Turn Short-Circuit," in IEEE Access, vol. 8, pp. 39454-39463, 2020, doi: 10.1109/ACCESS.2020.2976157.

[106] M. Tahir, S. Tenbholen and S. Miyazaki, "Analysis of Statistical Methods for Assessment of Power Transformer Frequency Response Measurements," in IEEE Transactions on Power Delivery, vol. 36, no. 2, pp. 618-626, April 2021, doi: 10.1109/TPWRD.2020.2987205.

[107] K. Samarawickrama, N. D. Jacob, A. M. Gole and B. Kordi, "Impulse Generator Optimum Setup for Transient Testing of Transformers Using Frequency-Response Analysis and Genetic Algorithm," in IEEE Transactions on Power Delivery, vol. 30, no. 4, pp. 1949-1957, Aug. 2015, doi: 10.1109/TPWRD.2015.2429554.

[108] P. Werelius, M. Ohlen, L. Adeen and E. Brynjebo, "Measurement considerations using SFRA for condition assessment of Power Transformers," 2008 International Conference on Condition Monitoring and Diagnosis, 2008, pp. 898-901, doi: 10.1109/CMD.2008.4580428.

[109] M. Bagheri, M. Salay Naderi, T. Blackburn, T. Phung, "Practical challenges in online transformer winding deformation diagnostics," *2011 2nd International Conference on Electric Power and Energy Conversion Systems, EPECS*, 2011. 1-6. 10.1109/EPECS.2011.6126848.

[110] V. Nurmanova, M. Bagheri, A. Zollanvari, K. Aliakhmet, Y. Akhmetov and G. B. Gharehpetian, "A New Transformer FRA Measurement Technique to Reach Smart Interpretation for Inter-Disk Faults," in *IEEE Transactions on Power Delivery*, vol. 34, no. 4, pp. 1508-1519, Aug. 2019, doi: 10.1109/TPWRD.2019.2909144.

[111] A. E. Shaban, K. H. Ibrahim and T. M. Barakat, "Modeling, Simulation and Classification of Power Transformer Faults Based on FRA Test," 2019 21st

International Middle East Power Systems Conference (MEPCON), 2019, pp. 908-913, doi: 10.1109/MEPCON47431.2019.9007984.

[112] O. Aljohani and A. Abu-Siada, "Application of digital image processing to detect transformer bushing faults and oil degradation using FRA polar plot signature," in IEEE Transactions on Dielectrics and Electrical Insulation, vol. 24, no. 1, pp. 428-436, Feb. 2017, doi: 10.1109/TDEI.2016.006088.

[113] D. A. K. Pham, T. M. T. Pham, M. H. Safari, V. N. C. Ho, H. Borsi and E. Gockenbach, "FRA-based transformer parameters at low frequencies," 2012 International Conference on High Voltage Engineering and Application, 2012, pp. 476-479, doi: 10.1109/ICHVE.2012.6357083.

[114] D. M. Sofian, Z. Wang and J. Li, "Interpretation of Transformer FRA Responses—Part II: Influence of Transformer Structure," in IEEE Transactions on Power Delivery, vol. 25, no. 4, pp. 2582-2589, Oct. 2010, doi: 10.1109/TPWRD.2010.2050342.

[115] M. Bagheri, B. T. Phung and T. Blackburn, "Transformer frequency response analysis: mathematical and practical approach to interpret mid-frequency oscillations," in *IEEE Transactions on Dielectrics and Electrical Insulation*, vol. 20, no. 6, pp. 1962-1970, December 2013, doi: 10.1109/TDEI.2013.6678842.

[116] A. Paleri, P. Preetha and K. Sunitha, "Frequency Response Analysis (FRA) in power transformers: An approach to locate inter-disk SC fault," *2017 IEEE PES Asia-Pacific Power and Energy Engineering Conference (APPEEC)*, 2017, pp. 1-5, doi: 10.1109/APPEEC.2017.8308951.

[117] K. M. Gawrylczyk and K. Trela, "Frequency Response Modeling of Transformer Windings Utilizing the Equivalent Parameters of a Laminated Core," in *Energies*, vol. 12, pp. 2371-2384, 2019, doi: https://doi.org/10.3390/en12122371.

[118] M. H. Samimi, A. A. Shayegani Akmal, H. Mohseni, S. Tenbohlen, "Detection of transformer mechanical deformations by comparing different FRA connections," in *International Journal of Electrical Power & Energy Systems*, vol. 86, pp. 53-60, 2017, doi: https://doi.org/10.1016/j.ijepes.2016.09.007.

[119] Tapan Kumar Saha and Prithwiraj Purkait, "Frequency Response Analysis Interpretation for Winding Deformation of Power Transformers," in *Transformer Ageing: Monitoring and Estimation Techniques*, IEEE, 2017, pp.303-328, doi: 10.1002/9781119239970.ch6.

[120] F. de León, A. Farazmand, S. Jazebi, D. Deswal and R. Levi, "Elimination of Residual Flux in Transformers by the Application of an Alternating Polarity DC Voltage Source," in IEEE Transactions on Power Delivery, vol. 30, no. 4, pp. 1727-1734, Aug. 2015, doi: 10.1109/TPWRD.2014.2377199.

[121] P. Vaca Vargas and E. Mombello, "Time-Frequency Analysis for the Interpretation of FRA Measurements," *VDE High Voltage Technology 2016; ETG-Symposium*, 2016, pp. 1-5.

REFERENCES

[122] D. M. Sofian, Z. D. Wang and P. Jarman, "Interpretation of transformer FRA measurement results using winding equivalent circuit modelling technique," *CEIDP '05. 2005 Annual Report Conference on Electrical Insulation and Dielectric Phenomena*, 2005., 2005, pp. 613-616, doi: 10.1109/CEIDP.2005.1560757.

[123] Z. Zhao, C. Tang, Y. Chen, Q. Zhou, C. Yao, and S. M. Islam, Interpretation of transformer winding deformation fault by the spectral clustering of FRA signature," in *International Journal of Electrical Power & Energy Systems*, vol. 130, no. 4, p. 106933, doi: 10.1016/j.ijepes.2021.106933.

[124] O. Aljohani and A. Abu-Siada, "Application of DIP to Detect Power Transformers Axial Displacement and Disk Space Variation Using FRA Polar Plot Signature," in *IEEE Transactions on Industrial Informatics*, vol. 13, no. 4, pp. 1794-1805, Aug. 2017, doi: 10.1109/TII.2016.2626779.

[125] Z. Zhao, C. Yao, C. Tang, C. Li, F. Yan and S. Islam, "Diagnosing Transformer Winding Deformation Faults Based on the Analysis of Binary Image Obtained From FRA Signature," in *IEEE Access*, vol. 7, pp. 40463-40474, 2019, doi: 10.1109/ACCESS.2019.2907648.

[126] T. Orynbassar, M. Bagheri and B. T. Phung, "Frequency response interpretation using statistical indices: A case study on 400 MVA transformer," *2017 3rd International Conference on Condition Assessment Techniques in Electrical Systems (CATCON)*, 2017, pp. 132-137, doi: 10.1109/CATCON.2017.8280199.

[127] V. Behjat, M. Mahvi and E. Rahimpour, "A new statistical approach to interpret power transformer frequency response analysis: Nonparametric statistical methods," *2015 30th International Power System Conference (PSC)*, 2015, pp. 142-148, doi: 10.1109/IPSC.2015.7827740.

[128] N. Wesley, S. Bhandari, A. Subramaniam, M. Bagheri and S. K. Panda, "Evaluation of statistical interpretation methods for frequency response analysis based winding fault detection of transformers," *2016 IEEE International Conference on Sustainable Energy Technologies (ICSET)*, 2016, pp. 36-41, doi: 10.1109/ICSET.2016.7811753.

[129] O. H. Aréu, A. M. G. Menéndez, J. I. H. Sánchez and E. S. Valdés, "Diagnosis of faults in power transformers through the interpretation of FRA testing with artificial intelligence," *2018 IEEE International Autumn Meeting on Power, Electronics and Computing (ROPEC)*, 2018, pp. 1-5, doi: 10.1109/ROPEC.2018.8661467.

[130] M. S. Chaouche, H. Houassine, S. Moulahoum and I. Colak, "Faults Investigation of Transformer Windings Using the Frequency Response Analysis FRA," 2016 15th IEEE International Conference on Machine Learning and Applications (ICMLA), 2016, pp. 452-459, doi: 10.1109/ICMLA.2016.0080.

[131] A. B. Mugarra, H. Mayora, J. M. Guerrero and C. A. Platero, "Frequency Response Analysis (FRA) Fault Diagram Assessment Method," in *IEEE Transactions on Industry Applications*, doi: 10.1109/TIA.2021.3131425.

REFERENCES

[132] Z. W. Zhang, J. D. Yan, W. H. Tang, L. J. Guo and S. M. Tao, "Experimental investigation of localized axial winding displacement in a high frequency range for power transformers," *2016 International Conference on Condition Monitoring and Diagnosis (CMD)*, 2016, pp. 388-391, doi: 10.1109/CMD.2016.7757841.

[133] S. Banaszak and W. Szoka, "Cross Test Comparison in Transformer Windings Frequency Response Analysis," in *Energies*, vol. 11, no. 6, p. 1349, May 2018, doi: 10.3390/en11061349.

[134] M. Tavakoli and M. Nafar, "Human reliability analysis in maintenance team of power transmission system protection," in *Prot Control Mod Power Syst*, vol. 5, no. 26, pp. 1-13, Nov. 2020, doi: https://doi.org/10.1186/s41601-020-00176-6.

[135] Y. Jin and Z. Li, "Analysis of Operator's Visual Process Using a Human Information Processing Model," *16th International Conference on Artificial Reality and Telexistence--Workshops (ICAT'06)*, 2006, pp. 594-598, doi: 10.1109/ICAT.2006.42.

[136] X. Wu, Y. He, C. Wang, W. Wu, C. Wang and J. Duan, "Hilbert ID Considering Multi-Window Feature Extraction for Transformer Deep Vision Fault Positioning," in *IEEE Access*, vol. 8, pp. 91276-91286, 2020, doi: 10.1109/ACCESS.2020.2991844.

[137] X. Mao, Z. Wang, P. Jarman and A. Fieldsend-Roxborough, "Winding Type Recognition through Supervised Machine Learning using Frequency Response Analysis (FRA) Data," *2019 2nd International Conference on Electrical Materials and Power Equipment (ICEMPE)*, 2019, pp. 588-591, doi: 10.1109/ICEMPE.2019.8727354.

[138] X. Mao, Z. Wang, P. Jarman and A. Fieldsend-Roxborough, "Winding Type Recognition through Supervised Machine Learning using Frequency Response Analysis (FRA) Data," *2019 2nd International Conference on Electrical Materials and Power Equipment (ICEMPE)*, 2019, pp. 588-591, doi: 10.1109/ICEMPE.2019.8727354.

[139] A. Moradzadeh, H. Moayyed, B. Mohammadi-Ivatloo, G. B. Gharehpetian and A. P. Aguiar, "Turn-to-Turn Short Circuit Fault Localization in Transformer Winding via Image Processing and Deep Learning Method," in *IEEE Transactions on Industrial Informatics*, doi: 10.1109/TII.2021.3105932.

[140] S. Ma and H. Ren, "Method for detecting system on power transformer winding deformation," *2009 International Conference on Electrical Machines and Systems*, 2009, pp. 1-5, doi: 10.1109/ICEMS.2009.5382646.

[141] Z. Zhao, C. Tang, Q. Zhou, L. Xu, Y. Gui, C. Yao, "Identification of power transformer winding mechanical fault types based on online IFRA by support vector machine," in *Energies*, vol. 10, no. 12, p. 2022, Dec. 2017.

REFERENCES

[142] M. Bigdeli, M. Vakilian, and E. Rahimpour, (2012). "Transformer winding faults classification based on transfer function analysis by support vector machine, " in *Electric Power Applications, IET*. 6, pp. 268-276, doi: 10.1049/iet-epa.2011.0232.

[143] E. Beshr, R. M. Sharkawy and A. S. Abd El-Hamid, "LVQ neural network for identification of abnormal conditions within transformers," *2015 50th International Universities Power Engineering Conference (UPEC), 2015*, pp. 1-6, doi: 10.1109/UPEC.2015.7339845.

[144] M. H. Samimi and S. Tenbohlen, "The Numerical Indices Proposed for the Interpretation of the FRA Results: A Review," VDE High Voltage Technology 2016; ETG-Symposium, 2016, pp. 1-7.

[145] S. Banaszak and W. Szoka, "Transformer Frequency Response Analysis With the Grouped Indices Method in End-to-End and Capacitive Inter-Winding Measurement Configurations," in IEEE Transactions on Power Delivery, vol. 35, no. 2, pp. 571-579, April 2020, doi: 10.1109/TPWRD.2019.2915570.

[146] V. Nurmanova, A. Khassenov, M. Bagheri, T. Phung and G. B. Gharehpetian, "The Influence of External Parameters on Transformer Frequency Response Signature and Numerical Indices," 2019 IEEE International Conference on Environment and Electrical Engineering and 2019 IEEE Industrial and Commercial Power Systems Europe (EEEIC/I&CPS Europe), 2019, pp. 1-4, doi: 10.1109/EEEIC.2019.8783609.

[147] R. S. De Andrade Ferreira, P. Picher, H. Ezzaidi and I. Fofana, "Frequency Response Analysis Interpretation Using Numerical Indices and Machine Learning: A Case Study Based on a Laboratory Model," in *IEEE Access*, vol. 9, pp. 67051-67063, 2021, doi: 10.1109/ACCESS.2021.3076154.

[148] V. Jeyabalan and S. Usa, "Frequency domain correlation technique for PD location in transformer winding," in I*EEE Transactions on Dielectrics and Electrical Insulation*, vol. 16, no. 4, pp. 1160-1167, August 2009, doi: 10.1109/TDEI.2009.5211871.

[149] S. M. A. N. Al-Ameri et al., “Understanding the Influence of Power Transformer Faults on the Frequency Response Signature Using Simulation Analysis and Statistical Indicators,” in *IEEE Access*, vol. 9, pp. 70935-70947, May. 2021.

[150] G. M. Kennedy, A. J. McGrail and J. A. Lapworth, “Using Cross-Correlation Coefficients to Analyze Transformer Sweep Frequency Response Analysis (SFRA) Traces,” in *2007 IEEE Power Engineering Society Conference and Exposition in Africa - PowerAfrica*, 16-20 Jul. 2007, pp. 1-6.

[151] J. C. Gonzales Arispe and E. E. Mombello, "Detection of Failures Within Transformers by FRA Using Multiresolution Decomposition," in IEEE Transactions on Power Delivery, vol. 29, no. 3, pp. 1127-1137, Jun. 2014.

[152] S. Miyazaki, Y. Mizutani, T. Okamoto, Y. Wada and C. Hayashida, "Abnormality diagnosis of transformer winding by frequency response analysis (FRA) using

circuit model," in *2012 IEEE International Conference on Condition Monitoring and Diagnosis*, 23-27 Sept. 2012, pp. 273-276.

[153] J. Kim, B. Park, S. C. Jeong, S. W. Kim and P. G. Park, "Fault diagnosis of a power transformer using an improved frequency-response analysis," in *IEEE Transactions on Power Delivery*, vol. 20, no. 1, pp. 169-178, Jan. 2005.

[154] M. H. Samimi, S. Tenbohlen, A. A. S. Akmal and H. Mohseni, "Effect of Different Connection Schemes, Terminating Resistors and Measurement Impedances on the Sensitivity of the FRA Method," in *IEEE Transactions on Power Delivery*, vol. 32, no. 4, pp. 1713-1720, Aug. 2017.

[155] E. Rahimpour, M. Jabbari and S. Tenbohlen, "Mathematical Comparison Methods to Assess Transfer Functions of Transformers to Detect Different Types of Mechanical Faults," in *IEEE Transactions on Power Delivery*, vol. 25, no. 4, pp. 2544-2555, Nov. 2010.

[156] L. Zhou, J. Jiang, X. Zhou, Z. Wu, T. Lin, D. Wang, "Detection of transformer winding faults using FRA and image features," in *IET Electric Power Applications*, vol. 14, no. 6, pp. 972-980, Jun. 2020, doi: 10.1049/iet-epa.2019.0933.

[157] Z. Zhao, C. Yao, C. Tang, C. Li, F. Yan and S. Islam, "Diagnosing Transformer Winding Deformation Faults Based on the Analysis of Binary Image Obtained From FRA Signature," in *IEEE Access*, vol. 7, pp. 40463-40474, 2019, doi: 10.1109/ACCESS.2019.2907648.

[158] A. Vosoughi and M. Hamed Samimi, "Evaluation of the Image Processing Technique in Interpretation of Polar Plot Characteristics of Transformer Frequency Response," *2022 International Conference on Machine Vision and Image Processing (MVIP)*, 2022, pp. 1-6, doi: 10.1109/MVIP53647.2022.9738771.

[159] CIGRÉ WG A2. 26, "Mechanical Condition Assessment of Transformer Windings using Frequency Response Analysis (FRA)", Brochure # 342 & Electra no. 237 and no. 228, April 2008.

[160] NCEPRI, "Application guideline for transformer winding distortion test technology," 1999.

[161] F. W. Grover, Inductance Calculations: Working Formulas and Tables, New York, NY, USA: Dover, 1962.

[162] M. Bagheri, S. Nezhivenko, B. Phung, T. Blackburn, "Air Core Transformer Winding Disk Deformation: A Precise Study on Mutual Inductance Variation and Its Influence on Frequency Response Spectrum," in *IEEE Access*, vol. 6, pp. 7476-7488, 2018.

[163] A. Massarini and M. Kazimierczuk, "Self-capacitance of inductors," in *IEEE Transactions on Power Electronics*, vol. 12, no. 4, pp. 671-676, 1997.

[164] W. Thue, Electrical power cable engineering. New York: Marcel Dekker, 1999.

[165] R. Jiang, W. Fu, C. C. Chen, "EPEEC: comprehensive SPICE-compatible reluctance extraction for high-speed interconnects above lossy multilayer

substrates," in *IEEE Transactions on Computer-Aided Design of Integrated Circuits and Systems*, vol. 24, no. 10, pp. 1562-1571, 2005.

[166] "Using Coilcraft's models in LTspice® | Coilcraft", *Coilcraft.com*, 2021. [Online]. Available: https://www.coilcraft.com/en-us/models/howto/using-coilcrafts-models-in-ltspice/.

[167] M. H. Samimi and S. Tenbohlen, "FRA interpretation using numerical indices: State-of-the-art," in *Int. J. Elec. Power*, vol. 89, pp. 115-125, 2017.

[168] P. M. Nirgude, D. Ashokraju, A. D. Rajkumar, and B. P. Singh, "Application of numerical evaluation techniques for interpreting frequency response measurements in power transformers," in *IET Sci. Meas. Technol*., vol. 2, no. 5, pp. 275-285, 2008.

[169] H. Tarimoradi and G. B. Gharehpetian, "Novel Calculation Method of Indices to Improve Classification of Transformer Winding Fault Type, Location, and Extent," in *IEEE Transactions on Industrial Informatics*, vol. 13, no. 4, pp. 1531-1540, Aug. 2017.

[170] K. P. Badgujar, M. Maoyafikuddin, and S. V. Kulkarni, "Alternative statistical techniques for aiding SFRA diagnostics in transformers," in *IET Gener. Transm. Dis*., 2011.

[171] A. J. Ghanizadeh and G. B. Gharehpetian, "ANN and cross-correlation based features for discrimination between electrical and mechanical defects and their localization in transformer winding," in *IEEE Trans. Dielectr. Electr. Insul*., vol. 21, no. 5, pp. 2374-2382, 2014.

[172] J. W. Kim, B. Park, S. C. Jeong, S. W. Kim, and P. Park, "Fault diagnosis of a power transformer using an improved frequency-response analysis," in *IEEE Trans. Power Del*., vol. 20, no. 1, pp. 169-178, 2005.

[173] M. H. Samimi, S. Tenbohlen, A. A. S. Akmal, and H. Mohseni, "Evaluation of numerical indices for the assessment of transformer frequency response," in *IET Gener. Transm. Dis*., vol. 11 no. 1, pp. 218-227, 2017.

[174] J. Secue and E. Mombello, "Sweep frequency response analysis (SFRA) for the assessment of winding displacements and deformation in power transformers," in *Electr. Pow. Syst. Res*., vol. 78, no. 6, pp. 1119-1128, 2008.

[175] M. Bagheri, S. Nezhivenko, and B. Phung, "Loss of low-frequency data in on-line frequency response analysis of transformers," in *IEEE Electrical Insulation Magazine*, vol. 33, no. 5, pp. 32-39, Sep./Oct. 2016.

[176] ABB, "1MRS 755916, Differential Protection RET 54_/Diff6T function, Application and Setting Guide," ver. A/17.08.2005, 2005.

[177] U. Braga-Neto and E. Dougherty, "Bolstered error estimation," in *Pattern Recognition*, vol. 37, no. 6, pp. 1267-1281, 2004.

[178] B. Efron and R. Tibshirani, *An introduction to the bootstrap*. New York: Chapman and Hall, 1993.

REFERENCES

[179] M. Tahir, S. Tenbholen and S. Miyazaki, "Analysis of Statistical Methods for Assessment of Power Transformer Frequency Response Measurements," in *IEEE Transactions on Power Delivery*, vol. 36, no. 2, pp. 618-626, Apr. 2021.

[180] Y. Akhmetov, V. Nurmanova, M. Bagheri, A. Zollanvari and G. B. Gharehpetian, "A New Diagnostic Technique for Reliable Decision-Making on Transformer FRA Data in Interturn Short-Circuit Condition," in *IEEE Transactions on Industrial Informatics*, vol. 17, no. 5, pp. 3020-3031, May 2021, doi: 10.1109/TII.2020.3007607.

[181] Y. Akhmetov, V. Nurmanova, M. Bagheri, A. Zollanvari and G. B. Gharehpetian, "A Bootstrapping Solution for Effective Interpretation of Transformer Winding Frequency Response," in *IEEE Transactions on Instrumentation and Measurement*, vol. 71, pp. 1-11, 2022, Art no. 3508811, doi: 10.1109/TIM.2022.3159012.

[182] V. Nurmanova, Y. Akhmetov, M. Bagheri, A. Zollanvari, G. B. Gharehpetian and T. Phung, "A New Transformer Winding RLC model to Study the Effect of the Disk Space Variation on FRA Signature," *2021 IEEE International Conference on Environment and Electrical Engineering and 2021 IEEE Industrial and Commercial Power Systems Europe (EEEIC / I&CPS Europe)*, 2021, pp. 1-6, doi: 10.1109/EEEIC/ICPSEurope51590.2021.9584786.

APPENDICES

Appendix A. Self- and Mutual inductances calculation

```
"""
Calculation of Self-inductances and Mutual inductances of coils

"""
import numpy as np

d = 2.99        # diameter of conductor (in mm)
t = 1.14        # thickness of insulator (in mm)
D_core = 110    # air core diameter (in mm)
N_d = 10        # number of disks
N_t = 6         # number of turns in each disk
e_r = 4         # relative permittivity of silicon rubber insulator
e_0 = 8.854e-12 # permittivity of free space

D_wire = d + 2*t                    # diameter of wire

R_turn = np.zeros((1,N_t))              # initializing turn radius vector (in mm)
R_mean = (N_t/2)*(2*t + d) + D_core/2   # mean radius of disk (in mm)

# Calculation of radii of turns
for i in range(N_t):
    R_turn[:,N_t-1-i] = (D_core/2) + (2*i + 1)*(t + d/2)

# Self-induction calculation using Kirchoff equation [59] Grover
L = 4*np.pi*(R_turn*1e-3)*(np.log(8*R_turn/(d/2))-1.75)*1e-7
#L_micro = np.round(L * 1e6, 4)
L_micro = L * 1e6

# Self-induction calculation using Geometric mean [60] Grover
ratio = (d/2)/R_turn
L_g = 4*np.pi*(R_turn*1e-3)*((1 + 0.1137*ratio**2)*np.log(8/ratio) - 0.0095*ratio**2 - 1.75)*1e-7
L_g_micro = np.round(L_g * 1e6, 4)

# Self-induction calculation for AC and high frequency [62] Grover
L_h = 4*np.pi*(R_turn*1e-3)*((1 + (3/16)*ratio**2)*np.log(8/ratio) - (1/16)*ratio**2 - 2)*1e-7
L_h_micro = np.round(L_h * 1e6, 4)

# Mutual inductance calculation for filament
M = np.zeros((12,12))       # initializing mutual inductance matrix
y = [0]*6 + [(d + 2*t)]*6   # distances between center of coils
R = np.concatenate((R_turn, np.flip(R_turn,axis=1)),axis=1)     # radial distances from central axis
for i in range(N_t*2):
    for j in range(i+1,N_t*2):
        # finding k^2 from Grover
        k_sq = ((y[i] - y[j])**2 + (R[:,i] - R[:,j])**2)/((y[i] - y[j])**2 + (R[:,i] + R[:,j])**2)
        # calculation of f
        f = 0.014468*(np.log10(1/k_sq)-0.53307)
        # calculation of mutual inductance
```

```
        M[i,j] = f*(R[:,i]*R[:,j]*1e-2)**0.5*1e-6
#M_micro = np.round(M * 1e6, 4)      # converting to microhenries
M_micro = M * 1e6

M_trans = np.transpose(M_micro)     # transposing the inductances
M_tot = M_micro + M_trans           # adding matrices
k = 0
for h in range(2*N_t):
    if h >= N_t:
        k = -(1+2*(h-N_t))
    M_tot[h,h] = L_micro[:,k+h]     # adding diagonal elements

M2_fin = M_tot * 1e-6               # from micro to true value 2 disks
K2_rel = np.linalg.inv(M2_fin)      # 2 disks reluctance

M1_fin = M_tot[:N_t,:N_t] * 1e-6    # inductance matrix for 1 disk
K1_rel = np.linalg.inv(M1_fin)      # reluctance matrix for 1 disk
L1 = 1 / np.diag(K1_rel) * 1e6      # new inductances in microHenries

alpha = np.zeros((N_t,N_t))
for i in range(N_t):
    alpha[i,:] = K1_rel[i,:]/K1_rel[i,i]
```

APPENDICES

Appendix B. Mutual inductance function

Inductance_calculation_complex.py

```
""" Function for calculating mutual inductance
"""
import numpy as np

# Table of constant f for k_sq > 0.1
k_sq_L = np.round(np.arange(0.01, 1.01, 0.01), 2)
f_L = np.array([0.021474, .017315, .014937, .013284, .012026, .011017, .010179, .009464, .008843,
.008297, .007810, .007371, .006974, .006611, .006278, .005970, .005685, .005420, .005173, .004941,
.004723, .004518, .004325, .004142, .003969, .003805, .003649, .003500, .003359, .003224, .003095,
.002971, .002853, .002740, .0026317, .0025276, .0024276, .0023315, .0022391, .0021502, .0020646,
.0019821, .0029026, .0018259, .0017519, .0016805, .0016116, .00015451, .0014808, .0014186, .0013585,
.0013004, .0012443, .0011900, .0011374, .0010865, .0010373, .0009897, .0009436, .0008990, .0008558,
.0008141, .0007736, .0007345, .0006966, .0006600, .0006246, .0005903, .0005571, .0005251, .0004941,
.0004642, .0004353, .0004074, .0003805, .0003545, .0003295, .0003054, .0002823, .00025998, .00023859,
.00021806, .00019840, .00017959, .00016162, .00014450, .00012821, .00011276, .00009815, .00008438,
.00007146, .00005940, .00004824, .00003798, .00002866, .00002035, .00001312, .00000708, .00000249,
.0])
diff_L1 = f_L[1:] - f_L[:-1]
diff_L2 = diff_L1[1:] - diff_L1[:-1]
# Table of constant f for k_sq <= 0.1
log_k_sq_S = np.round(np.arange(-6.0, -0.9, 0.1), 1)
k_sq_S = 10**(log_k_sq_S)
f_S = np.array([.079093, .077647, .076200, .074753, .073306, .071860, .070413, .068966, .067520, .066073,
.064626, .063180, .061733, .060287, .058840, .057394, .055947, .054500, .053055, .051609, .050163,
.048717, .047272, .045827, .044382, .042938, .041494, .040051, .038608, .037167, .035727, .034288,
.032851, .031416, .029984, .028554, .027128, .025707, .024291, .022881, .021478, .020084, .018700,
.017329, .015972, .014632, .013311, .012013, .010742, .009502, .008297])
diff_S1 = f_S[1:] - f_S[:-1]
diff_S2 = diff_S1[1:] - diff_S1[:-1]

def f_calc(k_sq):
    if k_sq <= 1e-6:
        # estimating f
        f = 0.014468 * (np.log10(1/k_sq) - 0.53307)
    elif k_sq <= 0.01:
        # calculating log10 of k_sq
        log_k_sq = np.log10(k_sq)
        # flooring the number to the first decimal
        log_k_sq_floor = np.floor(log_k_sq * 10) / 10
        # finding the corresponding value of f
        f1 = f_S[log_k_sq_floor*10 == log_k_sq_S*10]
        # finding the first order difference
        diff1 = diff_S1[(log_k_sq_floor == log_k_sq_S)[:-1]]
        # finding the second-order difference
        diff2 = diff_S2[(log_k_sq_floor == log_k_sq_S)[:-2]]
        # calculating the value of "u"
        u = (log_k_sq - log_k_sq_floor) * 10
        # calculating u2 = (1-u)/2
        u2 = (1 - u) / 2
        # estimating f
        f = f1 + u * (diff1 - u2*diff2)
```

```
        print(log_k_sq_floor, f1, diff1, diff2)
    elif k_sq < 1:
        # flooring the number to the second decimal
        k_sq_floor = np.floor(k_sq * 100) / 100
        # finding corresponding value of f
        f1 = f_L[k_sq_floor == k_sq_L]
        # finding the first-order difference
        diff1 = diff_L1[(k_sq_floor == k_sq_L)[:-1]]
        # finding the second-order difference
        diff2 = diff_L2[(k_sq_floor == k_sq_L)[:-2]]
        # calculating the value "u"
        u = (k_sq - k_sq_floor) * 100
        # calculating u2 = (1-u)/2
        u2 = (1 - u) / 2
        # estimating f
        f = f1 + u * (diff1 - u2*diff2)
    elif k_sq == 1:
        f = 0
    elif k_sq > 1:
        f = []
        print("Error in k_sq")
    return f
```

APPENDICES

Appendix C. AC resistance calculation

```
"""
Resistance calculation

"""
import numpy as np

d = 2.3622      # diameter of conductor (in mm)
t = 1.143       # thickness of insulator (in mm)
D_core = 89     # air core diameter (in mm)
N_d = 10        # number of disks
N_t = 6         # number of turns in each disk
e_r = 4         # relative permittivity of silicon rubber insulator
e_0 = 8.854e-12 # permittivity of free space
Res_dc = 0.00574# DC resistance (Ohm/m)

D_wire = d + 2*t                    # diameter of wire

R_turn = np.zeros((1,N_t))              # initializing turn radius vector (in mm)
R_mean = (N_t/2)*(2*t + d) + D_core/2   # mean radius of disk (in mm)

# Calculation of radii of turns
for i in range(N_t):
   R_turn[:,N_t-1-i] = (D_core/2) + (2*i + 1)*(t + d/2)

# Calculation of AC resistance of coils (coef*sqrt(f))
Res_ac_coef = 0.027678/(Res_dc*(2*np.pi*R_turn*1e-3))**0.5
```

APPENDICES

Appendix D. Turn-to-turn and disk-to-disk capacitances calculation

```
"""
Calculation of turn-to-turn and disk-to-disk capacitances

"""
import numpy as np

d = 2.99        # diameter of conductor (in mm)
t = 1.14        # thickness of insulator (in mm)
D_core = 110    # air core diameter (in mm)
N_d = 10        # number of disks
N_t = 6         # number of turns in each disk
e_r = 4         # relative permittivity of silicon rubber insulator
e_0 = 8.854e-12 # permittivity of free space

D_wire = d + 2*t                    # diameter of wire

R_turn = np.zeros((1,N_t))          # initializing turn radius vector (in mm)
R_mean = (N_t/2)*(2*t + d) + D_core/2   # mean radius of disk (in mm)

# Calculation of radii of turns
for i in range(N_t):
    R_turn[:,N_t-1-i] = (D_core/2) + (2*i + 1)*(t + d/2)

# Calculation of radie of middle of conductors (in mm)
R_mid = R_turn[:,:N_t-1] - (d/2) - t

# Calculation of length of middle of conductors lt (in mm)
l_mid = 2 * np.pi * R_mid

# Calculation of turn-to-turn capacitances between turns of same disk
theta = np.arccos(1 - np.log(D_wire/d)/e_r)     # crossing angle Theta*
Ctt = e_0 * (l_mid*1e-3) * (e_r * theta / np.log(D_wire/d) + 1/np.tan(theta/2) - 1/np.tan(np.pi/12))
Ctt_piko = Ctt * 1e12

# Calculation of disk-to-disk capacitances between turns of adjacent disks
Cdd = e_0 * (2*np.pi*R_turn*1e-3) * (e_r * theta / np.log(D_wire/d) + 1/np.tan(theta/2) - 1/np.tan(np.pi/12))
Cdd_piko = Cdd * 1e12
```

APPENDICES

Appendix E. Netlist generation for winding with 10 disks with 6 turns per disk

```
"""
Generating a netlist for 10 disks

"""

import numpy as np

d = 2.9972      # diameter of conductor (in mm)
t = 1.143       # thickness of insulator (in mm)
D_core = 110    # air core diameter (in mm)
N_d = 10        # number of disks
N_t = 6         # number of turns in each disk
e_r = 4         # relative permittivity of silicon rubber insulator
e_0 = 8.854e-12 # permittivity of free space
r_dc_m = 0.00354# DC resistance (Ohm/m)
r_dc_ft = 1.08  # DC resistance (Ohm/1000feet)
ft_to_m = 0.3048# meter to feet conversion

D_wire = d + 2*t                    # diameter of wire

R_turn = np.zeros((1,N_t))              # initializing turn radius vector (in mm)
R_mean = (N_t/2)*(2*t + d) + D_core/2   # mean radius of disk (in mm)

# Calculation of radii of turns
for i in range(N_t):
    R_turn[:,N_t-1-i] = (D_core/2) + (2*i + 1)*(t + d/2)

# %% Inductance calculation

# Self-induction calculation using Kirchoff equation [59] Grover
L = 4*np.pi*(R_turn*1e-3)*(np.log(8*R_turn/(d/2))-1.75)*1e-7
#L_micro = np.round(L * 1e6, 4)
L_micro = L * 1e6

# Mutual inductance calculation for filament (3 or more disks)
M = np.zeros((N_t*N_d,N_t*N_d))     # initializing mutual inductance matrix
y = []                          # vertical distance of center of coils from top coil
R = R_turn                          # initialize the radial distance vector
Rflip = R_turn                      # flipping radial dimensions
for i in range(N_d):
    y += [i * (d + 2*t)]*6   # distances between center of coils
for i in range(N_d-1):
    R = np.concatenate((R, np.flip(Rflip,axis=1)),axis=1)     # radial distances from central axis
    Rflip = np.flip(Rflip,axis=1)

for i in range(N_t*N_d):
    for j in range(i+1,N_t*N_d):
        # finding k^2 from Grover
        k_sq = ((y[i] - y[j])**2 + (R[:,i] - R[:,j])**2)/((y[i] - y[j])**2 + (R[:,i] + R[:,j])**2)
        # calculation of f
        f = 0.014468*(np.log10(1/k_sq)-0.53307)
        # calculation of mutual inductance
        M[i,j] = f*(R[:,i]*R[:,j]*1e-2)**0.5*1e-6
```

APPENDICES

```
#M_micro = np.round(M * 1e6, 4)      # converting to microhenries
M_micro = M * 1e6

M_trans = np.transpose(M_micro)     # transposing the inductances
M_tot = M_micro + M_trans           # adding matrices
index_flip = np.arange(N_t)         # index of self-inductance
cur_disk = 1                        # current disk
cc = 0                              # counter of turns
for h in range(N_d*N_t):
    M_tot[h,h] = L_micro[:,index_flip[h-N_t*(cur_disk-1)]]     # adding diagonal elements
    cc += 1                         # increment turn number
    if cc == N_t:
        cur_disk += 1               # increment disk counter
        cc = 0                      # nullify turn counter
        index_flip = np.flip(index_flip, axis=0)        # flip index vector


M_fin = M_tot * 1e-6                # from micro to true value 2 disks
K_rel = np.linalg.inv(M_fin)      # 2 disks reluctance

#M1_fin = M_tot[:N_t,:N_t] * 1e-6    # inductance matrix for 1 disk
#K1_rel = np.linalg.inv(M1_fin)      # reluctance matrix for 1 disk
Lnew = 1 / np.diag(K_rel) * 1e6      # new inductances in microHenries

alpha = np.zeros((N_t*N_d,N_t*N_d))
for i in range(N_t*N_d):
    alpha[i,:] = K_rel[i,:]/K_rel[i,i]

# %% Capacitance calculation

# Calculation of radie of middle of conductors (in mm)
R_mid = R_turn[:,:N_t-1] - (d/2) - t

# Calculation of length of middle of conductors lt (in mm)
l_mid = 2 * np.pi * R_mid

# Calculation of turn-to-turn capacitances between turns of same disk
theta = np.arccos(1 - np.log(D_wire/d)/e_r)     # crossing angle Theta*
Ctt = e_0 * (l_mid*1e-3) * (e_r * theta / np.log(D_wire/d) + 1/np.tan(theta/2) - 1/np.tan(np.pi/12))
Ctt_piko = Ctt * 1e12
Ctt_p = Ctt_piko

# Calculation of disk-to-disk capacitances between turns of adjacent disks
Cdd = e_0 * (2*np.pi*R_turn*1e-3) * (e_r * theta / np.log(D_wire/d) + 1/np.tan(theta/2) - 1/np.tan(np.pi/12))
Cdd_piko = Cdd * 1e12

# %% Calculation of AC resistance coefficient

# Calculation of AC resistance of coils (coef*sqrt(f))
Res_ac_coef = 0.027678/(r_dc_ft)**0.5
Res_ac_wire = ((2*np.pi*R_turn*1e-3) * (r_dc_ft/(ft_to_m*1e3))) * Res_ac_coef
r_ac = Res_ac_wire

# %% Generating a SPICE netlist for 10 disks
filename = "netlist_10disk.txt"  # name of the txt file
N_d = 10                         # number of disks
```

APPENDICES

```
cc = 0                      # counter of turns of disk
cur_disk = 1                # current disk number
with open(filename, "w") as nt:
   for i in range(N_t*N_d):
      nt.write("\nL{} N{}P1 N{}P2 {:0.4f}u\n".format(i+1, i+1, i+1, Lnew[i]))
      pn = 2                # node point N1P2
      for j in range(N_t*N_d):
         if j!=i:
            pn += 1         # move through node
            nt.write("E{}_{} N{}P{} N{}P{} N{}P{} N{}P{} {:0.4f}\n".format(i+1, j+1, i+1, pn, i+1, pn-1,
j+1, 1, j+1, N_t*N_d+1, alpha[i,j]))

      nt.write("R%d N%dP%d N%dP%d R=1 LAPLACE=+1/{K%d}/(-S*S/4/3.14^2)^0.25\n" % (i+1, i+1,
pn, i+2, 1, i+1))
      nt.write(".param K%d=%0.4e\n" % (i+1, r_ac[:,i-N_t*(cur_disk-1)]))

      cc += 1               # increment counter
      if cc < N_t:
         nt.write("Ctt%d_%d N%dP%d N%dP%d %0.2fp\n" % (i+1, i+2, i+1, 1, i+2, 1, Ctt_p[:,i-
N_t*(cur_disk-1)])) #

      elif cc == N_t:
         cc = 0             # nullify the counter (new disk)
         Ctt_p = np.flip(Ctt_p, axis=1)
         cur_disk += 1      # increment disk number
         r_ac = np.flip(r_ac, axis=1)

   nt.write("\n")
   Cdd_flip = Cdd_piko        # vector of disk-to-disk capacitance
   Cdd_print = Cdd_piko       # first 6 Cdds
   for i in range(N_d-2):
      Cdd_print = np.concatenate((Cdd_print, np.flip(Cdd_flip, axis=1)),axis=1)
      Cdd_flip = np.flip(Cdd_flip, axis=1)
   cur_disk = 1               # current disk number
   cc = 0                     # counter of turn
   for i in range(N_t*(N_d-1)):
      nt.write("Cdd%d_%d N%dP%d N%dP%d %0.2fp\n" % (i+1, 2*cur_disk*N_t-i, i+1, 1,
2*cur_disk*N_t-i, 1, Cdd_print[:,i]))
      cc += 1
      if cc == N_t:
         cur_disk += 1
         cc = 0


   nt.write("\nV1 In 0 AC 10\n")
   nt.write("Rin In N1P1 50\n")
   nt.write("Rout N{}P1 0 50\n".format(N_d*N_t+1))
   nt.write(".print V(N{}P1)\n".format(N_d*N_t+1))
   nt.write(".print V(In)\n")
   nt.write("\n.ac dec 1000 10 200000k\n.backanno\n.end\n")
```

APPENDICES

Appendix F. Netlist for winding with 10 disks with 6 turns per disk

```
L1 N1P1 N1P2 0.2086u
E1_2 N1P3 N1P2 N2P1 N2P61 -0.3780
E1_3 N1P4 N1P3 N3P1 N3P61 -0.0246
E1_4 N1P5 N1P4 N4P1 N4P61 -0.0200
E1_5 N1P6 N1P5 N5P1 N5P61 -0.0118
E1_6 N1P7 N1P6 N6P1 N6P61 -0.0103
E1_7 N1P8 N1P7 N7P1 N7P61 -0.0002
E1_8 N1P9 N1P8 N8P1 N8P61 0.0008
E1_9 N1P10 N1P9 N9P1 N9P61 0.0010
E1_10 N1P11 N1P10 N10P1 N10P61 0.0072
E1_11 N1P12 N1P11 N11P1 N11P61 -0.0515
E1_12 N1P13 N1P12 N12P1 N12P61 -0.3663
E1_13 N1P14 N1P13 N13P1 N13P61 -0.0235
E1_14 N1P15 N1P14 N14P1 N14P61 0.0070
E1_15 N1P16 N1P15 N15P1 N15P61 0.0006
E1_16 N1P17 N1P16 N16P1 N16P61 -0.0002
E1_17 N1P18 N1P17 N17P1 N17P61 -0.0001
E1_18 N1P19 N1P18 N18P1 N18P61 0.0002
E1_19 N1P20 N1P19 N19P1 N19P61 0.0006
E1_20 N1P21 N1P20 N20P1 N20P61 -0.0000
E1_21 N1P22 N1P21 N21P1 N21P61 -0.0000
E1_22 N1P23 N1P22 N22P1 N22P61 -0.0002
E1_23 N1P24 N1P23 N23P1 N23P61 0.0010
E1_24 N1P25 N1P24 N24P1 N24P61 -0.0186
E1_25 N1P26 N1P25 N25P1 N25P61 -0.0109
E1_26 N1P27 N1P26 N26P1 N26P61 0.0007
E1_27 N1P28 N1P27 N27P1 N27P61 -0.0000
E1_28 N1P29 N1P28 N28P1 N28P61 0.0000
E1_29 N1P30 N1P29 N29P1 N29P61 -0.0000
E1_30 N1P31 N1P30 N30P1 N30P61 0.0008
E1_31 N1P32 N1P31 N31P1 N31P61 0.0010
E1_32 N1P33 N1P32 N32P1 N32P61 -0.0001
E1_33 N1P34 N1P33 N33P1 N33P61 0.0000
E1_34 N1P35 N1P34 N34P1 N34P61 -0.0000
E1_35 N1P36 N1P35 N35P1 N35P61 0.0005
E1_36 N1P37 N1P36 N36P1 N36P61 -0.0074
E1_37 N1P38 N1P37 N37P1 N37P61 -0.0053
E1_38 N1P39 N1P38 N38P1 N38P61 0.0003
E1_39 N1P40 N1P39 N39P1 N39P61 -0.0000
E1_40 N1P41 N1P40 N40P1 N40P61 0.0000
E1_41 N1P42 N1P41 N41P1 N41P61 -0.0001
E1_42 N1P43 N1P42 N42P1 N42P61 0.0011
E1_43 N1P44 N1P43 N43P1 N43P61 0.0013
E1_44 N1P45 N1P44 N44P1 N44P61 -0.0001
E1_45 N1P46 N1P45 N45P1 N45P61 0.0000
E1_46 N1P47 N1P46 N46P1 N46P61 -0.0000
E1_47 N1P48 N1P47 N47P1 N47P61 0.0003
E1_48 N1P49 N1P48 N48P1 N48P61 -0.0041
E1_49 N1P50 N1P49 N49P1 N49P61 -0.0032
E1_50 N1P51 N1P50 N50P1 N50P61 0.0002
E1_51 N1P52 N1P51 N51P1 N51P61 -0.0000
E1_52 N1P53 N1P52 N52P1 N52P61 -0.0000
E1_53 N1P54 N1P53 N53P1 N53P61 -0.0001
E1_54 N1P55 N1P54 N54P1 N54P61 0.0014
E1_55 N1P56 N1P55 N55P1 N55P61 0.0029
E1_56 N1P57 N1P56 N56P1 N56P61 0.0007
E1_57 N1P58 N1P57 N57P1 N57P61 0.0003
E1_58 N1P59 N1P58 N58P1 N58P61 -0.0000
E1_59 N1P60 N1P59 N59P1 N59P61 -0.0003
E1_60 N1P61 N1P60 N60P1 N60P61 -0.0038
R1 N1P61 N2P1 R=1 LAPLACE=+1/{K1}/(-
S*S/4/3.14^2)^0.25
.param K1=4.9841e-05
Ctt1_2 N1P1 N2P1 16.72p

L2 N2P1 N2P2 0.1660u
E2_1 N2P3 N2P2 N1P1 N1P61 -0.3008
E2_3 N2P4 N2P3 N3P1 N3P61 -0.3127
E2_4 N2P5 N2P4 N4P1 N4P61 -0.0130
E2_5 N2P6 N2P5 N5P1 N5P61 -0.0124
E2_6 N2P7 N2P6 N6P1 N6P61 -0.0093
E2_7 N2P8 N2P7 N7P1 N7P61 -0.0005
E2_8 N2P9 N2P8 N8P1 N8P61 0.0006
E2_9 N2P10 N2P9 N9P1 N9P61 0.0059
E2_10 N2P11 N2P10 N10P1 N10P61 -0.0494
E2_11 N2P12 N2P11 N11P1 N11P61 -0.2364
E2_12 N2P13 N2P12 N12P1 N12P61 -0.0491
E2_13 N2P14 N2P13 N13P1 N13P61 0.0018
E2_14 N2P15 N2P14 N14P1 N14P61 0.0109
E2_15 N2P16 N2P15 N15P1 N15P61 0.0037
E2_16 N2P17 N2P16 N16P1 N16P61 0.0007
E2_17 N2P18 N2P17 N17P1 N17P61 -0.0001
E2_18 N2P19 N2P18 N18P1 N18P61 -0.0003
E2_19 N2P20 N2P19 N19P1 N19P61 -0.0000
E2_20 N2P21 N2P20 N20P1 N20P61 -0.0000
E2_21 N2P22 N2P21 N21P1 N21P61 -0.0001
E2_22 N2P23 N2P22 N22P1 N22P61 -0.0003
E2_23 N2P24 N2P23 N23P1 N23P61 -0.0005
E2_24 N2P25 N2P24 N24P1 N24P61 -0.0016
E2_25 N2P26 N2P25 N25P1 N25P61 -0.0010
E2_26 N2P27 N2P26 N26P1 N26P61 0.0001
E2_27 N2P28 N2P27 N27P1 N27P61 0.0000
E2_28 N2P29 N2P28 N28P1 N28P61 0.0000
E2_29 N2P30 N2P29 N29P1 N29P61 -0.0000
E2_30 N2P31 N2P30 N30P1 N30P61 0.0002
E2_31 N2P32 N2P31 N31P1 N31P61 0.0003
E2_32 N2P33 N2P32 N32P1 N32P61 -0.0000
E2_33 N2P34 N2P33 N33P1 N33P61 0.0000
E2_34 N2P35 N2P34 N34P1 N34P61 -0.0000
E2_35 N2P36 N2P35 N35P1 N35P61 0.0000
E2_36 N2P37 N2P36 N36P1 N36P61 -0.0008
E2_37 N2P38 N2P37 N37P1 N37P61 -0.0006
E2_38 N2P39 N2P38 N38P1 N38P61 0.0000
E2_39 N2P40 N2P39 N39P1 N39P61 -0.0000
```

E2_40 N2P41 N2P40 N40P1 N40P61 0.0000
E2_41 N2P42 N2P41 N41P1 N41P61 -0.0000
E2_42 N2P43 N2P42 N42P1 N42P61 0.0004
E2_43 N2P44 N2P43 N43P1 N43P61 0.0004
E2_44 N2P45 N2P44 N44P1 N44P61 -0.0000
E2_45 N2P46 N2P45 N45P1 N45P61 0.0000
E2_46 N2P47 N2P46 N46P1 N46P61 -0.0000
E2_47 N2P48 N2P47 N47P1 N47P61 0.0000
E2_48 N2P49 N2P48 N48P1 N48P61 -0.0005
E2_49 N2P50 N2P49 N49P1 N49P61 -0.0004
E2_50 N2P51 N2P50 N50P1 N50P61 0.0000
E2_51 N2P52 N2P51 N51P1 N51P61 -0.0000
E2_52 N2P53 N2P52 N52P1 N52P61 -0.0000
E2_53 N2P54 N2P53 N53P1 N53P61 -0.0001
E2_54 N2P55 N2P54 N54P1 N54P61 0.0005
E2_55 N2P56 N2P55 N55P1 N55P61 0.0012
E2_56 N2P57 N2P56 N56P1 N56P61 0.0004
E2_57 N2P58 N2P57 N57P1 N57P61 0.0003
E2_58 N2P59 N2P58 N58P1 N58P61 0.0002
E2_59 N2P60 N2P59 N59P1 N59P61 0.0001
E2_60 N2P61 N2P60 N60P1 N60P61 -0.0003
R2 N2P61 N3P1 R=1 LAPLACE=+1/{K2}/(-S*S/4/3.14^2)^0.25
.param K2=4.6709e-05
Ctt2_3 N2P1 N3P1 15.64p

L3 N3P1 N3P2 0.1548u
E3_1 N3P3 N3P2 N1P1 N1P61 -0.0183
E3_2 N3P4 N3P3 N2P1 N2P61 -0.2916
E3_4 N3P5 N3P4 N4P1 N4P61 -0.3130
E3_5 N3P6 N3P5 N5P1 N5P61 -0.0129
E3_6 N3P7 N3P6 N6P1 N6P61 -0.0160
E3_7 N3P8 N3P7 N7P1 N7P61 -0.0011
E3_8 N3P9 N3P8 N8P1 N8P61 0.0060
E3_9 N3P10 N3P9 N9P1 N9P61 -0.0495
E3_10 N3P11 N3P10 N10P1 N10P61 -0.2365
E3_11 N3P12 N3P11 N11P1 N11P61 -0.0458
E3_12 N3P13 N3P12 N12P1 N12P61 0.0018
E3_13 N3P14 N3P13 N13P1 N13P61 -0.0012
E3_14 N3P15 N3P14 N14P1 N14P61 0.0036
E3_15 N3P16 N3P15 N15P1 N15P61 0.0108
E3_16 N3P17 N3P16 N16P1 N16P61 0.0037
E3_17 N3P18 N3P17 N17P1 N17P61 0.0007
E3_18 N3P19 N3P18 N18P1 N18P61 -0.0008
E3_19 N3P20 N3P19 N19P1 N19P61 -0.0002
E3_20 N3P21 N3P20 N20P1 N20P61 -0.0000
E3_21 N3P22 N3P21 N21P1 N21P61 -0.0003
E3_22 N3P23 N3P22 N22P1 N22P61 -0.0006
E3_23 N3P24 N3P23 N23P1 N23P61 -0.0002
E3_24 N3P25 N3P24 N24P1 N24P61 -0.0012
E3_25 N3P26 N3P25 N25P1 N25P61 -0.0008
E3_26 N3P27 N3P26 N26P1 N26P61 0.0001
E3_27 N3P28 N3P27 N27P1 N27P61 0.0000
E3_28 N3P29 N3P28 N28P1 N28P61 0.0000
E3_29 N3P30 N3P29 N29P1 N29P61 0.0000
E3_30 N3P31 N3P30 N30P1 N30P61 0.0000
E3_31 N3P32 N3P31 N31P1 N31P61 0.0002
E3_32 N3P33 N3P32 N32P1 N32P61 -0.0000
E3_33 N3P34 N3P33 N33P1 N33P61 -0.0000
E3_34 N3P35 N3P34 N34P1 N34P61 -0.0000
E3_35 N3P36 N3P35 N35P1 N35P61 0.0000
E3_36 N3P37 N3P36 N36P1 N36P61 -0.0006
E3_37 N3P38 N3P37 N37P1 N37P61 -0.0004
E3_38 N3P39 N3P38 N38P1 N38P61 0.0000
E3_39 N3P40 N3P39 N39P1 N39P61 -0.0000
E3_40 N3P41 N3P40 N40P1 N40P61 0.0000
E3_41 N3P42 N3P41 N41P1 N41P61 -0.0000
E3_42 N3P43 N3P42 N42P1 N42P61 0.0003
E3_43 N3P44 N3P43 N43P1 N43P61 0.0004
E3_44 N3P45 N3P44 N44P1 N44P61 -0.0000
E3_45 N3P46 N3P45 N45P1 N45P61 0.0000
E3_46 N3P47 N3P46 N46P1 N46P61 -0.0000
E3_47 N3P48 N3P47 N47P1 N47P61 0.0000
E3_48 N3P49 N3P48 N48P1 N48P61 -0.0003
E3_49 N3P50 N3P49 N49P1 N49P61 -0.0002
E3_50 N3P51 N3P50 N50P1 N50P61 0.0000
E3_51 N3P52 N3P51 N51P1 N51P61 -0.0000
E3_52 N3P53 N3P52 N52P1 N52P61 -0.0000
E3_53 N3P54 N3P53 N53P1 N53P61 -0.0001
E3_54 N3P55 N3P54 N54P1 N54P61 0.0005
E3_55 N3P56 N3P55 N55P1 N55P61 0.0012
E3_56 N3P57 N3P56 N56P1 N56P61 0.0004
E3_57 N3P58 N3P57 N57P1 N57P61 0.0003
E3_58 N3P59 N3P58 N58P1 N58P61 0.0002
E3_59 N3P60 N3P59 N59P1 N59P61 0.0002
E3_60 N3P61 N3P60 N60P1 N60P61 -0.0000
R3 N3P61 N4P1 R=1 LAPLACE=+1/{K3}/(-S*S/4/3.14^2)^0.25
.param K3=4.3576e-05
Ctt3_4 N3P1 N4P1 14.55p

L4 N4P1 N4P2 0.1436u
E4_1 N4P3 N4P2 N1P1 N1P61 -0.0138
E4_2 N4P4 N4P3 N2P1 N2P61 -0.0113
E4_3 N4P5 N4P4 N3P1 N3P61 -0.2904
E4_5 N4P6 N4P5 N5P1 N5P61 -0.3139
E4_6 N4P7 N4P6 N6P1 N6P61 -0.0195
E4_7 N4P8 N4P7 N7P1 N7P61 0.0030
E4_8 N4P9 N4P8 N8P1 N8P61 -0.0494
E4_9 N4P10 N4P9 N9P1 N9P61 -0.2365
E4_10 N4P11 N4P10 N10P1 N10P61 -0.0459
E4_11 N4P12 N4P11 N11P1 N11P61 0.0052
E4_12 N4P13 N4P12 N12P1 N12P61 -0.0014
E4_13 N4P14 N4P13 N13P1 N13P61 -0.0011
E4_14 N4P15 N4P14 N14P1 N14P61 0.0007
E4_15 N4P16 N4P15 N15P1 N15P61 0.0035
E4_16 N4P17 N4P16 N16P1 N16P61 0.0108
E4_17 N4P18 N4P17 N17P1 N17P61 0.0038
E4_18 N4P19 N4P18 N18P1 N18P61 -0.0006
E4_19 N4P20 N4P19 N19P1 N19P61 -0.0006
E4_20 N4P21 N4P20 N20P1 N20P61 -0.0002
E4_21 N4P22 N4P21 N21P1 N21P61 -0.0006

E4_22 N4P23 N4P22 N22P1 N22P61 -0.0002
E4_23 N4P24 N4P23 N23P1 N23P61 -0.0000
E4_24 N4P25 N4P24 N24P1 N24P61 -0.0007
E4_25 N4P26 N4P25 N25P1 N25P61 -0.0005
E4_26 N4P27 N4P26 N26P1 N26P61 0.0000
E4_27 N4P28 N4P27 N27P1 N27P61 0.0000
E4_28 N4P29 N4P28 N28P1 N28P61 0.0000
E4_29 N4P30 N4P29 N29P1 N29P61 0.0000
E4_30 N4P31 N4P30 N30P1 N30P61 -0.0002
E4_31 N4P32 N4P31 N31P1 N31P61 0.0000
E4_32 N4P33 N4P32 N32P1 N32P61 -0.0000
E4_33 N4P34 N4P33 N33P1 N33P61 -0.0000
E4_34 N4P35 N4P34 N34P1 N34P61 -0.0000
E4_35 N4P36 N4P35 N35P1 N35P61 0.0000
E4_36 N4P37 N4P36 N36P1 N36P61 -0.0003
E4_37 N4P38 N4P37 N37P1 N37P61 -0.0002
E4_38 N4P39 N4P38 N38P1 N38P61 0.0000
E4_39 N4P40 N4P39 N39P1 N39P61 -0.0000
E4_40 N4P41 N4P40 N40P1 N40P61 0.0000
E4_41 N4P42 N4P41 N41P1 N41P61 -0.0000
E4_42 N4P43 N4P42 N42P1 N42P61 0.0002
E4_43 N4P44 N4P43 N43P1 N43P61 0.0003
E4_44 N4P45 N4P44 N44P1 N44P61 -0.0000
E4_45 N4P46 N4P45 N45P1 N45P61 0.0000
E4_46 N4P47 N4P46 N46P1 N46P61 0.0000
E4_47 N4P48 N4P47 N47P1 N47P61 0.0000
E4_48 N4P49 N4P48 N48P1 N48P61 -0.0001
E4_49 N4P50 N4P49 N49P1 N49P61 -0.0001
E4_50 N4P51 N4P50 N50P1 N50P61 -0.0000
E4_51 N4P52 N4P51 N51P1 N51P61 -0.0000
E4_52 N4P53 N4P52 N52P1 N52P61 -0.0000
E4_53 N4P54 N4P53 N53P1 N53P61 -0.0001
E4_54 N4P55 N4P54 N54P1 N54P61 0.0004
E4_55 N4P56 N4P55 N55P1 N55P61 0.0012
E4_56 N4P57 N4P56 N56P1 N56P61 0.0004
E4_57 N4P58 N4P57 N57P1 N57P61 0.0003
E4_58 N4P59 N4P58 N58P1 N58P61 0.0003
E4_59 N4P60 N4P59 N59P1 N59P61 0.0002
E4_60 N4P61 N4P60 N60P1 N60P61 0.0002
R4 N4P61 N5P1 R=1 LAPLACE=+1/{K4}/(-
S*S/4/3.14^2)^0.25
.param K4=4.0443e-05
Ctt4_5 N4P1 N5P1 13.47p

L5 N5P1 N5P2 0.1325u
E5_1 N5P3 N5P2 N1P1 N1P61 -0.0075
E5_2 N5P4 N5P3 N2P1 N2P61 -0.0099
E5_3 N5P5 N5P4 N3P1 N3P61 -0.0111
E5_4 N5P6 N5P5 N4P1 N4P61 -0.2896
E5_6 N5P7 N5P6 N6P1 N6P61 -0.3222
E5_7 N5P8 N5P7 N7P1 N7P61 -0.0519
E5_8 N5P9 N5P8 N8P1 N8P61 -0.2364
E5_9 N5P10 N5P9 N9P1 N9P61 -0.0458
E5_10 N5P11 N5P10 N10P1 N10P61 0.0051
E5_11 N5P12 N5P11 N11P1 N11P61 0.0005
E5_12 N5P13 N5P12 N12P1 N12P61 -0.0008
E5_13 N5P14 N5P13 N13P1 N13P61 -0.0007
E5_14 N5P15 N5P14 N14P1 N14P61 -0.0001
E5_15 N5P16 N5P15 N15P1 N15P61 0.0006
E5_16 N5P17 N5P16 N16P1 N16P61 0.0035
E5_17 N5P18 N5P17 N17P1 N17P61 0.0108
E5_18 N5P19 N5P18 N18P1 N18P61 0.0030
E5_19 N5P20 N5P19 N19P1 N19P61 -0.0008
E5_20 N5P21 N5P20 N20P1 N20P61 -0.0006
E5_21 N5P22 N5P21 N21P1 N21P61 -0.0002
E5_22 N5P23 N5P22 N22P1 N22P61 -0.0000
E5_23 N5P24 N5P23 N23P1 N23P61 0.0000
E5_24 N5P25 N5P24 N24P1 N24P61 -0.0004
E5_25 N5P26 N5P25 N25P1 N25P61 -0.0003
E5_26 N5P27 N5P26 N26P1 N26P61 0.0000
E5_27 N5P28 N5P27 N27P1 N27P61 0.0000
E5_28 N5P29 N5P28 N28P1 N28P61 0.0000
E5_29 N5P30 N5P29 N29P1 N29P61 0.0000
E5_30 N5P31 N5P30 N30P1 N30P61 -0.0002
E5_31 N5P32 N5P31 N31P1 N31P61 -0.0000
E5_32 N5P33 N5P32 N32P1 N32P61 0.0000
E5_33 N5P34 N5P33 N33P1 N33P61 -0.0000
E5_34 N5P35 N5P34 N34P1 N34P61 -0.0000
E5_35 N5P36 N5P35 N35P1 N35P61 0.0000
E5_36 N5P37 N5P36 N36P1 N36P61 -0.0002
E5_37 N5P38 N5P37 N37P1 N37P61 -0.0001
E5_38 N5P39 N5P38 N38P1 N38P61 0.0000
E5_39 N5P40 N5P39 N39P1 N39P61 -0.0000
E5_40 N5P41 N5P40 N40P1 N40P61 0.0000
E5_41 N5P42 N5P41 N41P1 N41P61 -0.0000
E5_42 N5P43 N5P42 N42P1 N42P61 0.0001
E5_43 N5P44 N5P43 N43P1 N43P61 0.0003
E5_44 N5P45 N5P44 N44P1 N44P61 -0.0000
E5_45 N5P46 N5P45 N45P1 N45P61 0.0000
E5_46 N5P47 N5P46 N46P1 N46P61 0.0000
E5_47 N5P48 N5P47 N47P1 N47P61 0.0000
E5_48 N5P49 N5P48 N48P1 N48P61 -0.0000
E5_49 N5P50 N5P49 N49P1 N49P61 0.0000
E5_50 N5P51 N5P50 N50P1 N50P61 -0.0000
E5_51 N5P52 N5P51 N51P1 N51P61 -0.0000
E5_52 N5P53 N5P52 N52P1 N52P61 -0.0000
E5_53 N5P54 N5P53 N53P1 N53P61 -0.0001
E5_54 N5P55 N5P54 N54P1 N54P61 0.0004
E5_55 N5P56 N5P55 N55P1 N55P61 0.0012
E5_56 N5P57 N5P56 N56P1 N56P61 0.0005
E5_57 N5P58 N5P57 N57P1 N57P61 0.0004
E5_58 N5P59 N5P58 N58P1 N58P61 0.0003
E5_59 N5P60 N5P59 N59P1 N59P61 0.0003
E5_60 N5P61 N5P60 N60P1 N60P61 0.0004
R5 N5P61 N6P1 R=1 LAPLACE=+1/{K5}/(-
S*S/4/3.14^2)^0.25
.param K5=3.7311e-05
Ctt5_6 N5P1 N6P1 12.38p

L6 N6P1 N6P2 0.1417u
E6_1 N6P3 N6P2 N1P1 N1P61 -0.0070
E6_2 N6P4 N6P3 N2P1 N2P61 -0.0079

APPENDICES

E6_3 N6P5 N6P4 N3P1 N3P61 -0.0147
E6_4 N6P6 N6P5 N4P1 N4P61 -0.0192
E6_5 N6P7 N6P6 N5P1 N5P61 -0.3447
E6_7 N6P8 N6P7 N7P1 N7P61 -0.3588
E6_8 N6P9 N6P8 N8P1 N8P61 -0.0477
E6_9 N6P10 N6P9 N9P1 N9P61 0.0060
E6_10 N6P11 N6P10 N10P1 N10P61 0.0007
E6_11 N6P12 N6P11 N11P1 N11P61 0.0006
E6_12 N6P13 N6P12 N12P1 N12P61 -0.0006
E6_13 N6P14 N6P13 N13P1 N13P61 -0.0004
E6_14 N6P15 N6P14 N14P1 N14P61 -0.0000
E6_15 N6P16 N6P15 N15P1 N15P61 -0.0001
E6_16 N6P17 N6P16 N16P1 N16P61 0.0005
E6_17 N6P18 N6P17 N17P1 N17P61 0.0062
E6_18 N6P19 N6P18 N18P1 N18P61 -0.0194
E6_19 N6P20 N6P19 N19P1 N19P61 -0.0148
E6_20 N6P21 N6P20 N20P1 N20P61 0.0007
E6_21 N6P22 N6P21 N21P1 N21P61 -0.0001
E6_22 N6P23 N6P22 N22P1 N22P61 -0.0000
E6_23 N6P24 N6P23 N23P1 N23P61 0.0000
E6_24 N6P25 N6P24 N24P1 N24P61 -0.0001
E6_25 N6P26 N6P25 N25P1 N25P61 0.0000
E6_26 N6P27 N6P26 N26P1 N26P61 -0.0000
E6_27 N6P28 N6P27 N27P1 N27P61 0.0000
E6_28 N6P29 N6P28 N28P1 N28P61 -0.0000
E6_29 N6P30 N6P29 N29P1 N29P61 0.0005
E6_30 N6P31 N6P30 N30P1 N30P61 -0.0073
E6_31 N6P32 N6P31 N31P1 N31P61 -0.0040
E6_32 N6P33 N6P32 N32P1 N32P61 0.0002
E6_33 N6P34 N6P33 N33P1 N33P61 -0.0000
E6_34 N6P35 N6P34 N34P1 N34P61 0.0000
E6_35 N6P36 N6P35 N35P1 N35P61 -0.0000
E6_36 N6P37 N6P36 N36P1 N36P61 0.0002
E6_37 N6P38 N6P37 N37P1 N37P61 0.0003
E6_38 N6P39 N6P38 N38P1 N38P61 -0.0000
E6_39 N6P40 N6P39 N39P1 N39P61 0.0000
E6_40 N6P41 N6P40 N40P1 N40P61 -0.0000
E6_41 N6P42 N6P41 N41P1 N41P61 0.0001
E6_42 N6P43 N6P42 N42P1 N42P61 -0.0020
E6_43 N6P44 N6P43 N43P1 N43P61 -0.0007
E6_44 N6P45 N6P44 N44P1 N44P61 0.0001
E6_45 N6P46 N6P45 N45P1 N45P61 0.0000
E6_46 N6P47 N6P46 N46P1 N46P61 0.0000
E6_47 N6P48 N6P47 N47P1 N47P61 -0.0000
E6_48 N6P49 N6P48 N48P1 N48P61 0.0004
E6_49 N6P50 N6P49 N49P1 N49P61 0.0006
E6_50 N6P51 N6P50 N50P1 N50P61 -0.0001
E6_51 N6P52 N6P51 N51P1 N51P61 -0.0001
E6_52 N6P53 N6P52 N52P1 N52P61 -0.0001
E6_53 N6P54 N6P53 N53P1 N53P61 -0.0001
E6_54 N6P55 N6P54 N54P1 N54P61 0.0001
E6_55 N6P56 N6P55 N55P1 N55P61 0.0027
E6_56 N6P57 N6P56 N56P1 N56P61 0.0013
E6_57 N6P58 N6P57 N57P1 N57P61 0.0012
E6_58 N6P59 N6P58 N58P1 N58P61 0.0011
E6_59 N6P60 N6P59 N59P1 N59P61 0.0010
E6_60 N6P61 N6P60 N60P1 N60P61 0.0020
R6 N6P61 N7P1 R=1 LAPLACE=+1/{K6}/(-S*S/4/3.14^2)^0.25
.param K6=3.4178e-05

L7 N7P1 N7P2 0.1213u
E7_1 N7P3 N7P2 N1P1 N1P61 -0.0001
E7_2 N7P4 N7P3 N2P1 N2P61 -0.0004
E7_3 N7P5 N7P4 N3P1 N3P61 -0.0008
E7_4 N7P6 N7P5 N4P1 N4P61 0.0025
E7_5 N7P7 N7P6 N5P1 N5P61 -0.0475
E7_6 N7P8 N7P7 N6P1 N6P61 -0.3070
E7_8 N7P9 N7P8 N8P1 N8P61 -0.2261
E7_9 N7P10 N7P9 N9P1 N9P61 0.0100
E7_10 N7P11 N7P10 N10P1 N10P61 -0.0005
E7_11 N7P12 N7P11 N11P1 N11P61 0.0000
E7_12 N7P13 N7P12 N12P1 N12P61 0.0001
E7_13 N7P14 N7P13 N13P1 N13P61 0.0001
E7_14 N7P15 N7P14 N14P1 N14P61 0.0000
E7_15 N7P16 N7P15 N15P1 N15P61 -0.0002
E7_16 N7P17 N7P16 N16P1 N16P61 0.0033
E7_17 N7P18 N7P17 N17P1 N17P61 -0.0456
E7_18 N7P19 N7P18 N18P1 N18P61 -0.3003
E7_19 N7P20 N7P19 N19P1 N19P61 -0.0108
E7_20 N7P21 N7P20 N20P1 N20P61 0.0052
E7_21 N7P22 N7P21 N21P1 N21P61 0.0006
E7_22 N7P23 N7P22 N22P1 N22P61 -0.0000
E7_23 N7P24 N7P23 N23P1 N23P61 -0.0000
E7_24 N7P25 N7P24 N24P1 N24P61 0.0002
E7_25 N7P26 N7P25 N25P1 N25P61 0.0002
E7_26 N7P27 N7P26 N26P1 N26P61 -0.0000
E7_27 N7P28 N7P27 N27P1 N27P61 -0.0000
E7_28 N7P29 N7P28 N28P1 N28P61 -0.0001
E7_29 N7P30 N7P29 N29P1 N29P61 0.0004
E7_30 N7P31 N7P30 N30P1 N30P61 -0.0099
E7_31 N7P32 N7P31 N31P1 N31P61 -0.0048
E7_32 N7P33 N7P32 N32P1 N32P61 0.0003
E7_33 N7P34 N7P33 N33P1 N33P61 -0.0000
E7_34 N7P35 N7P34 N34P1 N34P61 0.0000
E7_35 N7P36 N7P35 N35P1 N35P61 -0.0000
E7_36 N7P37 N7P36 N36P1 N36P61 0.0002
E7_37 N7P38 N7P37 N37P1 N37P61 0.0002
E7_38 N7P39 N7P38 N38P1 N38P61 -0.0000
E7_39 N7P40 N7P39 N39P1 N39P61 0.0000
E7_40 N7P41 N7P40 N40P1 N40P61 -0.0000
E7_41 N7P42 N7P41 N41P1 N41P61 0.0002
E7_42 N7P43 N7P42 N42P1 N42P61 -0.0027
E7_43 N7P44 N7P43 N43P1 N43P61 -0.0015
E7_44 N7P45 N7P44 N44P1 N44P61 0.0001
E7_45 N7P46 N7P45 N45P1 N45P61 -0.0000
E7_46 N7P47 N7P46 N46P1 N46P61 0.0000
E7_47 N7P48 N7P47 N47P1 N47P61 -0.0000
E7_48 N7P49 N7P48 N48P1 N48P61 0.0002
E7_49 N7P50 N7P49 N49P1 N49P61 0.0003
E7_50 N7P51 N7P50 N50P1 N50P61 -0.0000
E7_51 N7P52 N7P51 N51P1 N51P61 -0.0000

```
E7_52 N7P53 N7P52 N52P1 N52P61 -0.0000
E7_53 N7P54 N7P53 N53P1 N53P61 0.0000
E7_54 N7P55 N7P54 N54P1 N54P61 -0.0008
E7_55 N7P56 N7P55 N55P1 N55P61 0.0001
E7_56 N7P57 N7P56 N56P1 N56P61 0.0004
E7_57 N7P58 N7P57 N57P1 N57P61 0.0004
E7_58 N7P59 N7P58 N58P1 N58P61 0.0004
E7_59 N7P60 N7P59 N59P1 N59P61 0.0004
E7_60 N7P61 N7P60 N60P1 N60P61 0.0008
R7 N7P61 N8P1 R=1 LAPLACE=+1/{K7}/(-
S*S/4/3.14^2)^0.25
.param K7=3.4178e-05
Ctt7_8 N7P1 N8P1 12.38p

L8 N8P1 N8P2 0.1207u
E8_1 N8P3 N8P2 N1P1 N1P61 0.0005
E8_2 N8P4 N8P3 N2P1 N2P61 0.0004
E8_3 N8P5 N8P4 N3P1 N3P61 0.0047
E8_4 N8P6 N8P5 N4P1 N4P61 -0.0416
E8_5 N8P7 N8P6 N5P1 N5P61 -0.2154
E8_6 N8P8 N8P7 N6P1 N6P61 -0.0406
E8_7 N8P9 N8P8 N7P1 N7P61 -0.2251
E8_9 N8P10 N8P9 N9P1 N9P61 -0.2117
E8_10 N8P11 N8P10 N10P1 N10P61 0.0092
E8_11 N8P12 N8P11 N11P1 N11P61 -0.0006
E8_12 N8P13 N8P12 N12P1 N12P61 0.0001
E8_13 N8P14 N8P13 N13P1 N13P61 0.0000
E8_14 N8P15 N8P14 N14P1 N14P61 -0.0002
E8_15 N8P16 N8P15 N15P1 N15P61 0.0032
E8_16 N8P17 N8P16 N16P1 N16P61 -0.0448
E8_17 N8P18 N8P17 N17P1 N17P61 -0.2204
E8_18 N8P19 N8P18 N18P1 N18P61 -0.0453
E8_19 N8P20 N8P19 N19P1 N19P61 0.0052
E8_20 N8P21 N8P20 N20P1 N20P61 0.0100
E8_21 N8P22 N8P21 N21P1 N21P61 0.0034
E8_22 N8P23 N8P22 N22P1 N22P61 0.0006
E8_23 N8P24 N8P23 N23P1 N23P61 -0.0000
E8_24 N8P25 N8P24 N24P1 N24P61 0.0000
E8_25 N8P26 N8P25 N25P1 N25P61 0.0000
E8_26 N8P27 N8P26 N26P1 N26P61 -0.0000
E8_27 N8P28 N8P27 N27P1 N27P61 -0.0000
E8_28 N8P29 N8P28 N28P1 N28P61 -0.0002
E8_29 N8P30 N8P29 N29P1 N29P61 -0.0006
E8_30 N8P31 N8P30 N30P1 N30P61 0.0004
E8_31 N8P32 N8P31 N31P1 N31P61 0.0003
E8_32 N8P33 N8P32 N32P1 N32P61 0.0000
E8_33 N8P34 N8P33 N33P1 N33P61 0.0000
E8_34 N8P35 N8P34 N34P1 N34P61 0.0000
E8_35 N8P36 N8P35 N35P1 N35P61 0.0000
E8_36 N8P37 N8P36 N36P1 N36P61 -0.0000
E8_37 N8P38 N8P37 N37P1 N37P61 -0.0000
E8_38 N8P39 N8P38 N38P1 N38P61 0.0000
E8_39 N8P40 N8P39 N39P1 N39P61 -0.0000
E8_40 N8P41 N8P40 N40P1 N40P61 -0.0000
E8_41 N8P42 N8P41 N41P1 N41P61 -0.0000
E8_42 N8P43 N8P42 N42P1 N42P61 0.0002
E8_43 N8P44 N8P43 N43P1 N43P61 0.0001
E8_44 N8P45 N8P44 N44P1 N44P61 -0.0000
E8_45 N8P46 N8P45 N45P1 N45P61 0.0000
E8_46 N8P47 N8P46 N46P1 N46P61 -0.0000
E8_47 N8P48 N8P47 N47P1 N47P61 0.0000
E8_48 N8P49 N8P48 N48P1 N48P61 -0.0000
E8_49 N8P50 N8P49 N49P1 N49P61 -0.0000
E8_50 N8P51 N8P50 N50P1 N50P61 0.0000
E8_51 N8P52 N8P51 N51P1 N51P61 0.0000
E8_52 N8P53 N8P52 N52P1 N52P61 0.0000
E8_53 N8P54 N8P53 N53P1 N53P61 0.0000
E8_54 N8P55 N8P54 N54P1 N54P61 0.0000
E8_55 N8P56 N8P55 N55P1 N55P61 -0.0001
E8_56 N8P57 N8P56 N56P1 N56P61 -0.0000
E8_57 N8P58 N8P57 N57P1 N57P61 -0.0000
E8_58 N8P59 N8P58 N58P1 N58P61 -0.0000
E8_59 N8P60 N8P59 N59P1 N59P61 -0.0000
E8_60 N8P61 N8P60 N60P1 N60P61 -0.0001
R8 N8P61 N9P1 R=1 LAPLACE=+1/{K8}/(-
S*S/4/3.14^2)^0.25
.param K8=3.7311e-05
Ctt8_9 N8P1 N9P1 13.47p

L9 N9P1 N9P2 0.1308u
E9_1 N9P3 N9P2 N1P1 N1P61 0.0006
E9_2 N9P4 N9P3 N2P1 N2P61 0.0047
E9_3 N9P5 N9P4 N3P1 N3P61 -0.0418
E9_4 N9P6 N9P5 N4P1 N4P61 -0.2155
E9_5 N9P7 N9P6 N5P1 N5P61 -0.0452
E9_6 N9P8 N9P7 N6P1 N6P61 0.0056
E9_7 N9P9 N9P8 N7P1 N7P61 0.0107
E9_8 N9P10 N9P9 N8P1 N8P61 -0.2294
E9_10 N9P11 N9P10 N10P1 N10P61 -0.2122
E9_11 N9P12 N9P11 N11P1 N11P61 0.0093
E9_12 N9P13 N9P12 N12P1 N12P61 -0.0004
E9_13 N9P14 N9P13 N13P1 N13P61 -0.0001
E9_14 N9P15 N9P14 N14P1 N14P61 0.0032
E9_15 N9P16 N9P15 N15P1 N15P61 -0.0449
E9_16 N9P17 N9P16 N16P1 N16P61 -0.2201
E9_17 N9P18 N9P17 N17P1 N17P61 -0.0485
E9_18 N9P19 N9P18 N18P1 N18P61 0.0037
E9_19 N9P20 N9P19 N19P1 N19P61 0.0007
E9_20 N9P21 N9P20 N20P1 N20P61 0.0036
E9_21 N9P22 N9P21 N21P1 N21P61 0.0101
E9_22 N9P23 N9P22 N22P1 N22P61 0.0034
E9_23 N9P24 N9P23 N23P1 N23P61 0.0006
E9_24 N9P25 N9P24 N24P1 N24P61 -0.0000
E9_25 N9P26 N9P25 N25P1 N25P61 0.0000
E9_26 N9P27 N9P26 N26P1 N26P61 -0.0001
E9_27 N9P28 N9P27 N27P1 N27P61 -0.0002
E9_28 N9P29 N9P28 N28P1 N28P61 -0.0006
E9_29 N9P30 N9P29 N29P1 N29P61 -0.0002
E9_30 N9P31 N9P30 N30P1 N30P61 -0.0001
E9_31 N9P32 N9P31 N31P1 N31P61 -0.0000
E9_32 N9P33 N9P32 N32P1 N32P61 0.0000
E9_33 N9P34 N9P33 N33P1 N33P61 0.0000
```

E9_34 N9P35 N9P34 N34P1 N34P61 0.0000
E9_35 N9P36 N9P35 N35P1 N35P61 0.0000
E9_36 N9P37 N9P36 N36P1 N36P61 0.0000
E9_37 N9P38 N9P37 N37P1 N37P61 0.0000
E9_38 N9P39 N9P38 N38P1 N38P61 -0.0000
E9_39 N9P40 N9P39 N39P1 N39P61 -0.0000
E9_40 N9P41 N9P40 N40P1 N40P61 -0.0000
E9_41 N9P42 N9P41 N41P1 N41P61 0.0000
E9_42 N9P43 N9P42 N42P1 N42P61 -0.0000
E9_43 N9P44 N9P43 N43P1 N43P61 -0.0000
E9_44 N9P45 N9P44 N44P1 N44P61 0.0000
E9_45 N9P46 N9P45 N45P1 N45P61 -0.0000
E9_46 N9P47 N9P46 N46P1 N46P61 0.0000
E9_47 N9P48 N9P47 N47P1 N47P61 -0.0000
E9_48 N9P49 N9P48 N48P1 N48P61 0.0000
E9_49 N9P50 N9P49 N49P1 N49P61 0.0000
E9_50 N9P51 N9P50 N50P1 N50P61 0.0000
E9_51 N9P52 N9P51 N51P1 N51P61 0.0000
E9_52 N9P53 N9P52 N52P1 N52P61 0.0000
E9_53 N9P54 N9P53 N53P1 N53P61 0.0000
E9_54 N9P55 N9P54 N54P1 N54P61 -0.0000
E9_55 N9P56 N9P55 N55P1 N55P61 -0.0001
E9_56 N9P57 N9P56 N56P1 N56P61 -0.0000
E9_57 N9P58 N9P57 N57P1 N57P61 -0.0000
E9_58 N9P59 N9P58 N58P1 N58P61 -0.0000
E9_59 N9P60 N9P59 N59P1 N59P61 -0.0000
E9_60 N9P61 N9P60 N60P1 N60P61 -0.0000
R9 N9P61 N10P1 R=1 LAPLACE=+1/{K9}/(-S*S/4/3.14^2)^0.25
.param K9=4.0443e-05
Ctt9_10 N9P1 N10P1 14.55p

L10 N10P1 N10P2 0.1410u
E10_1 N10P3 N10P2 N1P1 N1P61 0.0049
E10_2 N10P4 N10P3 N2P1 N2P61 -0.0419
E10_3 N10P5 N10P4 N3P1 N3P61 -0.2155
E10_4 N10P6 N10P5 N4P1 N4P61 -0.0451
E10_5 N10P7 N10P6 N5P1 N5P61 0.0054
E10_6 N10P8 N10P7 N6P1 N6P61 0.0007
E10_7 N10P9 N10P8 N7P1 N7P61 -0.0006
E10_8 N10P10 N10P9 N8P1 N8P61 0.0108
E10_9 N10P11 N10P10 N9P1 N9P61 -0.2287
E10_11 N10P12 N10P11 N11P1 N11P61 -0.2128
E10_12 N10P13 N10P12 N12P1 N12P61 0.0093
E10_13 N10P14 N10P13 N13P1 N13P61 0.0032
E10_14 N10P15 N10P14 N14P1 N14P61 -0.0450
E10_15 N10P16 N10P15 N15P1 N15P61 -0.2201
E10_16 N10P17 N10P16 N16P1 N16P61 -0.0484
E10_17 N10P18 N10P17 N17P1 N17P61 0.0038
E10_18 N10P19 N10P18 N18P1 N18P61 -0.0002
E10_19 N10P20 N10P19 N19P1 N19P61 -0.0000
E10_20 N10P21 N10P20 N20P1 N20P61 0.0007
E10_21 N10P22 N10P21 N21P1 N21P61 0.0036
E10_22 N10P23 N10P22 N22P1 N22P61 0.0101
E10_23 N10P24 N10P23 N23P1 N23P61 0.0034
E10_24 N10P25 N10P24 N24P1 N24P61 0.0006
E10_25 N10P26 N10P25 N25P1 N25P61 -0.0001
E10_26 N10P27 N10P26 N26P1 N26P61 -0.0002
E10_27 N10P28 N10P27 N27P1 N27P61 -0.0006
E10_28 N10P29 N10P28 N28P1 N28P61 -0.0003
E10_29 N10P30 N10P29 N29P1 N29P61 -0.0001
E10_30 N10P31 N10P30 N30P1 N30P61 -0.0000
E10_31 N10P32 N10P31 N31P1 N31P61 -0.0000
E10_32 N10P33 N10P32 N32P1 N32P61 0.0000
E10_33 N10P34 N10P33 N33P1 N33P61 0.0000
E10_34 N10P35 N10P34 N34P1 N34P61 0.0000
E10_35 N10P36 N10P35 N35P1 N35P61 0.0000
E10_36 N10P37 N10P36 N36P1 N36P61 0.0000
E10_37 N10P38 N10P37 N37P1 N37P61 0.0000
E10_38 N10P39 N10P38 N38P1 N38P61 -0.0000
E10_39 N10P40 N10P39 N39P1 N39P61 -0.0000
E10_40 N10P41 N10P40 N40P1 N40P61 -0.0000
E10_41 N10P42 N10P41 N41P1 N41P61 0.0000
E10_42 N10P43 N10P42 N42P1 N42P61 -0.0000
E10_43 N10P44 N10P43 N43P1 N43P61 -0.0000
E10_44 N10P45 N10P44 N44P1 N44P61 0.0000
E10_45 N10P46 N10P45 N45P1 N45P61 -0.0000
E10_46 N10P47 N10P46 N46P1 N46P61 0.0000
E10_47 N10P48 N10P47 N47P1 N47P61 -0.0000
E10_48 N10P49 N10P48 N48P1 N48P61 0.0000
E10_49 N10P50 N10P49 N49P1 N49P61 0.0000
E10_50 N10P51 N10P50 N50P1 N50P61 0.0000
E10_51 N10P52 N10P51 N51P1 N51P61 0.0000
E10_52 N10P53 N10P52 N52P1 N52P61 0.0000
E10_53 N10P54 N10P53 N53P1 N53P61 0.0000
E10_54 N10P55 N10P54 N54P1 N54P61 -0.0000
E10_55 N10P56 N10P55 N55P1 N55P61 -0.0001
E10_56 N10P57 N10P56 N56P1 N56P61 -0.0000
E10_57 N10P58 N10P57 N57P1 N57P61 -0.0000
E10_58 N10P59 N10P58 N58P1 N58P61 -0.0000
E10_59 N10P60 N10P59 N59P1 N59P61 -0.0000
E10_60 N10P61 N10P60 N60P1 N60P61 -0.0000
R10 N10P61 N11P1 R=1 LAPLACE=+1/{K10}/(-S*S/4/3.14^2)^0.25
.param K10=4.3576e-05
Ctt10_11 N10P1 N11P1 15.64p

L11 N11P1 N11P2 0.1512u
E11_1 N11P3 N11P2 N1P1 N1P61 -0.0373
E11_2 N11P4 N11P3 N2P1 N2P61 -0.2153
E11_3 N11P5 N11P4 N3P1 N3P61 -0.0447
E11_4 N11P6 N11P5 N4P1 N4P61 0.0055
E11_5 N11P7 N11P6 N5P1 N5P61 0.0006
E11_6 N11P8 N11P7 N6P1 N6P61 0.0006
E11_7 N11P9 N11P8 N7P1 N7P61 0.0001
E11_8 N11P10 N11P9 N8P1 N8P61 -0.0007
E11_9 N11P11 N11P10 N9P1 N9P61 0.0107
E11_10 N11P12 N11P11 N10P1 N10P61 -0.2281
E11_12 N11P13 N11P12 N12P1 N12P61 -0.2084
E11_13 N11P14 N11P13 N13P1 N13P61 -0.0418
E11_14 N11P15 N11P14 N14P1 N14P61 -0.2204
E11_15 N11P16 N11P15 N15P1 N15P61 -0.0482

E11_16 N11P17 N11P16 N16P1 N16P61 0.0038
E11_17 N11P18 N11P17 N17P1 N17P61 -0.0003
E11_18 N11P19 N11P18 N18P1 N18P61 0.0000
E11_19 N11P20 N11P19 N19P1 N19P61 -0.0000
E11_20 N11P21 N11P20 N20P1 N20P61 -0.0001
E11_21 N11P22 N11P21 N21P1 N21P61 0.0007
E11_22 N11P23 N11P22 N22P1 N22P61 0.0036
E11_23 N11P24 N11P23 N23P1 N23P61 0.0100
E11_24 N11P25 N11P24 N24P1 N24P61 0.0050
E11_25 N11P26 N11P25 N25P1 N25P61 0.0005
E11_26 N11P27 N11P26 N26P1 N26P61 -0.0006
E11_27 N11P28 N11P27 N27P1 N27P61 -0.0002
E11_28 N11P29 N11P28 N28P1 N28P61 -0.0001
E11_29 N11P30 N11P29 N29P1 N29P61 -0.0000
E11_30 N11P31 N11P30 N30P1 N30P61 -0.0000
E11_31 N11P32 N11P31 N31P1 N31P61 -0.0000
E11_32 N11P33 N11P32 N32P1 N32P61 0.0000
E11_33 N11P34 N11P33 N33P1 N33P61 0.0000
E11_34 N11P35 N11P34 N34P1 N34P61 0.0000
E11_35 N11P36 N11P35 N35P1 N35P61 0.0000
E11_36 N11P37 N11P36 N36P1 N36P61 0.0004
E11_37 N11P38 N11P37 N37P1 N37P61 0.0003
E11_38 N11P39 N11P38 N38P1 N38P61 -0.0000
E11_39 N11P40 N11P39 N39P1 N39P61 0.0000
E11_40 N11P41 N11P40 N40P1 N40P61 -0.0000
E11_41 N11P42 N11P41 N41P1 N41P61 0.0000
E11_42 N11P43 N11P42 N42P1 N42P61 -0.0000
E11_43 N11P44 N11P43 N43P1 N43P61 -0.0000
E11_44 N11P45 N11P44 N44P1 N44P61 0.0000
E11_45 N11P46 N11P45 N45P1 N45P61 -0.0000
E11_46 N11P47 N11P46 N46P1 N46P61 0.0000
E11_47 N11P48 N11P47 N47P1 N47P61 -0.0000
E11_48 N11P49 N11P48 N48P1 N48P61 0.0002
E11_49 N11P50 N11P49 N49P1 N49P61 0.0001
E11_50 N11P51 N11P50 N50P1 N50P61 -0.0000
E11_51 N11P52 N11P51 N51P1 N51P61 0.0000
E11_52 N11P53 N11P52 N52P1 N52P61 0.0000
E11_53 N11P54 N11P53 N53P1 N53P61 0.0000
E11_54 N11P55 N11P54 N54P1 N54P61 -0.0001
E11_55 N11P56 N11P55 N55P1 N55P61 -0.0001
E11_56 N11P57 N11P56 N56P1 N56P61 -0.0000
E11_57 N11P58 N11P57 N57P1 N57P61 -0.0000
E11_58 N11P59 N11P58 N58P1 N58P61 0.0000
E11_59 N11P60 N11P59 N59P1 N59P61 0.0000
E11_60 N11P61 N11P60 N60P1 N60P61 0.0002
R11 N11P61 N12P1 R=1
LAPLACE=+1/{K11}/(-S*S/4/3.14^2)^0.25
.param K11=4.6709e-05
Ctt11_12 N11P1 N12P1 16.72p

L12 N12P1 N12P2 0.1771u
E12_1 N12P3 N12P2 N1P1 N1P61 -0.3111
E12_2 N12P4 N12P3 N2P1 N2P61 -0.0524
E12_3 N12P5 N12P4 N3P1 N3P61 0.0021
E12_4 N12P6 N12P5 N4P1 N4P61 -0.0018
E12_5 N12P7 N12P6 N5P1 N5P61 -0.0011
E12_6 N12P8 N12P7 N6P1 N6P61 -0.0008
E12_7 N12P9 N12P8 N7P1 N7P61 0.0002
E12_8 N12P10 N12P9 N8P1 N8P61 0.0001
E12_9 N12P11 N12P10 N9P1 N9P61 -0.0006
E12_10 N12P12 N12P11 N10P1 N10P61 0.0117
E12_11 N12P13 N12P12 N11P1 N11P61 -0.2442
E12_13 N12P14 N12P13 N13P1 N13P61 -0.3024
E12_14 N12P15 N12P14 N14P1 N14P61 -0.0492
E12_15 N12P16 N12P15 N15P1 N15P61 0.0038
E12_16 N12P17 N12P16 N16P1 N16P61 -0.0003
E12_17 N12P18 N12P17 N17P1 N17P61 0.0000
E12_18 N12P19 N12P18 N18P1 N18P61 0.0002
E12_19 N12P20 N12P19 N19P1 N19P61 0.0003
E12_20 N12P21 N12P20 N20P1 N20P61 -0.0000
E12_21 N12P22 N12P21 N21P1 N21P61 -0.0001
E12_22 N12P23 N12P22 N22P1 N22P61 0.0007
E12_23 N12P24 N12P23 N23P1 N23P61 0.0057
E12_24 N12P25 N12P24 N24P1 N24P61 -0.0124
E12_25 N12P26 N12P25 N25P1 N25P61 -0.0113
E12_26 N12P27 N12P26 N26P1 N26P61 0.0005
E12_27 N12P28 N12P27 N27P1 N27P61 -0.0001
E12_28 N12P29 N12P28 N28P1 N28P61 -0.0000
E12_29 N12P30 N12P29 N29P1 N29P61 -0.0000
E12_30 N12P31 N12P30 N30P1 N30P61 0.0003
E12_31 N12P32 N12P31 N31P1 N31P61 0.0003
E12_32 N12P33 N12P32 N32P1 N32P61 -0.0000
E12_33 N12P34 N12P33 N33P1 N33P61 0.0000
E12_34 N12P35 N12P34 N34P1 N34P61 -0.0000
E12_35 N12P36 N12P35 N35P1 N35P61 0.0004
E12_36 N12P37 N12P36 N36P1 N36P61 -0.0062
E12_37 N12P38 N12P37 N37P1 N37P61 -0.0041
E12_38 N12P39 N12P38 N38P1 N38P61 0.0003
E12_39 N12P40 N12P39 N39P1 N39P61 -0.0000
E12_40 N12P41 N12P40 N40P1 N40P61 0.0000
E12_41 N12P42 N12P41 N41P1 N41P61 -0.0000
E12_42 N12P43 N12P42 N42P1 N42P61 0.0004
E12_43 N12P44 N12P43 N43P1 N43P61 0.0004
E12_44 N12P45 N12P44 N44P1 N44P61 -0.0000
E12_45 N12P46 N12P45 N45P1 N45P61 0.0000
E12_46 N12P47 N12P46 N46P1 N46P61 -0.0000
E12_47 N12P48 N12P47 N47P1 N47P61 0.0002
E12_48 N12P49 N12P48 N48P1 N48P61 -0.0029
E12_49 N12P50 N12P49 N49P1 N49P61 -0.0022
E12_50 N12P51 N12P50 N50P1 N50P61 0.0002
E12_51 N12P52 N12P51 N51P1 N51P61 0.0000
E12_52 N12P53 N12P52 N52P1 N52P61 0.0000
E12_53 N12P54 N12P53 N53P1 N53P61 -0.0000
E12_54 N12P55 N12P54 N54P1 N54P61 0.0004
E12_55 N12P56 N12P55 N55P1 N55P61 0.0007
E12_56 N12P57 N12P56 N56P1 N56P61 0.0000
E12_57 N12P58 N12P57 N57P1 N57P61 -0.0001
E12_58 N12P59 N12P58 N58P1 N58P61 -0.0003
E12_59 N12P60 N12P59 N59P1 N59P61 -0.0004
E12_60 N12P61 N12P60 N60P1 N60P61 -0.0027
R12 N12P61 N13P1 R=1
LAPLACE=+1/{K12}/(-S*S/4/3.14^2)^0.25

APPENDICES

```
.param K12=4.9841e-05

L13 N13P1 N13P2 0.1770u
E13_1 N13P3 N13P2 N1P1 N1P61 -0.0199
E13_2 N13P4 N13P3 N2P1 N2P61 0.0020
E13_3 N13P5 N13P4 N3P1 N3P61 -0.0014
E13_4 N13P6 N13P5 N4P1 N4P61 -0.0014
E13_5 N13P7 N13P6 N5P1 N5P61 -0.0009
E13_6 N13P8 N13P7 N6P1 N6P61 -0.0005
E13_7 N13P9 N13P8 N7P1 N7P61 0.0002
E13_8 N13P10 N13P9 N8P1 N8P61 0.0001
E13_9 N13P11 N13P10 N9P1 N9P61 -0.0002
E13_10 N13P12 N13P11 N10P1 N10P61 0.0040
E13_11 N13P13 N13P12 N11P1 N11P61 -0.0490
E13_12 N13P14 N13P13 N12P1 N12P61 -0.3022
E13_14 N13P15 N13P14 N14P1 N14P61 -0.2444
E13_15 N13P16 N13P15 N15P1 N15P61 0.0115
E13_16 N13P17 N13P16 N16P1 N16P61 -0.0007
E13_17 N13P18 N13P17 N17P1 N17P61 0.0000
E13_18 N13P19 N13P18 N18P1 N18P61 0.0002
E13_19 N13P20 N13P19 N19P1 N19P61 0.0003
E13_20 N13P21 N13P20 N20P1 N20P61 0.0000
E13_21 N13P22 N13P21 N21P1 N21P61 -0.0003
E13_22 N13P23 N13P22 N22P1 N22P61 0.0039
E13_23 N13P24 N13P23 N23P1 N23P61 -0.0492
E13_24 N13P25 N13P24 N24P1 N24P61 -0.3018
E13_25 N13P26 N13P25 N25P1 N25P61 -0.0121
E13_26 N13P27 N13P26 N26P1 N26P61 0.0057
E13_27 N13P28 N13P27 N27P1 N27P61 0.0007
E13_28 N13P29 N13P28 N28P1 N28P61 -0.0001
E13_29 N13P30 N13P29 N29P1 N29P61 -0.0000
E13_30 N13P31 N13P30 N30P1 N30P61 0.0003
E13_31 N13P32 N13P31 N31P1 N31P61 0.0003
E13_32 N13P33 N13P32 N32P1 N32P61 -0.0000
E13_33 N13P34 N13P33 N33P1 N33P61 -0.0000
E13_34 N13P35 N13P34 N34P1 N34P61 -0.0001
E13_35 N13P36 N13P35 N35P1 N35P61 0.0005
E13_36 N13P37 N13P36 N36P1 N36P61 -0.0111
E13_37 N13P38 N13P37 N37P1 N37P61 -0.0061
E13_38 N13P39 N13P38 N38P1 N38P61 0.0004
E13_39 N13P40 N13P39 N39P1 N39P61 -0.0000
E13_40 N13P41 N13P40 N40P1 N40P61 0.0000
E13_41 N13P42 N13P41 N41P1 N41P61 -0.0000
E13_42 N13P43 N13P42 N42P1 N42P61 0.0003
E13_43 N13P44 N13P43 N43P1 N43P61 0.0003
E13_44 N13P45 N13P44 N44P1 N44P61 -0.0000
E13_45 N13P46 N13P45 N45P1 N45P61 0.0000
E13_46 N13P47 N13P46 N46P1 N46P61 -0.0000
E13_47 N13P48 N13P47 N47P1 N47P61 0.0003
E13_48 N13P49 N13P48 N48P1 N48P61 -0.0040
E13_49 N13P50 N13P49 N49P1 N49P61 -0.0029
E13_50 N13P51 N13P50 N50P1 N50P61 0.0002
E13_51 N13P52 N13P51 N51P1 N51P61 0.0000
E13_52 N13P53 N13P52 N52P1 N52P61 0.0000
E13_53 N13P54 N13P53 N53P1 N53P61 -0.0000
E13_54 N13P55 N13P54 N54P1 N54P61 0.0003
E13_55 N13P56 N13P55 N55P1 N55P61 0.0005
E13_56 N13P57 N13P56 N56P1 N56P61 -0.0000
E13_57 N13P58 N13P57 N57P1 N57P61 -0.0002
E13_58 N13P59 N13P58 N58P1 N58P61 -0.0004
E13_59 N13P60 N13P59 N59P1 N59P61 -0.0005
E13_60 N13P61 N13P60 N60P1 N60P61 -0.0035
R13 N13P61 N14P1 R=1
LAPLACE=+1/{K13}/(-S*S/4/3.14^2)^0.25
.param K13=4.9841e-05
Ctt13_14 N13P1 N14P1 16.72p

L14 N14P1 N14P2 0.1511u
E14_1 N14P3 N14P2 N1P1 N1P61 0.0051
E14_2 N14P4 N14P3 N2P1 N2P61 0.0099
E14_3 N14P5 N14P4 N3P1 N3P61 0.0035
E14_4 N14P6 N14P5 N4P1 N4P61 0.0007
E14_5 N14P7 N14P6 N5P1 N5P61 -0.0001
E14_6 N14P8 N14P7 N6P1 N6P61 -0.0000
E14_7 N14P9 N14P8 N7P1 N7P61 0.0000
E14_8 N14P10 N14P9 N8P1 N8P61 -0.0003
E14_9 N14P11 N14P10 N9P1 N9P61 0.0037
E14_10 N14P12 N14P11 N10P1 N10P61 -0.0482
E14_11 N14P13 N14P12 N11P1 N11P61 -0.2203
E14_12 N14P14 N14P13 N12P1 N12P61 -0.0420
E14_13 N14P15 N14P14 N13P1 N13P61 -0.2086
E14_15 N14P16 N14P15 N15P1 N15P61 -0.2279
E14_16 N14P17 N14P16 N16P1 N16P61 0.0109
E14_17 N14P18 N14P17 N17P1 N17P61 -0.0006
E14_18 N14P19 N14P18 N18P1 N18P61 0.0000
E14_19 N14P20 N14P19 N19P1 N19P61 0.0000
E14_20 N14P21 N14P20 N20P1 N20P61 -0.0003
E14_21 N14P22 N14P21 N21P1 N21P61 0.0037
E14_22 N14P23 N14P22 N22P1 N22P61 -0.0482
E14_23 N14P24 N14P23 N23P1 N23P61 -0.2203
E14_24 N14P25 N14P24 N24P1 N24P61 -0.0420
E14_25 N14P26 N14P25 N25P1 N25P61 0.0048
E14_26 N14P27 N14P26 N26P1 N26P61 0.0100
E14_27 N14P28 N14P27 N27P1 N27P61 0.0036
E14_28 N14P29 N14P28 N28P1 N28P61 0.0007
E14_29 N14P30 N14P29 N29P1 N29P61 -0.0001
E14_30 N14P31 N14P30 N30P1 N30P61 -0.0000
E14_31 N14P32 N14P31 N31P1 N31P61 -0.0000
E14_32 N14P33 N14P32 N32P1 N32P61 -0.0000
E14_33 N14P34 N14P33 N33P1 N33P61 -0.0001
E14_34 N14P35 N14P34 N34P1 N34P61 -0.0002
E14_35 N14P36 N14P35 N35P1 N35P61 -0.0006
E14_36 N14P37 N14P36 N36P1 N36P61 0.0004
E14_37 N14P38 N14P37 N37P1 N37P61 0.0004
E14_38 N14P39 N14P38 N38P1 N38P61 0.0000
E14_39 N14P40 N14P39 N39P1 N39P61 0.0000
E14_40 N14P41 N14P40 N40P1 N40P61 0.0000
E14_41 N14P42 N14P41 N41P1 N41P61 0.0000
E14_42 N14P43 N14P42 N42P1 N42P61 -0.0000
E14_43 N14P44 N14P43 N43P1 N43P61 -0.0000
E14_44 N14P45 N14P44 N44P1 N44P61 0.0000
E14_45 N14P46 N14P45 N45P1 N45P61 -0.0000
```

E14_46 N14P47 N14P46 N46P1 N46P61 0.0000
E14_47 N14P48 N14P47 N47P1 N47P61 -0.0000
E14_48 N14P49 N14P48 N48P1 N48P61 0.0002
E14_49 N14P50 N14P49 N49P1 N49P61 0.0002
E14_50 N14P51 N14P50 N50P1 N50P61 -0.0000
E14_51 N14P52 N14P51 N51P1 N51P61 -0.0000
E14_52 N14P53 N14P52 N52P1 N52P61 -0.0000
E14_53 N14P54 N14P53 N53P1 N53P61 0.0000
E14_54 N14P55 N14P54 N54P1 N54P61 -0.0000
E14_55 N14P56 N14P55 N55P1 N55P61 -0.0000
E14_56 N14P57 N14P56 N56P1 N56P61 0.0000
E14_57 N14P58 N14P57 N57P1 N57P61 0.0000
E14_58 N14P59 N14P58 N58P1 N58P61 0.0000
E14_59 N14P60 N14P59 N59P1 N59P61 0.0000
E14_60 N14P61 N14P60 N60P1 N60P61 0.0002
R14 N14P61 N15P1 R=1
LAPLACE=+1/{K14}/(-S*S/4/3.14^2)^0.25
.param K14=4.6709e-05
Ctt14_15 N14P1 N15P1 15.64p

L15 N15P1 N15P2 0.1409u
E15_1 N15P3 N15P2 N1P1 N1P61 0.0004
E15_2 N15P4 N15P3 N2P1 N2P61 0.0032
E15_3 N15P5 N15P4 N3P1 N3P61 0.0098
E15_4 N15P6 N15P5 N4P1 N4P61 0.0034
E15_5 N15P7 N15P6 N5P1 N5P61 0.0006
E15_6 N15P8 N15P7 N6P1 N6P61 -0.0001
E15_7 N15P9 N15P8 N7P1 N7P61 -0.0003
E15_8 N15P10 N15P9 N8P1 N8P61 0.0038
E15_9 N15P11 N15P10 N9P1 N9P61 -0.0483
E15_10 N15P12 N15P11 N10P1 N10P61 -0.2200
E15_11 N15P13 N15P12 N11P1 N11P61 -0.0450
E15_12 N15P14 N15P13 N12P1 N12P61 0.0031
E15_13 N15P15 N15P14 N13P1 N13P61 0.0092
E15_14 N15P16 N15P15 N14P1 N14P61 -0.2125
E15_16 N15P17 N15P16 N16P1 N16P61 -0.2284
E15_17 N15P18 N15P17 N17P1 N17P61 0.0109
E15_18 N15P19 N15P18 N18P1 N18P61 -0.0006
E15_19 N15P20 N15P19 N19P1 N19P61 -0.0003
E15_20 N15P21 N15P20 N20P1 N20P61 0.0038
E15_21 N15P22 N15P21 N21P1 N21P61 -0.0484
E15_22 N15P23 N15P22 N22P1 N22P61 -0.2201
E15_23 N15P24 N15P23 N23P1 N23P61 -0.0450
E15_24 N15P25 N15P24 N24P1 N24P61 0.0031
E15_25 N15P26 N15P25 N25P1 N25P61 0.0005
E15_26 N15P27 N15P26 N26P1 N26P61 0.0034
E15_27 N15P28 N15P27 N27P1 N27P61 0.0101
E15_28 N15P29 N15P28 N28P1 N28P61 0.0036
E15_29 N15P30 N15P29 N29P1 N29P61 0.0007
E15_30 N15P31 N15P30 N30P1 N30P61 -0.0001
E15_31 N15P32 N15P31 N31P1 N31P61 -0.0000
E15_32 N15P33 N15P32 N32P1 N32P61 -0.0001
E15_33 N15P34 N15P33 N33P1 N33P61 -0.0003
E15_34 N15P35 N15P34 N34P1 N34P61 -0.0006
E15_35 N15P36 N15P35 N35P1 N35P61 -0.0002
E15_36 N15P37 N15P36 N36P1 N36P61 -0.0001
E15_37 N15P38 N15P37 N37P1 N37P61 -0.0000
E15_38 N15P39 N15P38 N38P1 N38P61 0.0000
E15_39 N15P40 N15P39 N39P1 N39P61 0.0000
E15_40 N15P41 N15P40 N40P1 N40P61 0.0000
E15_41 N15P42 N15P41 N41P1 N41P61 0.0000
E15_42 N15P43 N15P42 N42P1 N42P61 0.0000
E15_43 N15P44 N15P43 N43P1 N43P61 0.0000
E15_44 N15P45 N15P44 N44P1 N44P61 -0.0000
E15_45 N15P46 N15P45 N45P1 N45P61 -0.0000
E15_46 N15P47 N15P46 N46P1 N46P61 -0.0000
E15_47 N15P48 N15P47 N47P1 N47P61 0.0000
E15_48 N15P49 N15P48 N48P1 N48P61 -0.0000
E15_49 N15P50 N15P49 N49P1 N49P61 -0.0000
E15_50 N15P51 N15P50 N50P1 N50P61 0.0000
E15_51 N15P52 N15P51 N51P1 N51P61 0.0000
E15_52 N15P53 N15P52 N52P1 N52P61 0.0000
E15_53 N15P54 N15P53 N53P1 N53P61 -0.0000
E15_54 N15P55 N15P54 N54P1 N54P61 0.0000
E15_55 N15P56 N15P55 N55P1 N55P61 0.0000
E15_56 N15P57 N15P56 N56P1 N56P61 0.0000
E15_57 N15P58 N15P57 N57P1 N57P61 0.0000
E15_58 N15P59 N15P58 N58P1 N58P61 -0.0000
E15_59 N15P60 N15P59 N59P1 N59P61 -0.0000
E15_60 N15P61 N15P60 N60P1 N60P61 -0.0000
R15 N15P61 N16P1 R=1
LAPLACE=+1/{K15}/(-S*S/4/3.14^2)^0.25
.param K15=4.3576e-05
Ctt15_16 N15P1 N16P1 14.55p

L16 N16P1 N16P2 0.1308u
E16_1 N16P3 N16P2 N1P1 N1P61 -0.0001
E16_2 N16P4 N16P3 N2P1 N2P61 0.0005
E16_3 N16P5 N16P4 N3P1 N3P61 0.0032
E16_4 N16P6 N16P5 N4P1 N4P61 0.0098
E16_5 N16P7 N16P6 N5P1 N5P61 0.0034
E16_6 N16P8 N16P7 N6P1 N6P61 0.0005
E16_7 N16P9 N16P8 N7P1 N7P61 0.0036
E16_8 N16P10 N16P9 N8P1 N8P61 -0.0485
E16_9 N16P11 N16P10 N9P1 N9P61 -0.2200
E16_10 N16P12 N16P11 N10P1 N10P61 -0.0449
E16_11 N16P13 N16P12 N11P1 N11P61 0.0032
E16_12 N16P14 N16P13 N12P1 N12P61 -0.0002
E16_13 N16P15 N16P14 N13P1 N13P61 -0.0005
E16_14 N16P16 N16P15 N14P1 N14P61 0.0094
E16_15 N16P17 N16P16 N15P1 N15P61 -0.2120
E16_17 N16P18 N16P17 N17P1 N17P61 -0.2291
E16_18 N16P19 N16P18 N18P1 N18P61 0.0107
E16_19 N16P20 N16P19 N19P1 N19P61 0.0036
E16_20 N16P21 N16P20 N20P1 N20P61 -0.0485
E16_21 N16P22 N16P21 N21P1 N21P61 -0.2201
E16_22 N16P23 N16P22 N22P1 N22P61 -0.0449
E16_23 N16P24 N16P23 N23P1 N23P61 0.0032
E16_24 N16P25 N16P24 N24P1 N24P61 -0.0002
E16_25 N16P26 N16P25 N25P1 N25P61 -0.0000
E16_26 N16P27 N16P26 N26P1 N26P61 0.0006
E16_27 N16P28 N16P27 N27P1 N27P61 0.0034

E16_28 N16P29 N16P28 N28P1 N28P61 0.0101
E16_29 N16P30 N16P29 N29P1 N29P61 0.0036
E16_30 N16P31 N16P30 N30P1 N30P61 0.0006
E16_31 N16P32 N16P31 N31P1 N31P61 -0.0001
E16_32 N16P33 N16P32 N32P1 N32P61 -0.0002
E16_33 N16P34 N16P33 N33P1 N33P61 -0.0006
E16_34 N16P35 N16P34 N34P1 N34P61 -0.0002
E16_35 N16P36 N16P35 N35P1 N35P61 -0.0001
E16_36 N16P37 N16P36 N36P1 N36P61 -0.0000
E16_37 N16P38 N16P37 N37P1 N37P61 0.0000
E16_38 N16P39 N16P38 N38P1 N38P61 0.0000
E16_39 N16P40 N16P39 N39P1 N39P61 0.0000
E16_40 N16P41 N16P40 N40P1 N40P61 0.0000
E16_41 N16P42 N16P41 N41P1 N41P61 0.0000
E16_42 N16P43 N16P42 N42P1 N42P61 -0.0000
E16_43 N16P44 N16P43 N43P1 N43P61 -0.0000
E16_44 N16P45 N16P44 N44P1 N44P61 -0.0000
E16_45 N16P46 N16P45 N45P1 N45P61 -0.0000
E16_46 N16P47 N16P46 N46P1 N46P61 -0.0000
E16_47 N16P48 N16P47 N47P1 N47P61 -0.0000
E16_48 N16P49 N16P48 N48P1 N48P61 0.0000
E16_49 N16P50 N16P49 N49P1 N49P61 0.0000
E16_50 N16P51 N16P50 N50P1 N50P61 -0.0000
E16_51 N16P52 N16P51 N51P1 N51P61 -0.0000
E16_52 N16P53 N16P52 N52P1 N52P61 -0.0000
E16_53 N16P54 N16P53 N53P1 N53P61 0.0000
E16_54 N16P55 N16P54 N54P1 N54P61 -0.0000
E16_55 N16P56 N16P55 N55P1 N55P61 0.0000
E16_56 N16P57 N16P56 N56P1 N56P61 0.0000
E16_57 N16P58 N16P57 N57P1 N57P61 0.0000
E16_58 N16P59 N16P58 N58P1 N58P61 0.0000
E16_59 N16P60 N16P59 N59P1 N59P61 0.0000
E16_60 N16P61 N16P60 N60P1 N60P61 0.0000
R16 N16P61 N17P1 R=1
LAPLACE=+1/{K16}/(-S*S/4/3.14^2)^0.25
.param K16=4.0443e-05
Ctt16_17 N16P1 N17P1 13.47p

L17 N17P1 N17P2 0.1207u
E17_1 N17P3 N17P2 N1P1 N1P61 -0.0000
E17_2 N17P4 N17P3 N2P1 N2P61 -0.0001
E17_3 N17P5 N17P4 N3P1 N3P61 0.0006
E17_4 N17P6 N17P5 N4P1 N4P61 0.0032
E17_5 N17P7 N17P6 N5P1 N5P61 0.0099
E17_6 N17P8 N17P7 N6P1 N6P61 0.0053
E17_7 N17P9 N17P8 N7P1 N7P61 -0.0454
E17_8 N17P10 N17P9 N8P1 N8P61 -0.2203
E17_9 N17P11 N17P10 N9P1 N9P61 -0.0447
E17_10 N17P12 N17P11 N10P1 N10P61 0.0032
E17_11 N17P13 N17P12 N11P1 N11P61 -0.0002
E17_12 N17P14 N17P13 N12P1 N12P61 0.0000
E17_13 N17P15 N17P14 N13P1 N13P61 0.0000
E17_14 N17P16 N17P15 N14P1 N14P61 -0.0005
E17_15 N17P17 N17P16 N15P1 N15P61 0.0093
E17_16 N17P18 N17P17 N16P1 N16P61 -0.2114
E17_18 N17P19 N17P18 N18P1 N18P61 -0.2252
E17_19 N17P20 N17P19 N19P1 N19P61 -0.0454
E17_20 N17P21 N17P20 N20P1 N20P61 -0.2203
E17_21 N17P22 N17P21 N21P1 N21P61 -0.0448
E17_22 N17P23 N17P22 N22P1 N22P61 0.0032
E17_23 N17P24 N17P23 N23P1 N23P61 -0.0002
E17_24 N17P25 N17P24 N24P1 N24P61 0.0000
E17_25 N17P26 N17P25 N25P1 N25P61 -0.0000
E17_26 N17P27 N17P26 N26P1 N26P61 -0.0000
E17_27 N17P28 N17P27 N27P1 N27P61 0.0006
E17_28 N17P29 N17P28 N28P1 N28P61 0.0034
E17_29 N17P30 N17P29 N29P1 N29P61 0.0100
E17_30 N17P31 N17P30 N30P1 N30P61 0.0051
E17_31 N17P32 N17P31 N31P1 N31P61 0.0004
E17_32 N17P33 N17P32 N32P1 N32P61 -0.0006
E17_33 N17P34 N17P33 N33P1 N33P61 -0.0002
E17_34 N17P35 N17P34 N34P1 N34P61 -0.0001
E17_35 N17P36 N17P35 N35P1 N35P61 -0.0000
E17_36 N17P37 N17P36 N36P1 N36P61 -0.0000
E17_37 N17P38 N17P37 N37P1 N37P61 -0.0000
E17_38 N17P39 N17P38 N38P1 N38P61 0.0000
E17_39 N17P40 N17P39 N39P1 N39P61 0.0000
E17_40 N17P41 N17P40 N40P1 N40P61 0.0000
E17_41 N17P42 N17P41 N41P1 N41P61 0.0000
E17_42 N17P43 N17P42 N42P1 N42P61 0.0003
E17_43 N17P44 N17P43 N43P1 N43P61 0.0002
E17_44 N17P45 N17P44 N44P1 N44P61 -0.0000
E17_45 N17P46 N17P45 N45P1 N45P61 -0.0000
E17_46 N17P47 N17P46 N46P1 N46P61 -0.0000
E17_47 N17P48 N17P47 N47P1 N47P61 0.0000
E17_48 N17P49 N17P48 N48P1 N48P61 -0.0000
E17_49 N17P50 N17P49 N49P1 N49P61 -0.0000
E17_50 N17P51 N17P50 N50P1 N50P61 0.0000
E17_51 N17P52 N17P51 N51P1 N51P61 0.0000
E17_52 N17P53 N17P52 N52P1 N52P61 0.0000
E17_53 N17P54 N17P53 N53P1 N53P61 -0.0000
E17_54 N17P55 N17P54 N54P1 N54P61 0.0001
E17_55 N17P56 N17P55 N55P1 N55P61 0.0000
E17_56 N17P57 N17P56 N56P1 N56P61 -0.0000
E17_57 N17P58 N17P57 N57P1 N57P61 -0.0000
E17_58 N17P59 N17P58 N58P1 N58P61 -0.0000
E17_59 N17P60 N17P59 N59P1 N59P61 -0.0000
E17_60 N17P61 N17P60 N60P1 N60P61 -0.0000
R17 N17P61 N18P1 R=1
LAPLACE=+1/{K17}/(-S*S/4/3.14^2)^0.25
.param K17=3.7311e-05
Ctt17_18 N17P1 N18P1 12.38p

L18 N18P1 N18P2 0.1212u
E18_1 N18P3 N18P2 N1P1 N1P61 0.0001
E18_2 N18P4 N18P3 N2P1 N2P61 -0.0003
E18_3 N18P5 N18P4 N3P1 N3P61 -0.0006
E18_4 N18P6 N18P5 N4P1 N4P61 -0.0005
E18_5 N18P7 N18P6 N5P1 N5P61 0.0027
E18_6 N18P8 N18P7 N6P1 N6P61 -0.0166
E18_7 N18P9 N18P8 N7P1 N7P61 -0.3002
E18_8 N18P10 N18P9 N8P1 N8P61 -0.0454

E18_9 N18P11 N18P10 N9P1 N9P61 0.0034
E18_10 N18P12 N18P11 N10P1 N10P61 -0.0002
E18_11 N18P13 N18P12 N11P1 N11P61 0.0000
E18_12 N18P14 N18P13 N12P1 N12P61 0.0002
E18_13 N18P15 N18P14 N13P1 N13P61 0.0002
E18_14 N18P16 N18P15 N14P1 N14P61 0.0000
E18_15 N18P17 N18P16 N15P1 N15P61 -0.0005
E18_16 N18P18 N18P17 N16P1 N16P61 0.0099
E18_17 N18P19 N18P18 N17P1 N17P61 -0.2262
E18_19 N18P20 N18P19 N19P1 N19P61 -0.2999
E18_20 N18P21 N18P20 N20P1 N20P61 -0.0456
E18_21 N18P22 N18P21 N21P1 N21P61 0.0033
E18_22 N18P23 N18P22 N22P1 N22P61 -0.0002
E18_23 N18P24 N18P23 N23P1 N23P61 0.0000
E18_24 N18P25 N18P24 N24P1 N24P61 0.0002
E18_25 N18P26 N18P25 N25P1 N25P61 0.0002
E18_26 N18P27 N18P26 N26P1 N26P61 -0.0000
E18_27 N18P28 N18P27 N27P1 N27P61 -0.0000
E18_28 N18P29 N18P28 N28P1 N28P61 0.0006
E18_29 N18P30 N18P29 N29P1 N29P61 0.0052
E18_30 N18P31 N18P30 N30P1 N30P61 -0.0107
E18_31 N18P32 N18P31 N31P1 N31P61 -0.0098
E18_32 N18P33 N18P32 N32P1 N32P61 0.0004
E18_33 N18P34 N18P33 N33P1 N33P61 -0.0001
E18_34 N18P35 N18P34 N34P1 N34P61 -0.0000
E18_35 N18P36 N18P35 N35P1 N35P61 -0.0000
E18_36 N18P37 N18P36 N36P1 N36P61 0.0002
E18_37 N18P38 N18P37 N37P1 N37P61 0.0002
E18_38 N18P39 N18P38 N38P1 N38P61 -0.0000
E18_39 N18P40 N18P39 N39P1 N39P61 0.0000
E18_40 N18P41 N18P40 N40P1 N40P61 -0.0000
E18_41 N18P42 N18P41 N41P1 N41P61 0.0003
E18_42 N18P43 N18P42 N42P1 N42P61 -0.0047
E18_43 N18P44 N18P43 N43P1 N43P61 -0.0027
E18_44 N18P45 N18P44 N44P1 N44P61 0.0002
E18_45 N18P46 N18P45 N45P1 N45P61 -0.0000
E18_46 N18P47 N18P46 N46P1 N46P61 0.0000
E18_47 N18P48 N18P47 N47P1 N47P61 -0.0000
E18_48 N18P49 N18P48 N48P1 N48P61 0.0002
E18_49 N18P50 N18P49 N49P1 N49P61 0.0003
E18_50 N18P51 N18P50 N50P1 N50P61 -0.0000
E18_51 N18P52 N18P51 N51P1 N51P61 -0.0000
E18_52 N18P53 N18P52 N52P1 N52P61 -0.0000
E18_53 N18P54 N18P53 N53P1 N53P61 0.0001
E18_54 N18P55 N18P54 N54P1 N54P61 -0.0015
E18_55 N18P56 N18P55 N55P1 N55P61 -0.0006
E18_56 N18P57 N18P56 N56P1 N56P61 0.0003
E18_57 N18P58 N18P57 N57P1 N57P61 0.0003
E18_58 N18P59 N18P58 N58P1 N58P61 0.0003
E18_59 N18P60 N18P59 N59P1 N59P61 0.0003
E18_60 N18P61 N18P60 N60P1 N60P61 0.0007
R18 N18P61 N19P1 R=1
LAPLACE=+1/{K18}/(-S*S/4/3.14^2)^0.25
.param K18=3.4178e-05

L19 N19P1 N19P2 0.1212u

E19_1 N19P3 N19P2 N1P1 N1P61 0.0003
E19_2 N19P4 N19P3 N2P1 N2P61 -0.0000
E19_3 N19P5 N19P4 N3P1 N3P61 -0.0002
E19_4 N19P6 N19P5 N4P1 N4P61 -0.0005
E19_5 N19P7 N19P6 N5P1 N5P61 -0.0008
E19_6 N19P8 N19P7 N6P1 N6P61 -0.0126
E19_7 N19P9 N19P8 N7P1 N7P61 -0.0108
E19_8 N19P10 N19P9 N8P1 N8P61 0.0053
E19_9 N19P11 N19P10 N9P1 N9P61 0.0006
E19_10 N19P12 N19P11 N10P1 N10P61 -0.0000
E19_11 N19P13 N19P12 N11P1 N11P61 -0.0000
E19_12 N19P14 N19P13 N12P1 N12P61 0.0002
E19_13 N19P15 N19P14 N13P1 N13P61 0.0002
E19_14 N19P16 N19P15 N14P1 N14P61 0.0000
E19_15 N19P17 N19P16 N15P1 N15P61 -0.0002
E19_16 N19P18 N19P17 N16P1 N16P61 0.0033
E19_17 N19P19 N19P18 N17P1 N17P61 -0.0456
E19_18 N19P20 N19P19 N18P1 N18P61 -0.2998
E19_20 N19P21 N19P20 N20P1 N20P61 -0.2261
E19_21 N19P22 N19P21 N21P1 N21P61 0.0099
E19_22 N19P23 N19P22 N22P1 N22P61 -0.0005
E19_23 N19P24 N19P23 N23P1 N23P61 0.0000
E19_24 N19P25 N19P24 N24P1 N24P61 0.0002
E19_25 N19P26 N19P25 N25P1 N25P61 0.0002
E19_26 N19P27 N19P26 N26P1 N26P61 0.0000
E19_27 N19P28 N19P27 N27P1 N27P61 -0.0002
E19_28 N19P29 N19P28 N28P1 N28P61 0.0033
E19_29 N19P30 N19P29 N29P1 N29P61 -0.0456
E19_30 N19P31 N19P30 N30P1 N30P61 -0.2997
E19_31 N19P32 N19P31 N31P1 N31P61 -0.0107
E19_32 N19P33 N19P32 N32P1 N32P61 0.0052
E19_33 N19P34 N19P33 N33P1 N33P61 0.0006
E19_34 N19P35 N19P34 N34P1 N34P61 -0.0000
E19_35 N19P36 N19P35 N35P1 N35P61 -0.0000
E19_36 N19P37 N19P36 N36P1 N36P61 0.0002
E19_37 N19P38 N19P37 N37P1 N37P61 0.0002
E19_38 N19P39 N19P38 N38P1 N38P61 -0.0000
E19_39 N19P40 N19P39 N39P1 N39P61 -0.0000
E19_40 N19P41 N19P40 N40P1 N40P61 -0.0001
E19_41 N19P42 N19P41 N41P1 N41P61 0.0004
E19_42 N19P43 N19P42 N42P1 N42P61 -0.0098
E19_43 N19P44 N19P43 N43P1 N43P61 -0.0047
E19_44 N19P45 N19P44 N44P1 N44P61 0.0003
E19_45 N19P46 N19P45 N45P1 N45P61 -0.0000
E19_46 N19P47 N19P46 N46P1 N46P61 0.0000
E19_47 N19P48 N19P47 N47P1 N47P61 -0.0000
E19_48 N19P49 N19P48 N48P1 N48P61 0.0002
E19_49 N19P50 N19P49 N49P1 N49P61 0.0002
E19_50 N19P51 N19P50 N50P1 N50P61 -0.0000
E19_51 N19P52 N19P51 N51P1 N51P61 -0.0000
E19_52 N19P53 N19P52 N52P1 N52P61 -0.0000
E19_53 N19P54 N19P53 N53P1 N53P61 0.0002
E19_54 N19P55 N19P54 N54P1 N54P61 -0.0027
E19_55 N19P56 N19P55 N55P1 N55P61 -0.0017
E19_56 N19P57 N19P56 N56P1 N56P61 0.0001
E19_57 N19P58 N19P57 N57P1 N57P61 0.0002

E19_58 N19P59 N19P58 N58P1 N58P61 0.0002
E19_59 N19P60 N19P59 N59P1 N59P61 0.0003
E19_60 N19P61 N19P60 N60P1 N60P61 0.0007
R19 N19P61 N20P1 R=1
LAPLACE=+1/{K19}/(-S*S/4/3.14^2)^0.25
.param K19=3.4178e-05
Ctt19_20 N19P1 N20P1 12.38p

L20 N20P1 N20P2 0.1207u
E20_1 N20P3 N20P2 N1P1 N1P61 -0.0000
E20_2 N20P4 N20P3 N2P1 N2P61 -0.0000
E20_3 N20P5 N20P4 N3P1 N3P61 -0.0000
E20_4 N20P6 N20P5 N4P1 N4P61 -0.0002
E20_5 N20P7 N20P6 N5P1 N5P61 -0.0005
E20_6 N20P8 N20P7 N6P1 N6P61 0.0006
E20_7 N20P9 N20P8 N7P1 N7P61 0.0052
E20_8 N20P10 N20P9 N8P1 N8P61 0.0100
E20_9 N20P11 N20P10 N9P1 N9P61 0.0034
E20_10 N20P12 N20P11 N10P1 N10P61 0.0006
E20_11 N20P13 N20P12 N11P1 N11P61 -0.0000
E20_12 N20P14 N20P13 N12P1 N12P61 -0.0000
E20_13 N20P15 N20P14 N13P1 N13P61 0.0000
E20_14 N20P16 N20P15 N14P1 N14P61 -0.0002
E20_15 N20P17 N20P16 N15P1 N15P61 0.0032
E20_16 N20P18 N20P17 N16P1 N16P61 -0.0448
E20_17 N20P19 N20P18 N17P1 N17P61 -0.2203
E20_18 N20P20 N20P19 N18P1 N18P61 -0.0454
E20_19 N20P21 N20P20 N19P1 N19P61 -0.2252
E20_21 N20P22 N20P21 N21P1 N21P61 -0.2114
E20_22 N20P23 N20P22 N22P1 N22P61 0.0093
E20_23 N20P24 N20P23 N23P1 N23P61 -0.0005
E20_24 N20P25 N20P24 N24P1 N24P61 0.0000
E20_25 N20P26 N20P25 N25P1 N25P61 0.0000
E20_26 N20P27 N20P26 N26P1 N26P61 -0.0002
E20_27 N20P28 N20P27 N27P1 N27P61 0.0032
E20_28 N20P29 N20P28 N28P1 N28P61 -0.0448
E20_29 N20P30 N20P29 N29P1 N29P61 -0.2203
E20_30 N20P31 N20P30 N30P1 N30P61 -0.0454
E20_31 N20P32 N20P31 N31P1 N31P61 0.0051
E20_32 N20P33 N20P32 N32P1 N32P61 0.0100
E20_33 N20P34 N20P33 N33P1 N33P61 0.0034
E20_34 N20P35 N20P34 N34P1 N34P61 0.0006
E20_35 N20P36 N20P35 N35P1 N35P61 -0.0000
E20_36 N20P37 N20P36 N36P1 N36P61 -0.0000
E20_37 N20P38 N20P37 N37P1 N37P61 -0.0000
E20_38 N20P39 N20P38 N38P1 N38P61 -0.0000
E20_39 N20P40 N20P39 N39P1 N39P61 -0.0001
E20_40 N20P41 N20P40 N40P1 N40P61 -0.0002
E20_41 N20P42 N20P41 N41P1 N41P61 -0.0006
E20_42 N20P43 N20P42 N42P1 N42P61 0.0004
E20_43 N20P44 N20P43 N43P1 N43P61 0.0003
E20_44 N20P45 N20P44 N44P1 N44P61 0.0000
E20_45 N20P46 N20P45 N45P1 N45P61 0.0000
E20_46 N20P47 N20P46 N46P1 N46P61 0.0000
E20_47 N20P48 N20P47 N47P1 N47P61 0.0000
E20_48 N20P49 N20P48 N48P1 N48P61 -0.0000
E20_49 N20P50 N20P49 N49P1 N49P61 -0.0000
E20_50 N20P51 N20P50 N50P1 N50P61 0.0000
E20_51 N20P52 N20P51 N51P1 N51P61 0.0000
E20_52 N20P53 N20P52 N52P1 N52P61 0.0000
E20_53 N20P54 N20P53 N53P1 N53P61 -0.0000
E20_54 N20P55 N20P54 N54P1 N54P61 0.0002
E20_55 N20P56 N20P55 N55P1 N55P61 0.0001
E20_56 N20P57 N20P56 N56P1 N56P61 -0.0000
E20_57 N20P58 N20P57 N57P1 N57P61 -0.0000
E20_58 N20P59 N20P58 N58P1 N58P61 -0.0000
E20_59 N20P60 N20P59 N59P1 N59P61 -0.0000
E20_60 N20P61 N20P60 N60P1 N60P61 -0.0000
R20 N20P61 N21P1 R=1
LAPLACE=+1/{K20}/(-S*S/4/3.14^2)^0.25
.param K20=3.7311e-05
Ctt20_21 N20P1 N21P1 13.47p

L21 N21P1 N21P2 0.1308u
E21_1 N21P3 N21P2 N1P1 N1P61 -0.0000
E21_2 N21P4 N21P3 N2P1 N2P61 -0.0000
E21_3 N21P5 N21P4 N3P1 N3P61 -0.0002
E21_4 N21P6 N21P5 N4P1 N4P61 -0.0006
E21_5 N21P7 N21P6 N5P1 N5P61 -0.0002
E21_6 N21P8 N21P7 N6P1 N6P61 -0.0001
E21_7 N21P9 N21P8 N7P1 N7P61 0.0006
E21_8 N21P10 N21P9 N8P1 N8P61 0.0036
E21_9 N21P11 N21P10 N9P1 N9P61 0.0101
E21_10 N21P12 N21P11 N10P1 N10P61 0.0034
E21_11 N21P13 N21P12 N11P1 N11P61 0.0006
E21_12 N21P14 N21P13 N12P1 N12P61 -0.0000
E21_13 N21P15 N21P14 N13P1 N13P61 -0.0002
E21_14 N21P16 N21P15 N14P1 N14P61 0.0032
E21_15 N21P17 N21P16 N15P1 N15P61 -0.0449
E21_16 N21P18 N21P17 N16P1 N16P61 -0.2201
E21_17 N21P19 N21P18 N17P1 N17P61 -0.0485
E21_18 N21P20 N21P19 N18P1 N18P61 0.0036
E21_19 N21P21 N21P20 N19P1 N19P61 0.0107
E21_20 N21P22 N21P21 N20P1 N20P61 -0.2291
E21_22 N21P23 N21P22 N22P1 N22P61 -0.2120
E21_23 N21P24 N21P23 N23P1 N23P61 0.0094
E21_24 N21P25 N21P24 N24P1 N24P61 -0.0005
E21_25 N21P26 N21P25 N25P1 N25P61 -0.0002
E21_26 N21P27 N21P26 N26P1 N26P61 0.0032
E21_27 N21P28 N21P27 N27P1 N27P61 -0.0449
E21_28 N21P29 N21P28 N28P1 N28P61 -0.2201
E21_29 N21P30 N21P29 N29P1 N29P61 -0.0485
E21_30 N21P31 N21P30 N30P1 N30P61 0.0036
E21_31 N21P32 N21P31 N31P1 N31P61 0.0006
E21_32 N21P33 N21P32 N32P1 N32P61 0.0036
E21_33 N21P34 N21P33 N33P1 N33P61 0.0101
E21_34 N21P35 N21P34 N34P1 N34P61 0.0034
E21_35 N21P36 N21P35 N35P1 N35P61 0.0006
E21_36 N21P37 N21P36 N36P1 N36P61 -0.0000
E21_37 N21P38 N21P37 N37P1 N37P61 -0.0000
E21_38 N21P39 N21P38 N38P1 N38P61 -0.0001
E21_39 N21P40 N21P39 N39P1 N39P61 -0.0002

```
E21_40 N21P41 N21P40 N40P1 N40P61 -0.0006
E21_41 N21P42 N21P41 N41P1 N41P61 -0.0002
E21_42 N21P43 N21P42 N42P1 N42P61 -0.0001
E21_43 N21P44 N21P43 N43P1 N43P61 -0.0000
E21_44 N21P45 N21P44 N44P1 N44P61 0.0000
E21_45 N21P46 N21P45 N45P1 N45P61 0.0000
E21_46 N21P47 N21P46 N46P1 N46P61 0.0000
E21_47 N21P48 N21P47 N47P1 N47P61 0.0000
E21_48 N21P49 N21P48 N48P1 N48P61 0.0000
E21_49 N21P50 N21P49 N49P1 N49P61 0.0000
E21_50 N21P51 N21P50 N50P1 N50P61 -0.0000
E21_51 N21P52 N21P51 N51P1 N51P61 -0.0000
E21_52 N21P53 N21P52 N52P1 N52P61 -0.0000
E21_53 N21P54 N21P53 N53P1 N53P61 -0.0000
E21_54 N21P55 N21P54 N54P1 N54P61 -0.0000
E21_55 N21P56 N21P55 N55P1 N55P61 -0.0000
E21_56 N21P57 N21P56 N56P1 N56P61 0.0000
E21_57 N21P58 N21P57 N57P1 N57P61 0.0000
E21_58 N21P59 N21P58 N58P1 N58P61 0.0000
E21_59 N21P60 N21P59 N59P1 N59P61 0.0000
E21_60 N21P61 N21P60 N60P1 N60P61 0.0000
R21 N21P61 N22P1 R=1
LAPLACE=+1/{K21}/(-S*S/4/3.14^2)^0.25
.param K21=4.0443e-05
Ctt21_22 N21P1 N22P1 14.55p

L22 N22P1 N22P2 0.1409u
E22_1 N22P3 N22P2 N1P1 N1P61 -0.0001
E22_2 N22P4 N22P3 N2P1 N2P61 -0.0002
E22_3 N22P5 N22P4 N3P1 N3P61 -0.0006
E22_4 N22P6 N22P5 N4P1 N4P61 -0.0002
E22_5 N22P7 N22P6 N5P1 N5P61 -0.0001
E22_6 N22P8 N22P7 N6P1 N6P61 -0.0000
E22_7 N22P9 N22P8 N7P1 N7P61 -0.0001
E22_8 N22P10 N22P9 N8P1 N8P61 0.0007
E22_9 N22P11 N22P10 N9P1 N9P61 0.0036
E22_10 N22P12 N22P11 N10P1 N10P61 0.0101
E22_11 N22P13 N22P12 N11P1 N11P61 0.0034
E22_12 N22P14 N22P13 N12P1 N12P61 0.0006
E22_13 N22P15 N22P14 N13P1 N13P61 0.0031
E22_14 N22P16 N22P15 N14P1 N14P61 -0.0450
E22_15 N22P17 N22P16 N15P1 N15P61 -0.2201
E22_16 N22P18 N22P17 N16P1 N16P61 -0.0484
E22_17 N22P19 N22P18 N17P1 N17P61 0.0038
E22_18 N22P20 N22P19 N18P1 N18P61 -0.0003
E22_19 N22P21 N22P20 N19P1 N19P61 -0.0006
E22_20 N22P22 N22P21 N20P1 N20P61 0.0109
E22_21 N22P23 N22P22 N21P1 N21P61 -0.2284
E22_23 N22P24 N22P23 N23P1 N23P61 -0.2125
E22_24 N22P25 N22P24 N24P1 N24P61 0.0092
E22_25 N22P26 N22P25 N25P1 N25P61 0.0031
E22_26 N22P27 N22P26 N26P1 N26P61 -0.0450
E22_27 N22P28 N22P27 N27P1 N27P61 -0.2201
E22_28 N22P29 N22P28 N28P1 N28P61 -0.0484
E22_29 N22P30 N22P29 N29P1 N29P61 0.0038
E22_30 N22P31 N22P30 N30P1 N30P61 -0.0003
E22_31 N22P32 N22P31 N31P1 N31P61 -0.0001
E22_32 N22P33 N22P32 N32P1 N32P61 0.0007
E22_33 N22P34 N22P33 N33P1 N33P61 0.0036
E22_34 N22P35 N22P34 N34P1 N34P61 0.0101
E22_35 N22P36 N22P35 N35P1 N35P61 0.0034
E22_36 N22P37 N22P36 N36P1 N36P61 0.0006
E22_37 N22P38 N22P37 N37P1 N37P61 -0.0001
E22_38 N22P39 N22P38 N38P1 N38P61 -0.0002
E22_39 N22P40 N22P39 N39P1 N39P61 -0.0006
E22_40 N22P41 N22P40 N40P1 N40P61 -0.0003
E22_41 N22P42 N22P41 N41P1 N41P61 -0.0001
E22_42 N22P43 N22P42 N42P1 N42P61 -0.0000
E22_43 N22P44 N22P43 N43P1 N43P61 0.0000
E22_44 N22P45 N22P44 N44P1 N44P61 0.0000
E22_45 N22P46 N22P45 N45P1 N45P61 0.0000
E22_46 N22P47 N22P46 N46P1 N46P61 0.0000
E22_47 N22P48 N22P47 N47P1 N47P61 0.0000
E22_48 N22P49 N22P48 N48P1 N48P61 -0.0000
E22_49 N22P50 N22P49 N49P1 N49P61 -0.0000
E22_50 N22P51 N22P50 N50P1 N50P61 0.0000
E22_51 N22P52 N22P51 N51P1 N51P61 -0.0000
E22_52 N22P53 N22P52 N52P1 N52P61 -0.0000
E22_53 N22P54 N22P53 N53P1 N53P61 -0.0000
E22_54 N22P55 N22P54 N54P1 N54P61 0.0000
E22_55 N22P56 N22P55 N55P1 N55P61 0.0000
E22_56 N22P57 N22P56 N56P1 N56P61 -0.0000
E22_57 N22P58 N22P57 N57P1 N57P61 -0.0000
E22_58 N22P59 N22P58 N58P1 N58P61 -0.0000
E22_59 N22P60 N22P59 N59P1 N59P61 -0.0000
E22_60 N22P61 N22P60 N60P1 N60P61 -0.0000
R22 N22P61 N23P1 R=1
LAPLACE=+1/{K22}/(-S*S/4/3.14^2)^0.25
.param K22=4.3576e-05
Ctt22_23 N22P1 N23P1 15.64p

L23 N23P1 N23P2 0.1511u
E23_1 N23P3 N23P2 N1P1 N1P61 0.0007
E23_2 N23P4 N23P3 N2P1 N2P61 -0.0005
E23_3 N23P5 N23P4 N3P1 N3P61 -0.0002
E23_4 N23P6 N23P5 N4P1 N4P61 -0.0000
E23_5 N23P7 N23P6 N5P1 N5P61 0.0000
E23_6 N23P8 N23P7 N6P1 N6P61 0.0000
E23_7 N23P9 N23P8 N7P1 N7P61 -0.0000
E23_8 N23P10 N23P9 N8P1 N8P61 -0.0001
E23_9 N23P11 N23P10 N9P1 N9P61 0.0007
E23_10 N23P12 N23P11 N10P1 N10P61 0.0036
E23_11 N23P13 N23P12 N11P1 N11P61 0.0100
E23_12 N23P14 N23P13 N12P1 N12P61 0.0049
E23_13 N23P15 N23P14 N13P1 N13P61 -0.0420
E23_14 N23P16 N23P15 N14P1 N14P61 -0.2203
E23_15 N23P17 N23P16 N15P1 N15P61 -0.0482
E23_16 N23P18 N23P17 N16P1 N16P61 0.0037
E23_17 N23P19 N23P18 N17P1 N17P61 -0.0003
E23_18 N23P20 N23P19 N18P1 N18P61 0.0000
E23_19 N23P21 N23P20 N19P1 N19P61 0.0000
E23_20 N23P22 N23P21 N20P1 N20P61 -0.0006
```

E23_21 N23P23 N23P22 N21P1 N21P61 0.0109
E23_22 N23P24 N23P23 N22P1 N22P61 -0.2279
E23_24 N23P25 N23P24 N24P1 N24P61 -0.2086
E23_25 N23P26 N23P25 N25P1 N25P61 -0.0420
E23_26 N23P27 N23P26 N26P1 N26P61 -0.2203
E23_27 N23P28 N23P27 N27P1 N27P61 -0.0482
E23_28 N23P29 N23P28 N28P1 N28P61 0.0037
E23_29 N23P30 N23P29 N29P1 N29P61 -0.0003
E23_30 N23P31 N23P30 N30P1 N30P61 0.0000
E23_31 N23P32 N23P31 N31P1 N31P61 -0.0000
E23_32 N23P33 N23P32 N32P1 N32P61 -0.0001
E23_33 N23P34 N23P33 N33P1 N33P61 0.0007
E23_34 N23P35 N23P34 N34P1 N34P61 0.0036
E23_35 N23P36 N23P35 N35P1 N35P61 0.0100
E23_36 N23P37 N23P36 N36P1 N36P61 0.0048
E23_37 N23P38 N23P37 N37P1 N37P61 0.0004
E23_38 N23P39 N23P38 N38P1 N38P61 -0.0006
E23_39 N23P40 N23P39 N39P1 N39P61 -0.0002
E23_40 N23P41 N23P40 N40P1 N40P61 -0.0001
E23_41 N23P42 N23P41 N41P1 N41P61 -0.0000
E23_42 N23P43 N23P42 N42P1 N42P61 -0.0000
E23_43 N23P44 N23P43 N43P1 N43P61 -0.0000
E23_44 N23P45 N23P44 N44P1 N44P61 0.0000
E23_45 N23P46 N23P45 N45P1 N45P61 0.0000
E23_46 N23P47 N23P46 N46P1 N46P61 0.0000
E23_47 N23P48 N23P47 N47P1 N47P61 0.0000
E23_48 N23P49 N23P48 N48P1 N48P61 0.0004
E23_49 N23P50 N23P49 N49P1 N49P61 0.0002
E23_50 N23P51 N23P50 N50P1 N50P61 -0.0000
E23_51 N23P52 N23P51 N51P1 N51P61 -0.0000
E23_52 N23P53 N23P52 N52P1 N52P61 -0.0000
E23_53 N23P54 N23P53 N53P1 N53P61 0.0000
E23_54 N23P55 N23P54 N54P1 N54P61 -0.0000
E23_55 N23P56 N23P55 N55P1 N55P61 -0.0000
E23_56 N23P57 N23P56 N56P1 N56P61 0.0000
E23_57 N23P58 N23P57 N57P1 N57P61 0.0000
E23_58 N23P59 N23P58 N58P1 N58P61 0.0000
E23_59 N23P60 N23P59 N59P1 N59P61 0.0000
E23_60 N23P61 N23P60 N60P1 N60P61 0.0002
R23 N23P61 N24P1 R=1
LAPLACE=+1/{K23}/(-S*S/4/3.14^2)^0.25
.param K23=4.6709e-05
Ctt23_24 N23P1 N24P1 16.72p

L24 N24P1 N24P2 0.1770u
E24_1 N24P3 N24P2 N1P1 N1P61 -0.0158
E24_2 N24P4 N24P3 N2P1 N2P61 -0.0017
E24_3 N24P5 N24P4 N3P1 N3P61 -0.0014
E24_4 N24P6 N24P5 N4P1 N4P61 -0.0008
E24_5 N24P7 N24P6 N5P1 N5P61 -0.0005
E24_6 N24P8 N24P7 N6P1 N6P61 -0.0002
E24_7 N24P9 N24P8 N7P1 N7P61 0.0002
E24_8 N24P10 N24P9 N8P1 N8P61 0.0000
E24_9 N24P11 N24P10 N9P1 N9P61 -0.0000
E24_10 N24P12 N24P11 N10P1 N10P61 0.0008
E24_11 N24P13 N24P12 N11P1 N11P61 0.0058
E24_12 N24P14 N24P13 N12P1 N12P61 -0.0123
E24_13 N24P15 N24P14 N13P1 N13P61 -0.3017
E24_14 N24P16 N24P15 N14P1 N14P61 -0.0492
E24_15 N24P17 N24P16 N15P1 N15P61 0.0038
E24_16 N24P18 N24P17 N16P1 N16P61 -0.0003
E24_17 N24P19 N24P18 N17P1 N17P61 0.0000
E24_18 N24P20 N24P19 N18P1 N18P61 0.0002
E24_19 N24P21 N24P20 N19P1 N19P61 0.0003
E24_20 N24P22 N24P21 N20P1 N20P61 0.0000
E24_21 N24P23 N24P22 N21P1 N21P61 -0.0007
E24_22 N24P24 N24P23 N22P1 N22P61 0.0115
E24_23 N24P25 N24P24 N23P1 N23P61 -0.2443
E24_25 N24P26 N24P25 N25P1 N25P61 -0.3015
E24_26 N24P27 N24P26 N26P1 N26P61 -0.0492
E24_27 N24P28 N24P27 N27P1 N27P61 0.0039
E24_28 N24P29 N24P28 N28P1 N28P61 -0.0003
E24_29 N24P30 N24P29 N29P1 N29P61 0.0000
E24_30 N24P31 N24P30 N30P1 N30P61 0.0003
E24_31 N24P32 N24P31 N31P1 N31P61 0.0003
E24_32 N24P33 N24P32 N32P1 N32P61 -0.0000
E24_33 N24P34 N24P33 N33P1 N33P61 -0.0001
E24_34 N24P35 N24P34 N34P1 N34P61 0.0007
E24_35 N24P36 N24P35 N35P1 N35P61 0.0057
E24_36 N24P37 N24P36 N36P1 N36P61 -0.0120
E24_37 N24P38 N24P37 N37P1 N37P61 -0.0111
E24_38 N24P39 N24P38 N38P1 N38P61 0.0005
E24_39 N24P40 N24P39 N39P1 N39P61 -0.0001
E24_40 N24P41 N24P40 N40P1 N40P61 -0.0000
E24_41 N24P42 N24P41 N41P1 N41P61 -0.0000
E24_42 N24P43 N24P42 N42P1 N42P61 0.0003
E24_43 N24P44 N24P43 N43P1 N43P61 0.0003
E24_44 N24P45 N24P44 N44P1 N44P61 -0.0000
E24_45 N24P46 N24P45 N45P1 N45P61 0.0000
E24_46 N24P47 N24P46 N46P1 N46P61 -0.0000
E24_47 N24P48 N24P47 N47P1 N47P61 0.0004
E24_48 N24P49 N24P48 N48P1 N48P61 -0.0061
E24_49 N24P50 N24P49 N49P1 N49P61 -0.0041
E24_50 N24P51 N24P50 N50P1 N50P61 0.0003
E24_51 N24P52 N24P51 N51P1 N51P61 0.0000
E24_52 N24P53 N24P52 N52P1 N52P61 0.0000
E24_53 N24P54 N24P53 N53P1 N53P61 -0.0000
E24_54 N24P55 N24P54 N54P1 N54P61 0.0003
E24_55 N24P56 N24P55 N55P1 N55P61 0.0004
E24_56 N24P57 N24P56 N56P1 N56P61 -0.0001
E24_57 N24P58 N24P57 N57P1 N57P61 -0.0003
E24_58 N24P59 N24P58 N58P1 N58P61 -0.0005
E24_59 N24P60 N24P59 N59P1 N59P61 -0.0007
E24_60 N24P61 N24P60 N60P1 N60P61 -0.0045
R24 N24P61 N25P1 R=1
LAPLACE=+1/{K24}/(-S*S/4/3.14^2)^0.25
.param K24=4.9841e-05

L25 N25P1 N25P2 0.1770u
E25_1 N25P3 N25P2 N1P1 N1P61 -0.0092
E25_2 N25P4 N25P3 N2P1 N2P61 -0.0011
E25_3 N25P5 N25P4 N3P1 N3P61 -0.0009

APPENDICES

E25_4 N25P6 N25P5 N4P1 N4P61 -0.0006
E25_5 N25P7 N25P6 N5P1 N5P61 -0.0004
E25_6 N25P8 N25P7 N6P1 N6P61 0.0000
E25_7 N25P9 N25P8 N7P1 N7P61 0.0002
E25_8 N25P10 N25P9 N8P1 N8P61 0.0000
E25_9 N25P11 N25P10 N9P1 N9P61 0.0000
E25_10 N25P12 N25P11 N10P1 N10P61 -0.0001
E25_11 N25P13 N25P12 N11P1 N11P61 0.0006
E25_12 N25P14 N25P13 N12P1 N12P61 -0.0113
E25_13 N25P15 N25P14 N13P1 N13P61 -0.0121
E25_14 N25P16 N25P15 N14P1 N14P61 0.0057
E25_15 N25P17 N25P16 N15P1 N15P61 0.0007
E25_16 N25P18 N25P17 N16P1 N16P61 -0.0001
E25_17 N25P19 N25P18 N17P1 N17P61 -0.0000
E25_18 N25P20 N25P19 N18P1 N18P61 0.0003
E25_19 N25P21 N25P20 N19P1 N19P61 0.0003
E25_20 N25P22 N25P21 N20P1 N20P61 0.0000
E25_21 N25P23 N25P22 N21P1 N21P61 -0.0003
E25_22 N25P24 N25P23 N22P1 N22P61 0.0039
E25_23 N25P25 N25P24 N23P1 N23P61 -0.0492
E25_24 N25P26 N25P25 N24P1 N24P61 -0.3014
E25_26 N25P27 N25P26 N26P1 N26P61 -0.2443
E25_27 N25P28 N25P27 N27P1 N27P61 0.0115
E25_28 N25P29 N25P28 N28P1 N28P61 -0.0007
E25_29 N25P30 N25P29 N29P1 N29P61 0.0000
E25_30 N25P31 N25P30 N30P1 N30P61 0.0003
E25_31 N25P32 N25P31 N31P1 N31P61 0.0003
E25_32 N25P33 N25P32 N32P1 N32P61 0.0000
E25_33 N25P34 N25P33 N33P1 N33P61 -0.0003
E25_34 N25P35 N25P34 N34P1 N34P61 0.0039
E25_35 N25P36 N25P35 N35P1 N35P61 -0.0492
E25_36 N25P37 N25P36 N36P1 N36P61 -0.3014
E25_37 N25P38 N25P37 N37P1 N37P61 -0.0120
E25_38 N25P39 N25P38 N38P1 N38P61 0.0057
E25_39 N25P40 N25P39 N39P1 N39P61 0.0007
E25_40 N25P41 N25P40 N40P1 N40P61 -0.0001
E25_41 N25P42 N25P41 N41P1 N41P61 -0.0000
E25_42 N25P43 N25P42 N42P1 N42P61 0.0003
E25_43 N25P44 N25P43 N43P1 N43P61 0.0003
E25_44 N25P45 N25P44 N44P1 N44P61 -0.0000
E25_45 N25P46 N25P45 N45P1 N45P61 -0.0000
E25_46 N25P47 N25P46 N46P1 N46P61 -0.0001
E25_47 N25P48 N25P47 N47P1 N47P61 0.0005
E25_48 N25P49 N25P48 N48P1 N48P61 -0.0111
E25_49 N25P50 N25P49 N49P1 N49P61 -0.0062
E25_50 N25P51 N25P50 N50P1 N50P61 0.0005
E25_51 N25P52 N25P51 N51P1 N51P61 0.0000
E25_52 N25P53 N25P52 N52P1 N52P61 0.0000
E25_53 N25P54 N25P53 N53P1 N53P61 -0.0000
E25_54 N25P55 N25P54 N54P1 N54P61 0.0003
E25_55 N25P56 N25P55 N55P1 N55P61 0.0002
E25_56 N25P57 N25P56 N56P1 N56P61 -0.0002
E25_57 N25P58 N25P57 N57P1 N57P61 -0.0004
E25_58 N25P59 N25P58 N58P1 N58P61 -0.0007
E25_59 N25P60 N25P59 N59P1 N59P61 -0.0009
E25_60 N25P61 N25P60 N60P1 N60P61 -0.0063

R25 N25P61 N26P1 R=1
LAPLACE=+1/{K25}/(-S*S/4/3.14^2)^0.25
.param K25=4.9841e-05
Ctt25_26 N25P1 N26P1 16.72p

L26 N26P1 N26P2 0.1511u
E26_1 N26P3 N26P2 N1P1 N1P61 0.0005
E26_2 N26P4 N26P3 N2P1 N2P61 0.0001
E26_3 N26P5 N26P4 N3P1 N3P61 0.0001
E26_4 N26P6 N26P5 N4P1 N4P61 0.0000
E26_5 N26P7 N26P6 N5P1 N5P61 0.0000
E26_6 N26P8 N26P7 N6P1 N6P61 -0.0000
E26_7 N26P9 N26P8 N7P1 N7P61 -0.0000
E26_8 N26P10 N26P9 N8P1 N8P61 -0.0000
E26_9 N26P11 N26P10 N9P1 N9P61 -0.0001
E26_10 N26P12 N26P11 N10P1 N10P61 -0.0002
E26_11 N26P13 N26P12 N11P1 N11P61 -0.0006
E26_12 N26P14 N26P13 N12P1 N12P61 0.0004
E26_13 N26P15 N26P14 N13P1 N13P61 0.0048
E26_14 N26P16 N26P15 N14P1 N14P61 0.0100
E26_15 N26P17 N26P16 N15P1 N15P61 0.0036
E26_16 N26P18 N26P17 N16P1 N16P61 0.0007
E26_17 N26P19 N26P18 N17P1 N17P61 -0.0001
E26_18 N26P20 N26P19 N18P1 N18P61 -0.0000
E26_19 N26P21 N26P20 N19P1 N19P61 0.0000
E26_20 N26P22 N26P21 N20P1 N20P61 -0.0003
E26_21 N26P23 N26P22 N21P1 N21P61 0.0037
E26_22 N26P24 N26P23 N22P1 N22P61 -0.0482
E26_23 N26P25 N26P24 N23P1 N23P61 -0.2203
E26_24 N26P26 N26P25 N24P1 N24P61 -0.0420
E26_25 N26P27 N26P26 N25P1 N25P61 -0.2086
E26_27 N26P28 N26P27 N27P1 N27P61 -0.2279
E26_28 N26P29 N26P28 N28P1 N28P61 0.0109
E26_29 N26P30 N26P29 N29P1 N29P61 -0.0006
E26_30 N26P31 N26P30 N30P1 N30P61 0.0000
E26_31 N26P32 N26P31 N31P1 N31P61 0.0000
E26_32 N26P33 N26P32 N32P1 N32P61 -0.0003
E26_33 N26P34 N26P33 N33P1 N33P61 0.0037
E26_34 N26P35 N26P34 N34P1 N34P61 -0.0482
E26_35 N26P36 N26P35 N35P1 N35P61 -0.2203
E26_36 N26P37 N26P36 N36P1 N36P61 -0.0420
E26_37 N26P38 N26P37 N37P1 N37P61 0.0048
E26_38 N26P39 N26P38 N38P1 N38P61 0.0100
E26_39 N26P40 N26P39 N39P1 N39P61 0.0036
E26_40 N26P41 N26P40 N40P1 N40P61 0.0007
E26_41 N26P42 N26P41 N41P1 N41P61 -0.0001
E26_42 N26P43 N26P42 N42P1 N42P61 -0.0000
E26_43 N26P44 N26P43 N43P1 N43P61 -0.0000
E26_44 N26P45 N26P44 N44P1 N44P61 -0.0000
E26_45 N26P46 N26P45 N45P1 N45P61 -0.0001
E26_46 N26P47 N26P46 N46P1 N46P61 -0.0002
E26_47 N26P48 N26P47 N47P1 N47P61 -0.0006
E26_48 N26P49 N26P48 N48P1 N48P61 0.0004
E26_49 N26P50 N26P49 N49P1 N49P61 0.0004
E26_50 N26P51 N26P50 N50P1 N50P61 0.0000
E26_51 N26P52 N26P51 N51P1 N51P61 0.0000

APPENDICES

E26_52 N26P53 N26P52 N52P1 N52P61 0.0000
E26_53 N26P54 N26P53 N53P1 N53P61 0.0000
E26_54 N26P55 N26P54 N54P1 N54P61 -0.0000
E26_55 N26P56 N26P55 N55P1 N55P61 -0.0000
E26_56 N26P57 N26P56 N56P1 N56P61 0.0000
E26_57 N26P58 N26P57 N57P1 N57P61 0.0000
E26_58 N26P59 N26P58 N58P1 N58P61 0.0000
E26_59 N26P60 N26P59 N59P1 N59P61 0.0000
E26_60 N26P61 N26P60 N60P1 N60P61 0.0003
R26 N26P61 N27P1 R=1
LAPLACE=+1/{K26}/(-S*S/4/3.14^2)^0.25
.param K26=4.6709e-05
Ctt26_27 N26P1 N27P1 15.64p

L27 N27P1 N27P2 0.1409u
E27_1 N27P3 N27P2 N1P1 N1P61 -0.0000
E27_2 N27P4 N27P3 N2P1 N2P61 0.0000
E27_3 N27P5 N27P4 N3P1 N3P61 0.0000
E27_4 N27P6 N27P5 N4P1 N4P61 0.0000
E27_5 N27P7 N27P6 N5P1 N5P61 0.0000
E27_6 N27P8 N27P7 N6P1 N6P61 0.0000
E27_7 N27P9 N27P8 N7P1 N7P61 -0.0000
E27_8 N27P10 N27P9 N8P1 N8P61 -0.0001
E27_9 N27P11 N27P10 N9P1 N9P61 -0.0003
E27_10 N27P12 N27P11 N10P1 N10P61 -0.0006
E27_11 N27P13 N27P12 N11P1 N11P61 -0.0002
E27_12 N27P14 N27P13 N12P1 N12P61 -0.0001
E27_13 N27P15 N27P14 N13P1 N13P61 0.0006
E27_14 N27P16 N27P15 N14P1 N14P61 0.0034
E27_15 N27P17 N27P16 N15P1 N15P61 0.0101
E27_16 N27P18 N27P17 N16P1 N16P61 0.0036
E27_17 N27P19 N27P18 N17P1 N17P61 0.0007
E27_18 N27P20 N27P19 N18P1 N18P61 -0.0001
E27_19 N27P21 N27P20 N19P1 N19P61 -0.0003
E27_20 N27P22 N27P21 N20P1 N20P61 0.0038
E27_21 N27P23 N27P22 N21P1 N21P61 -0.0484
E27_22 N27P24 N27P23 N22P1 N22P61 -0.2201
E27_23 N27P25 N27P24 N23P1 N23P61 -0.0450
E27_24 N27P26 N27P25 N24P1 N24P61 0.0031
E27_25 N27P27 N27P26 N25P1 N25P61 0.0092
E27_26 N27P28 N27P27 N26P1 N26P61 -0.2125
E27_28 N27P29 N27P28 N28P1 N28P61 -0.2284
E27_29 N27P30 N27P29 N29P1 N29P61 0.0109
E27_30 N27P31 N27P30 N30P1 N30P61 -0.0006
E27_31 N27P32 N27P31 N31P1 N31P61 -0.0003
E27_32 N27P33 N27P32 N32P1 N32P61 0.0038
E27_33 N27P34 N27P33 N33P1 N33P61 -0.0484
E27_34 N27P35 N27P34 N34P1 N34P61 -0.2201
E27_35 N27P36 N27P35 N35P1 N35P61 -0.0450
E27_36 N27P37 N27P36 N36P1 N36P61 0.0031
E27_37 N27P38 N27P37 N37P1 N37P61 0.0006
E27_38 N27P39 N27P38 N38P1 N38P61 0.0034
E27_39 N27P40 N27P39 N39P1 N39P61 0.0101
E27_40 N27P41 N27P40 N40P1 N40P61 0.0036
E27_41 N27P42 N27P41 N41P1 N41P61 0.0007
E27_42 N27P43 N27P42 N42P1 N42P61 -0.0001
E27_43 N27P44 N27P43 N43P1 N43P61 -0.0000
E27_44 N27P45 N27P44 N44P1 N44P61 -0.0001
E27_45 N27P46 N27P45 N45P1 N45P61 -0.0003
E27_46 N27P47 N27P46 N46P1 N46P61 -0.0006
E27_47 N27P48 N27P47 N47P1 N47P61 -0.0002
E27_48 N27P49 N27P48 N48P1 N48P61 -0.0001
E27_49 N27P50 N27P49 N49P1 N49P61 -0.0000
E27_50 N27P51 N27P50 N50P1 N50P61 0.0000
E27_51 N27P52 N27P51 N51P1 N51P61 0.0000
E27_52 N27P53 N27P52 N52P1 N52P61 0.0000
E27_53 N27P54 N27P53 N53P1 N53P61 0.0000
E27_54 N27P55 N27P54 N54P1 N54P61 0.0000
E27_55 N27P56 N27P55 N55P1 N55P61 0.0000
E27_56 N27P57 N27P56 N56P1 N56P61 -0.0000
E27_57 N27P58 N27P57 N57P1 N57P61 -0.0000
E27_58 N27P59 N27P58 N58P1 N58P61 -0.0000
E27_59 N27P60 N27P59 N59P1 N59P61 -0.0000
E27_60 N27P61 N27P60 N60P1 N60P61 -0.0000
R27 N27P61 N28P1 R=1
LAPLACE=+1/{K27}/(-S*S/4/3.14^2)^0.25
.param K27=4.3576e-05
Ctt27_28 N27P1 N28P1 14.55p

L28 N28P1 N28P2 0.1308u
E28_1 N28P3 N28P2 N1P1 N1P61 0.0000
E28_2 N28P4 N28P3 N2P1 N2P61 0.0000
E28_3 N28P5 N28P4 N3P1 N3P61 0.0000
E28_4 N28P6 N28P5 N4P1 N4P61 0.0000
E28_5 N28P7 N28P6 N5P1 N5P61 0.0000
E28_6 N28P8 N28P7 N6P1 N6P61 -0.0000
E28_7 N28P9 N28P8 N7P1 N7P61 -0.0001
E28_8 N28P10 N28P9 N8P1 N8P61 -0.0002
E28_9 N28P11 N28P10 N9P1 N9P61 -0.0006
E28_10 N28P12 N28P11 N10P1 N10P61 -0.0002
E28_11 N28P13 N28P12 N11P1 N11P61 -0.0001
E28_12 N28P14 N28P13 N12P1 N12P61 -0.0000
E28_13 N28P15 N28P14 N13P1 N13P61 -0.0000
E28_14 N28P16 N28P15 N14P1 N14P61 0.0006
E28_15 N28P17 N28P16 N15P1 N15P61 0.0034
E28_16 N28P18 N28P17 N16P1 N16P61 0.0101
E28_17 N28P19 N28P18 N17P1 N17P61 0.0036
E28_18 N28P20 N28P19 N18P1 N18P61 0.0006
E28_19 N28P21 N28P20 N19P1 N19P61 0.0036
E28_20 N28P22 N28P21 N20P1 N20P61 -0.0485
E28_21 N28P23 N28P22 N21P1 N21P61 -0.2201
E28_22 N28P24 N28P23 N22P1 N22P61 -0.0449
E28_23 N28P25 N28P24 N23P1 N23P61 0.0032
E28_24 N28P26 N28P25 N24P1 N24P61 -0.0002
E28_25 N28P27 N28P26 N25P1 N25P61 -0.0005
E28_26 N28P28 N28P27 N26P1 N26P61 0.0094
E28_27 N28P29 N28P28 N27P1 N27P61 -0.2120
E28_29 N28P30 N28P29 N29P1 N29P61 -0.2291
E28_30 N28P31 N28P30 N30P1 N30P61 0.0107
E28_31 N28P32 N28P31 N31P1 N31P61 0.0036
E28_32 N28P33 N28P32 N32P1 N32P61 -0.0485
E28_33 N28P34 N28P33 N33P1 N33P61 -0.2201

E28_34 N28P35 N28P34 N34P1 N34P61 -0.0449
E28_35 N28P36 N28P35 N35P1 N35P61 0.0032
E28_36 N28P37 N28P36 N36P1 N36P61 -0.0002
E28_37 N28P38 N28P37 N37P1 N37P61 -0.0000
E28_38 N28P39 N28P38 N38P1 N38P61 0.0006
E28_39 N28P40 N28P39 N39P1 N39P61 0.0034
E28_40 N28P41 N28P40 N40P1 N40P61 0.0101
E28_41 N28P42 N28P41 N41P1 N41P61 0.0036
E28_42 N28P43 N28P42 N42P1 N42P61 0.0006
E28_43 N28P44 N28P43 N43P1 N43P61 -0.0001
E28_44 N28P45 N28P44 N44P1 N44P61 -0.0002
E28_45 N28P46 N28P45 N45P1 N45P61 -0.0006
E28_46 N28P47 N28P46 N46P1 N46P61 -0.0002
E28_47 N28P48 N28P47 N47P1 N47P61 -0.0001
E28_48 N28P49 N28P48 N48P1 N48P61 -0.0000
E28_49 N28P50 N28P49 N49P1 N49P61 0.0000
E28_50 N28P51 N28P50 N50P1 N50P61 0.0000
E28_51 N28P52 N28P51 N51P1 N51P61 0.0000
E28_52 N28P53 N28P52 N52P1 N52P61 0.0000
E28_53 N28P54 N28P53 N53P1 N53P61 0.0000
E28_54 N28P55 N28P54 N54P1 N54P61 -0.0000
E28_55 N28P56 N28P55 N55P1 N55P61 -0.0000
E28_56 N28P57 N28P56 N56P1 N56P61 -0.0000
E28_57 N28P58 N28P57 N57P1 N57P61 -0.0000
E28_58 N28P59 N28P58 N58P1 N58P61 -0.0000
E28_59 N28P60 N28P59 N59P1 N59P61 0.0000
E28_60 N28P61 N28P60 N60P1 N60P61 0.0000
R28 N28P61 N29P1 R=1
LAPLACE=+1/{K28}/(-S*S/4/3.14^2)^0.25
.param K28=4.0443e-05
Ctt28_29 N28P1 N29P1 13.47p

L29 N29P1 N29P2 0.1207u
E29_1 N29P3 N29P2 N1P1 N1P61 -0.0000
E29_2 N29P4 N29P3 N2P1 N2P61 -0.0000
E29_3 N29P5 N29P4 N3P1 N3P61 0.0000
E29_4 N29P6 N29P5 N4P1 N4P61 0.0000
E29_5 N29P7 N29P6 N5P1 N5P61 0.0000
E29_6 N29P8 N29P7 N6P1 N6P61 0.0004
E29_7 N29P9 N29P8 N7P1 N7P61 0.0004
E29_8 N29P10 N29P9 N8P1 N8P61 -0.0006
E29_9 N29P11 N29P10 N9P1 N9P61 -0.0002
E29_10 N29P12 N29P11 N10P1 N10P61 -0.0001
E29_11 N29P13 N29P12 N11P1 N11P61 -0.0000
E29_12 N29P14 N29P13 N12P1 N12P61 -0.0000
E29_13 N29P15 N29P14 N13P1 N13P61 -0.0000
E29_14 N29P16 N29P15 N14P1 N14P61 -0.0000
E29_15 N29P17 N29P16 N15P1 N15P61 0.0006
E29_16 N29P18 N29P17 N16P1 N16P61 0.0034
E29_17 N29P19 N29P18 N17P1 N17P61 0.0100
E29_18 N29P20 N29P19 N18P1 N18P61 0.0052
E29_19 N29P21 N29P20 N19P1 N19P61 -0.0454
E29_20 N29P22 N29P21 N20P1 N20P61 -0.2203
E29_21 N29P23 N29P22 N21P1 N21P61 -0.0448
E29_22 N29P24 N29P23 N22P1 N22P61 0.0032
E29_23 N29P25 N29P24 N23P1 N23P61 -0.0002
E29_24 N29P26 N29P25 N24P1 N24P61 0.0000
E29_25 N29P27 N29P26 N25P1 N25P61 0.0000
E29_26 N29P28 N29P27 N26P1 N26P61 -0.0005
E29_27 N29P29 N29P28 N27P1 N27P61 0.0093
E29_28 N29P30 N29P29 N28P1 N28P61 -0.2114
E29_30 N29P31 N29P30 N30P1 N30P61 -0.2252
E29_31 N29P32 N29P31 N31P1 N31P61 -0.0454
E29_32 N29P33 N29P32 N32P1 N32P61 -0.2203
E29_33 N29P34 N29P33 N33P1 N33P61 -0.0448
E29_34 N29P35 N29P34 N34P1 N34P61 0.0032
E29_35 N29P36 N29P35 N35P1 N35P61 -0.0002
E29_36 N29P37 N29P36 N36P1 N36P61 0.0000
E29_37 N29P38 N29P37 N37P1 N37P61 -0.0000
E29_38 N29P39 N29P38 N38P1 N38P61 -0.0000
E29_39 N29P40 N29P39 N39P1 N39P61 0.0006
E29_40 N29P41 N29P40 N40P1 N40P61 0.0034
E29_41 N29P42 N29P41 N41P1 N41P61 0.0100
E29_42 N29P43 N29P42 N42P1 N42P61 0.0051
E29_43 N29P44 N29P43 N43P1 N43P61 0.0004
E29_44 N29P45 N29P44 N44P1 N44P61 -0.0006
E29_45 N29P46 N29P45 N45P1 N45P61 -0.0002
E29_46 N29P47 N29P46 N46P1 N46P61 -0.0001
E29_47 N29P48 N29P47 N47P1 N47P61 -0.0000
E29_48 N29P49 N29P48 N48P1 N48P61 -0.0000
E29_49 N29P50 N29P49 N49P1 N49P61 -0.0000
E29_50 N29P51 N29P50 N50P1 N50P61 0.0000
E29_51 N29P52 N29P51 N51P1 N51P61 0.0000
E29_52 N29P53 N29P52 N52P1 N52P61 0.0000
E29_53 N29P54 N29P53 N53P1 N53P61 0.0000
E29_54 N29P55 N29P54 N54P1 N54P61 0.0003
E29_55 N29P56 N29P55 N55P1 N55P61 0.0002
E29_56 N29P57 N29P56 N56P1 N56P61 0.0000
E29_57 N29P58 N29P57 N57P1 N57P61 -0.0000
E29_58 N29P59 N29P58 N58P1 N58P61 -0.0000
E29_59 N29P60 N29P59 N59P1 N59P61 -0.0000
E29_60 N29P61 N29P60 N60P1 N60P61 -0.0000
R29 N29P61 N30P1 R=1
LAPLACE=+1/{K29}/(-S*S/4/3.14^2)^0.25
.param K29=3.7311e-05
Ctt29_30 N29P1 N30P1 12.38p

L30 N30P1 N30P2 0.1212u
E30_1 N30P3 N30P2 N1P1 N1P61 0.0005
E30_2 N30P4 N30P3 N2P1 N2P61 0.0001
E30_3 N30P5 N30P4 N3P1 N3P61 0.0000
E30_4 N30P6 N30P5 N4P1 N4P61 -0.0002
E30_5 N30P7 N30P6 N5P1 N5P61 -0.0002
E30_6 N30P8 N30P7 N6P1 N6P61 -0.0062
E30_7 N30P9 N30P8 N7P1 N7P61 -0.0098
E30_8 N30P10 N30P9 N8P1 N8P61 0.0004
E30_9 N30P11 N30P10 N9P1 N9P61 -0.0001
E30_10 N30P12 N30P11 N10P1 N10P61 -0.0000
E30_11 N30P13 N30P12 N11P1 N11P61 -0.0000
E30_12 N30P14 N30P13 N12P1 N12P61 0.0002
E30_13 N30P15 N30P14 N13P1 N13P61 0.0002
E30_14 N30P16 N30P15 N14P1 N14P61 -0.0000

E30_15 N30P17 N30P16 N15P1 N15P61 -0.0000
E30_16 N30P18 N30P17 N16P1 N16P61 0.0006
E30_17 N30P19 N30P18 N17P1 N17P61 0.0052
E30_18 N30P20 N30P19 N18P1 N18P61 -0.0107
E30_19 N30P21 N30P20 N19P1 N19P61 -0.2997
E30_20 N30P22 N30P21 N20P1 N20P61 -0.0456
E30_21 N30P23 N30P22 N21P1 N21P61 0.0033
E30_22 N30P24 N30P23 N22P1 N22P61 -0.0002
E30_23 N30P25 N30P24 N23P1 N23P61 0.0000
E30_24 N30P26 N30P25 N24P1 N24P61 0.0002
E30_25 N30P27 N30P26 N25P1 N25P61 0.0002
E30_26 N30P28 N30P27 N26P1 N26P61 0.0000
E30_27 N30P29 N30P28 N27P1 N27P61 -0.0005
E30_28 N30P30 N30P29 N28P1 N28P61 0.0099
E30_29 N30P31 N30P30 N29P1 N29P61 -0.2261
E30_31 N30P32 N30P31 N31P1 N31P61 -0.2997
E30_32 N30P33 N30P32 N32P1 N32P61 -0.0456
E30_33 N30P34 N30P33 N33P1 N33P61 0.0033
E30_34 N30P35 N30P34 N34P1 N34P61 -0.0002
E30_35 N30P36 N30P35 N35P1 N35P61 0.0000
E30_36 N30P37 N30P36 N36P1 N36P61 0.0002
E30_37 N30P38 N30P37 N37P1 N37P61 0.0002
E30_38 N30P39 N30P38 N38P1 N38P61 -0.0000
E30_39 N30P40 N30P39 N39P1 N39P61 -0.0000
E30_40 N30P41 N30P40 N40P1 N40P61 0.0006
E30_41 N30P42 N30P41 N41P1 N41P61 0.0052
E30_42 N30P43 N30P42 N42P1 N42P61 -0.0107
E30_43 N30P44 N30P43 N43P1 N43P61 -0.0098
E30_44 N30P45 N30P44 N44P1 N44P61 0.0004
E30_45 N30P46 N30P45 N45P1 N45P61 -0.0001
E30_46 N30P47 N30P46 N46P1 N46P61 -0.0000
E30_47 N30P48 N30P47 N47P1 N47P61 -0.0000
E30_48 N30P49 N30P48 N48P1 N48P61 0.0002
E30_49 N30P50 N30P49 N49P1 N49P61 0.0002
E30_50 N30P51 N30P50 N50P1 N50P61 -0.0000
E30_51 N30P52 N30P51 N51P1 N51P61 -0.0000
E30_52 N30P53 N30P52 N52P1 N52P61 -0.0000
E30_53 N30P54 N30P53 N53P1 N53P61 0.0003
E30_54 N30P55 N30P54 N54P1 N54P61 -0.0048
E30_55 N30P56 N30P55 N55P1 N55P61 -0.0034
E30_56 N30P57 N30P56 N56P1 N56P61 -0.0000
E30_57 N30P58 N30P57 N57P1 N57P61 0.0000
E30_58 N30P59 N30P58 N58P1 N58P61 0.0001
E30_59 N30P60 N30P59 N59P1 N59P61 0.0002
E30_60 N30P61 N30P60 N60P1 N60P61 0.0006
R30 N30P61 N31P1 R=1
LAPLACE=+1/{K30}/(-S*S/4/3.14^2)^0.25
.param K30=3.4178e-05

L31 N31P1 N31P2 0.1212u
E31_1 N31P3 N31P2 N1P1 N1P61 0.0006
E31_2 N31P4 N31P3 N2P1 N2P61 0.0002
E31_3 N31P5 N31P4 N3P1 N3P61 0.0001
E31_4 N31P6 N31P5 N4P1 N4P61 0.0000
E31_5 N31P7 N31P6 N5P1 N5P61 -0.0000
E31_6 N31P8 N31P7 N6P1 N6P61 -0.0034
E31_7 N31P9 N31P8 N7P1 N7P61 -0.0048
E31_8 N31P10 N31P9 N8P1 N8P61 0.0003
E31_9 N31P11 N31P10 N9P1 N9P61 -0.0000
E31_10 N31P12 N31P11 N10P1 N10P61 -0.0000
E31_11 N31P13 N31P12 N11P1 N11P61 -0.0000
E31_12 N31P14 N31P13 N12P1 N12P61 0.0002
E31_13 N31P15 N31P14 N13P1 N13P61 0.0002
E31_14 N31P16 N31P15 N14P1 N14P61 -0.0000
E31_15 N31P17 N31P16 N15P1 N15P61 -0.0000
E31_16 N31P18 N31P17 N16P1 N16P61 -0.0001
E31_17 N31P19 N31P18 N17P1 N17P61 0.0004
E31_18 N31P20 N31P19 N18P1 N18P61 -0.0098
E31_19 N31P21 N31P20 N19P1 N19P61 -0.0107
E31_20 N31P22 N31P21 N20P1 N20P61 0.0052
E31_21 N31P23 N31P22 N21P1 N21P61 0.0006
E31_22 N31P24 N31P23 N22P1 N22P61 -0.0000
E31_23 N31P25 N31P24 N23P1 N23P61 -0.0000
E31_24 N31P26 N31P25 N24P1 N24P61 0.0002
E31_25 N31P27 N31P26 N25P1 N25P61 0.0002
E31_26 N31P28 N31P27 N26P1 N26P61 0.0000
E31_27 N31P29 N31P28 N27P1 N27P61 -0.0002
E31_28 N31P30 N31P29 N28P1 N28P61 0.0033
E31_29 N31P31 N31P30 N29P1 N29P61 -0.0456
E31_30 N31P32 N31P31 N30P1 N30P61 -0.2997
E31_32 N31P33 N31P32 N32P1 N32P61 -0.2261
E31_33 N31P34 N31P33 N33P1 N33P61 0.0099
E31_34 N31P35 N31P34 N34P1 N34P61 -0.0005
E31_35 N31P36 N31P35 N35P1 N35P61 0.0000
E31_36 N31P37 N31P36 N36P1 N36P61 0.0002
E31_37 N31P38 N31P37 N37P1 N37P61 0.0002
E31_38 N31P39 N31P38 N38P1 N38P61 0.0000
E31_39 N31P40 N31P39 N39P1 N39P61 -0.0002
E31_40 N31P41 N31P40 N40P1 N40P61 0.0033
E31_41 N31P42 N31P41 N41P1 N41P61 -0.0456
E31_42 N31P43 N31P42 N42P1 N42P61 -0.2997
E31_43 N31P44 N31P43 N43P1 N43P61 -0.0107
E31_44 N31P45 N31P44 N44P1 N44P61 0.0052
E31_45 N31P46 N31P45 N45P1 N45P61 0.0006
E31_46 N31P47 N31P46 N46P1 N46P61 -0.0000
E31_47 N31P48 N31P47 N47P1 N47P61 -0.0000
E31_48 N31P49 N31P48 N48P1 N48P61 0.0002
E31_49 N31P50 N31P49 N49P1 N49P61 0.0002
E31_50 N31P51 N31P50 N50P1 N50P61 -0.0000
E31_51 N31P52 N31P51 N51P1 N51P61 -0.0000
E31_52 N31P53 N31P52 N52P1 N52P61 -0.0001
E31_53 N31P54 N31P53 N53P1 N53P61 0.0004
E31_54 N31P55 N31P54 N54P1 N54P61 -0.0098
E31_55 N31P56 N31P55 N55P1 N55P61 -0.0062
E31_56 N31P57 N31P56 N56P1 N56P61 -0.0002
E31_57 N31P58 N31P57 N57P1 N57P61 -0.0002
E31_58 N31P59 N31P58 N58P1 N58P61 0.0000
E31_59 N31P60 N31P59 N59P1 N59P61 0.0001
E31_60 N31P61 N31P60 N60P1 N60P61 0.0005
R31 N31P61 N32P1 R=1
LAPLACE=+1/{K31}/(-S*S/4/3.14^2)^0.25
.param K31=3.4178e-05

APPENDICES

Ctt31_32 N31P1 N32P1 12.38p

L32 N32P1 N32P2 0.1207u
E32_1 N32P3 N32P2 N1P1 N1P61 -0.0000
E32_2 N32P4 N32P3 N2P1 N2P61 -0.0000
E32_3 N32P5 N32P4 N3P1 N3P61 -0.0000
E32_4 N32P6 N32P5 N4P1 N4P61 -0.0000
E32_5 N32P7 N32P6 N5P1 N5P61 0.0000
E32_6 N32P8 N32P7 N6P1 N6P61 0.0002
E32_7 N32P9 N32P8 N7P1 N7P61 0.0003
E32_8 N32P10 N32P9 N8P1 N8P61 0.0000
E32_9 N32P11 N32P10 N9P1 N9P61 0.0000
E32_10 N32P12 N32P11 N10P1 N10P61 0.0000
E32_11 N32P13 N32P12 N11P1 N11P61 0.0000
E32_12 N32P14 N32P13 N12P1 N12P61 -0.0000
E32_13 N32P15 N32P14 N13P1 N13P61 -0.0000
E32_14 N32P16 N32P15 N14P1 N14P61 -0.0000
E32_15 N32P17 N32P16 N15P1 N15P61 -0.0001
E32_16 N32P18 N32P17 N16P1 N16P61 -0.0002
E32_17 N32P19 N32P18 N17P1 N17P61 -0.0006
E32_18 N32P20 N32P19 N18P1 N18P61 0.0004
E32_19 N32P21 N32P20 N19P1 N19P61 0.0051
E32_20 N32P22 N32P21 N20P1 N20P61 0.0100
E32_21 N32P23 N32P22 N21P1 N21P61 0.0034
E32_22 N32P24 N32P23 N22P1 N22P61 0.0006
E32_23 N32P25 N32P24 N23P1 N23P61 -0.0000
E32_24 N32P26 N32P25 N24P1 N24P61 -0.0000
E32_25 N32P27 N32P26 N25P1 N25P61 0.0000
E32_26 N32P28 N32P27 N26P1 N26P61 -0.0002
E32_27 N32P29 N32P28 N27P1 N27P61 0.0032
E32_28 N32P30 N32P29 N28P1 N28P61 -0.0448
E32_29 N32P31 N32P30 N29P1 N29P61 -0.2203
E32_30 N32P32 N32P31 N30P1 N30P61 -0.0454
E32_31 N32P33 N32P32 N31P1 N31P61 -0.2252
E32_33 N32P34 N32P33 N33P1 N33P61 -0.2114
E32_34 N32P35 N32P34 N34P1 N34P61 0.0093
E32_35 N32P36 N32P35 N35P1 N35P61 -0.0005
E32_36 N32P37 N32P36 N36P1 N36P61 0.0000
E32_37 N32P38 N32P37 N37P1 N37P61 0.0000
E32_38 N32P39 N32P38 N38P1 N38P61 -0.0002
E32_39 N32P40 N32P39 N39P1 N39P61 0.0032
E32_40 N32P41 N32P40 N40P1 N40P61 -0.0448
E32_41 N32P42 N32P41 N41P1 N41P61 -0.2203
E32_42 N32P43 N32P42 N42P1 N42P61 -0.0454
E32_43 N32P44 N32P43 N43P1 N43P61 0.0052
E32_44 N32P45 N32P44 N44P1 N44P61 0.0100
E32_45 N32P46 N32P45 N45P1 N45P61 0.0034
E32_46 N32P47 N32P46 N46P1 N46P61 0.0006
E32_47 N32P48 N32P47 N47P1 N47P61 -0.0000
E32_48 N32P49 N32P48 N48P1 N48P61 -0.0000
E32_49 N32P50 N32P49 N49P1 N49P61 -0.0000
E32_50 N32P51 N32P50 N50P1 N50P61 -0.0000
E32_51 N32P52 N32P51 N51P1 N51P61 -0.0001
E32_52 N32P53 N32P52 N52P1 N52P61 -0.0002
E32_53 N32P54 N32P53 N53P1 N53P61 -0.0006
E32_54 N32P55 N32P54 N54P1 N54P61 0.0004
E32_55 N32P56 N32P55 N55P1 N55P61 0.0004
E32_56 N32P57 N32P56 N56P1 N56P61 0.0000
E32_57 N32P58 N32P57 N57P1 N57P61 0.0000
E32_58 N32P59 N32P58 N58P1 N58P61 0.0000
E32_59 N32P60 N32P59 N59P1 N59P61 -0.0000
E32_60 N32P61 N32P60 N60P1 N60P61 -0.0000
R32 N32P61 N33P1 R=1
LAPLACE=+1/{K32}/(-S*S/4/3.14^2)^0.25
.param K32=3.7311e-05
Ctt32_33 N32P1 N33P1 13.47p

L33 N33P1 N33P2 0.1308u
E33_1 N33P3 N33P2 N1P1 N1P61 0.0000
E33_2 N33P4 N33P3 N2P1 N2P61 0.0000
E33_3 N33P5 N33P4 N3P1 N3P61 -0.0000
E33_4 N33P6 N33P5 N4P1 N4P61 -0.0000
E33_5 N33P7 N33P6 N5P1 N5P61 -0.0000
E33_6 N33P8 N33P7 N6P1 N6P61 -0.0000
E33_7 N33P9 N33P8 N7P1 N7P61 -0.0000
E33_8 N33P10 N33P9 N8P1 N8P61 0.0000
E33_9 N33P11 N33P10 N9P1 N9P61 0.0000
E33_10 N33P12 N33P11 N10P1 N10P61 0.0000
E33_11 N33P13 N33P12 N11P1 N11P61 0.0000
E33_12 N33P14 N33P13 N12P1 N12P61 0.0000
E33_13 N33P15 N33P14 N13P1 N13P61 -0.0000
E33_14 N33P16 N33P15 N14P1 N14P61 -0.0001
E33_15 N33P17 N33P16 N15P1 N15P61 -0.0002
E33_16 N33P18 N33P17 N16P1 N16P61 -0.0006
E33_17 N33P19 N33P18 N17P1 N17P61 -0.0002
E33_18 N33P20 N33P19 N18P1 N18P61 -0.0001
E33_19 N33P21 N33P20 N19P1 N19P61 0.0006
E33_20 N33P22 N33P21 N20P1 N20P61 0.0036
E33_21 N33P23 N33P22 N21P1 N21P61 0.0101
E33_22 N33P24 N33P23 N22P1 N22P61 0.0034
E33_23 N33P25 N33P24 N23P1 N23P61 0.0006
E33_24 N33P26 N33P25 N24P1 N24P61 -0.0000
E33_25 N33P27 N33P26 N25P1 N25P61 -0.0002
E33_26 N33P28 N33P27 N26P1 N26P61 0.0032
E33_27 N33P29 N33P28 N27P1 N27P61 -0.0449
E33_28 N33P30 N33P29 N28P1 N28P61 -0.2201
E33_29 N33P31 N33P30 N29P1 N29P61 -0.0485
E33_30 N33P32 N33P31 N30P1 N30P61 0.0036
E33_31 N33P33 N33P32 N31P1 N31P61 0.0107
E33_32 N33P34 N33P33 N32P1 N32P61 -0.2291
E33_34 N33P35 N33P34 N34P1 N34P61 -0.2120
E33_35 N33P36 N33P35 N35P1 N35P61 0.0094
E33_36 N33P37 N33P36 N36P1 N36P61 -0.0005
E33_37 N33P38 N33P37 N37P1 N37P61 -0.0002
E33_38 N33P39 N33P38 N38P1 N38P61 0.0032
E33_39 N33P40 N33P39 N39P1 N39P61 -0.0449
E33_40 N33P41 N33P40 N40P1 N40P61 -0.2201
E33_41 N33P42 N33P41 N41P1 N41P61 -0.0485
E33_42 N33P43 N33P42 N42P1 N42P61 0.0036
E33_43 N33P44 N33P43 N43P1 N43P61 0.0006
E33_44 N33P45 N33P44 N44P1 N44P61 0.0036
E33_45 N33P46 N33P45 N45P1 N45P61 0.0101

E33_46 N33P47 N33P46 N46P1 N46P61 0.0034
E33_47 N33P48 N33P47 N47P1 N47P61 0.0006
E33_48 N33P49 N33P48 N48P1 N48P61 -0.0000
E33_49 N33P50 N33P49 N49P1 N49P61 -0.0000
E33_50 N33P51 N33P50 N50P1 N50P61 -0.0001
E33_51 N33P52 N33P51 N51P1 N51P61 -0.0002
E33_52 N33P53 N33P52 N52P1 N52P61 -0.0006
E33_53 N33P54 N33P53 N53P1 N53P61 -0.0002
E33_54 N33P55 N33P54 N54P1 N54P61 -0.0001
E33_55 N33P56 N33P55 N55P1 N55P61 -0.0000
E33_56 N33P57 N33P56 N56P1 N56P61 0.0000
E33_57 N33P58 N33P57 N57P1 N57P61 0.0000
E33_58 N33P59 N33P58 N58P1 N58P61 0.0000
E33_59 N33P60 N33P59 N59P1 N59P61 0.0000
E33_60 N33P61 N33P60 N60P1 N60P61 0.0000
R33 N33P61 N34P1 R=1
LAPLACE=+1/{K33}/(-S*S/4/3.14^2)^0.25
.param K33=4.0443e-05
Ctt33_34 N33P1 N34P1 14.55p

L34 N34P1 N34P2 0.1409u
E34_1 N34P3 N34P2 N1P1 N1P61 -0.0000
E34_2 N34P4 N34P3 N2P1 N2P61 -0.0000
E34_3 N34P5 N34P4 N3P1 N3P61 -0.0000
E34_4 N34P6 N34P5 N4P1 N4P61 -0.0000
E34_5 N34P7 N34P6 N5P1 N5P61 -0.0000
E34_6 N34P8 N34P7 N6P1 N6P61 0.0000
E34_7 N34P9 N34P8 N7P1 N7P61 0.0000
E34_8 N34P10 N34P9 N8P1 N8P61 0.0000
E34_9 N34P11 N34P10 N9P1 N9P61 0.0000
E34_10 N34P12 N34P11 N10P1 N10P61 0.0000
E34_11 N34P13 N34P12 N11P1 N11P61 0.0000
E34_12 N34P14 N34P13 N12P1 N12P61 -0.0000
E34_13 N34P15 N34P14 N13P1 N13P61 -0.0001
E34_14 N34P16 N34P15 N14P1 N14P61 -0.0002
E34_15 N34P17 N34P16 N15P1 N15P61 -0.0006
E34_16 N34P18 N34P17 N16P1 N16P61 -0.0003
E34_17 N34P19 N34P18 N17P1 N17P61 -0.0001
E34_18 N34P20 N34P19 N18P1 N18P61 -0.0000
E34_19 N34P21 N34P20 N19P1 N19P61 -0.0001
E34_20 N34P22 N34P21 N20P1 N20P61 0.0007
E34_21 N34P23 N34P22 N21P1 N21P61 0.0036
E34_22 N34P24 N34P23 N22P1 N22P61 0.0101
E34_23 N34P25 N34P24 N23P1 N23P61 0.0034
E34_24 N34P26 N34P25 N24P1 N24P61 0.0006
E34_25 N34P27 N34P26 N25P1 N25P61 0.0031
E34_26 N34P28 N34P27 N26P1 N26P61 -0.0450
E34_27 N34P29 N34P28 N27P1 N27P61 -0.2201
E34_28 N34P30 N34P29 N28P1 N28P61 -0.0484
E34_29 N34P31 N34P30 N29P1 N29P61 0.0038
E34_30 N34P32 N34P31 N30P1 N30P61 -0.0003
E34_31 N34P33 N34P32 N31P1 N31P61 -0.0006
E34_32 N34P34 N34P33 N32P1 N32P61 0.0109
E34_33 N34P35 N34P34 N33P1 N33P61 -0.2284
E34_35 N34P36 N34P35 N35P1 N35P61 -0.2125
E34_36 N34P37 N34P36 N36P1 N36P61 0.0092
E34_37 N34P38 N34P37 N37P1 N37P61 0.0031
E34_38 N34P39 N34P38 N38P1 N38P61 -0.0450
E34_39 N34P40 N34P39 N39P1 N39P61 -0.2201
E34_40 N34P41 N34P40 N40P1 N40P61 -0.0484
E34_41 N34P42 N34P41 N41P1 N41P61 0.0038
E34_42 N34P43 N34P42 N42P1 N42P61 -0.0003
E34_43 N34P44 N34P43 N43P1 N43P61 -0.0001
E34_44 N34P45 N34P44 N44P1 N44P61 0.0007
E34_45 N34P46 N34P45 N45P1 N45P61 0.0036
E34_46 N34P47 N34P46 N46P1 N46P61 0.0101
E34_47 N34P48 N34P47 N47P1 N47P61 0.0034
E34_48 N34P49 N34P48 N48P1 N48P61 0.0006
E34_49 N34P50 N34P49 N49P1 N49P61 -0.0001
E34_50 N34P51 N34P50 N50P1 N50P61 -0.0002
E34_51 N34P52 N34P51 N51P1 N51P61 -0.0006
E34_52 N34P53 N34P52 N52P1 N52P61 -0.0003
E34_53 N34P54 N34P53 N53P1 N53P61 -0.0001
E34_54 N34P55 N34P54 N54P1 N54P61 -0.0000
E34_55 N34P56 N34P55 N55P1 N55P61 0.0000
E34_56 N34P57 N34P56 N56P1 N56P61 0.0000
E34_57 N34P58 N34P57 N57P1 N57P61 0.0000
E34_58 N34P59 N34P58 N58P1 N58P61 0.0000
E34_59 N34P60 N34P59 N59P1 N59P61 0.0000
E34_60 N34P61 N34P60 N60P1 N60P61 -0.0000
R34 N34P61 N35P1 R=1
LAPLACE=+1/{K34}/(-S*S/4/3.14^2)^0.25
.param K34=4.3576e-05
Ctt34_35 N34P1 N35P1 15.64p

L35 N35P1 N35P2 0.1511u
E35_1 N35P3 N35P2 N1P1 N1P61 0.0003
E35_2 N35P4 N35P3 N2P1 N2P61 0.0000
E35_3 N35P5 N35P4 N3P1 N3P61 0.0000
E35_4 N35P6 N35P5 N4P1 N4P61 0.0000
E35_5 N35P7 N35P6 N5P1 N5P61 0.0000
E35_6 N35P8 N35P7 N6P1 N6P61 -0.0000
E35_7 N35P9 N35P8 N7P1 N7P61 -0.0000
E35_8 N35P10 N35P9 N8P1 N8P61 0.0000
E35_9 N35P11 N35P10 N9P1 N9P61 0.0000
E35_10 N35P12 N35P11 N10P1 N10P61 0.0000
E35_11 N35P13 N35P12 N11P1 N11P61 0.0000
E35_12 N35P14 N35P13 N12P1 N12P61 0.0004
E35_13 N35P15 N35P14 N13P1 N13P61 0.0004
E35_14 N35P16 N35P15 N14P1 N14P61 -0.0006
E35_15 N35P17 N35P16 N15P1 N15P61 -0.0002
E35_16 N35P18 N35P17 N16P1 N16P61 -0.0001
E35_17 N35P19 N35P18 N17P1 N17P61 -0.0000
E35_18 N35P20 N35P19 N18P1 N18P61 -0.0000
E35_19 N35P21 N35P20 N19P1 N19P61 -0.0000
E35_20 N35P22 N35P21 N20P1 N20P61 -0.0001
E35_21 N35P23 N35P22 N21P1 N21P61 0.0007
E35_22 N35P24 N35P23 N22P1 N22P61 0.0036
E35_23 N35P25 N35P24 N23P1 N23P61 0.0100
E35_24 N35P26 N35P25 N24P1 N24P61 0.0048
E35_25 N35P27 N35P26 N25P1 N25P61 -0.0420
E35_26 N35P28 N35P27 N26P1 N26P61 -0.2203

E35_27 N35P29 N35P28 N27P1 N27P61 -0.0482
E35_28 N35P30 N35P29 N28P1 N28P61 0.0037
E35_29 N35P31 N35P30 N29P1 N29P61 -0.0003
E35_30 N35P32 N35P31 N30P1 N30P61 0.0000
E35_31 N35P33 N35P32 N31P1 N31P61 0.0000
E35_32 N35P34 N35P33 N32P1 N32P61 -0.0006
E35_33 N35P35 N35P34 N33P1 N33P61 0.0109
E35_34 N35P36 N35P35 N34P1 N34P61 -0.2279
E35_36 N35P37 N35P36 N36P1 N36P61 -0.2086
E35_37 N35P38 N35P37 N37P1 N37P61 -0.0420
E35_38 N35P39 N35P38 N38P1 N38P61 -0.2203
E35_39 N35P40 N35P39 N39P1 N39P61 -0.0482
E35_40 N35P41 N35P40 N40P1 N40P61 0.0037
E35_41 N35P42 N35P41 N41P1 N41P61 -0.0003
E35_42 N35P43 N35P42 N42P1 N42P61 0.0000
E35_43 N35P44 N35P43 N43P1 N43P61 -0.0000
E35_44 N35P45 N35P44 N44P1 N44P61 -0.0001
E35_45 N35P46 N35P45 N45P1 N45P61 0.0007
E35_46 N35P47 N35P46 N46P1 N46P61 0.0036
E35_47 N35P48 N35P47 N47P1 N47P61 0.0100
E35_48 N35P49 N35P48 N48P1 N48P61 0.0048
E35_49 N35P50 N35P49 N49P1 N49P61 0.0004
E35_50 N35P51 N35P50 N50P1 N50P61 -0.0006
E35_51 N35P52 N35P51 N51P1 N51P61 -0.0002
E35_52 N35P53 N35P52 N52P1 N52P61 -0.0001
E35_53 N35P54 N35P53 N53P1 N53P61 -0.0000
E35_54 N35P55 N35P54 N54P1 N54P61 -0.0000
E35_55 N35P56 N35P55 N55P1 N55P61 -0.0000
E35_56 N35P57 N35P56 N56P1 N56P61 0.0000
E35_57 N35P58 N35P57 N57P1 N57P61 0.0000
E35_58 N35P59 N35P58 N58P1 N58P61 0.0001
E35_59 N35P60 N35P59 N59P1 N59P61 0.0001
E35_60 N35P61 N35P60 N60P1 N60P61 0.0005
R35 N35P61 N36P1 R=1
LAPLACE=+1/{K35}/(-S*S/4/3.14^2)^0.25
.param K35=4.6709e-05
Ctt35_36 N35P1 N36P1 16.72p

L36 N36P1 N36P2 0.1770u
E36_1 N36P3 N36P2 N1P1 N1P61 -0.0063
E36_2 N36P4 N36P3 N2P1 N2P61 -0.0009
E36_3 N36P5 N36P4 N3P1 N3P61 -0.0007
E36_4 N36P6 N36P5 N4P1 N4P61 -0.0004
E36_5 N36P7 N36P6 N5P1 N5P61 -0.0002
E36_6 N36P8 N36P7 N6P1 N6P61 0.0002
E36_7 N36P9 N36P8 N7P1 N7P61 0.0003
E36_8 N36P10 N36P9 N8P1 N8P61 -0.0000
E36_9 N36P11 N36P10 N9P1 N9P61 0.0000
E36_10 N36P12 N36P11 N10P1 N10P61 0.0000
E36_11 N36P13 N36P12 N11P1 N11P61 0.0005
E36_12 N36P14 N36P13 N12P1 N12P61 -0.0062
E36_13 N36P15 N36P14 N13P1 N13P61 -0.0111
E36_14 N36P16 N36P15 N14P1 N14P61 0.0005
E36_15 N36P17 N36P16 N15P1 N15P61 -0.0001
E36_16 N36P18 N36P17 N16P1 N16P61 -0.0000
E36_17 N36P19 N36P18 N17P1 N17P61 -0.0000
E36_18 N36P20 N36P19 N18P1 N18P61 0.0003
E36_19 N36P21 N36P20 N19P1 N19P61 0.0003
E36_20 N36P22 N36P21 N20P1 N20P61 -0.0000
E36_21 N36P23 N36P22 N21P1 N21P61 -0.0001
E36_22 N36P24 N36P23 N22P1 N22P61 0.0007
E36_23 N36P25 N36P24 N23P1 N23P61 0.0057
E36_24 N36P26 N36P25 N24P1 N24P61 -0.0120
E36_25 N36P27 N36P26 N25P1 N25P61 -0.3014
E36_26 N36P28 N36P27 N26P1 N26P61 -0.0492
E36_27 N36P29 N36P28 N27P1 N27P61 0.0039
E36_28 N36P30 N36P29 N28P1 N28P61 -0.0003
E36_29 N36P31 N36P30 N29P1 N29P61 0.0000
E36_30 N36P32 N36P31 N30P1 N30P61 0.0003
E36_31 N36P33 N36P32 N31P1 N31P61 0.0003
E36_32 N36P34 N36P33 N32P1 N32P61 0.0000
E36_33 N36P35 N36P34 N33P1 N33P61 -0.0007
E36_34 N36P36 N36P35 N34P1 N34P61 0.0115
E36_35 N36P37 N36P36 N35P1 N35P61 -0.2443
E36_37 N36P38 N36P37 N37P1 N37P61 -0.3014
E36_38 N36P39 N36P38 N38P1 N38P61 -0.0492
E36_39 N36P40 N36P39 N39P1 N39P61 0.0039
E36_40 N36P41 N36P40 N40P1 N40P61 -0.0003
E36_41 N36P42 N36P41 N41P1 N41P61 0.0000
E36_42 N36P43 N36P42 N42P1 N42P61 0.0003
E36_43 N36P44 N36P43 N43P1 N43P61 0.0003
E36_44 N36P45 N36P44 N44P1 N44P61 -0.0000
E36_45 N36P46 N36P45 N45P1 N45P61 -0.0001
E36_46 N36P47 N36P46 N46P1 N46P61 0.0007
E36_47 N36P48 N36P47 N47P1 N47P61 0.0057
E36_48 N36P49 N36P48 N48P1 N48P61 -0.0121
E36_49 N36P50 N36P49 N49P1 N49P61 -0.0113
E36_50 N36P51 N36P50 N50P1 N50P61 0.0006
E36_51 N36P52 N36P51 N51P1 N51P61 -0.0001
E36_52 N36P53 N36P52 N52P1 N52P61 0.0000
E36_53 N36P54 N36P53 N53P1 N53P61 0.0000
E36_54 N36P55 N36P54 N54P1 N54P61 0.0002
E36_55 N36P56 N36P55 N55P1 N55P61 0.0000
E36_56 N36P57 N36P56 N56P1 N56P61 -0.0004
E36_57 N36P58 N36P57 N57P1 N57P61 -0.0006
E36_58 N36P59 N36P58 N58P1 N58P61 -0.0009
E36_59 N36P60 N36P59 N59P1 N59P61 -0.0011
E36_60 N36P61 N36P60 N60P1 N60P61 -0.0092
R36 N36P61 N37P1 R=1
LAPLACE=+1/{K36}/(-S*S/4/3.14^2)^0.25
.param K36=4.9841e-05

L37 N37P1 N37P2 0.1770u
E37_1 N37P3 N37P2 N1P1 N1P61 -0.0045
E37_2 N37P4 N37P3 N2P1 N2P61 -0.0007
E37_3 N37P5 N37P4 N3P1 N3P61 -0.0005
E37_4 N37P6 N37P5 N4P1 N4P61 -0.0003
E37_5 N37P7 N37P6 N5P1 N5P61 -0.0001
E37_6 N37P8 N37P7 N6P1 N6P61 0.0004
E37_7 N37P9 N37P8 N7P1 N7P61 0.0003
E37_8 N37P10 N37P9 N8P1 N8P61 -0.0000
E37_9 N37P11 N37P10 N9P1 N9P61 0.0000

E37_10 N37P12 N37P11 N10P1 N10P61 0.0000
E37_11 N37P13 N37P12 N11P1 N11P61 0.0003
E37_12 N37P14 N37P13 N12P1 N12P61 -0.0041
E37_13 N37P15 N37P14 N13P1 N13P61 -0.0061
E37_14 N37P16 N37P15 N14P1 N14P61 0.0004
E37_15 N37P17 N37P16 N15P1 N15P61 -0.0000
E37_16 N37P18 N37P17 N16P1 N16P61 0.0000
E37_17 N37P19 N37P18 N17P1 N17P61 -0.0000
E37_18 N37P20 N37P19 N18P1 N18P61 0.0003
E37_19 N37P21 N37P20 N19P1 N19P61 0.0003
E37_20 N37P22 N37P21 N20P1 N20P61 -0.0000
E37_21 N37P23 N37P22 N21P1 N21P61 -0.0000
E37_22 N37P24 N37P23 N22P1 N22P61 -0.0001
E37_23 N37P25 N37P24 N23P1 N23P61 0.0005
E37_24 N37P26 N37P25 N24P1 N24P61 -0.0111
E37_25 N37P27 N37P26 N25P1 N25P61 -0.0120
E37_26 N37P28 N37P27 N26P1 N26P61 0.0057
E37_27 N37P29 N37P28 N27P1 N27P61 0.0007
E37_28 N37P30 N37P29 N28P1 N28P61 -0.0001
E37_29 N37P31 N37P30 N29P1 N29P61 -0.0000
E37_30 N37P32 N37P31 N30P1 N30P61 0.0003
E37_31 N37P33 N37P32 N31P1 N31P61 0.0003
E37_32 N37P34 N37P33 N32P1 N32P61 0.0000
E37_33 N37P35 N37P34 N33P1 N33P61 -0.0003
E37_34 N37P36 N37P35 N34P1 N34P61 0.0039
E37_35 N37P37 N37P36 N35P1 N35P61 -0.0492
E37_36 N37P38 N37P37 N36P1 N36P61 -0.3015
E37_38 N37P39 N37P38 N38P1 N38P61 -0.2443
E37_39 N37P40 N37P39 N39P1 N39P61 0.0115
E37_40 N37P41 N37P40 N40P1 N40P61 -0.0007
E37_41 N37P42 N37P41 N41P1 N41P61 0.0000
E37_42 N37P43 N37P42 N42P1 N42P61 0.0003
E37_43 N37P44 N37P43 N43P1 N43P61 0.0002
E37_44 N37P45 N37P44 N44P1 N44P61 0.0000
E37_45 N37P46 N37P45 N45P1 N45P61 -0.0003
E37_46 N37P47 N37P46 N46P1 N46P61 0.0038
E37_47 N37P48 N37P47 N47P1 N47P61 -0.0492
E37_48 N37P49 N37P48 N48P1 N48P61 -0.3017
E37_49 N37P50 N37P49 N49P1 N49P61 -0.0123
E37_50 N37P51 N37P50 N50P1 N50P61 0.0058
E37_51 N37P52 N37P51 N51P1 N51P61 0.0008
E37_52 N37P53 N37P52 N52P1 N52P61 -0.0000
E37_53 N37P54 N37P53 N53P1 N53P61 0.0000
E37_54 N37P55 N37P54 N54P1 N54P61 0.0002
E37_55 N37P56 N37P55 N55P1 N55P61 -0.0002
E37_56 N37P57 N37P56 N56P1 N56P61 -0.0005
E37_57 N37P58 N37P57 N57P1 N57P61 -0.0008
E37_58 N37P59 N37P58 N58P1 N58P61 -0.0014
E37_59 N37P60 N37P59 N59P1 N59P61 -0.0017
E37_60 N37P61 N37P60 N60P1 N60P61 -0.0158
R37 N37P61 N38P1 R=1
LAPLACE=+1/{K37}/(-S*S/4/3.14^2)^0.25
.param K37=4.9841e-05
Ctt37_38 N37P1 N38P1 16.72p

L38 N38P1 N38P2 0.1511u

E38_1 N38P3 N38P2 N1P1 N1P61 0.0002
E38_2 N38P4 N38P3 N2P1 N2P61 0.0000
E38_3 N38P5 N38P4 N3P1 N3P61 0.0000
E38_4 N38P6 N38P5 N4P1 N4P61 0.0000
E38_5 N38P7 N38P6 N5P1 N5P61 0.0000
E38_6 N38P8 N38P7 N6P1 N6P61 -0.0000
E38_7 N38P9 N38P8 N7P1 N7P61 -0.0000
E38_8 N38P10 N38P9 N8P1 N8P61 0.0000
E38_9 N38P11 N38P10 N9P1 N9P61 -0.0000
E38_10 N38P12 N38P11 N10P1 N10P61 -0.0000
E38_11 N38P13 N38P12 N11P1 N11P61 -0.0000
E38_12 N38P14 N38P13 N12P1 N12P61 0.0002
E38_13 N38P15 N38P14 N13P1 N13P61 0.0004
E38_14 N38P16 N38P15 N14P1 N14P61 0.0000
E38_15 N38P17 N38P16 N15P1 N15P61 0.0000
E38_16 N38P18 N38P17 N16P1 N16P61 0.0000
E38_17 N38P19 N38P18 N17P1 N17P61 0.0000
E38_18 N38P20 N38P19 N18P1 N18P61 -0.0000
E38_19 N38P21 N38P20 N19P1 N19P61 -0.0000
E38_20 N38P22 N38P21 N20P1 N20P61 -0.0000
E38_21 N38P23 N38P22 N21P1 N21P61 -0.0001
E38_22 N38P24 N38P23 N22P1 N22P61 -0.0002
E38_23 N38P25 N38P24 N23P1 N23P61 -0.0006
E38_24 N38P26 N38P25 N24P1 N24P61 0.0004
E38_25 N38P27 N38P26 N25P1 N25P61 0.0048
E38_26 N38P28 N38P27 N26P1 N26P61 0.0100
E38_27 N38P29 N38P28 N27P1 N27P61 0.0036
E38_28 N38P30 N38P29 N28P1 N28P61 0.0007
E38_29 N38P31 N38P30 N29P1 N29P61 -0.0001
E38_30 N38P32 N38P31 N30P1 N30P61 -0.0000
E38_31 N38P33 N38P32 N31P1 N31P61 0.0000
E38_32 N38P34 N38P33 N32P1 N32P61 -0.0003
E38_33 N38P35 N38P34 N33P1 N33P61 0.0037
E38_34 N38P36 N38P35 N34P1 N34P61 -0.0482
E38_35 N38P37 N38P36 N35P1 N35P61 -0.2203
E38_36 N38P38 N38P37 N36P1 N36P61 -0.0420
E38_37 N38P39 N38P38 N37P1 N37P61 -0.2086
E38_39 N38P40 N38P39 N39P1 N39P61 -0.2279
E38_40 N38P41 N38P40 N40P1 N40P61 0.0109
E38_41 N38P42 N38P41 N41P1 N41P61 -0.0006
E38_42 N38P43 N38P42 N42P1 N42P61 0.0000
E38_43 N38P44 N38P43 N43P1 N43P61 0.0000
E38_44 N38P45 N38P44 N44P1 N44P61 -0.0003
E38_45 N38P46 N38P45 N45P1 N45P61 0.0037
E38_46 N38P47 N38P46 N46P1 N46P61 -0.0482
E38_47 N38P48 N38P47 N47P1 N47P61 -0.2203
E38_48 N38P49 N38P48 N48P1 N48P61 -0.0420
E38_49 N38P50 N38P49 N49P1 N49P61 0.0049
E38_50 N38P51 N38P50 N50P1 N50P61 0.0100
E38_51 N38P52 N38P51 N51P1 N51P61 0.0036
E38_52 N38P53 N38P52 N52P1 N52P61 0.0007
E38_53 N38P54 N38P53 N53P1 N53P61 -0.0001
E38_54 N38P55 N38P54 N54P1 N54P61 -0.0000
E38_55 N38P56 N38P55 N55P1 N55P61 0.0000
E38_56 N38P57 N38P56 N56P1 N56P61 0.0000
E38_57 N38P58 N38P57 N57P1 N57P61 -0.0000

E38_58 N38P59 N38P58 N58P1 N58P61 -0.0002
E38_59 N38P60 N38P59 N59P1 N59P61 -0.0005
E38_60 N38P61 N38P60 N60P1 N60P61 0.0007
R38 N38P61 N39P1 R=1
LAPLACE=+1/{K38}/(-S*S/4/3.14^2)^0.25
.param K38=4.6709e-05
Ctt38_39 N38P1 N39P1 15.64p

L39 N39P1 N39P2 0.1409u
E39_1 N39P3 N39P2 N1P1 N1P61 -0.0000
E39_2 N39P4 N39P3 N2P1 N2P61 -0.0000
E39_3 N39P5 N39P4 N3P1 N3P61 -0.0000
E39_4 N39P6 N39P5 N4P1 N4P61 -0.0000
E39_5 N39P7 N39P6 N5P1 N5P61 -0.0000
E39_6 N39P8 N39P7 N6P1 N6P61 0.0000
E39_7 N39P9 N39P8 N7P1 N7P61 0.0000
E39_8 N39P10 N39P9 N8P1 N8P61 -0.0000
E39_9 N39P11 N39P10 N9P1 N9P61 -0.0000
E39_10 N39P12 N39P11 N10P1 N10P61 -0.0000
E39_11 N39P13 N39P12 N11P1 N11P61 0.0000
E39_12 N39P14 N39P13 N12P1 N12P61 -0.0000
E39_13 N39P15 N39P14 N13P1 N13P61 -0.0000
E39_14 N39P16 N39P15 N14P1 N14P61 0.0000
E39_15 N39P17 N39P16 N15P1 N15P61 0.0000
E39_16 N39P18 N39P17 N16P1 N16P61 0.0000
E39_17 N39P19 N39P18 N17P1 N17P61 0.0000
E39_18 N39P20 N39P19 N18P1 N18P61 0.0000
E39_19 N39P21 N39P20 N19P1 N19P61 -0.0000
E39_20 N39P22 N39P21 N20P1 N20P61 -0.0001
E39_21 N39P23 N39P22 N21P1 N21P61 -0.0003
E39_22 N39P24 N39P23 N22P1 N22P61 -0.0006
E39_23 N39P25 N39P24 N23P1 N23P61 -0.0002
E39_24 N39P26 N39P25 N24P1 N24P61 -0.0001
E39_25 N39P27 N39P26 N25P1 N25P61 0.0006
E39_26 N39P28 N39P27 N26P1 N26P61 0.0034
E39_27 N39P29 N39P28 N27P1 N27P61 0.0101
E39_28 N39P30 N39P29 N28P1 N28P61 0.0036
E39_29 N39P31 N39P30 N29P1 N29P61 0.0007
E39_30 N39P32 N39P31 N30P1 N30P61 -0.0001
E39_31 N39P33 N39P32 N31P1 N31P61 -0.0003
E39_32 N39P34 N39P33 N32P1 N32P61 0.0038
E39_33 N39P35 N39P34 N33P1 N33P61 -0.0484
E39_34 N39P36 N39P35 N34P1 N34P61 -0.2201
E39_35 N39P37 N39P36 N35P1 N35P61 -0.0450
E39_36 N39P38 N39P37 N36P1 N36P61 0.0031
E39_37 N39P39 N39P38 N37P1 N37P61 0.0092
E39_38 N39P40 N39P39 N38P1 N38P61 -0.2125
E39_40 N39P41 N39P40 N40P1 N40P61 -0.2284
E39_41 N39P42 N39P41 N41P1 N41P61 0.0109
E39_42 N39P43 N39P42 N42P1 N42P61 -0.0006
E39_43 N39P44 N39P43 N43P1 N43P61 -0.0003
E39_44 N39P45 N39P44 N44P1 N44P61 0.0038
E39_45 N39P46 N39P45 N45P1 N45P61 -0.0484
E39_46 N39P47 N39P46 N46P1 N46P61 -0.2201
E39_47 N39P48 N39P47 N47P1 N47P61 -0.0450
E39_48 N39P49 N39P48 N48P1 N48P61 0.0031
E39_49 N39P50 N39P49 N49P1 N49P61 0.0006
E39_50 N39P51 N39P50 N50P1 N50P61 0.0034
E39_51 N39P52 N39P51 N51P1 N51P61 0.0101
E39_52 N39P53 N39P52 N52P1 N52P61 0.0036
E39_53 N39P54 N39P53 N53P1 N53P61 0.0007
E39_54 N39P55 N39P54 N54P1 N54P61 -0.0001
E39_55 N39P56 N39P55 N55P1 N55P61 -0.0000
E39_56 N39P57 N39P56 N56P1 N56P61 -0.0001
E39_57 N39P58 N39P57 N57P1 N57P61 -0.0002
E39_58 N39P59 N39P58 N58P1 N58P61 -0.0006
E39_59 N39P60 N39P59 N59P1 N59P61 -0.0002
E39_60 N39P61 N39P60 N60P1 N60P61 -0.0001
R39 N39P61 N40P1 R=1
LAPLACE=+1/{K39}/(-S*S/4/3.14^2)^0.25
.param K39=4.3576e-05
Ctt39_40 N39P1 N40P1 14.55p

L40 N40P1 N40P2 0.1308u
E40_1 N40P3 N40P2 N1P1 N1P61 0.0000
E40_2 N40P4 N40P3 N2P1 N2P61 0.0000
E40_3 N40P5 N40P4 N3P1 N3P61 0.0000
E40_4 N40P6 N40P5 N4P1 N4P61 0.0000
E40_5 N40P7 N40P6 N5P1 N5P61 0.0000
E40_6 N40P8 N40P7 N6P1 N6P61 -0.0000
E40_7 N40P9 N40P8 N7P1 N7P61 -0.0000
E40_8 N40P10 N40P9 N8P1 N8P61 -0.0000
E40_9 N40P11 N40P10 N9P1 N9P61 -0.0000
E40_10 N40P12 N40P11 N10P1 N10P61 -0.0000
E40_11 N40P13 N40P12 N11P1 N11P61 -0.0000
E40_12 N40P14 N40P13 N12P1 N12P61 0.0000
E40_13 N40P15 N40P14 N13P1 N13P61 0.0000
E40_14 N40P16 N40P15 N14P1 N14P61 0.0000
E40_15 N40P17 N40P16 N15P1 N15P61 0.0000
E40_16 N40P18 N40P17 N16P1 N16P61 0.0000
E40_17 N40P19 N40P18 N17P1 N17P61 0.0000
E40_18 N40P20 N40P19 N18P1 N18P61 -0.0000
E40_19 N40P21 N40P20 N19P1 N19P61 -0.0001
E40_20 N40P22 N40P21 N20P1 N20P61 -0.0002
E40_21 N40P23 N40P22 N21P1 N21P61 -0.0006
E40_22 N40P24 N40P23 N22P1 N22P61 -0.0002
E40_23 N40P25 N40P24 N23P1 N23P61 -0.0001
E40_24 N40P26 N40P25 N24P1 N24P61 -0.0000
E40_25 N40P27 N40P26 N25P1 N25P61 -0.0000
E40_26 N40P28 N40P27 N26P1 N26P61 0.0006
E40_27 N40P29 N40P28 N27P1 N27P61 0.0034
E40_28 N40P30 N40P29 N28P1 N28P61 0.0101
E40_29 N40P31 N40P30 N29P1 N29P61 0.0036
E40_30 N40P32 N40P31 N30P1 N30P61 0.0006
E40_31 N40P33 N40P32 N31P1 N31P61 0.0036
E40_32 N40P34 N40P33 N32P1 N32P61 -0.0485
E40_33 N40P35 N40P34 N33P1 N33P61 -0.2201
E40_34 N40P36 N40P35 N34P1 N34P61 -0.0449
E40_35 N40P37 N40P36 N35P1 N35P61 0.0032
E40_36 N40P38 N40P37 N36P1 N36P61 -0.0002
E40_37 N40P39 N40P38 N37P1 N37P61 -0.0005
E40_38 N40P40 N40P39 N38P1 N38P61 0.0094

E40_39 N40P41 N40P40 N39P1 N39P61 -0.2120
E40_41 N40P42 N40P41 N41P1 N41P61 -0.2291
E40_42 N40P43 N40P42 N42P1 N42P61 0.0107
E40_43 N40P44 N40P43 N43P1 N43P61 0.0036
E40_44 N40P45 N40P44 N44P1 N44P61 -0.0485
E40_45 N40P46 N40P45 N45P1 N45P61 -0.2201
E40_46 N40P47 N40P46 N46P1 N46P61 -0.0449
E40_47 N40P48 N40P47 N47P1 N47P61 0.0032
E40_48 N40P49 N40P48 N48P1 N48P61 -0.0002
E40_49 N40P50 N40P49 N49P1 N49P61 -0.0000
E40_50 N40P51 N40P50 N50P1 N50P61 0.0006
E40_51 N40P52 N40P51 N51P1 N51P61 0.0034
E40_52 N40P53 N40P52 N52P1 N52P61 0.0101
E40_53 N40P54 N40P53 N53P1 N53P61 0.0036
E40_54 N40P55 N40P54 N54P1 N54P61 0.0006
E40_55 N40P56 N40P55 N55P1 N55P61 -0.0001
E40_56 N40P57 N40P56 N56P1 N56P61 -0.0002
E40_57 N40P58 N40P57 N57P1 N57P61 -0.0006
E40_58 N40P59 N40P58 N58P1 N58P61 -0.0002
E40_59 N40P60 N40P59 N59P1 N59P61 -0.0000
E40_60 N40P61 N40P60 N60P1 N60P61 -0.0000
R40 N40P61 N41P1 R=1
LAPLACE=+1/{K40}/(-S*S/4/3.14^2)^0.25
.param K40=4.0443e-05
Ctt40_41 N40P1 N41P1 13.47p

L41 N41P1 N41P2 0.1207u
E41_1 N41P3 N41P2 N1P1 N1P61 -0.0000
E41_2 N41P4 N41P3 N2P1 N2P61 -0.0000
E41_3 N41P5 N41P4 N3P1 N3P61 -0.0000
E41_4 N41P6 N41P5 N4P1 N4P61 -0.0000
E41_5 N41P7 N41P6 N5P1 N5P61 -0.0000
E41_6 N41P8 N41P7 N6P1 N6P61 0.0001
E41_7 N41P9 N41P8 N7P1 N7P61 0.0002
E41_8 N41P10 N41P9 N8P1 N8P61 -0.0000
E41_9 N41P11 N41P10 N9P1 N9P61 0.0000
E41_10 N41P12 N41P11 N10P1 N10P61 0.0000
E41_11 N41P13 N41P12 N11P1 N11P61 0.0000
E41_12 N41P14 N41P13 N12P1 N12P61 -0.0000
E41_13 N41P15 N41P14 N13P1 N13P61 -0.0000
E41_14 N41P16 N41P15 N14P1 N14P61 0.0000
E41_15 N41P17 N41P16 N15P1 N15P61 0.0000
E41_16 N41P18 N41P17 N16P1 N16P61 0.0000
E41_17 N41P19 N41P18 N17P1 N17P61 0.0000
E41_18 N41P20 N41P19 N18P1 N18P61 0.0003
E41_19 N41P21 N41P20 N19P1 N19P61 0.0004
E41_20 N41P22 N41P21 N20P1 N20P61 -0.0006
E41_21 N41P23 N41P22 N21P1 N21P61 -0.0002
E41_22 N41P24 N41P23 N22P1 N22P61 -0.0001
E41_23 N41P25 N41P24 N23P1 N23P61 -0.0000
E41_24 N41P26 N41P25 N24P1 N24P61 -0.0000
E41_25 N41P27 N41P26 N25P1 N25P61 -0.0000
E41_26 N41P28 N41P27 N26P1 N26P61 -0.0000
E41_27 N41P29 N41P28 N27P1 N27P61 0.0006
E41_28 N41P30 N41P29 N28P1 N28P61 0.0034
E41_29 N41P31 N41P30 N29P1 N29P61 0.0100
E41_30 N41P32 N41P31 N30P1 N30P61 0.0051
E41_31 N41P33 N41P32 N31P1 N31P61 -0.0454
E41_32 N41P34 N41P33 N32P1 N32P61 -0.2203
E41_33 N41P35 N41P34 N33P1 N33P61 -0.0448
E41_34 N41P36 N41P35 N34P1 N34P61 0.0032
E41_35 N41P37 N41P36 N35P1 N35P61 -0.0002
E41_36 N41P38 N41P37 N36P1 N36P61 0.0000
E41_37 N41P39 N41P38 N37P1 N37P61 0.0000
E41_38 N41P40 N41P39 N38P1 N38P61 -0.0005
E41_39 N41P41 N41P40 N39P1 N39P61 0.0093
E41_40 N41P42 N41P41 N40P1 N40P61 -0.2114
E41_42 N41P43 N41P42 N42P1 N42P61 -0.2252
E41_43 N41P44 N41P43 N43P1 N43P61 -0.0454
E41_44 N41P45 N41P44 N44P1 N44P61 -0.2203
E41_45 N41P46 N41P45 N45P1 N45P61 -0.0448
E41_46 N41P47 N41P46 N46P1 N46P61 0.0032
E41_47 N41P48 N41P47 N47P1 N47P61 -0.0002
E41_48 N41P49 N41P48 N48P1 N48P61 0.0000
E41_49 N41P50 N41P49 N49P1 N49P61 -0.0000
E41_50 N41P51 N41P50 N50P1 N50P61 -0.0000
E41_51 N41P52 N41P51 N51P1 N51P61 0.0006
E41_52 N41P53 N41P52 N52P1 N52P61 0.0034
E41_53 N41P54 N41P53 N53P1 N53P61 0.0100
E41_54 N41P55 N41P54 N54P1 N54P61 0.0052
E41_55 N41P56 N41P55 N55P1 N55P61 0.0006
E41_56 N41P57 N41P56 N56P1 N56P61 -0.0005
E41_57 N41P58 N41P57 N57P1 N57P61 -0.0002
E41_58 N41P59 N41P58 N58P1 N58P61 -0.0000
E41_59 N41P60 N41P59 N59P1 N59P61 -0.0000
E41_60 N41P61 N41P60 N60P1 N60P61 -0.0000
R41 N41P61 N42P1 R=1
LAPLACE=+1/{K41}/(-S*S/4/3.14^2)^0.25
.param K41=3.7311e-05
Ctt41_42 N41P1 N42P1 12.38p

L42 N42P1 N42P2 0.1212u
E42_1 N42P3 N42P2 N1P1 N1P61 0.0007
E42_2 N42P4 N42P3 N2P1 N2P61 0.0003
E42_3 N42P5 N42P4 N3P1 N3P61 0.0002
E42_4 N42P6 N42P5 N4P1 N4P61 0.0002
E42_5 N42P7 N42P6 N5P1 N5P61 0.0001
E42_6 N42P8 N42P7 N6P1 N6P61 -0.0017
E42_7 N42P9 N42P8 N7P1 N7P61 -0.0027
E42_8 N42P10 N42P9 N8P1 N8P61 0.0002
E42_9 N42P11 N42P10 N9P1 N9P61 -0.0000
E42_10 N42P12 N42P11 N10P1 N10P61 -0.0000
E42_11 N42P13 N42P12 N11P1 N11P61 -0.0000
E42_12 N42P14 N42P13 N12P1 N12P61 0.0002
E42_13 N42P15 N42P14 N13P1 N13P61 0.0002
E42_14 N42P16 N42P15 N14P1 N14P61 -0.0000
E42_15 N42P17 N42P16 N15P1 N15P61 0.0000
E42_16 N42P18 N42P17 N16P1 N16P61 -0.0000
E42_17 N42P19 N42P18 N17P1 N17P61 0.0003
E42_18 N42P20 N42P19 N18P1 N18P61 -0.0047
E42_19 N42P21 N42P20 N19P1 N19P61 -0.0098
E42_20 N42P22 N42P21 N20P1 N20P61 0.0004

E42_21 N42P23 N42P22 N21P1 N21P61 -0.0001
E42_22 N42P24 N42P23 N22P1 N22P61 -0.0000
E42_23 N42P25 N42P24 N23P1 N23P61 -0.0000
E42_24 N42P26 N42P25 N24P1 N24P61 0.0002
E42_25 N42P27 N42P26 N25P1 N25P61 0.0002
E42_26 N42P28 N42P27 N26P1 N26P61 -0.0000
E42_27 N42P29 N42P28 N27P1 N27P61 -0.0000
E42_28 N42P30 N42P29 N28P1 N28P61 0.0006
E42_29 N42P31 N42P30 N29P1 N29P61 0.0052
E42_30 N42P32 N42P31 N30P1 N30P61 -0.0107
E42_31 N42P33 N42P32 N31P1 N31P61 -0.2997
E42_32 N42P34 N42P33 N32P1 N32P61 -0.0456
E42_33 N42P35 N42P34 N33P1 N33P61 0.0033
E42_34 N42P36 N42P35 N34P1 N34P61 -0.0002
E42_35 N42P37 N42P36 N35P1 N35P61 0.0000
E42_36 N42P38 N42P37 N36P1 N36P61 0.0002
E42_37 N42P39 N42P38 N37P1 N37P61 0.0002
E42_38 N42P40 N42P39 N38P1 N38P61 0.0000
E42_39 N42P41 N42P40 N39P1 N39P61 -0.0005
E42_40 N42P42 N42P41 N40P1 N40P61 0.0099
E42_41 N42P43 N42P42 N41P1 N41P61 -0.2261
E42_43 N42P44 N42P43 N43P1 N43P61 -0.2998
E42_44 N42P45 N42P44 N44P1 N44P61 -0.0456
E42_45 N42P46 N42P45 N45P1 N45P61 0.0033
E42_46 N42P47 N42P46 N46P1 N46P61 -0.0002
E42_47 N42P48 N42P47 N47P1 N47P61 0.0000
E42_48 N42P49 N42P48 N48P1 N48P61 0.0002
E42_49 N42P50 N42P49 N49P1 N49P61 0.0002
E42_50 N42P51 N42P50 N50P1 N50P61 -0.0000
E42_51 N42P52 N42P51 N51P1 N51P61 -0.0000
E42_52 N42P53 N42P52 N52P1 N52P61 0.0006
E42_53 N42P54 N42P53 N53P1 N53P61 0.0053
E42_54 N42P55 N42P54 N54P1 N54P61 -0.0108
E42_55 N42P56 N42P55 N55P1 N55P61 -0.0126
E42_56 N42P57 N42P56 N56P1 N56P61 -0.0008
E42_57 N42P58 N42P57 N57P1 N57P61 -0.0005
E42_58 N42P59 N42P58 N58P1 N58P61 -0.0002
E42_59 N42P60 N42P59 N59P1 N59P61 -0.0000
E42_60 N42P61 N42P60 N60P1 N60P61 0.0003
R42 N42P61 N43P1 R=1
LAPLACE=+1/{K42}/(-S*S/4/3.14^2)^0.25
.param K42=3.4178e-05

L43 N43P1 N43P2 0.1212u
E43_1 N43P3 N43P2 N1P1 N1P61 0.0007
E43_2 N43P4 N43P3 N2P1 N2P61 0.0003
E43_3 N43P5 N43P4 N3P1 N3P61 0.0003
E43_4 N43P6 N43P5 N4P1 N4P61 0.0003
E43_5 N43P7 N43P6 N5P1 N5P61 0.0003
E43_6 N43P8 N43P7 N6P1 N6P61 -0.0006
E43_7 N43P9 N43P8 N7P1 N7P61 -0.0015
E43_8 N43P10 N43P9 N8P1 N8P61 0.0001
E43_9 N43P11 N43P10 N9P1 N9P61 -0.0000
E43_10 N43P12 N43P11 N10P1 N10P61 -0.0000
E43_11 N43P13 N43P12 N11P1 N11P61 -0.0000
E43_12 N43P14 N43P13 N12P1 N12P61 0.0003
E43_13 N43P15 N43P14 N13P1 N13P61 0.0002
E43_14 N43P16 N43P15 N14P1 N14P61 -0.0000
E43_15 N43P17 N43P16 N15P1 N15P61 0.0000
E43_16 N43P18 N43P17 N16P1 N16P61 -0.0000
E43_17 N43P19 N43P18 N17P1 N17P61 0.0002
E43_18 N43P20 N43P19 N18P1 N18P61 -0.0027
E43_19 N43P21 N43P20 N19P1 N19P61 -0.0047
E43_20 N43P22 N43P21 N20P1 N20P61 0.0003
E43_21 N43P23 N43P22 N21P1 N21P61 -0.0000
E43_22 N43P24 N43P23 N22P1 N22P61 0.0000
E43_23 N43P25 N43P24 N23P1 N23P61 -0.0000
E43_24 N43P26 N43P25 N24P1 N24P61 0.0002
E43_25 N43P27 N43P26 N25P1 N25P61 0.0002
E43_26 N43P28 N43P27 N26P1 N26P61 -0.0000
E43_27 N43P29 N43P28 N27P1 N27P61 -0.0000
E43_28 N43P30 N43P29 N28P1 N28P61 -0.0001
E43_29 N43P31 N43P30 N29P1 N29P61 0.0004
E43_30 N43P32 N43P31 N30P1 N30P61 -0.0098
E43_31 N43P33 N43P32 N31P1 N31P61 -0.0107
E43_32 N43P34 N43P33 N32P1 N32P61 0.0052
E43_33 N43P35 N43P34 N33P1 N33P61 0.0006
E43_34 N43P36 N43P35 N34P1 N34P61 -0.0000
E43_35 N43P37 N43P36 N35P1 N35P61 -0.0000
E43_36 N43P38 N43P37 N36P1 N36P61 0.0002
E43_37 N43P39 N43P38 N37P1 N37P61 0.0002
E43_38 N43P40 N43P39 N38P1 N38P61 0.0000
E43_39 N43P41 N43P40 N39P1 N39P61 -0.0002
E43_40 N43P42 N43P41 N40P1 N40P61 0.0033
E43_41 N43P43 N43P42 N41P1 N41P61 -0.0456
E43_42 N43P44 N43P43 N42P1 N42P61 -0.2999
E43_44 N43P45 N43P44 N44P1 N44P61 -0.2262
E43_45 N43P46 N43P45 N45P1 N45P61 0.0099
E43_46 N43P47 N43P46 N46P1 N46P61 -0.0005
E43_47 N43P48 N43P47 N47P1 N47P61 0.0000
E43_48 N43P49 N43P48 N48P1 N48P61 0.0002
E43_49 N43P50 N43P49 N49P1 N49P61 0.0002
E43_50 N43P51 N43P50 N50P1 N50P61 0.0000
E43_51 N43P52 N43P51 N51P1 N51P61 -0.0002
E43_52 N43P53 N43P52 N52P1 N52P61 0.0034
E43_53 N43P54 N43P53 N53P1 N53P61 -0.0454
E43_54 N43P55 N43P54 N54P1 N54P61 -0.3002
E43_55 N43P56 N43P55 N55P1 N55P61 -0.0166
E43_56 N43P57 N43P56 N56P1 N56P61 0.0027
E43_57 N43P58 N43P57 N57P1 N57P61 -0.0005
E43_58 N43P59 N43P58 N58P1 N58P61 -0.0006
E43_59 N43P60 N43P59 N59P1 N59P61 -0.0003
E43_60 N43P61 N43P60 N60P1 N60P61 0.0001
R43 N43P61 N44P1 R=1
LAPLACE=+1/{K43}/(-S*S/4/3.14^2)^0.25
.param K43=3.4178e-05
Ctt43_44 N43P1 N44P1 12.38p

L44 N44P1 N44P2 0.1207u
E44_1 N44P3 N44P2 N1P1 N1P61 -0.0000
E44_2 N44P4 N44P3 N2P1 N2P61 -0.0000
E44_3 N44P5 N44P4 N3P1 N3P61 -0.0000

APPENDICES

E44_4 N44P6 N44P5 N4P1 N4P61 -0.0000
E44_5 N44P7 N44P6 N5P1 N5P61 -0.0000
E44_6 N44P8 N44P7 N6P1 N6P61 0.0000
E44_7 N44P9 N44P8 N7P1 N7P61 0.0001
E44_8 N44P10 N44P9 N8P1 N8P61 -0.0000
E44_9 N44P11 N44P10 N9P1 N9P61 0.0000
E44_10 N44P12 N44P11 N10P1 N10P61 0.0000
E44_11 N44P13 N44P12 N11P1 N11P61 0.0000
E44_12 N44P14 N44P13 N12P1 N12P61 -0.0000
E44_13 N44P15 N44P14 N13P1 N13P61 -0.0000
E44_14 N44P16 N44P15 N14P1 N14P61 0.0000
E44_15 N44P17 N44P16 N15P1 N15P61 -0.0000
E44_16 N44P18 N44P17 N16P1 N16P61 -0.0000
E44_17 N44P19 N44P18 N17P1 N17P61 -0.0000
E44_18 N44P20 N44P19 N18P1 N18P61 0.0002
E44_19 N44P21 N44P20 N19P1 N19P61 0.0003
E44_20 N44P22 N44P21 N20P1 N20P61 0.0000
E44_21 N44P23 N44P22 N21P1 N21P61 0.0000
E44_22 N44P24 N44P23 N22P1 N22P61 0.0000
E44_23 N44P25 N44P24 N23P1 N23P61 0.0000
E44_24 N44P26 N44P25 N24P1 N24P61 -0.0000
E44_25 N44P27 N44P26 N25P1 N25P61 -0.0000
E44_26 N44P28 N44P27 N26P1 N26P61 -0.0000
E44_27 N44P29 N44P28 N27P1 N27P61 -0.0001
E44_28 N44P30 N44P29 N28P1 N28P61 -0.0002
E44_29 N44P31 N44P30 N29P1 N29P61 -0.0006
E44_30 N44P32 N44P31 N30P1 N30P61 0.0004
E44_31 N44P33 N44P32 N31P1 N31P61 0.0051
E44_32 N44P34 N44P33 N32P1 N32P61 0.0100
E44_33 N44P35 N44P34 N33P1 N33P61 0.0034
E44_34 N44P36 N44P35 N34P1 N34P61 0.0006
E44_35 N44P37 N44P36 N35P1 N35P61 -0.0000
E44_36 N44P38 N44P37 N36P1 N36P61 -0.0000
E44_37 N44P39 N44P38 N37P1 N37P61 0.0000
E44_38 N44P40 N44P39 N38P1 N38P61 -0.0002
E44_39 N44P41 N44P40 N39P1 N39P61 0.0032
E44_40 N44P42 N44P41 N40P1 N40P61 -0.0448
E44_41 N44P43 N44P42 N41P1 N41P61 -0.2203
E44_42 N44P44 N44P43 N42P1 N42P61 -0.0454
E44_43 N44P45 N44P44 N43P1 N43P61 -0.2252
E44_45 N44P46 N44P45 N45P1 N45P61 -0.2114
E44_46 N44P47 N44P46 N46P1 N46P61 0.0093
E44_47 N44P48 N44P47 N47P1 N47P61 -0.0005
E44_48 N44P49 N44P48 N48P1 N48P61 0.0000
E44_49 N44P50 N44P49 N49P1 N49P61 0.0000
E44_50 N44P51 N44P50 N50P1 N50P61 -0.0002
E44_51 N44P52 N44P51 N51P1 N51P61 0.0032
E44_52 N44P53 N44P52 N52P1 N52P61 -0.0447
E44_53 N44P54 N44P53 N53P1 N53P61 -0.2203
E44_54 N44P55 N44P54 N54P1 N54P61 -0.0454
E44_55 N44P56 N44P55 N55P1 N55P61 0.0053
E44_56 N44P57 N44P56 N56P1 N56P61 0.0099
E44_57 N44P58 N44P57 N57P1 N57P61 0.0032
E44_58 N44P59 N44P58 N58P1 N58P61 0.0006
E44_59 N44P60 N44P59 N59P1 N59P61 -0.0001
E44_60 N44P61 N44P60 N60P1 N60P61 -0.0000

R44 N44P61 N45P1 R=1
LAPLACE=+1/{K44}/(-S*S/4/3.14^2)^0.25
.param K44=3.7311e-05
Ctt44_45 N44P1 N45P1 13.47p

L45 N45P1 N45P2 0.1308u
E45_1 N45P3 N45P2 N1P1 N1P61 0.0000
E45_2 N45P4 N45P3 N2P1 N2P61 0.0000
E45_3 N45P5 N45P4 N3P1 N3P61 0.0000
E45_4 N45P6 N45P5 N4P1 N4P61 0.0000
E45_5 N45P7 N45P6 N5P1 N5P61 0.0000
E45_6 N45P8 N45P7 N6P1 N6P61 0.0000
E45_7 N45P9 N45P8 N7P1 N7P61 -0.0000
E45_8 N45P10 N45P9 N8P1 N8P61 0.0000
E45_9 N45P11 N45P10 N9P1 N9P61 -0.0000
E45_10 N45P12 N45P11 N10P1 N10P61 -0.0000
E45_11 N45P13 N45P12 N11P1 N11P61 -0.0000
E45_12 N45P14 N45P13 N12P1 N12P61 0.0000
E45_13 N45P15 N45P14 N13P1 N13P61 0.0000
E45_14 N45P16 N45P15 N14P1 N14P61 -0.0000
E45_15 N45P17 N45P16 N15P1 N15P61 -0.0000
E45_16 N45P18 N45P17 N16P1 N16P61 -0.0000
E45_17 N45P19 N45P18 N17P1 N17P61 -0.0000
E45_18 N45P20 N45P19 N18P1 N18P61 -0.0000
E45_19 N45P21 N45P20 N19P1 N19P61 -0.0000
E45_20 N45P22 N45P21 N20P1 N20P61 0.0000
E45_21 N45P23 N45P22 N21P1 N21P61 0.0000
E45_22 N45P24 N45P23 N22P1 N22P61 0.0000
E45_23 N45P25 N45P24 N23P1 N23P61 0.0000
E45_24 N45P26 N45P25 N24P1 N24P61 0.0000
E45_25 N45P27 N45P26 N25P1 N25P61 -0.0000
E45_26 N45P28 N45P27 N26P1 N26P61 -0.0001
E45_27 N45P29 N45P28 N27P1 N27P61 -0.0002
E45_28 N45P30 N45P29 N28P1 N28P61 -0.0006
E45_29 N45P31 N45P30 N29P1 N29P61 -0.0002
E45_30 N45P32 N45P31 N30P1 N30P61 -0.0001
E45_31 N45P33 N45P32 N31P1 N31P61 0.0006
E45_32 N45P34 N45P33 N32P1 N32P61 0.0036
E45_33 N45P35 N45P34 N33P1 N33P61 0.0101
E45_34 N45P36 N45P35 N34P1 N34P61 0.0034
E45_35 N45P37 N45P36 N35P1 N35P61 0.0006
E45_36 N45P38 N45P37 N36P1 N36P61 -0.0000
E45_37 N45P39 N45P38 N37P1 N37P61 -0.0002
E45_38 N45P40 N45P39 N38P1 N38P61 0.0032
E45_39 N45P41 N45P40 N39P1 N39P61 -0.0449
E45_40 N45P42 N45P41 N40P1 N40P61 -0.2201
E45_41 N45P43 N45P42 N41P1 N41P61 -0.0485
E45_42 N45P44 N45P43 N42P1 N42P61 0.0036
E45_43 N45P45 N45P44 N43P1 N43P61 0.0107
E45_44 N45P46 N45P45 N44P1 N44P61 -0.2291
E45_46 N45P47 N45P46 N46P1 N46P61 -0.2120
E45_47 N45P48 N45P47 N47P1 N47P61 0.0094
E45_48 N45P49 N45P48 N48P1 N48P61 -0.0005
E45_49 N45P50 N45P49 N49P1 N49P61 -0.0002
E45_50 N45P51 N45P50 N50P1 N50P61 0.0032
E45_51 N45P52 N45P51 N51P1 N51P61 -0.0449

E45_52 N45P53 N45P52 N52P1 N52P61 -0.2200
E45_53 N45P54 N45P53 N53P1 N53P61 -0.0485
E45_54 N45P55 N45P54 N54P1 N54P61 0.0036
E45_55 N45P56 N45P55 N55P1 N55P61 0.0005
E45_56 N45P57 N45P56 N56P1 N56P61 0.0034
E45_57 N45P58 N45P57 N57P1 N57P61 0.0098
E45_58 N45P59 N45P58 N58P1 N58P61 0.0032
E45_59 N45P60 N45P59 N59P1 N59P61 0.0005
E45_60 N45P61 N45P60 N60P1 N60P61 -0.0001
R45 N45P61 N46P1 R=1
LAPLACE=+1/{K45}/(-S*S/4/3.14^2)^0.25
.param K45=4.0443e-05
Ctt45_46 N45P1 N46P1 14.55p

L46 N46P1 N46P2 0.1409u
E46_1 N46P3 N46P2 N1P1 N1P61 -0.0000
E46_2 N46P4 N46P3 N2P1 N2P61 -0.0000
E46_3 N46P5 N46P4 N3P1 N3P61 -0.0000
E46_4 N46P6 N46P5 N4P1 N4P61 0.0000
E46_5 N46P7 N46P6 N5P1 N5P61 0.0000
E46_6 N46P8 N46P7 N6P1 N6P61 0.0000
E46_7 N46P9 N46P8 N7P1 N7P61 0.0000
E46_8 N46P10 N46P9 N8P1 N8P61 -0.0000
E46_9 N46P11 N46P10 N9P1 N9P61 0.0000
E46_10 N46P12 N46P11 N10P1 N10P61 0.0000
E46_11 N46P13 N46P12 N11P1 N11P61 0.0000
E46_12 N46P14 N46P13 N12P1 N12P61 -0.0000
E46_13 N46P15 N46P14 N13P1 N13P61 -0.0000
E46_14 N46P16 N46P15 N14P1 N14P61 0.0000
E46_15 N46P17 N46P16 N15P1 N15P61 -0.0000
E46_16 N46P18 N46P17 N16P1 N16P61 -0.0000
E46_17 N46P19 N46P18 N17P1 N17P61 -0.0000
E46_18 N46P20 N46P19 N18P1 N18P61 0.0000
E46_19 N46P21 N46P20 N19P1 N19P61 0.0000
E46_20 N46P22 N46P21 N20P1 N20P61 0.0000
E46_21 N46P23 N46P22 N21P1 N21P61 0.0000
E46_22 N46P24 N46P23 N22P1 N22P61 0.0000
E46_23 N46P25 N46P24 N23P1 N23P61 0.0000
E46_24 N46P26 N46P25 N24P1 N24P61 -0.0000
E46_25 N46P27 N46P26 N25P1 N25P61 -0.0001
E46_26 N46P28 N46P27 N26P1 N26P61 -0.0002
E46_27 N46P29 N46P28 N27P1 N27P61 -0.0006
E46_28 N46P30 N46P29 N28P1 N28P61 -0.0003
E46_29 N46P31 N46P30 N29P1 N29P61 -0.0001
E46_30 N46P32 N46P31 N30P1 N30P61 -0.0000
E46_31 N46P33 N46P32 N31P1 N31P61 -0.0001
E46_32 N46P34 N46P33 N32P1 N32P61 0.0007
E46_33 N46P35 N46P34 N33P1 N33P61 0.0036
E46_34 N46P36 N46P35 N34P1 N34P61 0.0101
E46_35 N46P37 N46P36 N35P1 N35P61 0.0034
E46_36 N46P38 N46P37 N36P1 N36P61 0.0005
E46_37 N46P39 N46P38 N37P1 N37P61 0.0031
E46_38 N46P40 N46P39 N38P1 N38P61 -0.0450
E46_39 N46P41 N46P40 N39P1 N39P61 -0.2201
E46_40 N46P42 N46P41 N40P1 N40P61 -0.0484
E46_41 N46P43 N46P42 N41P1 N41P61 0.0038
E46_42 N46P44 N46P43 N42P1 N42P61 -0.0003
E46_43 N46P45 N46P44 N43P1 N43P61 -0.0006
E46_44 N46P46 N46P45 N44P1 N44P61 0.0109
E46_45 N46P47 N46P46 N45P1 N45P61 -0.2284
E46_47 N46P48 N46P47 N47P1 N47P61 -0.2125
E46_48 N46P49 N46P48 N48P1 N48P61 0.0092
E46_49 N46P50 N46P49 N49P1 N49P61 0.0031
E46_50 N46P51 N46P50 N50P1 N50P61 -0.0450
E46_51 N46P52 N46P51 N51P1 N51P61 -0.2200
E46_52 N46P53 N46P52 N52P1 N52P61 -0.0483
E46_53 N46P54 N46P53 N53P1 N53P61 0.0038
E46_54 N46P55 N46P54 N54P1 N54P61 -0.0003
E46_55 N46P56 N46P55 N55P1 N55P61 -0.0001
E46_56 N46P57 N46P56 N56P1 N56P61 0.0006
E46_57 N46P58 N46P57 N57P1 N57P61 0.0034
E46_58 N46P59 N46P58 N58P1 N58P61 0.0098
E46_59 N46P60 N46P59 N59P1 N59P61 0.0032
E46_60 N46P61 N46P60 N60P1 N60P61 0.0004
R46 N46P61 N47P1 R=1
LAPLACE=+1/{K46}/(-S*S/4/3.14^2)^0.25
.param K46=4.3576e-05
Ctt46_47 N46P1 N47P1 15.64p

L47 N47P1 N47P2 0.1511u
E47_1 N47P3 N47P2 N1P1 N1P61 0.0002
E47_2 N47P4 N47P3 N2P1 N2P61 0.0000
E47_3 N47P5 N47P4 N3P1 N3P61 0.0000
E47_4 N47P6 N47P5 N4P1 N4P61 0.0000
E47_5 N47P7 N47P6 N5P1 N5P61 0.0000
E47_6 N47P8 N47P7 N6P1 N6P61 -0.0000
E47_7 N47P9 N47P8 N7P1 N7P61 -0.0000
E47_8 N47P10 N47P9 N8P1 N8P61 0.0000
E47_9 N47P11 N47P10 N9P1 N9P61 -0.0000
E47_10 N47P12 N47P11 N10P1 N10P61 -0.0000
E47_11 N47P13 N47P12 N11P1 N11P61 -0.0000
E47_12 N47P14 N47P13 N12P1 N12P61 0.0002
E47_13 N47P15 N47P14 N13P1 N13P61 0.0002
E47_14 N47P16 N47P15 N14P1 N14P61 -0.0000
E47_15 N47P17 N47P16 N15P1 N15P61 0.0000
E47_16 N47P18 N47P17 N16P1 N16P61 -0.0000
E47_17 N47P19 N47P18 N17P1 N17P61 0.0000
E47_18 N47P20 N47P19 N18P1 N18P61 -0.0000
E47_19 N47P21 N47P20 N19P1 N19P61 -0.0000
E47_20 N47P22 N47P21 N20P1 N20P61 0.0000
E47_21 N47P23 N47P22 N21P1 N21P61 0.0000
E47_22 N47P24 N47P23 N22P1 N22P61 0.0000
E47_23 N47P25 N47P24 N23P1 N23P61 0.0000
E47_24 N47P26 N47P25 N24P1 N24P61 0.0004
E47_25 N47P27 N47P26 N25P1 N25P61 0.0004
E47_26 N47P28 N47P27 N26P1 N26P61 -0.0006
E47_27 N47P29 N47P28 N27P1 N27P61 -0.0002
E47_28 N47P30 N47P29 N28P1 N28P61 -0.0001
E47_29 N47P31 N47P30 N29P1 N29P61 -0.0000
E47_30 N47P32 N47P31 N30P1 N30P61 -0.0000
E47_31 N47P33 N47P32 N31P1 N31P61 -0.0000
E47_32 N47P34 N47P33 N32P1 N32P61 -0.0001

E47_33 N47P35 N47P34 N33P1 N33P61 0.0007
E47_34 N47P36 N47P35 N34P1 N34P61 0.0036
E47_35 N47P37 N47P36 N35P1 N35P61 0.0100
E47_36 N47P38 N47P37 N36P1 N36P61 0.0048
E47_37 N47P39 N47P38 N37P1 N37P61 -0.0420
E47_38 N47P40 N47P39 N38P1 N38P61 -0.2203
E47_39 N47P41 N47P40 N39P1 N39P61 -0.0482
E47_40 N47P42 N47P41 N40P1 N40P61 0.0037
E47_41 N47P43 N47P42 N41P1 N41P61 -0.0003
E47_42 N47P44 N47P43 N42P1 N42P61 0.0000
E47_43 N47P45 N47P44 N43P1 N43P61 0.0000
E47_44 N47P46 N47P45 N44P1 N44P61 -0.0006
E47_45 N47P47 N47P46 N45P1 N45P61 0.0109
E47_46 N47P48 N47P47 N46P1 N46P61 -0.2279
E47_48 N47P49 N47P48 N48P1 N48P61 -0.2086
E47_49 N47P50 N47P49 N49P1 N49P61 -0.0420
E47_50 N47P51 N47P50 N50P1 N50P61 -0.2203
E47_51 N47P52 N47P51 N51P1 N51P61 -0.0482
E47_52 N47P53 N47P52 N52P1 N52P61 0.0037
E47_53 N47P54 N47P53 N53P1 N53P61 -0.0003
E47_54 N47P55 N47P54 N54P1 N54P61 0.0000
E47_55 N47P56 N47P55 N55P1 N55P61 -0.0000
E47_56 N47P57 N47P56 N56P1 N56P61 -0.0001
E47_57 N47P58 N47P57 N57P1 N57P61 0.0007
E47_58 N47P59 N47P58 N58P1 N58P61 0.0035
E47_59 N47P60 N47P59 N59P1 N59P61 0.0099
E47_60 N47P61 N47P60 N60P1 N60P61 0.0051
R47 N47P61 N48P1 R=1
LAPLACE=+1/{K47}/(-S*S/4/3.14^2)^0.25
.param K47=4.6709e-05
Ctt47_48 N47P1 N48P1 16.72p

L48 N48P1 N48P2 0.1770u
E48_1 N48P3 N48P2 N1P1 N1P61 -0.0035
E48_2 N48P4 N48P3 N2P1 N2P61 -0.0005
E48_3 N48P5 N48P4 N3P1 N3P61 -0.0004
E48_4 N48P6 N48P5 N4P1 N4P61 -0.0002
E48_5 N48P7 N48P6 N5P1 N5P61 -0.0000
E48_6 N48P8 N48P7 N6P1 N6P61 0.0005
E48_7 N48P9 N48P8 N7P1 N7P61 0.0003
E48_8 N48P10 N48P9 N8P1 N8P61 -0.0000
E48_9 N48P11 N48P10 N9P1 N9P61 0.0000
E48_10 N48P12 N48P11 N10P1 N10P61 0.0000
E48_11 N48P13 N48P12 N11P1 N11P61 0.0002
E48_12 N48P14 N48P13 N12P1 N12P61 -0.0029
E48_13 N48P15 N48P14 N13P1 N13P61 -0.0040
E48_14 N48P16 N48P15 N14P1 N14P61 0.0003
E48_15 N48P17 N48P16 N15P1 N15P61 -0.0000
E48_16 N48P18 N48P17 N16P1 N16P61 0.0000
E48_17 N48P19 N48P18 N17P1 N17P61 -0.0000
E48_18 N48P20 N48P19 N18P1 N18P61 0.0003
E48_19 N48P21 N48P20 N19P1 N19P61 0.0003
E48_20 N48P22 N48P21 N20P1 N20P61 -0.0000
E48_21 N48P23 N48P22 N21P1 N21P61 0.0000
E48_22 N48P24 N48P23 N22P1 N22P61 -0.0000
E48_23 N48P25 N48P24 N23P1 N23P61 0.0004
E48_24 N48P26 N48P25 N24P1 N24P61 -0.0061
E48_25 N48P27 N48P26 N25P1 N25P61 -0.0111
E48_26 N48P28 N48P27 N26P1 N26P61 0.0005
E48_27 N48P29 N48P28 N27P1 N27P61 -0.0001
E48_28 N48P30 N48P29 N28P1 N28P61 -0.0000
E48_29 N48P31 N48P30 N29P1 N29P61 -0.0000
E48_30 N48P32 N48P31 N30P1 N30P61 0.0003
E48_31 N48P33 N48P32 N31P1 N31P61 0.0003
E48_32 N48P34 N48P33 N32P1 N32P61 -0.0000
E48_33 N48P35 N48P34 N33P1 N33P61 -0.0001
E48_34 N48P36 N48P35 N34P1 N34P61 0.0007
E48_35 N48P37 N48P36 N35P1 N35P61 0.0057
E48_36 N48P38 N48P37 N36P1 N36P61 -0.0121
E48_37 N48P39 N48P38 N37P1 N37P61 -0.3018
E48_38 N48P40 N48P39 N38P1 N38P61 -0.0492
E48_39 N48P41 N48P40 N39P1 N39P61 0.0039
E48_40 N48P42 N48P41 N40P1 N40P61 -0.0003
E48_41 N48P43 N48P42 N41P1 N41P61 0.0000
E48_42 N48P44 N48P43 N42P1 N42P61 0.0003
E48_43 N48P45 N48P44 N43P1 N43P61 0.0002
E48_44 N48P46 N48P45 N44P1 N44P61 0.0000
E48_45 N48P47 N48P46 N45P1 N45P61 -0.0007
E48_46 N48P48 N48P47 N46P1 N46P61 0.0115
E48_47 N48P49 N48P48 N47P1 N47P61 -0.2444
E48_49 N48P50 N48P49 N49P1 N49P61 -0.3022
E48_50 N48P51 N48P50 N50P1 N50P61 -0.0490
E48_51 N48P52 N48P51 N51P1 N51P61 0.0040
E48_52 N48P53 N48P52 N52P1 N52P61 -0.0002
E48_53 N48P54 N48P53 N53P1 N53P61 0.0001
E48_54 N48P55 N48P54 N54P1 N54P61 0.0002
E48_55 N48P56 N48P55 N55P1 N55P61 -0.0005
E48_56 N48P57 N48P56 N56P1 N56P61 -0.0009
E48_57 N48P58 N48P57 N57P1 N57P61 -0.0014
E48_58 N48P59 N48P58 N58P1 N58P61 -0.0014
E48_59 N48P60 N48P59 N59P1 N59P61 0.0020
E48_60 N48P61 N48P60 N60P1 N60P61 -0.0199
R48 N48P61 N49P1 R=1
LAPLACE=+1/{K48}/(-S*S/4/3.14^2)^0.25
.param K48=4.9841e-05

L49 N49P1 N49P2 0.1771u
E49_1 N49P3 N49P2 N1P1 N1P61 -0.0027
E49_2 N49P4 N49P3 N2P1 N2P61 -0.0004
E49_3 N49P5 N49P4 N3P1 N3P61 -0.0003
E49_4 N49P6 N49P5 N4P1 N4P61 -0.0001
E49_5 N49P7 N49P6 N5P1 N5P61 0.0000
E49_6 N49P8 N49P7 N6P1 N6P61 0.0007
E49_7 N49P9 N49P8 N7P1 N7P61 0.0004
E49_8 N49P10 N49P9 N8P1 N8P61 -0.0000
E49_9 N49P11 N49P10 N9P1 N9P61 0.0000
E49_10 N49P12 N49P11 N10P1 N10P61 0.0000
E49_11 N49P13 N49P12 N11P1 N11P61 0.0002
E49_12 N49P14 N49P13 N12P1 N12P61 -0.0022
E49_13 N49P15 N49P14 N13P1 N13P61 -0.0029
E49_14 N49P16 N49P15 N14P1 N14P61 0.0002
E49_15 N49P17 N49P16 N15P1 N15P61 -0.0000

```
E49_16 N49P18 N49P17 N16P1 N16P61 0.0000
E49_17 N49P19 N49P18 N17P1 N17P61 -0.0000
E49_18 N49P20 N49P19 N18P1 N18P61 0.0004
E49_19 N49P21 N49P20 N19P1 N19P61 0.0004
E49_20 N49P22 N49P21 N20P1 N20P61 -0.0000
E49_21 N49P23 N49P22 N21P1 N21P61 0.0000
E49_22 N49P24 N49P23 N22P1 N22P61 -0.0000
E49_23 N49P25 N49P24 N23P1 N23P61 0.0003
E49_24 N49P26 N49P25 N24P1 N24P61 -0.0041
E49_25 N49P27 N49P26 N25P1 N25P61 -0.0062
E49_26 N49P28 N49P27 N26P1 N26P61 0.0004
E49_27 N49P29 N49P28 N27P1 N27P61 -0.0000
E49_28 N49P30 N49P29 N28P1 N28P61 0.0000
E49_29 N49P31 N49P30 N29P1 N29P61 -0.0000
E49_30 N49P32 N49P31 N30P1 N30P61 0.0003
E49_31 N49P33 N49P32 N31P1 N31P61 0.0003
E49_32 N49P34 N49P33 N32P1 N32P61 -0.0000
E49_33 N49P35 N49P34 N33P1 N33P61 -0.0000
E49_34 N49P36 N49P35 N34P1 N34P61 -0.0001
E49_35 N49P37 N49P36 N35P1 N35P61 0.0005
E49_36 N49P38 N49P37 N36P1 N36P61 -0.0113
E49_37 N49P39 N49P38 N37P1 N37P61 -0.0124
E49_38 N49P40 N49P39 N38P1 N38P61 0.0057
E49_39 N49P41 N49P40 N39P1 N39P61 0.0007
E49_40 N49P42 N49P41 N40P1 N40P61 -0.0001
E49_41 N49P43 N49P42 N41P1 N41P61 -0.0000
E49_42 N49P44 N49P43 N42P1 N42P61 0.0003
E49_43 N49P45 N49P44 N43P1 N43P61 0.0002
E49_44 N49P46 N49P45 N44P1 N44P61 0.0000
E49_45 N49P47 N49P46 N45P1 N45P61 -0.0003
E49_46 N49P48 N49P47 N46P1 N46P61 0.0038
E49_47 N49P49 N49P48 N47P1 N47P61 -0.0492
E49_48 N49P50 N49P49 N48P1 N48P61 -0.3024
E49_50 N49P51 N49P50 N50P1 N50P61 -0.2442
E49_51 N49P52 N49P51 N51P1 N51P61 0.0117
E49_52 N49P53 N49P52 N52P1 N52P61 -0.0006
E49_53 N49P54 N49P53 N53P1 N53P61 0.0001
E49_54 N49P55 N49P54 N54P1 N54P61 0.0002
E49_55 N49P56 N49P55 N55P1 N55P61 -0.0008
E49_56 N49P57 N49P56 N56P1 N56P61 -0.0011
E49_57 N49P58 N49P57 N57P1 N57P61 -0.0018
E49_58 N49P59 N49P58 N58P1 N58P61 0.0021
E49_59 N49P60 N49P59 N59P1 N59P61 -0.0524
E49_60 N49P61 N49P60 N60P1 N60P61 -0.3111
R49 N49P61 N50P1 R=1
LAPLACE=+1/{K49}/(-S*S/4/3.14^2)^0.25
.param K49=4.9841e-05
Ctt49_50 N49P1 N50P1 16.72p

L50 N50P1 N50P2 0.1512u
E50_1 N50P3 N50P2 N1P1 N1P61 0.0002
E50_2 N50P4 N50P3 N2P1 N2P61 0.0000
E50_3 N50P5 N50P4 N3P1 N3P61 0.0000
E50_4 N50P6 N50P5 N4P1 N4P61 -0.0000
E50_5 N50P7 N50P6 N5P1 N5P61 -0.0000
E50_6 N50P8 N50P7 N6P1 N6P61 -0.0001
E50_7 N50P9 N50P8 N7P1 N7P61 -0.0001
E50_8 N50P10 N50P9 N8P1 N8P61 0.0000
E50_9 N50P11 N50P10 N9P1 N9P61 0.0000
E50_10 N50P12 N50P11 N10P1 N10P61 0.0000
E50_11 N50P13 N50P12 N11P1 N11P61 -0.0000
E50_12 N50P14 N50P13 N12P1 N12P61 0.0001
E50_13 N50P15 N50P14 N13P1 N13P61 0.0002
E50_14 N50P16 N50P15 N14P1 N14P61 -0.0000
E50_15 N50P17 N50P16 N15P1 N15P61 0.0000
E50_16 N50P18 N50P17 N16P1 N16P61 -0.0000
E50_17 N50P19 N50P18 N17P1 N17P61 0.0000
E50_18 N50P20 N50P19 N18P1 N18P61 -0.0000
E50_19 N50P21 N50P20 N19P1 N19P61 -0.0000
E50_20 N50P22 N50P21 N20P1 N20P61 0.0000
E50_21 N50P23 N50P22 N21P1 N21P61 -0.0000
E50_22 N50P24 N50P23 N22P1 N22P61 0.0000
E50_23 N50P25 N50P24 N23P1 N23P61 -0.0000
E50_24 N50P26 N50P25 N24P1 N24P61 0.0003
E50_25 N50P27 N50P26 N25P1 N25P61 0.0004
E50_26 N50P28 N50P27 N26P1 N26P61 0.0000
E50_27 N50P29 N50P28 N27P1 N27P61 0.0000
E50_28 N50P30 N50P29 N28P1 N28P61 0.0000
E50_29 N50P31 N50P30 N29P1 N29P61 0.0000
E50_30 N50P32 N50P31 N30P1 N30P61 -0.0000
E50_31 N50P33 N50P32 N31P1 N31P61 -0.0000
E50_32 N50P34 N50P33 N32P1 N32P61 -0.0000
E50_33 N50P35 N50P34 N33P1 N33P61 -0.0001
E50_34 N50P36 N50P35 N34P1 N34P61 -0.0002
E50_35 N50P37 N50P36 N35P1 N35P61 -0.0006
E50_36 N50P38 N50P37 N36P1 N36P61 0.0005
E50_37 N50P39 N50P38 N37P1 N37P61 0.0050
E50_38 N50P40 N50P39 N38P1 N38P61 0.0100
E50_39 N50P41 N50P40 N39P1 N39P61 0.0036
E50_40 N50P42 N50P41 N40P1 N40P61 0.0007
E50_41 N50P43 N50P42 N41P1 N41P61 -0.0001
E50_42 N50P44 N50P43 N42P1 N42P61 -0.0000
E50_43 N50P45 N50P44 N43P1 N43P61 0.0000
E50_44 N50P46 N50P45 N44P1 N44P61 -0.0003
E50_45 N50P47 N50P46 N45P1 N45P61 0.0038
E50_46 N50P48 N50P47 N46P1 N46P61 -0.0482
E50_47 N50P49 N50P48 N47P1 N47P61 -0.2204
E50_48 N50P50 N50P49 N48P1 N48P61 -0.0418
E50_49 N50P51 N50P50 N49P1 N49P61 -0.2084
E50_51 N50P52 N50P51 N51P1 N51P61 -0.2281
E50_52 N50P53 N50P52 N52P1 N52P61 0.0107
E50_53 N50P54 N50P53 N53P1 N53P61 -0.0007
E50_54 N50P55 N50P54 N54P1 N54P61 0.0001
E50_55 N50P56 N50P55 N55P1 N55P61 0.0006
E50_56 N50P57 N50P56 N56P1 N56P61 0.0006
E50_57 N50P58 N50P57 N57P1 N57P61 0.0055
E50_58 N50P59 N50P58 N58P1 N58P61 -0.0447
E50_59 N50P60 N50P59 N59P1 N59P61 -0.2153
E50_60 N50P61 N50P60 N60P1 N60P61 -0.0373
R50 N50P61 N51P1 R=1
LAPLACE=+1/{K50}/(-S*S/4/3.14^2)^0.25
.param K50=4.6709e-05
```

APPENDICES

```
Ctt50_51 N50P1 N51P1 15.64p

L51 N51P1 N51P2 0.1410u
E51_1 N51P3 N51P2 N1P1 N1P61 -0.0000
E51_2 N51P4 N51P3 N2P1 N2P61 -0.0000
E51_3 N51P5 N51P4 N3P1 N3P61 -0.0000
E51_4 N51P6 N51P5 N4P1 N4P61 -0.0000
E51_5 N51P7 N51P6 N5P1 N5P61 -0.0000
E51_6 N51P8 N51P7 N6P1 N6P61 -0.0001
E51_7 N51P9 N51P8 N7P1 N7P61 -0.0000
E51_8 N51P10 N51P9 N8P1 N8P61 0.0000
E51_9 N51P11 N51P10 N9P1 N9P61 0.0000
E51_10 N51P12 N51P11 N10P1 N10P61 0.0000
E51_11 N51P13 N51P12 N11P1 N11P61 0.0000
E51_12 N51P14 N51P13 N12P1 N12P61 0.0000
E51_13 N51P15 N51P14 N13P1 N13P61 0.0000
E51_14 N51P16 N51P15 N14P1 N14P61 -0.0000
E51_15 N51P17 N51P16 N15P1 N15P61 0.0000
E51_16 N51P18 N51P17 N16P1 N16P61 -0.0000
E51_17 N51P19 N51P18 N17P1 N17P61 0.0000
E51_18 N51P20 N51P19 N18P1 N18P61 -0.0000
E51_19 N51P21 N51P20 N19P1 N19P61 -0.0000
E51_20 N51P22 N51P21 N20P1 N20P61 0.0000
E51_21 N51P23 N51P22 N21P1 N21P61 -0.0000
E51_22 N51P24 N51P23 N22P1 N22P61 -0.0000
E51_23 N51P25 N51P24 N23P1 N23P61 -0.0000
E51_24 N51P26 N51P25 N24P1 N24P61 0.0000
E51_25 N51P27 N51P26 N25P1 N25P61 0.0000
E51_26 N51P28 N51P27 N26P1 N26P61 0.0000
E51_27 N51P29 N51P28 N27P1 N27P61 0.0000
E51_28 N51P30 N51P29 N28P1 N28P61 0.0000
E51_29 N51P31 N51P30 N29P1 N29P61 0.0000
E51_30 N51P32 N51P31 N30P1 N30P61 -0.0000
E51_31 N51P33 N51P32 N31P1 N31P61 -0.0000
E51_32 N51P34 N51P33 N32P1 N32P61 -0.0001
E51_33 N51P35 N51P34 N33P1 N33P61 -0.0003
E51_34 N51P36 N51P35 N34P1 N34P61 -0.0006
E51_35 N51P37 N51P36 N35P1 N35P61 -0.0002
E51_36 N51P38 N51P37 N36P1 N36P61 -0.0001
E51_37 N51P39 N51P38 N37P1 N37P61 0.0006
E51_38 N51P40 N51P39 N38P1 N38P61 0.0034
E51_39 N51P41 N51P40 N39P1 N39P61 0.0101
E51_40 N51P42 N51P41 N40P1 N40P61 0.0036
E51_41 N51P43 N51P42 N41P1 N41P61 0.0007
E51_42 N51P44 N51P43 N42P1 N42P61 -0.0000
E51_43 N51P45 N51P44 N43P1 N43P61 -0.0002
E51_44 N51P46 N51P45 N44P1 N44P61 0.0038
E51_45 N51P47 N51P46 N45P1 N45P61 -0.0484
E51_46 N51P48 N51P47 N46P1 N46P61 -0.2201
E51_47 N51P49 N51P48 N47P1 N47P61 -0.0450
E51_48 N51P50 N51P49 N48P1 N48P61 0.0032
E51_49 N51P51 N51P50 N49P1 N49P61 0.0093
E51_50 N51P52 N51P51 N50P1 N50P61 -0.2128
E51_52 N51P53 N51P52 N52P1 N52P61 -0.2287
E51_53 N51P54 N51P53 N53P1 N53P61 0.0108
E51_54 N51P55 N51P54 N54P1 N54P61 -0.0006
E51_55 N51P56 N51P55 N55P1 N55P61 0.0007
E51_56 N51P57 N51P56 N56P1 N56P61 0.0054
E51_57 N51P58 N51P57 N57P1 N57P61 -0.0451
E51_58 N51P59 N51P58 N58P1 N58P61 -0.2155
E51_59 N51P60 N51P59 N59P1 N59P61 -0.0419
E51_60 N51P61 N51P60 N60P1 N60P61 0.0049
R51 N51P61 N52P1 R=1
LAPLACE=+1/{K51}/(-S*S/4/3.14^2)^0.25
.param K51=4.3576e-05
Ctt51_52 N51P1 N52P1 14.55p

L52 N52P1 N52P2 0.1308u
E52_1 N52P3 N52P2 N1P1 N1P61 -0.0000
E52_2 N52P4 N52P3 N2P1 N2P61 -0.0000
E52_3 N52P5 N52P4 N3P1 N3P61 -0.0000
E52_4 N52P6 N52P5 N4P1 N4P61 -0.0000
E52_5 N52P7 N52P6 N5P1 N5P61 -0.0000
E52_6 N52P8 N52P7 N6P1 N6P61 -0.0001
E52_7 N52P9 N52P8 N7P1 N7P61 -0.0000
E52_8 N52P10 N52P9 N8P1 N8P61 0.0000
E52_9 N52P11 N52P10 N9P1 N9P61 0.0000
E52_10 N52P12 N52P11 N10P1 N10P61 0.0000
E52_11 N52P13 N52P12 N11P1 N11P61 0.0000
E52_12 N52P14 N52P13 N12P1 N12P61 0.0000
E52_13 N52P15 N52P14 N13P1 N13P61 0.0000
E52_14 N52P16 N52P15 N14P1 N14P61 -0.0000
E52_15 N52P17 N52P16 N15P1 N15P61 0.0000
E52_16 N52P18 N52P17 N16P1 N16P61 -0.0000
E52_17 N52P19 N52P18 N17P1 N17P61 0.0000
E52_18 N52P20 N52P19 N18P1 N18P61 -0.0000
E52_19 N52P21 N52P20 N19P1 N19P61 -0.0000
E52_20 N52P22 N52P21 N20P1 N20P61 0.0000
E52_21 N52P23 N52P22 N21P1 N21P61 -0.0000
E52_22 N52P24 N52P23 N22P1 N22P61 -0.0000
E52_23 N52P25 N52P24 N23P1 N23P61 -0.0000
E52_24 N52P26 N52P25 N24P1 N24P61 0.0000
E52_25 N52P27 N52P26 N25P1 N25P61 0.0000
E52_26 N52P28 N52P27 N26P1 N26P61 0.0000
E52_27 N52P29 N52P28 N27P1 N27P61 0.0000
E52_28 N52P30 N52P29 N28P1 N28P61 0.0000
E52_29 N52P31 N52P30 N29P1 N29P61 0.0000
E52_30 N52P32 N52P31 N30P1 N30P61 -0.0000
E52_31 N52P33 N52P32 N31P1 N31P61 -0.0001
E52_32 N52P34 N52P33 N32P1 N32P61 -0.0002
E52_33 N52P35 N52P34 N33P1 N33P61 -0.0006
E52_34 N52P36 N52P35 N34P1 N34P61 -0.0002
E52_35 N52P37 N52P36 N35P1 N35P61 -0.0001
E52_36 N52P38 N52P37 N36P1 N36P61 0.0000
E52_37 N52P39 N52P38 N37P1 N37P61 -0.0000
E52_38 N52P40 N52P39 N38P1 N38P61 0.0006
E52_39 N52P41 N52P40 N39P1 N39P61 0.0034
E52_40 N52P42 N52P41 N40P1 N40P61 0.0101
E52_41 N52P43 N52P42 N41P1 N41P61 0.0036
E52_42 N52P44 N52P43 N42P1 N42P61 0.0007
E52_43 N52P45 N52P44 N43P1 N43P61 0.0037
E52_44 N52P46 N52P45 N44P1 N44P61 -0.0485
```

E52_45 N52P47 N52P46 N45P1 N45P61 -0.2201
E52_46 N52P48 N52P47 N46P1 N46P61 -0.0449
E52_47 N52P49 N52P48 N47P1 N47P61 0.0032
E52_48 N52P50 N52P49 N48P1 N48P61 -0.0001
E52_49 N52P51 N52P50 N49P1 N49P61 -0.0004
E52_50 N52P52 N52P51 N50P1 N50P61 0.0093
E52_51 N52P53 N52P52 N51P1 N51P61 -0.2122
E52_53 N52P54 N52P53 N53P1 N53P61 -0.2294
E52_54 N52P55 N52P54 N54P1 N54P61 0.0107
E52_55 N52P56 N52P55 N55P1 N55P61 0.0056
E52_56 N52P57 N52P56 N56P1 N56P61 -0.0452
E52_57 N52P58 N52P57 N57P1 N57P61 -0.2155
E52_58 N52P59 N52P58 N58P1 N58P61 -0.0418
E52_59 N52P60 N52P59 N59P1 N59P61 0.0047
E52_60 N52P61 N52P60 N60P1 N60P61 0.0006
R52 N52P61 N53P1 R=1
LAPLACE=+1/{K52}/(-S*S/4/3.14^2)^0.25
.param K52=4.0443e-05
Ctt52_53 N52P1 N53P1 13.47p

L53 N53P1 N53P2 0.1207u
E53_1 N53P3 N53P2 N1P1 N1P61 -0.0001
E53_2 N53P4 N53P3 N2P1 N2P61 -0.0000
E53_3 N53P5 N53P4 N3P1 N3P61 -0.0000
E53_4 N53P6 N53P5 N4P1 N4P61 -0.0000
E53_5 N53P7 N53P6 N5P1 N5P61 -0.0000
E53_6 N53P8 N53P7 N6P1 N6P61 -0.0001
E53_7 N53P9 N53P8 N7P1 N7P61 0.0000
E53_8 N53P10 N53P9 N8P1 N8P61 0.0000
E53_9 N53P11 N53P10 N9P1 N9P61 0.0000
E53_10 N53P12 N53P11 N10P1 N10P61 0.0000
E53_11 N53P13 N53P12 N11P1 N11P61 0.0000
E53_12 N53P14 N53P13 N12P1 N12P61 -0.0000
E53_13 N53P15 N53P14 N13P1 N13P61 -0.0000
E53_14 N53P16 N53P15 N14P1 N14P61 0.0000
E53_15 N53P17 N53P16 N15P1 N15P61 -0.0000
E53_16 N53P18 N53P17 N16P1 N16P61 0.0000
E53_17 N53P19 N53P18 N17P1 N17P61 -0.0000
E53_18 N53P20 N53P19 N18P1 N18P61 0.0001
E53_19 N53P21 N53P20 N19P1 N19P61 0.0002
E53_20 N53P22 N53P21 N20P1 N20P61 -0.0000
E53_21 N53P23 N53P22 N21P1 N21P61 -0.0000
E53_22 N53P24 N53P23 N22P1 N22P61 -0.0000
E53_23 N53P25 N53P24 N23P1 N23P61 0.0000
E53_24 N53P26 N53P25 N24P1 N24P61 -0.0000
E53_25 N53P27 N53P26 N25P1 N25P61 -0.0000
E53_26 N53P28 N53P27 N26P1 N26P61 0.0000
E53_27 N53P29 N53P28 N27P1 N27P61 0.0000
E53_28 N53P30 N53P29 N28P1 N28P61 0.0000
E53_29 N53P31 N53P30 N29P1 N29P61 0.0000
E53_30 N53P32 N53P31 N30P1 N30P61 0.0003
E53_31 N53P33 N53P32 N31P1 N31P61 0.0004
E53_32 N53P34 N53P33 N32P1 N32P61 -0.0006
E53_33 N53P35 N53P34 N33P1 N33P61 -0.0002
E53_34 N53P36 N53P35 N34P1 N34P61 -0.0000
E53_35 N53P37 N53P36 N35P1 N35P61 -0.0000
E53_36 N53P38 N53P37 N36P1 N36P61 0.0000
E53_37 N53P39 N53P38 N37P1 N37P61 0.0000
E53_38 N53P40 N53P39 N38P1 N38P61 -0.0000
E53_39 N53P41 N53P40 N39P1 N39P61 0.0006
E53_40 N53P42 N53P41 N40P1 N40P61 0.0034
E53_41 N53P43 N53P42 N41P1 N41P61 0.0100
E53_42 N53P44 N53P43 N42P1 N42P61 0.0052
E53_43 N53P45 N53P44 N43P1 N43P61 -0.0453
E53_44 N53P46 N53P45 N44P1 N44P61 -0.2204
E53_45 N53P47 N53P46 N45P1 N45P61 -0.0448
E53_46 N53P48 N53P47 N46P1 N46P61 0.0032
E53_47 N53P49 N53P48 N47P1 N47P61 -0.0002
E53_48 N53P50 N53P49 N48P1 N48P61 0.0000
E53_49 N53P51 N53P50 N49P1 N49P61 0.0001
E53_50 N53P52 N53P51 N50P1 N50P61 -0.0006
E53_51 N53P53 N53P52 N51P1 N51P61 0.0092
E53_52 N53P54 N53P53 N52P1 N52P61 -0.2117
E53_54 N53P55 N53P54 N54P1 N54P61 -0.2251
E53_55 N53P56 N53P55 N55P1 N55P61 -0.0406
E53_56 N53P57 N53P56 N56P1 N56P61 -0.2154
E53_57 N53P58 N53P57 N57P1 N57P61 -0.0416
E53_58 N53P59 N53P58 N58P1 N58P61 0.0047
E53_59 N53P60 N53P59 N59P1 N59P61 0.0004
E53_60 N53P61 N53P60 N60P1 N60P61 0.0005
R53 N53P61 N54P1 R=1
LAPLACE=+1/{K53}/(-S*S/4/3.14^2)^0.25
.param K53=3.7311e-05
Ctt53_54 N53P1 N54P1 12.38p

L54 N54P1 N54P2 0.1213u
E54_1 N54P3 N54P2 N1P1 N1P61 0.0008
E54_2 N54P4 N54P3 N2P1 N2P61 0.0004
E54_3 N54P5 N54P4 N3P1 N3P61 0.0004
E54_4 N54P6 N54P5 N4P1 N4P61 0.0004
E54_5 N54P7 N54P6 N5P1 N5P61 0.0004
E54_6 N54P8 N54P7 N6P1 N6P61 0.0001
E54_7 N54P9 N54P8 N7P1 N7P61 -0.0008
E54_8 N54P10 N54P9 N8P1 N8P61 0.0000
E54_9 N54P11 N54P10 N9P1 N9P61 -0.0000
E54_10 N54P12 N54P11 N10P1 N10P61 -0.0000
E54_11 N54P13 N54P12 N11P1 N11P61 -0.0000
E54_12 N54P14 N54P13 N12P1 N12P61 0.0003
E54_13 N54P15 N54P14 N13P1 N13P61 0.0002
E54_14 N54P16 N54P15 N14P1 N14P61 -0.0000
E54_15 N54P17 N54P16 N15P1 N15P61 0.0000
E54_16 N54P18 N54P17 N16P1 N16P61 -0.0000
E54_17 N54P19 N54P18 N17P1 N17P61 0.0001
E54_18 N54P20 N54P19 N18P1 N18P61 -0.0015
E54_19 N54P21 N54P20 N19P1 N19P61 -0.0027
E54_20 N54P22 N54P21 N20P1 N20P61 0.0002
E54_21 N54P23 N54P22 N21P1 N21P61 -0.0000
E54_22 N54P24 N54P23 N22P1 N22P61 0.0000
E54_23 N54P25 N54P24 N23P1 N23P61 -0.0000
E54_24 N54P26 N54P25 N24P1 N24P61 0.0002
E54_25 N54P27 N54P26 N25P1 N25P61 0.0002
E54_26 N54P28 N54P27 N26P1 N26P61 -0.0000

E54_27 N54P29 N54P28 N27P1 N27P61 0.0000
E54_28 N54P30 N54P29 N28P1 N28P61 -0.0000
E54_29 N54P31 N54P30 N29P1 N29P61 0.0003
E54_30 N54P32 N54P31 N30P1 N30P61 -0.0048
E54_31 N54P33 N54P32 N31P1 N31P61 -0.0099
E54_32 N54P34 N54P33 N32P1 N32P61 0.0004
E54_33 N54P35 N54P34 N33P1 N33P61 -0.0001
E54_34 N54P36 N54P35 N34P1 N34P61 -0.0000
E54_35 N54P37 N54P36 N35P1 N35P61 -0.0000
E54_36 N54P38 N54P37 N36P1 N36P61 0.0002
E54_37 N54P39 N54P38 N37P1 N37P61 0.0002
E54_38 N54P40 N54P39 N38P1 N38P61 -0.0000
E54_39 N54P41 N54P40 N39P1 N39P61 -0.0000
E54_40 N54P42 N54P41 N40P1 N40P61 0.0006
E54_41 N54P43 N54P42 N41P1 N41P61 0.0052
E54_42 N54P44 N54P43 N42P1 N42P61 -0.0108
E54_43 N54P45 N54P44 N43P1 N43P61 -0.3003
E54_44 N54P46 N54P45 N44P1 N44P61 -0.0456
E54_45 N54P47 N54P46 N45P1 N45P61 0.0033
E54_46 N54P48 N54P47 N46P1 N46P61 -0.0002
E54_47 N54P49 N54P48 N47P1 N47P61 0.0000
E54_48 N54P50 N54P49 N48P1 N48P61 0.0001
E54_49 N54P51 N54P50 N49P1 N49P61 0.0001
E54_50 N54P52 N54P51 N50P1 N50P61 0.0000
E54_51 N54P53 N54P52 N51P1 N51P61 -0.0005
E54_52 N54P54 N54P53 N52P1 N52P61 0.0100
E54_53 N54P55 N54P54 N53P1 N53P61 -0.2261
E54_55 N54P56 N54P55 N55P1 N55P61 -0.3070
E54_56 N54P57 N54P56 N56P1 N56P61 -0.0475
E54_57 N54P58 N54P57 N57P1 N57P61 0.0025
E54_58 N54P59 N54P58 N58P1 N58P61 -0.0008
E54_59 N54P60 N54P59 N59P1 N59P61 -0.0004
E54_60 N54P61 N54P60 N60P1 N60P61 -0.0001
R54 N54P61 N55P1 R=1
LAPLACE=+1/{K54}/(-S*S/4/3.14^2)^0.25
.param K54=3.4178e-05

L55 N55P1 N55P2 0.1417u
E55_1 N55P3 N55P2 N1P1 N1P61 0.0020
E55_2 N55P4 N55P3 N2P1 N2P61 0.0010
E55_3 N55P5 N55P4 N3P1 N3P61 0.0011
E55_4 N55P6 N55P5 N4P1 N4P61 0.0012
E55_5 N55P7 N55P6 N5P1 N5P61 0.0013
E55_6 N55P8 N55P7 N6P1 N6P61 0.0027
E55_7 N55P9 N55P8 N7P1 N7P61 0.0001
E55_8 N55P10 N55P9 N8P1 N8P61 -0.0001
E55_9 N55P11 N55P10 N9P1 N9P61 -0.0001
E55_10 N55P12 N55P11 N10P1 N10P61 -0.0001
E55_11 N55P13 N55P12 N11P1 N11P61 -0.0001
E55_12 N55P14 N55P13 N12P1 N12P61 0.0006
E55_13 N55P15 N55P14 N13P1 N13P61 0.0004
E55_14 N55P16 N55P15 N14P1 N14P61 -0.0000
E55_15 N55P17 N55P16 N15P1 N15P61 0.0000
E55_16 N55P18 N55P17 N16P1 N16P61 0.0000
E55_17 N55P19 N55P18 N17P1 N17P61 0.0001
E55_18 N55P20 N55P19 N18P1 N18P61 -0.0007
E55_19 N55P21 N55P20 N19P1 N19P61 -0.0020
E55_20 N55P22 N55P21 N20P1 N20P61 0.0001
E55_21 N55P23 N55P22 N21P1 N21P61 -0.0000
E55_22 N55P24 N55P23 N22P1 N22P61 0.0000
E55_23 N55P25 N55P24 N23P1 N23P61 -0.0000
E55_24 N55P26 N55P25 N24P1 N24P61 0.0003
E55_25 N55P27 N55P26 N25P1 N25P61 0.0002
E55_26 N55P28 N55P27 N26P1 N26P61 -0.0000
E55_27 N55P29 N55P28 N27P1 N27P61 0.0000
E55_28 N55P30 N55P29 N28P1 N28P61 -0.0000
E55_29 N55P31 N55P30 N29P1 N29P61 0.0002
E55_30 N55P32 N55P31 N30P1 N30P61 -0.0040
E55_31 N55P33 N55P32 N31P1 N31P61 -0.0073
E55_32 N55P34 N55P33 N32P1 N32P61 0.0005
E55_33 N55P35 N55P34 N33P1 N33P61 -0.0000
E55_34 N55P36 N55P35 N34P1 N34P61 0.0000
E55_35 N55P37 N55P36 N35P1 N35P61 -0.0000
E55_36 N55P38 N55P37 N36P1 N36P61 0.0000
E55_37 N55P39 N55P38 N37P1 N37P61 -0.0001
E55_38 N55P40 N55P39 N38P1 N38P61 0.0000
E55_39 N55P41 N55P40 N39P1 N39P61 -0.0000
E55_40 N55P42 N55P41 N40P1 N40P61 -0.0001
E55_41 N55P43 N55P42 N41P1 N41P61 0.0007
E55_42 N55P44 N55P43 N42P1 N42P61 -0.0148
E55_43 N55P45 N55P44 N43P1 N43P61 -0.0194
E55_44 N55P46 N55P45 N44P1 N44P61 0.0062
E55_45 N55P47 N55P46 N45P1 N45P61 0.0005
E55_46 N55P48 N55P47 N46P1 N46P61 -0.0001
E55_47 N55P49 N55P48 N47P1 N47P61 -0.0000
E55_48 N55P50 N55P49 N48P1 N48P61 -0.0004
E55_49 N55P51 N55P50 N49P1 N49P61 -0.0006
E55_50 N55P52 N55P51 N50P1 N50P61 0.0006
E55_51 N55P53 N55P52 N51P1 N51P61 0.0007
E55_52 N55P54 N55P53 N52P1 N52P61 0.0060
E55_53 N55P55 N55P54 N53P1 N53P61 -0.0477
E55_54 N55P56 N55P55 N54P1 N54P61 -0.3588
E55_56 N55P57 N55P56 N56P1 N56P61 -0.3447
E55_57 N55P58 N55P57 N57P1 N57P61 -0.0192
E55_58 N55P59 N55P58 N58P1 N58P61 -0.0147
E55_59 N55P60 N55P59 N59P1 N59P61 -0.0079
E55_60 N55P61 N55P60 N60P1 N60P61 -0.0070
R55 N55P61 N56P1 R=1
LAPLACE=+1/{K55}/(-S*S/4/3.14^2)^0.25
.param K55=3.4178e-05
Ctt55_56 N55P1 N56P1 12.38p

L56 N56P1 N56P2 0.1325u
E56_1 N56P3 N56P2 N1P1 N1P61 0.0004
E56_2 N56P4 N56P3 N2P1 N2P61 0.0003
E56_3 N56P5 N56P4 N3P1 N3P61 0.0003
E56_4 N56P6 N56P5 N4P1 N4P61 0.0004
E56_5 N56P7 N56P6 N5P1 N5P61 0.0005
E56_6 N56P8 N56P7 N6P1 N6P61 0.0012
E56_7 N56P9 N56P8 N7P1 N7P61 0.0004
E56_8 N56P10 N56P9 N8P1 N8P61 -0.0001
E56_9 N56P11 N56P10 N9P1 N9P61 -0.0000

E56_10 N56P12 N56P11 N10P1 N10P61 -0.0000
E56_11 N56P13 N56P12 N11P1 N11P61 -0.0000
E56_12 N56P14 N56P13 N12P1 N12P61 0.0000
E56_13 N56P15 N56P14 N13P1 N13P61 -0.0000
E56_14 N56P16 N56P15 N14P1 N14P61 0.0000
E56_15 N56P17 N56P16 N15P1 N15P61 0.0000
E56_16 N56P18 N56P17 N16P1 N16P61 0.0000
E56_17 N56P19 N56P18 N17P1 N17P61 -0.0000
E56_18 N56P20 N56P19 N18P1 N18P61 0.0003
E56_19 N56P21 N56P20 N19P1 N19P61 0.0001
E56_20 N56P22 N56P21 N20P1 N20P61 -0.0000
E56_21 N56P23 N56P22 N21P1 N21P61 0.0000
E56_22 N56P24 N56P23 N22P1 N22P61 -0.0000
E56_23 N56P25 N56P24 N23P1 N23P61 0.0000
E56_24 N56P26 N56P25 N24P1 N24P61 -0.0001
E56_25 N56P27 N56P26 N25P1 N25P61 -0.0002
E56_26 N56P28 N56P27 N26P1 N26P61 0.0000
E56_27 N56P29 N56P28 N27P1 N27P61 -0.0000
E56_28 N56P30 N56P29 N28P1 N28P61 -0.0000
E56_29 N56P31 N56P30 N29P1 N29P61 0.0000
E56_30 N56P32 N56P31 N30P1 N30P61 -0.0000
E56_31 N56P33 N56P32 N31P1 N31P61 -0.0002
E56_32 N56P34 N56P33 N32P1 N32P61 0.0000
E56_33 N56P35 N56P34 N33P1 N33P61 0.0000
E56_34 N56P36 N56P35 N34P1 N34P61 0.0000
E56_35 N56P37 N56P36 N35P1 N35P61 0.0000
E56_36 N56P38 N56P37 N36P1 N36P61 -0.0003
E56_37 N56P39 N56P38 N37P1 N37P61 -0.0004
E56_38 N56P40 N56P39 N38P1 N38P61 0.0000
E56_39 N56P41 N56P40 N39P1 N39P61 -0.0000
E56_40 N56P42 N56P41 N40P1 N40P61 -0.0002
E56_41 N56P43 N56P42 N41P1 N41P61 -0.0006
E56_42 N56P44 N56P43 N42P1 N42P61 -0.0008
E56_43 N56P45 N56P44 N43P1 N43P61 0.0030
E56_44 N56P46 N56P45 N44P1 N44P61 0.0108
E56_45 N56P47 N56P46 N45P1 N45P61 0.0035
E56_46 N56P48 N56P47 N46P1 N46P61 0.0006
E56_47 N56P49 N56P48 N47P1 N47P61 -0.0001
E56_48 N56P50 N56P49 N48P1 N48P61 -0.0007
E56_49 N56P51 N56P50 N49P1 N49P61 -0.0008
E56_50 N56P52 N56P51 N50P1 N50P61 0.0005
E56_51 N56P53 N56P52 N51P1 N51P61 0.0051
E56_52 N56P54 N56P53 N52P1 N52P61 -0.0458
E56_53 N56P55 N56P54 N53P1 N53P61 -0.2364
E56_54 N56P56 N56P55 N54P1 N54P61 -0.0519
E56_55 N56P57 N56P56 N55P1 N55P61 -0.3222
E56_57 N56P58 N56P57 N57P1 N57P61 -0.2896
E56_58 N56P59 N56P58 N58P1 N58P61 -0.0111
E56_59 N56P60 N56P59 N59P1 N59P61 -0.0099
E56_60 N56P61 N56P60 N60P1 N60P61 -0.0075
R56 N56P61 N57P1 R=1
LAPLACE=+1/{K56}/(-S*S/4/3.14^2)^0.25
.param K56=3.7311e-05
Ctt56_57 N56P1 N57P1 13.47p

L57 N57P1 N57P2 0.1436u

E57_1 N57P3 N57P2 N1P1 N1P61 0.0002
E57_2 N57P4 N57P3 N2P1 N2P61 0.0002
E57_3 N57P5 N57P4 N3P1 N3P61 0.0003
E57_4 N57P6 N57P5 N4P1 N4P61 0.0003
E57_5 N57P7 N57P6 N5P1 N5P61 0.0004
E57_6 N57P8 N57P7 N6P1 N6P61 0.0012
E57_7 N57P9 N57P8 N7P1 N7P61 0.0004
E57_8 N57P10 N57P9 N8P1 N8P61 -0.0001
E57_9 N57P11 N57P10 N9P1 N9P61 -0.0000
E57_10 N57P12 N57P11 N10P1 N10P61 -0.0000
E57_11 N57P13 N57P12 N11P1 N11P61 -0.0000
E57_12 N57P14 N57P13 N12P1 N12P61 -0.0001
E57_13 N57P15 N57P14 N13P1 N13P61 -0.0001
E57_14 N57P16 N57P15 N14P1 N14P61 0.0000
E57_15 N57P17 N57P16 N15P1 N15P61 0.0000
E57_16 N57P18 N57P17 N16P1 N16P61 0.0000
E57_17 N57P19 N57P18 N17P1 N17P61 -0.0000
E57_18 N57P20 N57P19 N18P1 N18P61 0.0003
E57_19 N57P21 N57P20 N19P1 N19P61 0.0002
E57_20 N57P22 N57P21 N20P1 N20P61 -0.0000
E57_21 N57P23 N57P22 N21P1 N21P61 0.0000
E57_22 N57P24 N57P23 N22P1 N22P61 -0.0000
E57_23 N57P25 N57P24 N23P1 N23P61 0.0000
E57_24 N57P26 N57P25 N24P1 N24P61 -0.0002
E57_25 N57P27 N57P26 N25P1 N25P61 -0.0003
E57_26 N57P28 N57P27 N26P1 N26P61 0.0000
E57_27 N57P29 N57P28 N27P1 N27P61 -0.0000
E57_28 N57P30 N57P29 N28P1 N28P61 -0.0000
E57_29 N57P31 N57P30 N29P1 N29P61 -0.0000
E57_30 N57P32 N57P31 N30P1 N30P61 0.0000
E57_31 N57P33 N57P32 N31P1 N31P61 -0.0002
E57_32 N57P34 N57P33 N32P1 N32P61 0.0000
E57_33 N57P35 N57P34 N33P1 N33P61 0.0000
E57_34 N57P36 N57P35 N34P1 N34P61 0.0000
E57_35 N57P37 N57P36 N35P1 N35P61 0.0000
E57_36 N57P38 N57P37 N36P1 N36P61 -0.0005
E57_37 N57P39 N57P38 N37P1 N37P61 -0.0007
E57_38 N57P40 N57P39 N38P1 N38P61 -0.0000
E57_39 N57P41 N57P40 N39P1 N39P61 -0.0002
E57_40 N57P42 N57P41 N40P1 N40P61 -0.0006
E57_41 N57P43 N57P42 N41P1 N41P61 -0.0002
E57_42 N57P44 N57P43 N42P1 N42P61 -0.0006
E57_43 N57P45 N57P44 N43P1 N43P61 -0.0006
E57_44 N57P46 N57P45 N44P1 N44P61 0.0038
E57_45 N57P47 N57P46 N45P1 N45P61 0.0108
E57_46 N57P48 N57P47 N46P1 N46P61 0.0035
E57_47 N57P49 N57P48 N47P1 N47P61 0.0007
E57_48 N57P50 N57P49 N48P1 N48P61 -0.0011
E57_49 N57P51 N57P50 N49P1 N49P61 -0.0014
E57_50 N57P52 N57P51 N50P1 N50P61 0.0052
E57_51 N57P53 N57P52 N51P1 N51P61 -0.0459
E57_52 N57P54 N57P53 N52P1 N52P61 -0.2365
E57_53 N57P55 N57P54 N53P1 N53P61 -0.0494
E57_54 N57P56 N57P55 N54P1 N54P61 0.0030
E57_55 N57P57 N57P56 N55P1 N55P61 -0.0195
E57_56 N57P58 N57P57 N56P1 N56P61 -0.3139

E57_58 N57P59 N57P58 N58P1 N58P61 -0.2904
E57_59 N57P60 N57P59 N59P1 N59P61 -0.0113
E57_60 N57P61 N57P60 N60P1 N60P61 -0.0138
R57 N57P61 N58P1 R=1
LAPLACE=+1/{K57}/(-S*S/4/3.14^2)^0.25
.param K57=4.0443e-05
Ctt57_58 N57P1 N58P1 14.55p

L58 N58P1 N58P2 0.1548u
E58_1 N58P3 N58P2 N1P1 N1P61 -0.0000
E58_2 N58P4 N58P3 N2P1 N2P61 0.0002
E58_3 N58P5 N58P4 N3P1 N3P61 0.0002
E58_4 N58P6 N58P5 N4P1 N4P61 0.0003
E58_5 N58P7 N58P6 N5P1 N5P61 0.0004
E58_6 N58P8 N58P7 N6P1 N6P61 0.0012
E58_7 N58P9 N58P8 N7P1 N7P61 0.0005
E58_8 N58P10 N58P9 N8P1 N8P61 -0.0001
E58_9 N58P11 N58P10 N9P1 N9P61 -0.0000
E58_10 N58P12 N58P11 N10P1 N10P61 -0.0000
E58_11 N58P13 N58P12 N11P1 N11P61 0.0000
E58_12 N58P14 N58P13 N12P1 N12P61 -0.0002
E58_13 N58P15 N58P14 N13P1 N13P61 -0.0003
E58_14 N58P16 N58P15 N14P1 N14P61 0.0000
E58_15 N58P17 N58P16 N15P1 N15P61 -0.0000
E58_16 N58P18 N58P17 N16P1 N16P61 0.0000
E58_17 N58P19 N58P18 N17P1 N17P61 -0.0000
E58_18 N58P20 N58P19 N18P1 N18P61 0.0004
E58_19 N58P21 N58P20 N19P1 N19P61 0.0003
E58_20 N58P22 N58P21 N20P1 N20P61 -0.0000
E58_21 N58P23 N58P22 N21P1 N21P61 0.0000
E58_22 N58P24 N58P23 N22P1 N22P61 -0.0000
E58_23 N58P25 N58P24 N23P1 N23P61 0.0000
E58_24 N58P26 N58P25 N24P1 N24P61 -0.0004
E58_25 N58P27 N58P26 N25P1 N25P61 -0.0006
E58_26 N58P28 N58P27 N26P1 N26P61 0.0000
E58_27 N58P29 N58P28 N27P1 N27P61 -0.0000
E58_28 N58P30 N58P29 N28P1 N28P61 -0.0000
E58_29 N58P31 N58P30 N29P1 N29P61 -0.0000
E58_30 N58P32 N58P31 N30P1 N30P61 0.0002
E58_31 N58P33 N58P32 N31P1 N31P61 0.0000
E58_32 N58P34 N58P33 N32P1 N32P61 0.0000
E58_33 N58P35 N58P34 N33P1 N33P61 0.0000
E58_34 N58P36 N58P35 N34P1 N34P61 0.0000
E58_35 N58P37 N58P36 N35P1 N35P61 0.0001
E58_36 N58P38 N58P37 N36P1 N36P61 -0.0008
E58_37 N58P39 N58P38 N37P1 N37P61 -0.0012
E58_38 N58P40 N58P39 N38P1 N38P61 -0.0002
E58_39 N58P41 N58P40 N39P1 N39P61 -0.0006
E58_40 N58P42 N58P41 N40P1 N40P61 -0.0003
E58_41 N58P43 N58P42 N41P1 N41P61 -0.0000
E58_42 N58P44 N58P43 N42P1 N42P61 -0.0002
E58_43 N58P45 N58P44 N43P1 N43P61 -0.0008
E58_44 N58P46 N58P45 N44P1 N44P61 0.0007
E58_45 N58P47 N58P46 N45P1 N45P61 0.0037
E58_46 N58P48 N58P47 N46P1 N46P61 0.0108
E58_47 N58P49 N58P48 N47P1 N47P61 0.0036
E58_48 N58P50 N58P49 N48P1 N48P61 -0.0012
E58_49 N58P51 N58P50 N49P1 N49P61 0.0018
E58_50 N58P52 N58P51 N50P1 N50P61 -0.0458
E58_51 N58P53 N58P52 N51P1 N51P61 -0.2365
E58_52 N58P54 N58P53 N52P1 N52P61 -0.0495
E58_53 N58P55 N58P54 N53P1 N53P61 0.0060
E58_54 N58P56 N58P55 N54P1 N54P61 -0.0011
E58_55 N58P57 N58P56 N55P1 N55P61 -0.0160
E58_56 N58P58 N58P57 N56P1 N56P61 -0.0129
E58_57 N58P59 N58P58 N57P1 N57P61 -0.3130
E58_59 N58P60 N58P59 N59P1 N59P61 -0.2916
E58_60 N58P61 N58P60 N60P1 N60P61 -0.0183
R58 N58P61 N59P1 R=1
LAPLACE=+1/{K58}/(-S*S/4/3.14^2)^0.25
.param K58=4.3576e-05
Ctt58_59 N58P1 N59P1 15.64p

L59 N59P1 N59P2 0.1660u
E59_1 N59P3 N59P2 N1P1 N1P61 -0.0003
E59_2 N59P4 N59P3 N2P1 N2P61 0.0001
E59_3 N59P5 N59P4 N3P1 N3P61 0.0002
E59_4 N59P6 N59P5 N4P1 N4P61 0.0003
E59_5 N59P7 N59P6 N5P1 N5P61 0.0004
E59_6 N59P8 N59P7 N6P1 N6P61 0.0012
E59_7 N59P9 N59P8 N7P1 N7P61 0.0005
E59_8 N59P10 N59P9 N8P1 N8P61 -0.0001
E59_9 N59P11 N59P10 N9P1 N9P61 -0.0000
E59_10 N59P12 N59P11 N10P1 N10P61 -0.0000
E59_11 N59P13 N59P12 N11P1 N11P61 0.0000
E59_12 N59P14 N59P13 N12P1 N12P61 -0.0004
E59_13 N59P15 N59P14 N13P1 N13P61 -0.0005
E59_14 N59P16 N59P15 N14P1 N14P61 0.0000
E59_15 N59P17 N59P16 N15P1 N15P61 -0.0000
E59_16 N59P18 N59P17 N16P1 N16P61 0.0000
E59_17 N59P19 N59P18 N17P1 N17P61 -0.0000
E59_18 N59P20 N59P19 N18P1 N18P61 0.0004
E59_19 N59P21 N59P20 N19P1 N19P61 0.0004
E59_20 N59P22 N59P21 N20P1 N20P61 -0.0000
E59_21 N59P23 N59P22 N21P1 N21P61 0.0000
E59_22 N59P24 N59P23 N22P1 N22P61 -0.0000
E59_23 N59P25 N59P24 N23P1 N23P61 0.0000
E59_24 N59P26 N59P25 N24P1 N24P61 -0.0006
E59_25 N59P27 N59P26 N25P1 N25P61 -0.0008
E59_26 N59P28 N59P27 N26P1 N26P61 0.0000
E59_27 N59P29 N59P28 N27P1 N27P61 -0.0000
E59_28 N59P30 N59P29 N28P1 N28P61 0.0000
E59_29 N59P31 N59P30 N29P1 N29P61 -0.0000
E59_30 N59P32 N59P31 N30P1 N30P61 0.0003
E59_31 N59P33 N59P32 N31P1 N31P61 0.0002
E59_32 N59P34 N59P33 N32P1 N32P61 -0.0000
E59_33 N59P35 N59P34 N33P1 N33P61 0.0000
E59_34 N59P36 N59P35 N34P1 N34P61 0.0000
E59_35 N59P37 N59P36 N35P1 N35P61 0.0001
E59_36 N59P38 N59P37 N36P1 N36P61 -0.0010
E59_37 N59P39 N59P38 N37P1 N37P61 -0.0016
E59_38 N59P40 N59P39 N38P1 N38P61 -0.0005

E59_39 N59P41 N59P40 N39P1 N39P61 -0.0003
E59_40 N59P42 N59P41 N40P1 N40P61 -0.0001
E59_41 N59P43 N59P42 N41P1 N41P61 -0.0000
E59_42 N59P44 N59P43 N42P1 N42P61 -0.0000
E59_43 N59P45 N59P44 N43P1 N43P61 -0.0003
E59_44 N59P46 N59P45 N44P1 N44P61 -0.0001
E59_45 N59P47 N59P46 N45P1 N45P61 0.0007
E59_46 N59P48 N59P47 N46P1 N46P61 0.0037
E59_47 N59P49 N59P48 N47P1 N47P61 0.0109
E59_48 N59P50 N59P49 N48P1 N48P61 0.0018
E59_49 N59P51 N59P50 N49P1 N49P61 -0.0491
E59_50 N59P52 N59P51 N50P1 N50P61 -0.2364
E59_51 N59P53 N59P52 N51P1 N51P61 -0.0494
E59_52 N59P54 N59P53 N52P1 N52P61 0.0059
E59_53 N59P55 N59P54 N53P1 N53P61 0.0006
E59_54 N59P56 N59P55 N54P1 N54P61 -0.0005
E59_55 N59P57 N59P56 N55P1 N55P61 -0.0093
E59_56 N59P58 N59P57 N56P1 N56P61 -0.0124
E59_57 N59P59 N59P58 N57P1 N57P61 -0.0130
E59_58 N59P60 N59P59 N58P1 N58P61 -0.3127
E59_60 N59P61 N59P60 N60P1 N60P61 -0.3008
R59 N59P61 N60P1 R=1
LAPLACE=+1/{K59}/(-S*S/4/3.14^2)^0.25
.param K59=4.6709e-05
Ctt59_60 N59P1 N60P1 16.72p

L60 N60P1 N60P2 0.2086u
E60_1 N60P3 N60P2 N1P1 N1P61 -0.0038
E60_2 N60P4 N60P3 N2P1 N2P61 -0.0003
E60_3 N60P5 N60P4 N3P1 N3P61 -0.0000
E60_4 N60P6 N60P5 N4P1 N4P61 0.0003
E60_5 N60P7 N60P6 N5P1 N5P61 0.0007
E60_6 N60P8 N60P7 N6P1 N6P61 0.0029
E60_7 N60P9 N60P8 N7P1 N7P61 0.0014
E60_8 N60P10 N60P9 N8P1 N8P61 -0.0001
E60_9 N60P11 N60P10 N9P1 N9P61 -0.0000
E60_10 N60P12 N60P11 N10P1 N10P61 -0.0000
E60_11 N60P13 N60P12 N11P1 N11P61 0.0002
E60_12 N60P14 N60P13 N12P1 N12P61 -0.0032
E60_13 N60P15 N60P14 N13P1 N13P61 -0.0041
E60_14 N60P16 N60P15 N14P1 N14P61 0.0003
E60_15 N60P17 N60P16 N15P1 N15P61 -0.0000
E60_16 N60P18 N60P17 N16P1 N16P61 0.0000
E60_17 N60P19 N60P18 N17P1 N17P61 -0.0001
E60_18 N60P20 N60P19 N18P1 N18P61 0.0013
E60_19 N60P21 N60P20 N19P1 N19P61 0.0011
E60_20 N60P22 N60P21 N20P1 N20P61 -0.0001
E60_21 N60P23 N60P22 N21P1 N21P61 0.0000
E60_22 N60P24 N60P23 N22P1 N22P61 -0.0000
E60_23 N60P25 N60P24 N23P1 N23P61 0.0003
E60_24 N60P26 N60P25 N24P1 N24P61 -0.0053
E60_25 N60P27 N60P26 N25P1 N25P61 -0.0074
E60_26 N60P28 N60P27 N26P1 N26P61 0.0005
E60_27 N60P29 N60P28 N27P1 N27P61 -0.0000
E60_28 N60P30 N60P29 N28P1 N28P61 0.0000
E60_29 N60P31 N60P30 N29P1 N29P61 -0.0001
E60_30 N60P32 N60P31 N30P1 N30P61 0.0010
E60_31 N60P33 N60P32 N31P1 N31P61 0.0008
E60_32 N60P34 N60P33 N32P1 N32P61 -0.0000
E60_33 N60P35 N60P34 N33P1 N33P61 0.0000
E60_34 N60P36 N60P35 N34P1 N34P61 -0.0000
E60_35 N60P37 N60P36 N35P1 N35P61 0.0007
E60_36 N60P38 N60P37 N36P1 N36P61 -0.0109
E60_37 N60P39 N60P38 N37P1 N37P61 -0.0186
E60_38 N60P40 N60P39 N38P1 N38P61 0.0010
E60_39 N60P41 N60P40 N39P1 N39P61 -0.0002
E60_40 N60P42 N60P41 N40P1 N40P61 -0.0000
E60_41 N60P43 N60P42 N41P1 N41P61 -0.0000
E60_42 N60P44 N60P43 N42P1 N42P61 0.0006
E60_43 N60P45 N60P44 N43P1 N43P61 0.0002
E60_44 N60P46 N60P45 N44P1 N44P61 -0.0001
E60_45 N60P47 N60P46 N45P1 N45P61 -0.0002
E60_46 N60P48 N60P47 N46P1 N46P61 0.0006
E60_47 N60P49 N60P48 N47P1 N47P61 0.0070
E60_48 N60P50 N60P49 N48P1 N48P61 -0.0235
E60_49 N60P51 N60P50 N49P1 N49P61 -0.3663
E60_50 N60P52 N60P51 N50P1 N50P61 -0.0515
E60_51 N60P53 N60P52 N51P1 N51P61 0.0072
E60_52 N60P54 N60P53 N52P1 N52P61 0.0010
E60_53 N60P55 N60P54 N53P1 N53P61 0.0008
E60_54 N60P56 N60P55 N54P1 N54P61 -0.0002
E60_55 N60P57 N60P56 N55P1 N55P61 -0.0103
E60_56 N60P58 N60P57 N56P1 N56P61 -0.0118
E60_57 N60P59 N60P58 N57P1 N57P61 -0.0200
E60_58 N60P60 N60P59 N58P1 N58P61 -0.0246
E60_59 N60P61 N60P60 N59P1 N59P61 -0.3780
R60 N60P61 N61P1 R=1
LAPLACE=+1/{K60}/(-S*S/4/3.14^2)^0.25
.param K60=4.9841e-05

Cdd1_12 N1P1 N12P1 17.26p
Cdd2_11 N2P1 N11P1 16.18p
Cdd3_10 N3P1 N10P1 15.09p
Cdd4_9 N4P1 N9P1 14.01p
Cdd5_8 N5P1 N8P1 12.92p
Cdd6_7 N6P1 N7P1 11.84p
Cdd7_18 N7P1 N18P1 11.84p
Cdd8_17 N8P1 N17P1 12.92p
Cdd9_16 N9P1 N16P1 14.01p
Cdd10_15 N10P1 N15P1 15.09p
Cdd11_14 N11P1 N14P1 16.18p
Cdd12_13 N12P1 N13P1 17.26p
Cdd13_24 N13P1 N24P1 17.26p
Cdd14_23 N14P1 N23P1 16.18p
Cdd15_22 N15P1 N22P1 15.09p
Cdd16_21 N16P1 N21P1 14.01p
Cdd17_20 N17P1 N20P1 12.92p
Cdd18_19 N18P1 N19P1 11.84p
Cdd19_30 N19P1 N30P1 11.84p
Cdd20_29 N20P1 N29P1 12.92p
Cdd21_28 N21P1 N28P1 14.01p
Cdd22_27 N22P1 N27P1 15.09p

```
Cdd23_26 N23P1 N26P1 16.18p
Cdd24_25 N24P1 N25P1 17.26p
Cdd25_36 N25P1 N36P1 17.26p
Cdd26_35 N26P1 N35P1 16.18p
Cdd27_34 N27P1 N34P1 15.09p
Cdd28_33 N28P1 N33P1 14.01p
Cdd29_32 N29P1 N32P1 12.92p
Cdd30_31 N30P1 N31P1 11.84p
Cdd31_42 N31P1 N42P1 11.84p
Cdd32_41 N32P1 N41P1 12.92p
Cdd33_40 N33P1 N40P1 14.01p
Cdd34_39 N34P1 N39P1 15.09p
Cdd35_38 N35P1 N38P1 16.18p
Cdd36_37 N36P1 N37P1 17.26p
Cdd37_48 N37P1 N48P1 17.26p
Cdd38_47 N38P1 N47P1 16.18p
Cdd39_46 N39P1 N46P1 15.09p
Cdd40_45 N40P1 N45P1 14.01p
Cdd41_44 N41P1 N44P1 12.92p
Cdd42_43 N42P1 N43P1 11.84p
Cdd43_54 N43P1 N54P1 11.84p
Cdd44_53 N44P1 N53P1 12.92p
Cdd45_52 N45P1 N52P1 14.01p
Cdd46_51 N46P1 N51P1 15.09p
Cdd47_50 N47P1 N50P1 16.18p
Cdd48_49 N48P1 N49P1 17.26p
Cdd49_60 N49P1 N60P1 17.26p
Cdd50_59 N50P1 N59P1 16.18p
Cdd51_58 N51P1 N58P1 15.09p
Cdd52_57 N52P1 N57P1 14.01p
Cdd53_56 N53P1 N56P1 12.92p
Cdd54_55 N54P1 N55P1 11.84p

V1 In 0 AC 10
Rin In N1P1 50
Rout N61P1 0 50
.print V(N61P1)
.print V(In)

.ac dec 1000 10 200000k
.backanno
.end
```

Appendix G. Coherence of SIs

SD	*SSE*	*ASLE*	*DABS*	*RMSE*	*ED*	*CSD*	*MM*	*SSRE*	*SSMMRE*	*ρ*
0.9179	0.9191	0.9375	0.9167	0.9681	0.9216	0.9167	0.9436	0.9314	0.9301	0.9179
0.9963	0.9963	0.9387	0.9743	0.9203	0.9963	0.9694	0.94	0.913	0.9118	0.9289
0.9387	0.9424	0.9424	0.9779	0.9216	0.9975	0.9706	0.9436	0.9142	0.9154	0.9277
0.9743	0.9779	0.9449	0.9449	0.9449	0.9424	0.9326	0.9767	0.9449	0.9485	0.9314
0.9203	0.9216	0.9449	0.9216	0.9216	0.9779	0.9632	0.9436	0.9118	0.9154	0.9326
0.9963	0.9975	0.9424	0.9779	0.924	0.924	0.9142	0.951	0.9314	0.9326	0.9301
0.9694	0.9706	0.9326	0.9632	0.9142	0.9706	0.9706	0.9412	0.9167	0.9154	0.9301
0.94	0.9436	0.9767	0.9436	0.951	0.9412	0.9412	0.9412	0.9363	0.9326	0.9203
0.913	0.9142	0.9449	0.9118	0.9314	0.9167	0.9363	0.951	0.951	0.9547	0.9252
0.9118	0.9154	0.9485	0.9154	0.9326	0.9154	0.9326	0.9547	0.9963	0.9963	0.9056
0.9289	0.9277	0.9314	0.9326	0.9301	0.9301	0.9203	0.9252	0.9056	0.9069	0.9069

Appendix H. Short-circuit monitoring and SIs for the green-to-yellow boundary

CC	Wind.%	15 kΩ	5 kΩ	4.5 kΩ	4 kΩ	3.5 kΩ	3 kΩ	2.5 kΩ	2 kΩ	1.5 kΩ	1 kΩ	500 Ω	200 Ω	1 Ω
1 phase														
400VA														
T1 5V	13,89%	0,9998	0,9997	0,9998	0,9997	0,9997	0,9998	0,9999	0,9997	0,9998	0,9999	0,9998	0,9977	0,9045
T1 12V	33,33%	0,9998	0,9997	0,9997	0,9997	0,9998	0,9999	0,9997	0,9998	0,9997	0,9998	0,9997	0,9992	0,8983
T1 24V	66,67%	0,9997	0,9999	0,9999	0,9999	0,9999	0,9999	0,9999	0,9998	0,9998	0,9995	0,9985	0,9939	0,8985
T1 36V	100%	0,9997	0,9989	0,9985	0,9986	0,9989	0,9989	0,9989	0,9989	0,9987	0,998	0,9949	0,982	0,9008
T2 24V	100%	0,9999	1	0,9999	0,9997	0,9998	0,9998	0,9999	0,9998	0,9997	0,9995	0,9984	0,9937	0,9385
T3 24V	100%	0,9986	0,9997	0,9999	0,9999	1	0,9999	0,9999	0,9999	0,9998	0,9992	0,9981	0,9941	0,9454
630VA														
T4 5V	2,27%	0,9998	0,9998	0,9997	0,9998	0,9997	0,9997	0,9997	0,9997	0,9997	0,9997	0,9997	0,9998	0,9449
T4 12V	5,40%	0,9998	1	0,9999	0,9999	0,9998	0,9999	0,9999	1	0,9999	1	1	0,9999	0,895
T4 22V	10%	0,9998	1	1	0,9999	1	1	1	1	1	1	0,9998	0,9992	0,8296
T4 42V	19,10%	0,9998	1	1	0,9997	0,9999	0,9999	0,9999	0,9999	0,9998	0,9996	0,9987	0,9953	0,7701
T4 110V	50%	0,9997	0,9993	0,9992	0,9984	0,9988	0,9985	0,998	0,9973	0,996	0,9933	0,9856	0,9659	0,7181
T4 220V	100%	0,9989	0,9951	0,9946	0,9936	0,9925	0,9911	0,9891	0,9862	0,9819	0,9726	0,9501	0,903	0,6842
T5 230V	100%	0,9995	0,9967	0,9962	0,9957	0,9947	0,9936	0,992	0,9895	0,9856	0,9778	0,9562	0,9079	0,6788
T6 220V	100%	0,9989	0,9954	0,995	0,9943	0,9932	0,9917	0,9897	0,9869	0,9824	0,9735	0,9509	0,9019	0,6649
750kVA														
T7 53V	13,25%	1	1	0,9999	0,9998	0,9999	0,9999	0,9999	0,9998	0,9998	0,9996	0,999	0,9967	0,8161
T7 200V	50%	0,9994	0,9983	0,9981	0,9976	0,9973	0,9967	0,9959	0,9947	0,9928	0,9893	0,9804	0,9611	0,7005
T7 400V	100%	0,9976	0,9912	0,9903	0,989	0,9876	0,9858	0,9834	0,98	0,9748	0,9659	0,9437	0,8947	0,648
T7 115V	50%	0,9994	0,9996	0,9995	0,9992	0,9992	0,999	0,9987	0,9982	0,9972	0,9953	0,9893	0,9739	0,7169
T7 230V	100%	0,999	0,9965	0,996	0,9952	0,9944	0,9933	0,9917	0,9893	0,9855	0,9783	0,9599	0,9186	0,7051
1kVA														
T8 5V	2,27%	0,9997	0,9997	0,9997	0,9998	0,9998	0,9997	0,9997	0,9997	0,9997	0,9997	0,9997	0,9997	0,9433
T8 12V	5,45%	0,9997	1	0,9999	0,9999	0,9999	0,9999	0,9999	0,9999	0,9999	0,9999	0,9999	0,9999	0,8978
T8 24V	10,90%	0,9997	1	1	1	1	1	1	1	1	1	0,9999	0,9996	0,8472
T8 36V	16,36%	0,9997	1	1	0,9999	0,9999	0,9999	0,9999	0,9999	0,9999	0,9997	0,9992	0,9966	0,7446
T8 110V	50%	0,9997	0,9996	0,9995	0,9994	0,9992	0,999	0,9987	0,9982	0,9972	0,9952	0,9888	0,9716	0,7103
T8 220V	100%	0,9993	0,9964	0,9959	0,9951	0,9942	0,993	0,9913	0,9889	0,9847	0,9769	0,9566	0,9143	0,7003
3 phase														
350VA														
T9 230V	57,50%	0,9993	0,9987	0,9984	0,9981	0,9975	0,9973	0,9967	0,9957	0,994	0,9906	0,9818	0,961	0,7048
T9 400V	100%	0,998	0,9925	0,9914	0,9906	0,9885	0,9873	0,9851	0,9816	0,9762	0,966	0,9409	0,886	0,6531
T9 230V	57,50%	0,9994	0,9982	0,9978	0,9975	0,9966	0,9964	0,9955	0,9943	0,9922	0,9882	0,9782	0,9547	0,7276
T9 400V	100%	0,9976	0,9908	0,9897	0,9891	0,9864	0,9851	0,9826	0,979	0,9733	0,9623	0,934	0,874	0,6224
T9 230V	57,50%	0,9986	0,9984	0,9979	0,9973	0,997	0,9966	0,9959	0,9948	0,9929	0,9894	0,9805	0,9585	0,7313
T9 400V	100%	0,9971	0,9917	0,991	0,9899	0,9886	0,9866	0,9842	0,9807	0,9755	0,9649	0,9382	0,8796	0,6217
1.2kVA														
T10 24V	57,10%	0,9993	0,9998	0,9998	0,9996	0,9997	0,9999	0,9999	0,9999	0,9999	0,9999	0,9999	0,9995	0,965

T10 42V	100%	0,9993	0,9997	0,9996	0,9997	0,9998	0,9998	0,9998	0,9998	0,9998	0,9997	0,9993	0,9971	0,9655
5kVA														
T11	100%	0,9997	0,9997	0,9998	0,9997	0,9998	0,9997	0,9999	0,9997	0,9998	0,9997	0,9997	0,9996	0,9926
20kVA														
T12	100%	0,9998	0,9996	0,9995	0,9994	0,9992	0,999	0,9985	0,998	0,9969	0,9942	0,9854	0,9602	0,8029
40kVA														
T13	100%	1	0,9998	0,9997	0,9997	0,9996	0,9994	0,9992	0,9987	0,9977	0,9956	0,9869	0,9616	0,8518
SD	**Wind.%**	**15 kΩ**	**5 kΩ**	**4.5 kΩ**	**4 kΩ**	**3.5 kΩ**	**3 kΩ**	**2.5 kΩ**	**2 kΩ**	**1.5 kΩ**	**1 kΩ**	**500 Ω**	**200 Ω**	**1 Ω**
400VA														
T1 5V	13,89%	1,9155	1,0909	1,2691	1,3889	1,2881	1,2656	1,2555	1,2389	1,2299	1,2231	1,2013	1,151	7,3829
T1 12V	33,33%	1,5758	0,4347	0,4793	0,7436	0,5391	0,5172	0,5368	0,5693	0,5319	0,5522	0,571	0,8413	7,9023
T1 24V	66,67%	1,7833	0,2358	0,2296	0,2329	0,228	0,2688	0,3117	0,3658	0,4546	0,6295	1,141	2,3066	8,0404
T1 36V	100%	1,8683	0,8045	0,9343	0,912	0,8123	0,8457	0,8411	0,8725	0,9869	1,289	2,148	3,9604	8,1097
T2 24V	100%	1,0823	0,1486	0,2086	0,4132	0,3278	0,2893	0,2919	0,3269	0,4029	0,5467	0,9656	1,8679	5,5971
T3 24V	100%	0,9851	0,4013	0,2717	0,2805	0,1922	0,2057	0,2505	0,2996	0,3884	0,6904	1,0527	1,9316	5,7617
630VA														
T4 5V	2,27%	1,5073	0,7353	0,8873	1,1266	1,006	0,9403	0,9158	0,9182	0,9048	0,8908	0,8558	0,8155	13,4734
T4 12V	5,40%	0,9671	0,3009	0,423	0,5836	0,6496	0,4962	0,4501	0,3779	0,4509	0,3938	0,3836	0,6671	17,6099
T4 22V	10%	0,6896	0,1531	0,1366	0,3957	0,1683	0,1744	0,185	0,2282	0,2991	0,4425	0,8402	1,8462	21,5171
T4 42V	19,10%	0,8053	0,3275	0,3729	0,9581	0,5517	0,5625	0,6409	0,7823	0,9997	1,4217	2,4926	4,7789	24,3227
T4 110V	50%	1,1296	1,806	1,9885	2,4665	2,4545	2,7461	3,1473	3,6806	4,5252	5,8298	8,6453	12,9662	26,5184
T4 220V	100%	2,3753	5,0946	5,4639	5,8977	6,3711	6,9895	7,7259	8,6937	10,003	12,1303	15,7323	20,2274	27,9812
T5 230V	100%	1,5439	3,7722	4,0824	4,4456	4,8607	5,3891	6,0282	6,8715	8,0927	9,9603	13,3872	17,7117	25,4741
T6 220V	100%	2,7133	5,537	5,925	6,3823	6,8924	7,5535	8,4145	9,455	10,916	13,0983	16,8719	21,4771	29,4361
750kVA														
T7 53V	13,25%	1,2284	0,3756	0,4701	0,7068	0,622	0,6554	0,6875	0,7636	0,9066	1,2005	2,0247	3,8615	23,6702
T7 200V	50%	1,4821	2,652	2,8759	3,1717	3,4525	3,8331	4,3066	4,9697	5,8976	7,3439	10,3054	14,6924	28,037
T7 400V	100%	3,3147	6,5141	6,9078	7,3847	7,9138	8,5458	9,3296	10,3398	11,748	13,7327	17,3651	21,8443	29,6568
T7 115V	50%	1,2613	1,0876	1,2149	1,4007	1,5155	1,6876	1,9395	2,2892	2,8397	3,7443	5,7848	9,1918	22,0984
T7 230V	100%	1,7778	3,2189	3,4703	3,7817	4,1122	4,5449	5,0851	5,8148	6,8071	8,4061	11,3634	15,3106	22,7032
1kVA														
T8 5V	2,27%	1,6915	0,8001	0,9311	1,1314	1,0566	1,027	0,9972	0,9969	0,9751	1,0096	0,9144	0,8958	12,1836
T8 12V	5,45%	0,8505	0,2705	0,319	0,3866	0,3533	0,3341	0,3278	0,3217	0,3219	0,3262	0,3487	0,4691	15,3249
T8 24V	10,90%	0,8041	0,1589	0,2105	0,2621	0,2242	0,2067	0,2077	0,2158	0,2558	0,3167	0,5532	1,2126	18,2617
T8 36V	16,36%	0,8223	0,2705	0,3289	0,3905	0,3872	0,4085	0,4548	0,5337	0,672	0,9466	1,7182	3,634	22,5608
T8 110V	50%	0,9392	1,2121	1,3353	1,4864	1,6541	1,8647	2,1586	2,5938	3,2208	4,2863	6,6567	10,549	23,8395
T8 220V	100%	1,7207	3,6678	3,9533	4,3025	4,7056	5,2044	5,834	6,6358	7,8225	9,5934	12,952	17,2109	24,6815
3 phase														
350VA														
T9 230V	57,50%	1,3588	2,0661	2,2899	2,5262	2,827	3,0376	3,4139	3,948	4,7573	6,0289	8,6177	12,5667	25,3161
T9 400V	100%	2,6345	5,3258	5,7085	6,1028	6,6009	7,1175	7,7878	8,6939	9,9266	11,7935	15,0269	19,1271	26,5609
T9 230V	57,50%	1,6583	3,3274	3,6302	3,956	4,4189	4,7753	5,3703	6,1249	7,264	9,0559	12,3979	17,142	29,8035

T9 400V	100%	4,0382	8,0685	8,5223	9,0781	9,7669	10,470	11,403	12,535	14,043	16,3493	20,3257	25,0254	33,0743
T9 230V	57,50%	2,4682	3,2512	3,8008	4,2478	4,5161	4,8808	5,4448	6,2144	7,3297	9,0691	12,349	17,1627	29,6813
T9 400V	100%	4,4731	8,0612	8,5321	9,1646	9,7741	10,49	11,356	12,537	14,134	16,3897	20,3054	25,0108	32,9953
1.2kVA														
T10 24V	57,10%	0,6415	0,2872	0,3602	0,4427	0,4029	0,2827	0,2552	0,2379	0,2259	0,2275	0,2926	0,5453	4,1345
T10 42V	100%	0,685	0,3784	0,4741	0,4539	0,3697	0,3571	0,3516	0,3689	0,3872	0,4755	0,6798	1,2844	4,1964
5kVA														
T11	100%	1,0015	0,4527	0,5743	0,6792	0,6299	0,5799	0,6146	0,5222	0,4724	0,4434	0,4445	0,5237	1,7993
20kVA														
T12	100%	0,4422	0,5629	0,7873	0,8604	0,9538	1,0757	1,221	1,5135	1,7866	2,232	3,0274	4,7851	7,6503
40kVA														
T13	100%	0,1256	0,4326	0,4811	0,5329	0,6054	0,7047	0,8354	1,0373	1,3644	1,8979	3,2081	5,4009	10,5056
SSE	**Wind.%**	**15 kΩ**	**5 kΩ**	**4.5 kΩ**	**4 kΩ**	**3.5 kΩ**	**3 kΩ**	**2.5 kΩ**	**2 kΩ**	**1.5 kΩ**	**1 kΩ**	**500 Ω**	**200 Ω**	**1 Ω**
400VA														
T1 5V	13,89%	3,6654	1,1887	1,609	1,9271	1,6574	1,6002	1,5748	1,5334	1,511	1,4946	1,4417	1,3234	54,452
T1 12V	33,33%	2,4806	0,1888	0,2295	0,5524	0,2903	0,2672	0,2878	0,3238	0,2826	0,3046	0,3257	0,707	62,3822
T1 24V	66,67%	3,1767	0,0556	0,0527	0,0542	0,0519	0,0722	0,097	0,1337	0,2064	0,3958	1,3006	5,3148	64,5812
T1 36V	100%	3,4868	0,6466	0,8721	0,8309	0,6591	0,7145	0,7066	0,7605	0,9729	1,6597	4,6094	15,6687	65,6998
T2 24V	100%	1,1702	0,0221	0,0434	0,1705	0,1073	0,0836	0,0851	0,1068	0,1622	0,2985	0,9315	3,4856	31,2951
T3 24V	100%	0,9693	0,1609	0,0738	0,0786	0,0369	0,0423	0,0627	0,0896	0,1507	0,4761	1,107	3,7271	33,1633
630VA														
T4 5V	2,27%	2,27	0,54	0,787	1,268	1,011	0,883	0,838	0,842	0,818	0,793	0,732	0,664	181,346
T4 12V	5,40%	0,934	0,09	0,179	0,34	0,422	0,246	0,202	0,143	0,203	0,155	0,147	0,445	309,791
T4 22V	10%	0,475	0,023	0,019	0,157	0,028	0,03	0,034	0,052	0,089	0,196	0,705	3,405	462,512
T4 42V	19,10%	0,648	0,107	0,139	0,917	0,304	0,316	0,41	0,611	0,998	2,019	6,207	22,814	590,987
T4 110V	50%	1,275	3,258	3,95	6,077	6,019	7,533	9,895	13,533	20,457	33,952	74,665	167,95	702,502
T4 220V	100%	5,636	25,928	29,824	34,747	40,55	48,803	59,629	75,502	99,951	146,995	247,252	408,727	782,144
T5 230V	100%	2,381	14,215	16,649	19,743	23,602	29,013	36,301	47,169	65,425	99,106	179,033	313,382	648,263
T6 220V	100%	7,354	30,627	35,07	40,692	47,456	56,997	70,731	89,305	119,029	171,39	284,37	460,791	865,598
750kVA														
T7 53V	13,25%	1,5073	0,1409	0,2208	0,4991	0,3865	0,4292	0,4722	0,5824	0,8211	1,4398	4,0951	14,8961	559,7025
T7 200V	50%	2,1943	7,0257	8,2622	10,050	11,907	14,677	18,528	24,672	34,745	53,8769	106,0923	215,6455	785,2688
T7 400V	100%	10,976	42,39	47,669	54,479	62,565	72,957	86,952	106,802	137,868	188,395	301,236	476,684	878,625
T7 115V	50%	1,589	1,182	1,475	1,96	2,294	2,845	3,758	5,235	8,056	14,006	33,43	84,403	487,838
T7 230V	100%	3,157	10,351	12,031	14,287	16,893	20,635	25,832	33,778	46,29	70,59	128,995	234,173	514,905
1kVA														
T8 5V	2,27%	2,8581	0,6395	0,8661	1,2788	1,1153	1,0536	0,9933	0,9928	0,9499	1,0183	0,8352	0,8017	148,2868
T8 12V	5,45%	0,7227	0,0731	0,1017	0,1493	0,1247	0,1115	0,1073	0,1034	0,1035	0,1063	0,1215	0,2198	234,6104
T8 24V	10,90%	0,646	0,0252	0,0443	0,0686	0,0502	0,0427	0,0431	0,0465	0,0654	0,1002	0,3057	1,469	333,1492
T8 36V	16,36%	0,6755	0,0731	0,1081	0,1524	0,1498	0,1667	0,2067	0,2845	0,4511	0,8951	2,9491	13,1923	508,4678
T8 110V	50%	0,8813	1,4678	1,7812	2,2072	2,7333	3,4736	4,6549	6,721	10,3632	18,3531	44,2657	111,1672	567,7382

T8 220V	100%	2,9578	13,439	15,613	18,493	22,120	27,058	34,001	43,988	61,128	91,9388	167,5825	295,9126	608,5494
3 phase														
350VA														
T9 230V	57,50%	1,8443	4,2643	5,2384	6,3751	7,9837	9,2173	11,643	15,571	22,609	36,3103	74,1889	157,7593	640,247
T9 400V	100%	6,9333	28,335	32,554	37,207	43,527	50,608	60,587	75,506	98,437	138,94	225,58	365,47	704,76
T9 230V	57,50%	2,7472	11,06	13,165	15,634	19,507	22,78	28,81	37,476	52,712	81,93	153,55	293,55	887,34
T9 400V	100%	16,290	65,035	72,556	82,328	95,294	109,51	130,03	156,95	197,02	267,02	412,71	625,63	1092,8
T9 230V	57,50%	6,0858	10,559	14,431	18,025	20,374	23,798	29,615	38,58	53,67	82,16	152,34	294,26	880,07
T9 400V	100%	19,988	64,917	72,722	83,903	95,434	109,93	128,82	157,01	199,56	268,35	411,89	624,9	1087,6
1.2kVA														
T10 24V	57,10%	0,4111	0,0824	0,1296	0,1958	0,1622	0,0799	0,0651	0,0565	0,051	0,0517	0,0855	0,2971	17,076
T10 42V	100%	0,4687	0,1431	0,2245	0,2059	0,1365	0,1274	0,1235	0,1359	0,1498	0,2259	0,4617	1,6481	17,592
5kVA														
T11	100%	1,002	0,2047	0,3295	0,4609	0,3964	0,3359	0,3773	0,2724	0,2229	0,1964	0,1974	0,274	3,234
20kVA														
T12	100%	0,1953	0,6191	0,7395	0,9089	1,1559	1,4893	2,2883	3,1886	4,9768	9,1559	22,874	58,4675	207,7306
40kVA														
T13	100%	0,0158	0,1869	0,2313	0,2836	0,3661	0,496	0,6971	1,0749	1,8598	3,5984	10,2812	29,1399	110,254
ASLE	**Wind.%**	**15 kΩ**	**5 kΩ**	**4.5 kΩ**	**4 kΩ**	**3.5 kΩ**	**3 kΩ**	**2.5 kΩ**	**2 kΩ**	**1.5 kΩ**	**1 kΩ**	**500 Ω**	**200 Ω**	**1 Ω**
400VA														
T1 5V	13,89%	0,301	0,061	0,065	0,068	0,063	0,061	0,061	0,061	0,061	0,063	0,068	0,083	3,621
T1 12V	33,33%	0,283	0,034	0,036	0,047	0,041	0,041	0,045	0,049	0,053	0,065	0,098	0,194	4,263
T1 24V	66,67%	0,292	0,04	0,042	0,044	0,048	0,056	0,065	0,079	0,101	0,145	0,275	0,616	4,389
T1 36V	100%	0,3005	0,1035	0,1142	0,1179	0,1236	0,1384	0,1567	0,1836	0,2285	0,3206	0,5772	1,2323	4,4734
T2 24V	100%	0,2889	0,0535	0,0637	0,0796	0,0845	0,0915	0,1046	0,1255	0,1614	0,2284	0,4209	0,8805	4,1995
T3 24V	100%	0,0674	0,0652	0,0677	0,076	0,0779	0,0888	0,1052	0,1273	0,1645	0,2454	0,4349	0,905	4,2322
630VA														
T4 5V	2,27%	0,1031	0,058	0,066	0,075	0,0695	0,0658	0,0644	0,0644	0,0642	0,0635	0,0643	0,0674	3,0013
T4 12V	5,40%	0,0596	0,0276	0,0344	0,0396	0,0444	0,0353	0,0335	0,0307	0,0365	0,0367	0,0453	0,0803	4,7915
T4 22V	10%	0,0428	0,0183	0,0192	0,029	0,0198	0,0208	0,0224	0,0255	0,0329	0,047	0,09	0,2103	6,8151
T4 42V	19,10%	0,0555	0,0419	0,0482	0,0639	0,0656	0,0664	0,0737	0,0888	0,1127	0,1584	0,2949	0,6477	8,6011
T4 110V	50%	0,118	0,2122	0,2396	0,2787	0,3021	0,3418	0,4009	0,4817	0,625	0,8652	1,4965	2,7445	10,6113
T4 220V	100%	0,3092	0,7314	0,8031	0,896	0,9872	1,126	1,2929	1,5354	1,8934	2,5348	3,8352	5,9227	12,2967
T5 230V	100%	0,2282	0,5891	0,6487	0,7179	0,8077	0,9242	1,0732	1,284	1,61	2,1721	3,4068	5,4073	11,7042
T6 220V	100%	0,4176	0,872	0,9596	1,0616	1,1644	1,3033	1,5008	1,7547	2,1453	2,7889	4,1333	6,226	12,5597
750kVA														
T7 53V	13,25%	0,1254	0,0309	0,0364	0,0476	0,0459	0,0491	0,0524	0,0591	0,0712	0,0953	0,168	0,3747	6,4439
T7 200V	50%	0,1777	0,2415	0,2677	0,3046	0,3379	0,3843	0,4474	0,5415	0,687	0,9427	1,5828	2,8264	10,069
T7 400V	100%	0,3823	0,7667	0,8401	0,9346	1,0332	1,1589	1,3271	1,5617	1,9233	2,5068	3,831	5,968	12,4449
T7 115V	50%	0,1575	0,1095	0,1251	0,1458	0,1599	0,1797	0,2113	0,2568	0,3353	0,4814	0,8865	1,8144	9,8277
T7 230V	100%	0,2457	0,3943	0,4387	0,4962	0,5533	0,6331	0,7411	0,8995	1,1396	1,5854	2,62	4,4965	10,781
1kVA														

T8 5V	2,27%	0,236	0,044	0,049	0,056	0,054	0,053	0,052	0,052	0,051	0,053	0,051	0,054	3,057
T8 12V	5,45%	0,181	0,027	0,03	0,034	0,032	0,031	0,031	0,031	0,032	0,035	0,042	0,065	4,564
T8 24V	10,90%	0,177	0,018	0,022	0,025	0,023	0,023	0,024	0,026	0,031	0,04	0,07	0,154	6,226
T8 36V	16,36%	0,177	0,037	0,043	0,048	0,049	0,053	0,059	0,069	0,086	0,122	0,226	0,532	9,072
T8 110V	50%	0,204	0,158	0,175	0,196	0,218	0,246	0,289	0,356	0,459	0,654	1,17	2,279	10,432
T8 220V	100%	0,324	0,536	0,589	0,657	0,734	0,834	0,97	1,156	1,459	1,976	3,176	5,192	11,516
3 phase														
350VA														
T9 230V	57,50%	0,102	0,173	0,1984	0,2264	0,2539	0,2812	0,3248	0,3973	0,5153	0,7266	1,2536	2,3194	9,474
T9 400V	100%	0,2555	0,6158	0,6856	0,7579	0,8443	0,9473	1,0831	1,2824	1,5826	2,0955	3,1752	4,9813	10,93
T9 230V	57,50%	0,1749	0,3605	0,4043	0,4495	0,5027	0,5588	0,6493	0,7656	0,9569	1,2892	2,0253	3,3092	9,341
T9 400V	100%	0,4857	1,1279	1,2197	1,343	1,4834	1,6419	1,8594	2,1377	2,541	3,2297	4,64	6,7619	13,145
T9 230V	57,50%	0,2377	0,3651	0,4547	0,5148	0,5504	0,6031	0,6884	0,812	1,003	1,3324	2,0556	3,3635	9,294
T9 400V	100%	0,5495	1,152	1,256	1,3933	1,5229	1,6734	1,8713	2,1649	2,6033	3,2713	4,6552	6,7727	13,061
1.2kVA														
T10 24V	57,10%	0,0631	0,0365	0,0419	0,049	0,0488	0,0391	0,0386	0,0408	0,0444	0,0552	0,0913	0,1928	2,708
T10 42V	100%	0,071	0,0542	0,0629	0,0646	0,0637	0,0659	0,0715	0,0822	0,0976	0,1353	0,2276	0,4769	2,777
5kVA														
T11	100%	0,0907	0,0467	0,0569	0,0619	0,0613	0,0572	0,062	0,0564	0,0584	0,0654	0,0939	0,1694	1,256
20kVA														
T12	100%	0,0858	0,1642	0,1826	0,1999	0,2318	0,2705	0,4075	0,4784	0,6125	0,8685	1,5419	2,9579	9,172
40kVA														
T13	100%	0,0307	0,101	0,1148	0,1279	0,1432	0,1663	0,1994	0,2509	0,3352	0,4798	0,8784	1,7367	6,386
DABS	**Wind.%**	**15 kΩ**	**5 kΩ**	**4.5 kΩ**	**4 kΩ**	**3.5 kΩ**	**3 kΩ**	**2.5 kΩ**	**2 kΩ**	**1.5 kΩ**	**1 kΩ**	**500 Ω**	**200 Ω**	**1 Ω**
400VA														
T1 5V	13,89%	0,628	0,2293	0,2502	0,2619	0,2441	0,239	0,2369	0,2345	0,2345	0,2377	0,247	0,2759	4,887
T1 12V	33,33%	0,5736	0,1161	0,1251	0,1703	0,1393	0,1388	0,147	0,1602	0,1643	0,1905	0,2565	0,4501	5,3124
T1 24V	66,67%	0,6051	0,1037	0,1063	0,1089	0,114	0,1332	0,1544	0,1825	0,2295	0,319	0,5908	1,2599	5,4784
T1 36V	100%	0,6349	0,2986	0,3319	0,3302	0,3282	0,3599	0,392	0,4408	0,526	0,7047	1,1902	2,3275	5,5998
T2 24V	100%	0,4476	0,0928	0,1141	0,1569	0,1551	0,1593	0,1749	0,2042	0,2567	0,3522	0,622	1,2245	4,3398
T3 24V	100%	0,2294	0,1429	0,1294	0,1448	0,1257	0,1386	0,1677	0,1982	0,2528	0,4067	0,6739	1,2854	4,3946
630VA														
T4 5V	2,27%	0,415	0,2234	0,2577	0,3	0,274	0,2588	0,2535	0,2539	0,2536	0,253	0,259	0,2794	9,8658
T4 12V	5,40%	0,2459	0,1065	0,1362	0,162	0,1807	0,1454	0,1388	0,1285	0,1554	0,1614	0,2104	0,3917	13,2379
T4 22V	10%	0,1767	0,082	0,0834	0,1325	0,092	0,099	0,1069	0,1263	0,1647	0,2378	0,4564	1,0357	16,8557
T4 42V	19,10%	0,2383	0,1964	0,2269	0,3129	0,3122	0,3234	0,3644	0,4422	0,5651	0,7962	1,4389	2,9666	19,4608
T4 110V	50%	0,5493	1,0447	1,1725	1,3676	1,4658	1,6473	1,9112	2,2649	2,869	3,8281	6,1194	9,9553	22,4322
T4 220V	100%	1,4501	3,2995	3,5913	3,9527	4,2965	4,8159	5,4149	6,2536	7,4337	9,3707	12,7978	17,1467	24,3385
T5 230V	100%	0,9783	2,4586	2,6864	2,938	3,2674	3,6768	4,1917	4,8905	5,9207	7,5661	10,7425	14,8505	21,9115
T6 220V	100%	1,8889	3,9243	4,2743	4,6735	5,0692	5,5937	6,3161	7,2081	8,5088	10,4854	14,0649	18,4375	25,5776
750kVA														
T7 53V	13,25%	0,3851	0,1471	0,1721	0,2183	0,2177	0,2376	0,2614	0,303	0,3759	0,5161	0,9218	1,9644	17,949

T7 200V	50%	0,6915	1,2846	1,4139	1,589	1,754	1,9808	2,2787	2,711	3,3516	4,4126	6,7933	10,6565	22,5893
T7 400V	100%	1,8046	3,7217	4,0249	4,4047	4,7966	5,2812	5,9069	6,7406	7,9492	9,7282	13,1885	17,5729	25,0576
T7 115V	50%	0,5284	0,4955	0,561	0,6465	0,7094	0,7958	0,9292	1,1177	1,4311	1,9864	3,3885	6,1082	18,1382
T7 230V	100%	0,9421	1,6564	1,8238	2,0369	2,2439	2,527	2,8989	3,4242	4,1798	5,4771	8,0828	11,8344	19,0058
1kVA														
T8 5V	2,27%	0,7294	0,1584	0,1781	0,2048	0,1931	0,1882	0,1836	0,1838	0,1813	0,1894	0,1846	0,2037	9,0657
T8 12V	5,45%	0,5344	0,0884	0,1	0,115	0,1101	0,1053	0,1067	0,1085	0,1131	0,1269	0,1633	0,2684	11,4946
T8 24V	10,90%	0,5138	0,0679	0,0816	0,0951	0,0902	0,0902	0,0967	0,1082	0,1337	0,1757	0,3132	0,6858	14,1035
T8 36V	16,36%	0,5248	0,1507	0,1752	0,1987	0,2075	0,2256	0,255	0,3024	0,3828	0,5411	0,9946	2,228	18,5204
T8 110V	50%	0,677	0,6996	0,774	0,8651	0,9603	1,0829	1,2631	1,5383	1,9491	2,6894	4,4845	7,7862	20,3332
T8 220V	100%	1,2378	2,2523	2,4551	2,7095	2,9934	3,3565	3,8312	4,4591	5,4262	6,9533	10,0429	14,1643	21,3515
3 phase														
350VA														
T9 230V	57,50%	0,5142	0,9001	1,031	1,1679	1,3067	1,4251	1,6222	1,9456	2,4494	3,3007	5,2048	8,4217	19,71
T9 400V	100%	1,2789	2,8609	3,1579	3,4435	3,7869	4,1545	4,6369	5,3221	6,3008	7,8334	10,607	14,2458	20,72
T9 230V	57,50%	0,9285	1,9736	2,2021	2,429	2,7077	2,972	3,4061	3,9433	4,7976	6,1959	8,9911	13,1024	23,635
T9 400V	100%	2,5588	5,5091	5,9013	6,4045	6,9828	7,5786	8,3811	9,3689	10,7237	12,8528	16,6136	21,0461	28,167
T9 230V	57,50%	1,1625	1,9673	2,3871	2,6682	2,862	3,1293	3,544	4,12	4,9738	6,3603	9,107	13,2996	23,572
T9 400V	100%	2,8308	5,5933	6,0274	6,5861	7,0978	7,6766	8,4112	9,4561	10,934	12,9776	16,6586	21,094	28,071
1.2kVA														
T10 24V	57,10%	0,1968	0,1026	0,1204	0,1434	0,1373	0,1024	0,0955	0,0943	0,0965	0,1093	0,1606	0,3024	2,692
T10 42V	100%	0,2176	0,1399	0,1623	0,1673	0,154	0,1501	0,1548	0,1693	0,1884	0,2459	0,3626	0,6935	2,779
5kVA														
T11	100%	0,2883	0,1404	0,1744	0,1933	0,1846	0,1663	0,1773	0,153	0,1447	0,1478	0,1783	0,2583	1,063
20kVA														
T12	100%	0,2545	0,4616	0,5112	0,5581	0,6396	0,7377	1,0571	1,238	1,5567	2,1448	3,552	6,0422	12,401
40kVA														
T13	100%	0,0743	0,2439	0,2743	0,3046	0,342	0,3958	0,47	0,5865	0,7745	1,0877	1,8997	3,4207	8,13
RMSE	**Wind.%**	**15 kΩ**	**5 kΩ**	**4.5 kΩ**	**4 kΩ**	**3.5 kΩ**	**3 kΩ**	**2.5 kΩ**	**2 kΩ**	**1.5 kΩ**	**1 kΩ**	**500 Ω**	**200 Ω**	**1 Ω**
400VA														
T1 5V	13,89%	0,1282	0,073	0,085	0,093	0,0862	0,0847	0,084	0,0829	0,0823	0,0819	0,0804	0,077	0,4942
T1 12V	33,33%	0,1051	0,029	0,032	0,0496	0,0359	0,0345	0,0358	0,038	0,0355	0,0368	0,0381	0,0561	0,5269
T1 24V	66,67%	0,1191	0,0157	0,0153	0,0156	0,0152	0,0179	0,0208	0,0244	0,0304	0,042	0,0762	0,154	0,537
T1 36V	100%	0,1245	0,0536	0,0623	0,0608	0,0541	0,0564	0,056	0,0581	0,0658	0,0859	0,1431	0,2639	0,5404
T2 24V	100%	0,0815	0,0112	0,0157	0,0311	0,0247	0,0218	0,022	0,0246	0,0303	0,0412	0,0727	0,1407	0,4215
T3 24V	100%	0,0675	0,0275	0,0186	0,0192	0,0132	0,0141	0,0172	0,0205	0,0266	0,0473	0,0721	0,1323	0,3947
630VA														
T4 5V	2,27%	0,0439	0,0214	0,0258	0,0328	0,0293	0,0274	0,0266	0,0267	0,0263	0,0259	0,0249	0,0237	0,3921
T4 12V	5,40%	0,0282	0,0088	0,0124	0,017	0,019	0,0145	0,0131	0,011	0,0132	0,0115	0,0112	0,0195	0,5143
T4 22V	10%	0,0202	0,0045	0,004	0,0116	0,0049	0,0051	0,0054	0,0067	0,0088	0,0129	0,0246	0,054	0,6296
T4 42V	19,10%	0,0235	0,0096	0,0109	0,028	0,0161	0,0164	0,0187	0,0228	0,0292	0,0415	0,0728	0,1396	0,7104
T4 110V	50%	0,0329	0,0527	0,058	0,0719	0,0716	0,0801	0,0918	0,1073	0,132	0,17	0,2521	0,3781	0,7734

T4 220V	100%	0,0693	0,1487	0,1595	0,1722	0,186	0,204	0,2255	0,2538	0,292	0,3541	0,4592	0,5905	0,8168
T5 230V	100%	0,049	0,1198	0,1296	0,1412	0,1543	0,1711	0,1914	0,2182	0,257	0,3163	0,4251	0,5624	0,8088
T6 220V	100%	0,076	0,155	0,1659	0,1787	0,1929	0,2114	0,2356	0,2647	0,3056	0,3667	0,4723	0,6012	0,824
750kVA														
T7 53V	13,25%	0,0364	0,0111	0,0139	0,021	0,0184	0,0194	0,0204	0,0226	0,0269	0,0356	0,06	0,1145	0,7019
T7 200V	50%	0,0439	0,0786	0,0852	0,094	0,1023	0,1136	0,1276	0,1473	0,1748	0,2177	0,3054	0,4355	0,831
T7 400V	100%	0,0984	0,1933	0,205	0,2192	0,2349	0,2536	0,2769	0,3069	0,3487	0,4076	0,5154	0,6483	0,8802
T7 115V	50%	0,0453	0,039	0,0436	0,0503	0,0544	0,0606	0,0696	0,0822	0,1019	0,1344	0,2077	0,33	0,7933
T7 230V	100%	0,0638	0,1156	0,1246	0,1358	0,1476	0,1632	0,1826	0,2088	0,2444	0,3018	0,408	0,5497	0,8151
1kVA														
T8 5V	2,27%	0,0554	0,0262	0,0305	0,0371	0,0346	0,0337	0,0327	0,0327	0,032	0,0331	0,03	0,0294	0,3992
T8 12V	5,45%	0,0282	0,009	0,0106	0,0128	0,0117	0,0111	0,0109	0,0107	0,0107	0,0108	0,0116	0,0156	0,5082
T8 24V	10,90%	0,0267	0,0053	0,007	0,0087	0,0074	0,0069	0,0069	0,0072	0,0085	0,0105	0,0183	0,0402	0,6057
T8 36V	16,36%	0,0273	0,009	0,0109	0,013	0,0128	0,0136	0,0151	0,0177	0,0223	0,0314	0,057	0,1206	0,7485
T8 110V	50%	0,0312	0,0402	0,0443	0,0493	0,0549	0,0619	0,0716	0,086	0,1068	0,1422	0,2208	0,3499	0,7908
T8 220V	100%	0,0571	0,1218	0,1313	0,1429	0,1563	0,1728	0,1938	0,2204	0,2598	0,3186	0,4302	0,5716	0,8197
3 phase														
350VA														
T9 230V	57,50%	0,0438	0,0665	0,0737	0,0813	0,091	0,0978	0,1099	0,1271	0,1532	0,1941	0,2775	0,4046	0,8152
T9 400V	100%	0,0847	0,1713	0,1836	0,1963	0,2123	0,229	0,2505	0,2797	0,3193	0,3794	0,4834	0,6153	0,8549
T9 230V	57,50%	0,0434	0,087	0,0949	0,1035	0,1156	0,1249	0,1405	0,1602	0,19	0,2368	0,3243	0,4483	0,7807
T9 400V	100%	0,1055	0,2109	0,2227	0,2372	0,2552	0,2736	0,2982	0,3276	0,367	0,4273	0,5312	0,654	0,8645
T9 230V	57,50%	0,0645	0,0849	0,0993	0,111	0,118	0,1275	0,1422	0,1623	0,1915	0,2369	0,3226	0,4483	0,7753
T9 400V	100%	0,1169	0,2107	0,223	0,2396	0,2555	0,2742	0,2968	0,3277	0,3695	0,4284	0,5308	0,6538	0,8625
1.2kVA														
T10 24V	57,10%	0,0486	0,0218	0,0273	0,0335	0,0305	0,0214	0,0193	0,018	0,0171	0,0172	0,0222	0,0413	0,3133
T10 42V	100%	0,0519	0,0287	0,0359	0,0344	0,028	0,0271	0,0266	0,028	0,0293	0,036	0,0515	0,0973	0,318
5kVA														
T11	100%	0,0865	0,0391	0,0496	0,0586	0,0544	0,0501	0,0531	0,0451	0,0408	0,0383	0,0384	0,0452	0,1553
20kVA														
T12	100%	0,0217	0,0386	0,0422	0,0468	0,0528	0,0599	0,0743	0,0877	0,1095	0,1486	0,2348	0,3755	0,708
40kVA														
T13	100%	0,008	0,0276	0,0307	0,034	0,0386	0,045	0,0533	0,0662	0,0871	0,1211	0,2048	0,3447	0,6706
ED	**Wind.%**	**15 kΩ**	**5 kΩ**	**4.5 kΩ**	**4 kΩ**	**3.5 kΩ**	**3 kΩ**	**2.5 kΩ**	**2 kΩ**	**1.5 kΩ**	**1 kΩ**	**500 Ω**	**200 Ω**	**1 Ω**
400VA														
T1 5V	13,89%	59,781	34,044	39,608	43,347	40,199	39,499	39,184	38,666	38,383	38,173	37,492	35,921	230,414
T1 12V	33,33%	49,179	13,567	14,957	23,207	16,824	16,14	16,753	17,769	16,6	17,234	17,819	26,255	246,622
T1 24V	66,67%	55,654	7,36	7,165	7,268	7,116	8,388	9,727	11,418	14,187	19,645	35,61	71,986	250,932
T1 36V	100%	58,307	25,109	29,159	28,463	25,35	26,395	26,248	27,231	30,799	40,227	67,038	123,6	253,095
T2 24V	100%	33,779	4,637	6,509	12,895	10,229	9,03	9,11	10,203	12,574	17,061	30,136	58,296	174,679
T3 24V	100%	30,743	12,524	8,48	8,754	5,997	6,421	7,817	9,349	12,123	21,546	32,853	60,282	179,817
630VA														

T4 5V	2,27%	47,042	22,949	27,692	35,159	31,397	29,346	28,58	28,656	28,237	27,801	26,708	25,451	420,49
T4 12V	5,40%	30,183	9,39	13,201	18,213	20,272	15,487	14,047	11,793	14,073	12,292	11,97	20,82	549,587
T4 22V	10%	21,521	4,779	4,263	12,351	5,252	5,443	5,775	7,12	9,334	13,81	26,222	57,619	671,527
T4 42V	19,10%	25,131	10,22	11,637	29,902	17,217	17,554	20,003	24,415	31,199	44,369	77,792	149,144	759,086
T4 110V	50%	35,252	56,363	62,061	76,977	76,603	85,701	98,225	114,87	141,23	181,942	269,812	404,662	827,611
T4 220V	100%	74,13	158,10	170,52	184,06	198,84	218,14	241,12	271,32	312,17	378,576	490,99	631,275	873,264
T5 230V	100%	48,185	117,73	127,41	138,74	151,70	168,19	188,13	214,45	252,57	310,851	417,801	552,763	795,02
T6 220V	100%	84,679	172,81	184,91	199,19	215,10	235,74	262,61	295,08	340,67	408,785	526,556	670,277	918,672
750kVA														
T7 53V	13,25%	38,336	11,723	14,673	22,059	19,413	20,456	21,457	23,83	28,295	37,467	63,188	120,514	738,722
T7 200V	50%	46,254	82,765	89,753	98,987	107,75	119,63	134,40	155,10	184,06	229,194	321,621	458,535	875,007
T7 400V	100%	103,45	203,30	215,59	230,47	246,98	266,71	291,17	322,70	366,64	428,585	541,946	681,738	925,559
T7 115V	50%	39,364	33,943	37,917	43,714	47,296	52,667	60,53	71,442	88,624	116,857	180,539	286,868	689,668
T7 230V	100%	55,484	100,46	108,31	118,02	128,34	141,84	158,70	181,48	212,44	262,346	354,641	477,827	708,542
1kVA														
T8 5V	2,27%	52,789	24,970	29,059	35,311	32,976	32,051	31,120	31,113	30,433	31,509	28,5363	27,9585	380,2363
T8 12V	5,45%	26,544	8,4422	9,9553	12,067	11,028	10,427	10,229	10,041	10,045	10,1801	10,8831	14,6396	478,2731
T8 24V	10,90%	25,096	4,959	6,571	8,179	6,998	6,451	6,481	6,736	7,983	9,885	17,263	37,845	569,93
T8 36V	16,36%	25,663	8,441	10,265	12,188	12,084	12,749	14,195	16,655	20,972	29,541	53,622	113,413	704,1
T8 110V	50%	29,313	37,829	41,674	46,39	51,623	58,196	67,369	80,951	100,52	133,77	207,748	329,223	744,006
T8 220V	100%	123,40	122,92	131,32	141,78	153,75	168,74	187,53	212,03	248,34	302,89	406,938	540,111	774,7858
3 phase														
350VA														
T9 230V	57,50%	42,405	64,48	71,466	78,84	88,228	94,799	106,55	123,21	148,47	188,16	268,95	392,19	790,09
T9 400V	100%	82,219	166,21	178,16	190,46	206,01	222,13	243,05	271,33	309,8	368,06	468,97	596,94	828,94
T9 230V	57,50%	51,755	103,85	113,29	123,46	137,91	149,03	167,6	191,15	226,7	282,63	386,93	534,99	930,14
T9 400V	100%	126,03	251,81	265,97	283,32	304,81	326,77	356,06	391,19	438,28	510,24	634,34	781,02	1032,2
T9 230V	57,50%	77,03	101,47	118,62	132,57	140,94	152,33	169,93	193,95	228,75	283,04	385,4	535,63	926,32
T9 400V	100%	139,6	251,58	266,28	286,02	305,04	327,38	354,41	391,26	441,11	511,51	633,71	780,56	1029,7
1.2kVA														
T10 24V	57,10%	20,02	8,9636	11,241	13,815	12,575	8,8236	7,9657	7,4232	7,0515	7,0996	9,1307	17,019	129,03
T10 42V	100%	21,378	11,811	14,796	14,167	11,537	11,146	10,972	11,513	12,086	14,84	21,216	40,086	130,97
5kVA														
T11	100%	31,257	14,129	17,925	21,198	19,659	18,097	19,18	16,297	14,743	13,838	13,872	16,345	56,155
20kVA														
T12	100%	13,799	24,57	26,853	29,769	33,572	38,107	47,235	55,758	69,659	94,483	149,34	238,76	450,04
40kVA														
T13	100%	3,9209	13,5	15,016	16,63	18,894	21,991	26,071	32,374	42,583	59,232	100,12	168,56	327,87
CSD	**Wind.%**	**15 kΩ**	**5 kΩ**	**4.5 kΩ**	**4 kΩ**	**3.5 kΩ**	**3 kΩ**	**2.5 kΩ**	**2 kΩ**	**1.5 kΩ**	**1 kΩ**	**500 Ω**	**200 Ω**	**1 Ω**
400VA														
T1 5V	13,89%	1,8973	1,0908	1,2691	1,3889	1,288	1,2656	1,2555	1,2388	1,2297	1,223	1,2009	1,1494	6,5474
T1 12V	33,33%	1,564	0,4322	0,4764	0,741	0,5352	0,5128	0,5319	0,5638	0,5244	0,5411	0,5449	0,7648	6,2932

T1 24V	66,67%	1,7719	0,2316	0,222	0,2212	0,2136	0,2522	0,2914	0,3401	0,4191	0,5753	1,0334	2,0509	6,1523
T1 36V	100%	1,8604	0,7978	0,9254	0,8995	0,795	0,8228	0,8073	0,8223	0,9111	1,1642	1,8937	3,3885	6,069
T2 24V	100%	1,0522	0,1346	0,1955	0,4059	0,3139	0,2672	0,2615	0,288	0,3516	0,4741	0,8296	1,5722	4,2368
T3 24V	100%	0,9604	0,4009	0,2673	0,2536	0,1674	0,1799	0,2264	0,2585	0,3379	0,6576	0,9603	1,668	4,0972
630VA														
T4 5V	2,27%	1,4533	0,7108	0,8581	1,1004	0,9746	0,911	0,8871	0,8891	0,8757	0,8625	0,8256	0,776	10,113
T4 12V	5,40%	0,9358	0,283	0,402	0,5671	0,6252	0,4757	0,4296	0,357	0,425	0,3617	0,3247	0,5475	12,609
T4 22V	10%	0,6687	0,1481	0,1126	0,3821	0,1482	0,1475	0,1604	0,1963	0,2564	0,386	0,716	1,5743	14,745
T4 42V	19,10%	0,7765	0,2752	0,3057	0,9347	0,4646	0,4701	0,5377	0,6568	0,8385	1,1962	2,0739	3,8423	15,673
T4 110V	50%	1,038	1,5058	1,647	2,148	2,0173	2,248	2,5636	2,9796	3,6109	4,5708	6,459	9,0404	15,81
T4 220V	100%	1,9448	3,9683	4,2042	4,5167	4,8507	5,2572	5,7482	6,3652	7,1449	8,3738	10,204	12,015	14,925
T5 230V	100%	1,2498	2,9955	3,2237	3,4547	3,7669	4,134	4,5758	5,1448	5,9195	7,0502	8,9891	11,093	14,451
T6 220V	100%	1,9857	4,0199	4,2297	4,5021	4,8448	5,2805	5,8076	6,4263	7,2444	8,4269	10,264	12,161	15,611
750kVA														
T7 53V	13,25%	1,2284	0,3553	0,4486	0,6902	0,5977	0,6263	0,6493	0,7137	0,8383	1,0999	1,8166	3,3494	16,468
T7 200V	50%	1,4493	2,3541	2,5448	2,8049	3,0304	3,3382	3,7178	4,2388	4,9451	5,9958	7,9592	10,505	17,713
T7 400V	100%	3,006	5,4219	5,7039	6,054	6,4167	6,8445	7,363	8,0088	8,8664	10,004	11,889	13,935	17,223
T7 115V	50%	1,2572	0,9838	1,0993	1,2799	1,3702	1,5161	1,7318	2,0296	2,4944	3,2355	4,8007	7,1085	14,042
T7 230V	100%	1,6925	2,8051	3,0069	3,2667	3,5229	3,8574	4,2693	4,8108	5,5181	6,5876	8,3638	10,351	13,449
1kVA														
T8 5V	2,27%	0,6399	0,7888	0,9202	0,8237	0,9472	0,8162	0,9859	0,9855	0,9638	0,998	0,9011	0,8781	9,31
T8 12V	5,45%	0,8487	0,2705	0,319	0,3866	0,3533	0,3339	0,3274	0,321	0,3207	0,3236	0,3402	0,4316	11,4
T8 24V	10,90%	0,8027	0,1577	0,2093	0,2611	0,2222	0,2028	0,2013	0,2056	0,2407	0,289	0,489	1,0441	13,001
T8 36V	16,36%	0,8204	0,2583	0,316	0,3778	0,3682	0,3816	0,4185	0,4837	0,6011	0,8343	1,4796	3,0127	14,767
T8 110V	50%	0,911	1,0618	1,1676	1,2994	1,4351	1,6068	1,8469	2,1993	2,6991	3,5247	5,2494	7,7887	14,705
T8 220V	100%	1,4854	3,0432	3,2633	3,534	3,8336	4,2001	4,6534	5,2161	6,019	7,1487	9,0646	10,992	13,778
3 phase														
350VA														
T9 230V	57,50%	1,3039	1,8936	2,1067	2,2975	2,5982	2,7436	3,0564	3,4988	4,154	5,1479	7,0324	9,6381	17,017
T9 400V	100%	2,3784	4,5997	4,9141	5,179	5,616	5,9574	6,4371	7,0778	7,9239	9,1579	11,162	13,5209	17,334
T9 230V	57,50%	1,4736	2,7641	3,0195	3,2265	3,6845	3,8775	4,3131	4,8365	5,6244	6,8097	8,8586	11,542	18,745
T9 400V	100%	3,2411	6,1019	6,4079	6,6855	7,2317	7,6032	8,1498	8,8027	9,6552	10,913	12,939	15,11	18,656
T9 230V	57,50%	2,1958	2,6333	3,013	3,3656	3,5612	3,823	4,2234	4,7609	5,5185	6,6397	8,6219	11,324	18,67
T9 400V	100%	3,4898	5,9587	6,2138	6,5752	6,9527	7,4232	7,955	8,6393	9,4995	10,759	12,764	14,947	18,731
1.2kVA														
T10 24V	57,10%	0,6198	0,2817	0,3516	0,4354	0,3895	0,2717	0,243	0,2252	0,2133	0,21	0,2671	0,4978	3,4025
T10 42V	100%	0,6509	0,3657	0,4532	0,4275	0,3412	0,3303	0,3231	0,3375	0,3517	0,427	0,6097	1,149	3,2154
5kVA														
T11	100%	0,9595	0,4313	0,548	0,6526	0,6032	0,5565	0,5897	0,5008	0,4527	0,4225	0,4165	0,4783	1,4902
20kVA														
T12	100%	0,4039	0,6875	0,7539	0,8367	0,9325	1,0462	1,2692	1,4895	1,8327	2,445	3,6945	5,4299	7,8475
40kVA														
T13	100%	0,1217	0,4035	0,4504	0,4971	0,564	0,6564	0,7766	0,9656	1,2643	1,7498	2,9264	4,7362	6,9818

CCF	**Wind.%**	**15 kΩ**	**5 kΩ**	**4.5 kΩ**	**4 kΩ**	**3.5 kΩ**	**3 kΩ**	**2.5 kΩ**	**2 kΩ**	**1.5 kΩ**	**1 kΩ**	**500 Ω**	**200 Ω**	**1 Ω**
400VA														
T1 5V	13,89%	0,9725	0,9911	0,988	0,9856	0,9876	0,9881	0,9882	0,9886	0,9887	0,9888	0,9892	0,99	0,6697
T1 12V	33,33%	0,9813	0,9986	0,9983	0,9958	0,9978	0,998	0,9979	0,9976	0,998	0,9979	0,998	0,9967	0,6864
T1 24V	66,67%	0,976	0,9996	0,9997	0,9997	0,9997	0,9996	0,9995	0,9993	0,999	0,9981	0,9939	0,9737	0,6952
T1 36V	100%	0,9742	0,9953	0,9937	0,994	0,9953	0,995	0,9953	0,9953	0,9946	0,9917	0,9786	0,9197	0,7045
T2 24V	100%	0,9998	0,9998	0,9995	0,998	0,9988	0,9992	0,9992	0,9991	0,9986	0,9973	0,9915	0,9685	0,7519
T3 24V	100%	0,9954	0,999	0,9995	0,9997	0,9998	0,9998	0,9996	0,9995	0,9991	0,997	0,9932	0,9791	0,8895
630VA														
T4 5V	2,27%	0,9889	0,9974	0,9961	0,9937	0,995	0,9957	0,9959	0,9959	0,996	0,9961	0,9964	0,9969	0,4351
T4 12V	5,40%	0,9997	0,9996	0,9992	0,9983	0,998	0,9988	0,999	0,9994	0,9991	0,9994	0,9996	0,9993	0,2115
T4 22V	10%	0,9976	0,9999	1	0,9992	0,9999	0,9999	0,9999	0,9999	0,9999	0,9996	0,9989	0,9938	-0,09
T4 42V	19,10%	0,9969	0,9998	0,9998	0,9955	0,9993	0,9995	0,9993	0,999	0,9984	0,9968	0,9896	0,9571	-0,229
T4 110V	50%	0,9954	0,9947	0,9937	0,9823	0,9906	0,9884	0,9845	0,978	0,966	0,9359	0,8166	0,3815	-0,312
T4 220V	100%	0,9905	0,9562	0,9508	0,9391	0,9266	0,9105	0,8798	0,8319	0,7486	0,528	0,1195	-0,12	-0,25
T5 230V	100%	0,9965	0,9697	0,9635	0,96	0,948	0,9345	0,9124	0,8756	0,8059	0,6419	0,2058	-0,142	-0,317
T6 220V	100%	0,9863	0,9554	0,9522	0,9459	0,9306	0,9075	0,8731	0,8142	0,691	0,3762	-0,157	-0,363	-0,478
750kVA														
T7 53V	13,25%	0,9998	0,9997	0,9994	0,9986	0,999	0,9989	0,9989	0,9988	0,9984	0,9975	0,994	0,9801	-0,472
T7 200V	50%	0,9975	0,9903	0,9886	0,9858	0,9837	0,9803	0,9757	0,9686	0,9571	0,9355	0,871	0,6393	-0,482
T7 400V	100%	0,9925	0,9479	0,9423	0,9339	0,9248	0,9126	0,8954	0,8692	0,8221	0,7183	0,3426	-0,161	-0,462
T7 115V	50%	0,9994	0,9975	0,9968	0,9951	0,9948	0,9938	0,9921	0,9892	0,9835	0,9714	0,9277	0,7512	-0,297
T7 230V	100%	0,9958	0,9786	0,9754	0,9702	0,965	0,9571	0,9454	0,9261	0,8922	0,81	0,5258	0,0874	-0,216
1kVA														
T8 5V	2,27%	0,998	0,9975	0,9987	0,9991	0,9984	0,9993	0,9987	0,9985	0,9984	0,9987	0,9981	0,9977	0,4907
T8 12V	5,45%	0,9994	0,9996	0,9995	0,9992	0,9993	0,9994	0,9994	0,9995	0,9995	0,9995	0,9994	0,9993	0,3002
T8 24V	10,90%	0,9989	0,9999	0,9998	0,9996	0,9997	0,9998	0,9998	0,9998	0,9998	0,9997	0,9993	0,9973	0,0779
T8 36V	16,36%	0,9997	0,9997	0,9996	0,9994	0,9994	0,9995	0,9994	0,9993	0,999	0,9982	0,9946	0,9767	-0,293
T8 110V	50%	0,9975	0,9971	0,9964	0,9955	0,9946	0,9934	0,9913	0,9876	0,9809	0,9655	0,907	0,6491	-0,345
T8 220V	100%	0,9927	0,9747	0,9701	0,9636	0,9561	0,9455	0,9296	0,9045	0,8545	0,7403	0,3567	-0,085	-0,275
3 phase														
350VA														
T9 230V	57,50%	0,9957	0,993	0,9908	0,9896	0,9854	0,9853	0,9821	0,9764	0,9662	0,9456	0,8839	0,7108	-0,078
T9 400V	100%	0,989	0,957	0,9488	0,9461	0,9297	0,9233	0,9083	0,8831	0,8406	0,7542	0,5443	0,2409	-0,068
T9 230V	57,50%	0,9948	0,9854	0,9814	0,9807	0,9695	0,9702	0,9625	0,9529	0,9328	0,8892	0,7523	0,383	-0,403
T9 400V	100%	0,9825	0,9173	0,9042	0,9038	0,8636	0,8516	0,8193	0,7676	0,6775	0,4941	0,1344	-0,142	-0,34
T9 230V	57,50%	0,9845	0,9879	0,9829	0,9765	0,9756	0,9733	0,9684	0,9599	0,9447	0,9131	0,8009	0,3567	-0,485
T9 400V	100%	0,9745	0,9346	0,9313	0,9229	0,9101	0,8888	0,8592	0,8106	0,7286	0,4994	0,0231	-0,277	-0,423
1.2kVA														
T10 24V	57,10%	0,9976	0,9994	0,9991	0,9986	0,999	0,9995	0,9997	0,9997	0,9997	0,9997	0,9995	0,9981	0,9172
T10 42V	100%	0,9979	0,9991	0,9988	0,9991	0,9995	0,9995	0,9995	0,9994	0,9993	0,9989	0,9972	0,9891	0,9248
5kVA														

T11	100%	0,9958	0,9992	0,9988	0,9981	0,9984	0,9985	0,9983	0,9988	0,999	0,9992	0,9992	0,9988	0,9852
20kVA														
T12	100%	0,9986	0,9964	0,9956	0,9946	0,9933	0,9917	0,987	0,9817	0,9714	0,9445	0,8516	0,641	0,35
40kVA														
T13	100%	0,9999	0,9989	0,9986	0,9983	0,9978	0,997	0,9959	0,9935	0,9886	0,9774	0,9293	0,78	0,4655
MM	**Wind.%**	**15 kΩ**	**5 kΩ**	**4.5 kΩ**	**4 kΩ**	**3.5 kΩ**	**3 kΩ**	**2.5 kΩ**	**2 kΩ**	**1.5 kΩ**	**1 kΩ**	**500 Ω**	**200 Ω**	**1 Ω**
400VA														
T1 5V	13,89%	1,0146	1,0155	1,0169	1,0177	1,0165	1,0161	1,016	1,0158	1,0158	1,0161	1,0167	1,0187	1,41
T1 12V	33,33%	1,014	1,0078	1,0084	1,0114	1,0094	1,0093	1,0099	1,0108	1,0111	1,0128	1,0174	1,0308	1,506
T1 24V	66,67%	1,0139	1,007	1,0071	1,0073	1,0077	1,009	1,0104	1,0123	1,0155	1,0217	1,0409	1,0912	1,55
T1 36V	100%	1,0147	1,0202	1,0225	1,0224	1,0222	1,0245	1,0267	1,0301	1,0362	1,049	1,0856	1,1817	1,577
T2 24V	100%	1,0043	1,007	1,0087	1,0119	1,0118	1,0121	1,0133	1,0156	1,0197	1,0272	1,0489	1,1007	1,428
T3 24V	100%	1,016	1,0098	1,0089	1,01	1,0087	1,0096	1,0116	1,0137	1,0176	1,0285	1,048	1,0955	1,4239
630VA														
T4 5V	2,27%	1,0122	1,0065	1,0076	1,0088	1,008	1,0076	1,0074	1,0074	1,0074	1,0074	1,0076	1,0082	1,3952
T4 12V	5,40%	1,0072	1,0031	1,004	1,0048	1,0053	1,0043	1,0041	1,0038	1,0046	1,0047	1,0062	1,0116	1,6169
T4 22V	10%	1,0052	1,0024	1,0024	1,0039	1,0027	1,0029	1,0031	1,0037	1,0048	1,007	1,0135	1,0312	1,9417
T4 42V	19,10%	1,007	1,0058	1,0067	1,0092	1,0092	1,0095	1,0108	1,0131	1,0168	1,0238	1,0439	1,0947	2,2808
T4 110V	50%	1,0163	1,0314	1,0354	1,0415	1,0446	1,0504	1,059	1,0706	1,0912	1,1253	1,2159	1,4039	2,8068
T4 220V	100%	1,0442	1,1065	1,117	1,1302	1,1431	1,1631	1,187	1,2221	1,2751	1,3723	1,5855	1,9779	3,3763
T5 230V	100%	1,032	1,0845	1,093	1,1027	1,1154	1,1317	1,1529	1,1828	1,2298	1,3129	1,5079	1,8657	3,1826
T6 220V	100%	1,0558	1,1233	1,1357	1,1502	1,165	1,1852	1,2141	1,2517	1,3109	1,412	1,6399	2,0453	3,449
750kVA														
T7 53V	13,25%	1,003	1,0044	1,0051	1,0065	1,0065	1,0071	1,0078	1,0091	1,0113	1,0155	1,0281	1,0618	2,0739
T7 200V	50%	1,0115	1,0396	1,0437	1,0494	1,0548	1,0623	1,0723	1,0873	1,1101	1,1501	1,2511	1,4581	2,8936
T7 400V	100%	1,0475	1,124	1,1354	1,15	1,1656	1,1855	1,212	1,2493	1,3075	1,4035	1,6354	2,0662	3,6778
T7 115V	50%	1,0073	1,0181	1,0205	1,0237	1,0261	1,0294	1,0345	1,0418	1,0541	1,0767	1,1381	1,2792	2,7145
T7 230V	100%	1,0233	1,0632	1,07	1,0787	1,0875	1,0996	1,1159	1,1398	1,1759	1,2435	1,4051	1,7268	3,0033
1kVA														
T8 5V	2,27%	1,0203	1,0052	1,0059	1,0067	1,0064	1,0062	1,0061	1,0061	1,006	1,0062	1,0061	1,0067	1,4113
T8 12V	5,45%	1,0179	1,0029	1,0033	1,0038	1,0037	1,0035	1,0035	1,0036	1,0038	1,0042	1,0054	1,009	1,5963
T8 24V	10,90%	1,0172	1,0023	1,0027	1,0032	1,003	1,003	1,0032	1,0036	1,0045	1,0059	1,0105	1,0235	1,8459
T8 36V	16,36%	1,0176	1,005	1,0058	1,0066	1,0069	1,0075	1,0085	1,0101	1,0129	1,0183	1,0341	1,0796	2,5007
T8 110V	50%	1,0228	1,0237	1,0263	1,0295	1,0328	1,0372	1,0436	1,0536	1,0689	1,0976	1,1735	1,3433	2,9208
T8 220V	100%	1,0426	1,0806	1,0885	1,0985	1,1099	1,1249	1,145	1,1727	1,2181	1,2969	1,4911	1,864	3,3246
3 phase														
350VA														
T9 230V	57,50%	1,0168	1,0298	1,0343	1,039	1,0438	1,048	1,055	1,0667	1,0855	1,1186	1,2006	1,3694	2,6676
T9 400V	100%	1,0428	1,1011	1,1126	1,1242	1,138	1,1536	1,1746	1,2056	1,2527	1,3342	1,5114	1,8289	2,9449
T9 230V	57,50%	1,0248	1,0544	1,061	1,0677	1,076	1,0841	1,0976	1,1147	1,1431	1,1928	1,306	1,5173	2,5949
T9 400V	100%	1,0716	1,1677	1,1817	1,2003	1,2219	1,2456	1,2788	1,3219	1,3859	1,4994	1,7516	2,1855	3,6791
T9 230V	57,50%	1,0313	1,0542	1,0665	1,0749	1,0807	1,0889	1,1019	1,1204	1,1491	1,1988	1,3109	1,5284	2,577

T9 400V	100%	1,0799	1,1709	1,1866	1,2074	1,2271	1,2501	1,2806	1,3264	1,397	1,5076	1,7567	2,1939	3,6417
1.2kVA														
T10 24V	57,10%	1,0151	1,0078	1,0092	1,011	1,0105	1,0078	1,0073	1,0072	1,0074	1,0084	1,0123	1,0234	1,2523
T10 42V	100%	1,0168	1,0107	1,0125	1,0128	1,0118	1,0115	1,0119	1,013	1,0145	1,019	1,0282	1,0552	1,2659
5kVA														
T11	100%	1,0255	1,0123	1,0153	1,017	1,0162	1,0146	1,0155	1,0134	1,0127	1,0129	1,0156	1,0228	1,1008
20kVA														
T12	100%	1,0126	1,0231	1,0257	1,0281	1,0323	1,0375	1,0544	1,0643	1,0822	1,1166	1,2081	1,4124	2,5275
40kVA														
T13	100%	1,0048	1,0158	1,0178	1,0198	1,0222	1,0258	1,0308	1,0386	1,0516	1,0738	1,1352	1,2704	2,0599
SSRE	**Wind.%**	**15 kΩ**	**5 kΩ**	**4.5 kΩ**	**4 kΩ**	**3.5 kΩ**	**3 kΩ**	**2.5 kΩ**	**2 kΩ**	**1.5 kΩ**	**1 kΩ**	**500 Ω**	**200 Ω**	**1 Ω**
400VA	**Wind.%**	**15 kΩ**	**5 kΩ**	**4.5 kΩ**	**4 kΩ**	**3.5 kΩ**	**3 kΩ**	**2.5 kΩ**	**2 kΩ**	**1.5 kΩ**	**1 kΩ**	**500 Ω**	**200 Ω**	**1 Ω**
T1 5V	13,89%	0,0005	0,001	0,0014	0,0016	0,0013	0,0012	0,0012	0,0012	0,0011	0,0011	0,0011	0,001	0,1586
T1 12V	33,33%	0,0005	0,0001	0,0002	0,0004	0,0002	0,0002	0,0002	0,0002	0,0002	0,0002	0,0003	0,0012	0,1734
T1 24V	66,67%	0,0004	0,0001	0,0001	0,0001	0,0001	0,0001	0,0002	0,0002	0,0004	0,0008	0,0026	0,0105	0,1804
T1 36V	100%	0,0004	0,0005	0,0007	0,0007	0,0006	0,0007	0,0009	0,0011	0,0017	0,0031	0,0092	0,032	0,1844
T2 24V	100%	0	0,0001	0,0001	0,0003	0,0002	0,0002	0,0003	0,0004	0,0007	0,0014	0,0044	0,0171	0,1656
T3 24V	100%	0,0005	0,0001	0,0001	0,0001	0,0002	0,0002	0,0003	0,0004	0,0007	0,0016	0,0048	0,0184	0,1754
630VA														
T4 5V	2,27%	0,0012	0,0003	0,0004	0,0007	0,0005	0,0005	0,0004	0,0005	0,0004	0,0004	0,0004	0,0004	0,1154
T4 12V	5,40%	0,0005	0,0001	0,0001	0,0002	0,0002	0,0001	0,0001	0,0001	0,0001	0,0001	0,0001	0,0002	0,2097
T4 22V	10%	0,0003	0	0	0,0001	0	0	0	0	0	0,0001	0,0003	0,0015	0,3036
T4 42V	19,10%	0,0004	0,0001	0,0001	0,0004	0,0001	0,0001	0,0002	0,0003	0,0004	0,0009	0,0027	0,0105	0,3797
T4 110V	50%	0,0006	0,0014	0,0018	0,0028	0,0027	0,0034	0,0045	0,0061	0,0094	0,0161	0,0381	0,0959	0,4805
T4 220V	100%	0,0027	0,0121	0,014	0,0165	0,0194	0,0237	0,0295	0,0383	0,0527	0,0827	0,1539	0,2639	0,5369
T5 230V	100%	0,0014	0,0081	0,0095	0,0114	0,0137	0,0171	0,0218	0,0291	0,0418	0,0673	0,1355	0,2453	0,5179
T6 220V	100%	0,0041	0,0147	0,017	0,0199	0,0234	0,0284	0,0357	0,0459	0,0629	0,0945	0,1672	0,2777	0,5386
750kVA														
T7 53V	13,25%	0,0001	0,0001	0,0001	0,0004	0,0003	0,0003	0,0003	0,0003	0,0004	0,0006	0,0014	0,0052	0,2845
T7 200V	50%	0,0003	0,0025	0,0029	0,0037	0,0043	0,0053	0,0067	0,009	0,0128	0,0206	0,0436	0,0987	0,4307
T7 400V	100%	0,0033	0,0157	0,0178	0,0207	0,0241	0,0285	0,0347	0,0438	0,0588	0,0853	0,1533	0,2739	0,5328
T7 115V	50%	0,0001	0,0006	0,0008	0,0011	0,0012	0,0014	0,0019	0,0026	0,0041	0,0073	0,0187	0,0534	0,4343
T7 230V	100%	0,0001	0,0053	0,0062	0,0076	0,009	0,0111	0,0142	0,019	0,027	0,0437	0,0895	0,1852	0,4343
1kVA														
T8 5V	2,27%	0,0007	0,0005	0,0006	0,0007	0,0006	0,0006	0,0007	0,0007	0,0007	0,0007	0,0006	0,0006	0,1148
T8 12V	5,45%	0,0007	0,0001	0,0001	0,0002	0,0001	0,0001	0,0001	0,0001	0,0001	0,0001	0,0001	0,0002	0,1958
T8 24V	10,90%	0,0006	0	0	0,0001	0,0001	0	0	0	0,0001	0,0001	0,0002	0,0008	0,274
T8 36V	16,36%	0,0005	0,0001	0,0001	0,0001	0,0001	0,0001	0,0001	0,0002	0,0003	0,0005	0,0016	0,0073	0,4106
T8 110V	50%	0,0007	0,0008	0,001	0,0012	0,0015	0,0019	0,0025	0,0036	0,0057	0,0103	0,0268	0,0772	0,4811
T8 220V	100%	0,0021	0,0074	0,0087	0,0103	0,0125	0,0154	0,0197	0,026	0,0375	0,0599	0,1243	0,234	0,5124
3 phase														
350VA														

T9 230V	57,50%	0,0008	0,0015	0,0019	0,0023	0,0029	0,0034	0,0043	0,0058	0,0087	0,0146	0,0325	0,0786	0,4434
T9 400V	100%	0,0026	0,0111	0,0129	0,015	0,0178	0,0211	0,0258	0,0332	0,045	0,0676	0,1217	0,222	0,4734
T9 230V	57,50%	0,0011	0,0038	0,0045	0,0054	0,0069	0,008	0,0102	0,0134	0,0192	0,0308	0,0611	0,1241	0,4022
T9 400V	100%	0,0058	0,0242	0,0273	0,0313	0,0367	0,0427	0,0517	0,0638	0,0827	0,118	0,199	0,3156	0,5595
T9 230V	57,50%	0,003	0,0037	0,0054	0,0069	0,0075	0,0087	0,0108	0,0141	0,0199	0,0313	0,0612	0,1255	0,4003
T9 400V	100%	0,0077	0,0243	0,0276	0,0324	0,0372	0,0432	0,0515	0,0643	0,0847	0,12	0,2009	0,3169	0,5571
1.2kVA														
T10 24V	57,10%	0,0004	0,0001	0,0001	0,0002	0,0002	0,0001	0,0001	0,0001	0,0001	0,0001	0,0003	0,0013	0,1056
T10 42V	100%	0,0005	0,0002	0,0003	0,0002	0,0002	0,0002	0,0002	0,0003	0,0003	0,0006	0,0019	0,0074	0,1062
5kVA														
T11	100%	0,0011	0,0002	0,0004	0,0004	0,0004	0,0004	0,0004	0,0003	0,0003	0,0003	0,0004	0,0011	0,0377
20kVA														
T12	100%	0,0002	0,0008	0,0009	0,0011	0,0015	0,0019	0,0032	0,0044	0,0071	0,0136	0,0378	0,1124	0,4241
40kVA														
T13	100%	0	0,0003	0,0004	0,0005	0,0006	0,0008	0,0012	0,0019	0,0033	0,0068	0,0223	0,0684	0,2763
SSMMRE	**Wind.%**	**15 kΩ**	**5 kΩ**	**4.5 kΩ**	**4 kΩ**	**3.5 kΩ**	**3 kΩ**	**2.5 kΩ**	**2 kΩ**	**1.5 kΩ**	**1 kΩ**	**500 Ω**	**200 Ω**	**1 Ω**
400VA														
T1 5V	13,89%	0,0005	0,0007	0,0009	0,0009	0,0008	0,0008	0,0007	0,0007	0,0007	0,0007	0,0007	0,0007	0,1422
T1 12V	33,33%	0,0004	0,0001	0,0001	0,0003	0,0002	0,0002	0,0002	0,0002	0,0002	0,0002	0,0003	0,0012	0,1729
T1 24V	66,67%	0,0004	0,0001	0,0001	0,0001	0,0001	0,0001	0,0002	0,0002	0,0004	0,0008	0,0025	0,0105	0,1804
T1 36V	100%	0,0004	0,0005	0,0006	0,0006	0,0006	0,0007	0,0008	0,0011	0,0016	0,0031	0,0091	0,0317	0,1844
T2 24V	100%	0	0,0001	0,0001	0,0002	0,0002	0,0002	0,0003	0,0004	0,0007	0,0013	0,0043	0,0165	0,1654
T3 24V	100%	0,0005	0,0001	0,0001	0,0001	0,0002	0,0002	0,0003	0,0004	0,0007	0,0015	0,0046	0,0174	0,1741
630VA														
T4 5V	2,27%	0,0012	0,0003	0,0004	0,0007	0,0005	0,0005	0,0004	0,0005	0,0004	0,0004	0,0004	0,0004	0,115
T4 12V	5,40%	0,0005	0,0001	0,0001	0,0002	0,0002	0,0001	0,0001	0,0001	0,0001	0,0001	0,0001	0,0002	0,2093
T4 22V	10%	0,0003	0	0	0,0001	0	0	0	0	0	0,0001	0,0003	0,0015	0,3019
T4 42V	19,10%	0,0004	0,0001	0,0001	0,0003	0,0001	0,0001	0,0002	0,0003	0,0004	0,0009	0,0027	0,0105	0,3781
T4 110V	50%	0,0006	0,0014	0,0018	0,0024	0,0027	0,0034	0,0045	0,0061	0,0094	0,0161	0,0375	0,0915	0,4594
T4 220V	100%	0,0026	0,0121	0,014	0,0164	0,0194	0,0236	0,0293	0,038	0,0518	0,0798	0,1434	0,2536	0,531
T5 230V	100%	0,0014	0,008	0,0095	0,0113	0,0136	0,017	0,0215	0,0286	0,0407	0,064	0,1228	0,2279	0,5076
T6 220V	100%	0,0041	0,0147	0,017	0,0199	0,0234	0,0283	0,0356	0,0456	0,0621	0,0922	0,1602	0,2716	0,535
750kVA														
T7 53V	13,25%	0,0001	0,0001	0,0001	0,0003	0,0003	0,0003	0,0003	0,0003	0,0004	0,0006	0,0014	0,0052	0,2838
T7 200V	50%	0,0003	0,0024	0,0029	0,0036	0,0043	0,0052	0,0067	0,0089	0,0128	0,0205	0,0435	0,0982	0,4297
T7 400V	100%	0,0033	0,0157	0,0178	0,0207	0,024	0,0285	0,0346	0,0437	0,0585	0,0843	0,148	0,2586	0,527
T7 115V	50%	0,0001	0,0006	0,0007	0,001	0,0012	0,0014	0,0019	0,0026	0,0041	0,0073	0,0187	0,053	0,4261
T7 230V	100%	0,0009	0,0053	0,0062	0,0075	0,009	0,0111	0,0141	0,019	0,0269	0,0434	0,088	0,1807	0,4688
1kVA														
T8 5V	2,27%	0,0007	0,0005	0,0006	0,0005	0,0004	0,0005	0,0006	0,0006	0,0007	0,0007	0,0006	0,0006	0,1138
T8 12V	5,45%	0,0006	0,0001	0,0001	0,0001	0,0001	0,0001	0,0001	0,0001	0,0001	0,0001	0,0001	0,0002	0,1953
T8 24V	10,90%	0,0007	0	0	0,0001	0	0	0	0	0,0001	0,0001	0,0002	0,0008	0,2732

T8 36V	16,36%	0,0007	0,0001	0,0001	0,0001	0,0001	0,0001	0,0001	0,0002	0,0003	0,0005	0,0016	0,0073	0,3973
T8 110V	50%	0,0007	0,0008	0,001	0,0012	0,0015	0,0019	0,0025	0,0036	0,0057	0,0103	0,0262	0,0713	0,4534
T8 220V	100%	0,002	0,0074	0,0086	0,0103	0,0124	0,0153	0,0195	0,0257	0,0368	0,0576	0,1129	0,2155	0,5027
3 phase														
350VA														
T9 230V	57,50%	0,0007	0,0015	0,0019	0,0023	0,0028	0,0033	0,0043	0,0058	0,0087	0,0146	0,0324	0,0778	0,4183
T9 400V	100%	0,0025	0,0111	0,0129	0,0149	0,0177	0,021	0,0258	0,0331	0,0448	0,067	0,1191	0,2129	0,4669
T9 230V	57,50%	0,001	0,0038	0,0045	0,0054	0,0067	0,0079	0,0101	0,0134	0,0192	0,0308	0,0608	0,1233	0,4015
T9 400V	100%	0,0057	0,0242	0,0272	0,0312	0,0364	0,0425	0,0514	0,0633	0,0816	0,115	0,1886	0,3008	0,5515
T9 230V	57,50%	0,003	0,0037	0,0054	0,0069	0,0075	0,0087	0,0108	0,0141	0,0199	0,0312	0,0608	0,1243	0,399
T9 400V	100%	0,0077	0,0243	0,0275	0,0323	0,0371	0,0431	0,0512	0,0637	0,0833	0,1163	0,1889	0,3009	0,5479
1.2kVA														
T10 24V	57,10%	0,0004	0,0001	0,0001	0,0002	0,0002	0,0001	0,0001	0,0001	0,0001	0,0001	0,0003	0,0013	0,103
T10 42V	100%	0,0005	0,0002	0,0003	0,0002	0,0002	0,0002	0,0002	0,0003	0,0003	0,0006	0,0019	0,0074	0,1062
5kVA														
T11	100%	0,0011	0,0002	0,0004	0,0004	0,0004	0,0004	0,0004	0,0003	0,0003	0,0003	0,0004	0,0011	0,0377
20kVA														
T12	100%	0,0002	0,0008	0,0009	0,0011	0,0015	0,0019	0,0032	0,0044	0,0069	0,0132	0,035	0,0974	0,4132
40kVA														
T13	100%	0	0,0003	0,0004	0,0005	0,0006	0,0008	0,0012	0,0018	0,0032	0,0063	0,0183	0,0525	0,2727
ρ	**Wind.%**	**15 kΩ**	**5 kΩ**	**4.5 kΩ**	**4 kΩ**	**3.5 kΩ**	**3 kΩ**	**2.5 kΩ**	**2 kΩ**	**1.5 kΩ**	**1 kΩ**	**500 Ω**	**200 Ω**	**1 Ω**
400VA														
T1 5V	13,89%	0,9998	0,9994	0,9992	0,999	0,9991	0,9992	0,9992	0,9992	0,9992	0,9992	0,9992	0,9993	0,9717
T1 12V	33,33%	0,9998	0,9999	0,9999	0,9997	0,9999	0,9999	0,9999	0,9998	0,9999	0,9999	0,9999	0,9998	0,9672
T1 24V	66,67%	0,9998	1	1	1	1	1	1	0,9999	0,9999	0,9999	0,9995	0,9982	0,9672
T1 36V	100%	0,9998	0,9997	0,9996	0,9996	0,9997	0,9997	0,9997	0,9997	0,9996	0,9994	0,9985	0,9946	0,9673
T2 24V	100%	1	1	1	0,9999	0,9999	1	1	0,9999	0,9999	0,9999	0,9995	0,9981	0,9785
T3 24V	100%	0,9996	0,9999	1	1	1	1	1	1	0,9999	0,9997	0,9994	0,9981	0,9797
630VA														
T4 5V	2,27%	0,9998	0,9999	0,9999	0,9999	0,9999	0,9999	0,9999	0,9999	0,9999	0,9999	0,9999	0,9999	0,9851
T4 12V	5,40%	0,9999	1	1	1	1	1	1	1	1	1	1	1	0,9706
T4 22V	10%	1	1	1	1	1	1	1	1	1	1	1	0,9998	0,9508
T4 42V	19,10%	0,9999	1	1	0,9999	1	1	1	1	0,9999	0,9999	0,9996	0,9988	0,9308
T4 110V	50%	0,9999	0,9998	0,9998	0,9996	0,9997	0,9996	0,9995	0,9993	0,9989	0,9982	0,9962	0,9911	0,9115
T4 220V	100%	0,9997	0,9987	0,9985	0,9983	0,998	0,9976	0,9971	0,9964	0,9952	0,9928	0,9869	0,974	0,8954
T5 230V	100%	0,9999	0,9991	0,999	0,9988	0,9986	0,9983	0,9979	0,9972	0,9962	0,9942	0,9885	0,9755	0,8946
T6 220V	100%	0,9997	0,9988	0,9987	0,9985	0,9982	0,9978	0,9973	0,9966	0,9954	0,9931	0,9873	0,9741	0,8906
750kVA														
T7 53V	13,25%	1	1	1	1	1	1	1	1	0,9999	0,9999	0,9997	0,9991	0,9488
T7 200V	50%	0,9999	0,9995	0,9995	0,9993	0,9992	0,9991	0,9988	0,9985	0,998	0,997	0,9946	0,9894	0,9109
T7 400V	100%	0,9994	0,9976	0,9973	0,9969	0,9966	0,9961	0,9954	0,9945	0,9931	0,9907	0,9848	0,9716	0,8881
T7 115V	50%	1	0,9999	0,9998	0,9998	0,9998	0,9997	0,9996	0,9995	0,9992	0,9987	0,9971	0,993	0,9126

T7 230V	100%	0,9998	0,999	0,9989	0,9987	0,9985	0,9981	0,9977	0,9971	0,996	0,9941	0,9892	0,9782	0,906
1kVA														
T8 5V	2,27%	1	0,9999	0,9999	0,9998	0,9999	0,9999	0,9999	0,9999	0,9999	0,9999	0,9999	0,9999	0,9849
T8 12V	5,45%	1	1	1	1	1	1	1	1	1	1	1	1	0,9727
T8 24V	10,90%	1	1	1	1	1	1	1	1	1	1	1	0,9999	0,9576
T8 36V	16,36%	1	1	1	1	1	1	1	1	1	0,9999	0,9998	0,9991	0,9252
T8 110V	50%	1	0,9999	0,9998	0,9998	0,9998	0,9997	0,9996	0,9995	0,9992	0,9987	0,997	0,9924	0,9128
T8 220V	100%	0,9998	0,999	0,9989	0,9987	0,9984	0,9981	0,9976	0,997	0,9959	0,9938	0,9885	0,9772	0,9072
3 phase														
350VA														
T9 230V	57,50%	0,9998	0,9996	0,9995	0,9995	0,9993	0,9992	0,9991	0,9988	0,9983	0,9973	0,9949	0,9891	0,9046
T9 400V	100%	0,9994	0,9979	0,9975	0,9973	0,9967	0,9964	0,9958	0,9948	0,9933	0,9905	0,9836	0,9679	0,8797
T9 230V	57,50%	0,9998	0,9995	0,9994	0,9993	0,9991	0,999	0,9988	0,9985	0,9979	0,9968	0,9942	0,988	0,918
T9 400V	100%	0,9993	0,9975	0,9972	0,9971	0,9963	0,996	0,9953	0,9944	0,9929	0,99	0,9825	0,9656	0,8709
T9 230V	57,50%	0,9996	0,9996	0,9994	0,9993	0,9992	0,9991	0,9989	0,9986	0,9981	0,9971	0,9948	0,989	0,9203
T9 400V	100%	0,9992	0,9977	0,9976	0,9973	0,9969	0,9964	0,9958	0,9948	0,9935	0,9907	0,9837	0,9676	0,8729
1.2kVA														
T10 24V	57,10%	0,9998	1	0,9999	0,9999	0,9999	1	1	1	1	1	1	0,9998	0,9875
T10 42V	100%	0,9998	0,9999	0,9999	0,9999	0,9999	0,9999	0,9999	0,9999	0,9999	0,9999	0,9998	0,9991	0,9874
5kVA														
T11	100%	0,9994	0,9999	0,9998	0,9997	0,9998	0,9998	0,9998	0,9998	0,9999	0,9999	0,9999	0,9999	0,9972
20kVA														
T12	100%	1	0,9999	0,9999	0,9998	0,9998	0,9997	0,9996	0,9994	0,9992	0,9984	0,9961	0,9892	0,9341
40kVA														
T13	100%	1	0,9999	0,9999	0,9999	0,9999	0,9998	0,9998	0,9996	0,9993	0,9987	0,9962	0,9889	0,9527

Appendix I. Bolstered error estimation method Python main function

```
""" Bolstered Error Estimation"""
import pandas as pd
import numpy as np
import matplotlib.pyplot as plt
from matplotlib.ticker import PercentFormatter
import scipy.stats as stats
import xlsxwriter
from math import inf, erf, sqrt

def true_mean_distance(x, y, categ):
    """ x - training samples (Ntr x d matrix)
        N - number of training samples
        d - dimensions
        y - label of the training samples (Ntr x d matrix)
        categ - number of categories
    """
    categories = categ
    num_dist = np.zeros((1, categories))# numerator of true mean calculation
    den_dist = np.zeros((1, categories))# denominator of true mean calcuation
    Ntr = len(x)                    # total number of training samples
    for k in range(Ntr):
        cur_sample = x[k,:]          # current sample
        cur_label = int(y[k,:])      # label of current sample
        min_diff = 1e10              # initialize min of euclidean distance
        for j in range(Ntr):
            if j != k and cur_label == int(y[j,:]) and cur_sample != x[j,:]:
                x2 = x[j,:]
                diff = (sum([(m - q) ** 2 for m, q in zip(cur_sample, x2)])) ** 0.5
                if diff < min_diff:
                    min_diff = diff     # assign minimum distance
        adder = np.zeros((1, categories))
        adder[0, cur_label] = min_diff
        num_dist += adder
        den_dist[0, cur_label] += 1

    d_est = num_dist / den_dist         # true mean distance
    return d_est

def integral(mu, sigma, a, b):
    # probability from Z=0 to lower bound
    double_prob = erf( (a-mu) / (sigma*sqrt(2)) )
    p_lower = double_prob/2
    # probability from Z=0 to upper bound
    double_prob = erf( (b-mu) / (sigma*sqrt(2)) )
    p_upper = double_prob/2
    # print the results
    Pin = (p_upper) - (p_lower)
    return round(Pin,4)

def coherence(x):
    """
    x - input vector (Ntr x Nsi)
    Nsi - number of statistical indicators
```

```
    Ntr - number of training samples
    """
    Ntr = np.size(x,0)         # length of the vector
    Nsi = np.size(x,1)         # number of indicators
    coh_mat = np.zeros((Nsi,Nsi))   # coherence matrix
    coh = np.zeros((Nsi-1,Nsi))
    for j in range(Nsi):
        x_cur = x[:,j]
        for k in range(j+1,N_si):
            diff = abs(x_cur - x[:,k])
            sum_diff = np.sum(diff)
            coh_mat[k,j] = 1 - sum_diff/Ntr
            coh_mat[j,k] = coh_mat[k,j]
        non_zero = np.nonzero(coh_mat[:,j])     # finding non-zero element indices of coherence matrix
        coh[:,j] = coh_mat[non_zero,j]
    return coh_mat, coh

def f_Gauss(mu, sigma, start, end):
    x = np.linspace(start, end, 100)
    y = stats.norm.pdf(x, mu, sigma)
    return x, y

# reading the data
data = pd.read_excel('data.xlsx')
mat = data.values
mat = mat[:,1:] # data
mat = np.round(mat,4)

N_si = 12       # number of statistical indicators
N_res = 12      # number of cases with resistors
N_tr = 37       # number of transformers (3 of them are removed due to incorrect measurement)
mat_data = np.zeros((N_tr,N_res,N_si))

# boundaries (green, yellow)
bound                                                                                          =
np.array([[0.99978,0.999],[0.72755,2.1],[0.57265,4.4],[0.09895,0.245],[0.394,1.12],[0.0286667,0.07],[22.7
052,67],[0.6403,1.3],[1.0153333,1.0354],[0.00035,0.0009],[0.00035,0.0009],[0.9999,0.9995]])
# limits of the indicators (for example, CC ~ [0,1])
limits = np.array([[0,1],[0,inf],[0,inf],[0,inf],[0,inf],[0,inf],[0,inf],[0,inf],[-inf,inf],[0,inf],[0,inf],[0,1]])

lab_mat = np.zeros(((N_tr-3),N_res))    # labels of samples in matrix form
lab_arr = np.zeros(((N_tr-3)*N_res,N_si))  # labels of samples in array form

for i in range(N_si):
    st = N_tr * i
    en = N_tr + N_tr * i
    mat_data[:N_tr,:,i] = mat[st:en,:]


# removing not correct data
mat_data = np.concatenate((mat_data[1:6,:,:], mat_data[7:19,:,:], mat_data[20:,:,:]))
N_sample = len(mat_data)
mat_global = np.zeros((N_sample * N_res, N_si))
mat_global = mat_data.reshape((N_sample*N_res,N_si))

#%% boundary estimation NOT VALID OR USED NOW
```

```
gy = np.zeros((12,6))
gy[:,0] = mat_data[0,9,:]
gy[:,1] = mat_data[1,7,:]
gy[:,2] = mat_data[6,9,:]
gy[:,3] = mat_data[7,7,:]
gy[:,4] = mat_data[18,9,:]
gy[:,5] = mat_data[19,8,:]
gy_avg = (gy[:,0]+gy[:,1]+gy[:,2]+gy[:,3]+gy[:,4]+gy[:,5])/6

yr = np.zeros((12,3))
yr[0,:] = np.array([0.9992, 0.9991, 0.9987])
yr[1,:] = np.array([1.82, 1.99, 2.49])
yr[2,:] = np.array([2.48, 4.71, 6.01])
yr[3,:] = np.array([0.189, 0.285, 0.261])
yr[4,:] = np.array([1.08, 0.98, 1.30])
yr[5,:] = np.array([0.068, 0.080, 0.062])
yr[6,:] = np.array([61.5, 52.48, 87.02])
yr[7,:] = np.array([1.41, 1.57, 0.92])
yr[8,:] = np.array([1.0385, 1.0400, 1.0277])
yr[9,:] = np.array([0.0008, 0.0007, 0.0012])
yr[10,:] = np.array([0.0005, 0.0010, 0.0012])
yr[11,:] = np.array([0.9992, 0.9996, 0.9997])
yr_avg = (yr[:,0] + yr[:,1] + yr[:,2])/3

N_resample = 100                    # size of sample
N_boundaries = 100                  # number of resampled boundaries
gy_sample = np.zeros((N_boundaries,N_resample,N_si))  # random samples of gy
gy_bound = np.zeros((N_boundaries,N_si))          # averaged gy boundaries
yr_sample = np.zeros((N_boundaries,N_resample,N_si))  # random samples of yr
yr_bound = np.zeros((N_boundaries,N_si))          # averaged yr boundaries

# boolean that defines if gy boundary is larger than yr
gy_greater_yr = [1,0,0,0,0,0,0,0,0,0,0,1]
# resampling boundaries
for j in range(N_si):
    gy_sample[:,:,j] = np.random.choice(gy[j,:], size=(N_boundaries,N_resample))
    gy_bound[:,j] = np.average(gy_sample[:,:,j], axis=1)
    yr_sample[:,:,j] = np.random.choice(yr[j,:], size=(N_boundaries,N_resample))
    yr_bound[:,j] = np.average(yr_sample[:,:,j], axis=1)


x_sam = mat_global[400,:]           # current observation
conf_green = np.zeros((N_si,1))       # initialize confidences
conf_yellow = np.zeros((N_si,1))
conf_red = np.zeros((N_si,1))
# classification
for i in range(N_si):
    n_g = 0
    n_y = 0
    n_r = 0
    count_gy = 0
    count_yr = 0
    x = x_sam[i]
    for j in range(N_boundaries):
        for k in range(N_boundaries):
            b_gy = gy_bound[j,i]
```

```
            b_yr = yr_bound[k,i]

            if (gy_greater_yr[i] == 1) and (b_gy > b_yr):
                if x > b_gy:
                    n_g += 1
                elif x <= b_yr:
                    n_r += 1
                else:
                    n_y += 1
                count_gy += 1

            if (gy_greater_yr[i] == 0) and (b_gy < b_yr):
                if x < b_gy:
                    n_g += 1
                elif x >= b_yr:
                    n_r += 1
                else:
                    n_y += 1
                count_yr += 1

        conf_green[i,0] = n_g / (n_g + n_y + n_r)
        conf_yellow[i,0] = n_y / (n_g + n_y + n_r)
        conf_red[i,0] = n_r / (n_g + n_y + n_r)

conf_overall = np.concatenate((conf_green, conf_yellow, conf_red), axis=1)


#%% USED CONFIDENCE ESTIMATION

# resampling boundaries unordered
unordered6 = np.load('unordered6.npy')
unordered3 = np.load('unordered3.npy')

gy_bound_unord = np.dot(unordered6, np.transpose(gy)) / 6
yr_bound_unord = np.dot(unordered3, np.transpose(yr)) / 3


x_sam = mat_global[404,:]              # current observation [244,376,406] [244,372,404]
conf_green_u = np.zeros((N_si,1))      # initialize confidences
conf_yellow_u = np.zeros((N_si,1))
conf_red_u = np.zeros((N_si,1))
# classification
for i in range(N_si):
    n_g = 0
    n_y = 0
    n_r = 0
    count_gy = 0
    count_yr = 0
    x = x_sam[i]
    for j in range(len(gy_bound_unord)):
        for k in range(len(yr_bound_unord)):
            b_gy = gy_bound_unord[j,i]
            b_yr = yr_bound_unord[k,i]

            if (gy_greater_yr[i] == 1) and (b_gy > b_yr):
                if x > b_gy:
```

```
            n_g += 1
        elif x <= b_yr:
            n_r += 1
        else:
            n_y += 1
        count_gy += 1

    if (gy_greater_yr[i] == 0) and (b_gy < b_yr):
        if x < b_gy:
            n_g += 1
        elif x >= b_yr:
            n_r += 1
        else:
            n_y += 1
        count_yr += 1

  conf_green_u[i,0] = n_g / (n_g + n_y + n_r)
  conf_yellow_u[i,0] = n_y / (n_g + n_y + n_r)
  conf_red_u[i,0] = n_r / (n_g + n_y + n_r)

conf_overall_u = np.concatenate((conf_green_u, conf_yellow_u, conf_red_u), axis=1)

#%% drawing histogram CC
plt.figure(figsize=(6,3),dpi=300)
# the histogram of the yr data
# n_yr, bins_yr, patches_yr = plt.hist(yr_bound_unord[:,0], 90, weights=np.ones(len(yr_bound_unord[:,0]))/len(yr_bound_unord[:,0]), rwidth=1, density=None, stacked = True, color='b', alpha=1)
plt.stem(yr_bound_unord[:,0],0.1*np.ones((len(yr_bound_unord[:,0]))),markerfmt=" ", basefmt=" ", linefmt="b",label="Y|R boundaries")

# the histogram of the gy data
n_gy, bins_gy, patches_gy = plt.hist(gy_bound_unord[:,0], 20, weights=np.ones(len(gy_bound_unord[:,0]))/len(gy_bound_unord[:,0]), rwidth=0.59, density=None, stacked = True, color='k', alpha=1)
plt.ylabel('Percentage', fontname='Arial', fontsize=13)
plt.xlabel('Correlation Coefficient (CC)', fontname='Arial', fontsize=13)

plt.stem([10,20],[0.1,0.1],markerfmt=" ", basefmt=" ",linefmt='k',label="G|Y boundaries")

plt.axis([0.9985, 1, 0, 0.3])

import matplotlib.font_manager as font_manager
font = font_manager.FontProperties(family='Arial',
                                   style='normal', size=11)
plt.legend(prop=font)

plt.gca().yaxis.set_major_formatter(PercentFormatter(1))
gradient = np.linspace(0, 0.1, 10).reshape(1, -1)
grad1 = np.arange(0, 0.33, 0.001).reshape(1, -1)
grad2 = np.arange(0.33, 0.67, 0.0005).reshape(1, -1)
grad3 = np.arange(0.67, 1, 0.002).reshape(1, -1)
gradient = np.concatenate((grad1, grad2, grad3), axis=1)
plt.imshow(gradient, extent=[0.9985, 1, 0, 2], cmap='RdYlGn', aspect='auto')
plt.savefig('Boundaries_CC.png',bbox_inches='tight')
plt.show()
```

```
# plt.imshow(gradient, extent=[0.9996, 1, 0, 19000], cmap='summer_r', aspect='auto')
# n_yr[n_yr==0] = -1
# n_gy[n_gy==0] = -1
# plt.scatter(bins_yr[:-1]+ 0.5*(bins_yr[1:] - bins_yr[:-1]), n_yr, marker='o', c='blue', s=10, alpha=1)
# plt.scatter(bins_gy[:-1]+ 0.5*(bins_gy[1:] - bins_gy[:-1]), n_gy, marker='D', c='k', s=10, alpha=1)



#%% drawing histogram SD
plt.figure(figsize=(6,3),dpi=300)
# the histogram of the yr data
n_yr, bins_yr, patches_yr = plt.hist(yr_bound_unord[:,1], 80, weights=np.ones(len(yr_bound_unord[:,0]))/len(yr_bound_unord[:,0]), rwidth=1.1, density=None, stacked = True, color='b', alpha=1)
# the histogram of the gy data
n_gy, bins_gy, patches_gy = plt.hist(gy_bound_unord[:,1], 20, weights=np.ones(len(gy_bound_unord[:,0]))/len(gy_bound_unord[:,0]), rwidth=0.59, density=None, stacked = True, color='k', alpha=1)
plt.ylabel('Percentage', fontname='Arial', fontsize=13)
plt.xlabel('Standard Deviation (SD)', fontname='Arial', fontsize=13)
# plt.axis([0.9985, 1, 0, 0.3])
plt.gca().yaxis.set_major_formatter(PercentFormatter(1))
gradient = np.linspace(0, 0.1, 10).reshape(1, -1)
grad1 = np.arange(0, 0.33, 0.001).reshape(1, -1)
grad2 = np.arange(0.33, 0.67, 0.0005).reshape(1, -1)
grad3 = np.arange(0.67, 1, 0.0008).reshape(1, -1)
gradient = np.concatenate((grad1, grad2, grad3), axis=1)
plt.imshow(gradient, extent=[0, 3, 0, 0.2], cmap='RdYlGn_r', aspect='auto')
plt.savefig('Boundaries_SD.png',bbox_inches='tight')
plt.show()

#%% drawing histogram CC for case 1
# plt.figure(figsize=(6,3),dpi=300)
# plt.plot([0.9,1],[0,0],linewidth=0.5, color='k',zorder=1)
# # the histogram of the yr data
# # n_yr, bins_yr, patches_yr = plt.hist(yr_bound_unord[:,0], 90, weights=np.ones(len(yr_bound_unord[:,0]))/len(yr_bound_unord[:,0]), rwidth=1, density=None, stacked = True, color='b', alpha=1)
# plt.stem(yr_bound_unord[:,0],0.1*np.ones((len(yr_bound_unord[:,0]))),markerfmt=" ", basefmt=" ", linefmt="b")
# # the histogram of the gy data
# n_gy, bins_gy, patches_gy = plt.hist(gy_bound_unord[:,0], 20, weights=np.ones(len(gy_bound_unord[:,0]))/len(gy_bound_unord[:,0]), rwidth=0.59, density=None, stacked = True, color='k', alpha=1)
# plt.ylabel('Percentage', fontname='Arial', fontsize=13)
# plt.xlabel('Correlation Coefficient (CC)', fontname='Arial', fontsize=13)
# plt.scatter([0.9990],[0],marker='x',c='k',s=65, linewidth=1.5,zorder=5)

# # markerline, stemlines, baseline=plt.stem([0.9990], [0.2], markerfmt='ok', linefmt='--k')
# # plt.setp(stemlines, 'linewidth', 2)

# arrowprops2 = dict(arrowstyle = "->", connectionstyle = "angle,angleA=0,angleB=60,rad=5")
# bbox = dict(boxstyle='round',fc='w')
# plt.annotate('Observation', xy=(0.999,0.0),xytext=(0.9993, 0.04),bbox=bbox,arrowprops=arrowprops2,zorder=10)
```

```
# plt.axis([0.9985, 1, -0.01, 0.3])
# plt.gca().yaxis.set_major_formatter(PercentFormatter(1))
# gradient = np.linspace(0, 0.1, 10).reshape(1, -1)
# grad1 = np.arange(0, 0.33, 0.001).reshape(1, -1)
# grad2 = np.arange(0.33, 0.67, 0.0005).reshape(1, -1)
# grad3 = np.arange(0.67, 1, 0.002).reshape(1, -1)
# gradient = np.concatenate((grad1, grad2, grad3), axis=1)
# plt.imshow(gradient, extent=[0.9985, 1, -0.5, 2], cmap='RdYlGn', aspect='auto')
# plt.savefig('Boundaries_CC_case1.png',bbox_inches='tight')
# plt.show()

#%% drawing histogram CC for case 1 type 2
plt.figure(figsize=(6,3),dpi=300)
plt.plot([0.9,1],[0,0],linewidth=0.5, color='k',zorder=1)
# the histogram of the yr data
# n_yr, bins_yr, patches_yr = plt.hist(yr_bound_unord[:,0], 90, weights=np.ones(len(yr_bound_unord[:,0]))/len(yr_bound_unord[:,0]), rwidth=1, density=None, stacked = True, color='b', alpha=1)
plt.stem(yr_bound_unord[:,0],0.1*np.ones((len(yr_bound_unord[:,0]))),markerfmt=" ", basefmt=" ", linefmt="b",label="Y|R boundaries")
# the histogram of the gy data
n_gy, bins_gy, patches_gy = plt.hist(gy_bound_unord[:,0], 20, weights=np.ones(len(gy_bound_unord[:,0]))/len(gy_bound_unord[:,0]), rwidth=0.59, density=None, stacked = True, color='k', alpha=1)
plt.ylabel('Percentage', fontname='Arial', fontsize=13)
plt.xlabel('Correlation Coefficient (CC)', fontname='Arial', fontsize=13)
plt.scatter([0.9990],[0],marker='x',c='k',s=65, linewidth=1.5,zorder=5,label="Test observation")


plt.stem([10,20],[0.1,0.1],markerfmt=" ", basefmt=" ",linefmt='k',label="G|Y boundaries")
# markerline, stemlines, baseline=plt.stem([0.9990], [0.2], markerfmt='ok', linefmt='--k')
# plt.setp(stemlines, 'linewidth', 2)

# arrowprops2 = dict(arrowstyle = "->", connectionstyle = "angle,angleA=0,angleB=60,rad=5")
# bbox = dict(boxstyle='round',fc='w')
# plt.annotate('Observation', xy=(0.999,0.0),xytext=(0.9993, 0.04),bbox=bbox,arrowprops=arrowprops2,zorder=10)
import matplotlib.font_manager as font_manager
font = font_manager.FontProperties(family='Arial',
                                   style='normal', size=11)
plt.legend(prop=font)

plt.axis([0.9985, 1, -0.01, 0.3])
plt.gca().yaxis.set_major_formatter(PercentFormatter(1))
gradient = np.linspace(0, 0.1, 10).reshape(1, -1)
grad1 = np.arange(0, 0.33, 0.001).reshape(1, -1)
grad2 = np.arange(0.33, 0.67, 0.0005).reshape(1, -1)
grad3 = np.arange(0.67, 1, 0.002).reshape(1, -1)
gradient = np.concatenate((grad1, grad2, grad3), axis=1)
plt.imshow(gradient, extent=[0.9985, 1, -0.5, 2], cmap='RdYlGn', aspect='auto')
plt.savefig('Boundaries_CC_case1_v2.png',bbox_inches='tight')
plt.show()

#%% drawing histogram CC for case 2 type 2
plt.figure(figsize=(6,3),dpi=300)
```

```
plt.plot([0.9,1],[0,0],linewidth=0.5, color='k',zorder=1)
# the histogram of the yr data
# n_yr, bins_yr, patches_yr = plt.hist(yr_bound_unord[:,0], 90, weights=np.ones(len(yr_bound_unord[:,0]))/len(yr_bound_unord[:,0]), rwidth=1, density=None, stacked = True, color='b', alpha=1)
plt.stem(yr_bound_unord[:,0],0.1*np.ones((len(yr_bound_unord[:,0]))),markerfmt=" ", basefmt=" ", linefmt="b",label="Y|R boundaries")
# the histogram of the gy data
n_gy, bins_gy, patches_gy = plt.hist(gy_bound_unord[:,0], 20, weights=np.ones(len(gy_bound_unord[:,0]))/len(gy_bound_unord[:,0]), rwidth=0.59, density=None, stacked = True, color='k', alpha=1)
plt.ylabel('Percentage', fontname='Arial', fontsize=13)
plt.xlabel('Correlation Coefficient (CC)', fontname='Arial', fontsize=13)
plt.scatter([0.9996],[0],marker='x',c='k',s=65, linewidth=1.5,zorder=5,label="Test observation")


plt.stem([10,20],[0.1,0.1],markerfmt=" ", basefmt=" ",linefmt='k',label="G|Y boundaries")
# markerline, stemlines, baseline=plt.stem([0.9990], [0.2], markerfmt='ok', linefmt='--k')
# plt.setp(stemlines, 'linewidth', 2)

# arrowprops2 = dict(arrowstyle = "->", connectionstyle = "angle,angleA=0,angleB=60,rad=5")
# bbox = dict(boxstyle='round',fc='w')
# plt.annotate('Observation', xy=(0.999,0.0),xytext=(0.9993, 0.04),bbox=bbox,arrowprops=arrowprops2,zorder=10)
import matplotlib.font_manager as font_manager
font = font_manager.FontProperties(family='Arial',
                                   style='normal', size=11)
plt.legend(prop=font)

plt.axis([0.9985, 1, -0.01, 0.3])
plt.gca().yaxis.set_major_formatter(PercentFormatter(1))
gradient = np.linspace(0, 0.1, 10).reshape(1, -1)
grad1 = np.arange(0, 0.33, 0.001).reshape(1, -1)
grad2 = np.arange(0.33, 0.67, 0.0005).reshape(1, -1)
grad3 = np.arange(0.67, 1, 0.002).reshape(1, -1)
gradient = np.concatenate((grad1, grad2, grad3), axis=1)
plt.imshow(gradient, extent=[0.9985, 1, -0.5, 2], cmap='RdYlGn', aspect='auto')
plt.savefig('Boundaries_CC_case2_v2.png',bbox_inches='tight')
plt.show()

#%% drawing histogram CC for case 3 type 2
plt.figure(figsize=(6,3),dpi=300)
plt.plot([0.9,1],[0,0],linewidth=0.5, color='k',zorder=1)
# the histogram of the yr data
# n_yr, bins_yr, patches_yr = plt.hist(yr_bound_unord[:,0], 90, weights=np.ones(len(yr_bound_unord[:,0]))/len(yr_bound_unord[:,0]), rwidth=1, density=None, stacked = True, color='b', alpha=1)
plt.stem(yr_bound_unord[:,0],0.1*np.ones((len(yr_bound_unord[:,0]))),markerfmt=" ", basefmt=" ", linefmt="b",label="Y|R boundaries")
# the histogram of the gy data
n_gy, bins_gy, patches_gy = plt.hist(gy_bound_unord[:,0], 20, weights=np.ones(len(gy_bound_unord[:,0]))/len(gy_bound_unord[:,0]), rwidth=0.59, density=None, stacked = True, color='k', alpha=1)
plt.ylabel('Percentage', fontname='Arial', fontsize=13)
plt.xlabel('Correlation Coefficient (CC)', fontname='Arial', fontsize=13)
plt.scatter([0.9987],[0],marker='x',c='k',s=65, linewidth=1.5,zorder=5,label="Test observation")
```

```
plt.stem([10,20],[0.1,0.1],markerfmt=" ", basefmt=" ",linefmt='k',label="G|Y boundaries")
# markerline, stemlines, baseline=plt.stem([0.9990], [0.2], markerfmt='ok', linefmt='--k')
# plt.setp(stemlines, 'linewidth', 2)

# arrowprops2 = dict(arrowstyle = "->", connectionstyle = "angle,angleA=0,angleB=60,rad=5")
# bbox = dict(boxstyle='round',fc='w')
# plt.annotate('Observation', xy=(0.999,0.0),xytext=(0.9993, 0.04),bbox=bbox,arrowprops=arrowprops2,zorder=10)
import matplotlib.font_manager as font_manager
font = font_manager.FontProperties(family='Arial',
                           style='normal', size=11)
plt.legend(prop=font)

plt.axis([0.9985, 1, -0.01, 0.3])
plt.gca().yaxis.set_major_formatter(PercentFormatter(1))
gradient = np.linspace(0, 0.1, 10).reshape(1, -1)
grad1 = np.arange(0, 0.33, 0.001).reshape(1, -1)
grad2 = np.arange(0.33, 0.67, 0.0005).reshape(1, -1)
grad3 = np.arange(0.67, 1, 0.002).reshape(1, -1)
gradient = np.concatenate((grad1, grad2, grad3), axis=1)
plt.imshow(gradient, extent=[0.9985, 1, -0.5, 2], cmap='RdYlGn', aspect='auto')
plt.savefig('Boundaries_CC_case3_v2.png',bbox_inches='tight')
plt.show()
#%% drawing histogram SD for case 1
# plt.figure(figsize=(6,3),dpi=300)
# # the histogram of the yr data
# # n_yr, bins_yr, patches_yr = plt.hist(yr_bound_unord[:,1], 80, weights=np.ones(len(yr_bound_unord[:,0]))/len(yr_bound_unord[:,0]), rwidth=1.1, density=None, stacked = True, color='b', alpha=1)
# plt.stem(yr_bound_unord[:,1],0.1*np.ones((len(yr_bound_unord[:,1]))),markerfmt=" ", basefmt=" ", linefmt="b")
# # the histogram of the gy data
# n_gy, bins_gy, patches_gy = plt.hist(gy_bound_unord[:,1], 20, weights=np.ones(len(gy_bound_unord[:,0]))/len(gy_bound_unord[:,0]), rwidth=0.59, density=None, stacked = True, color='k', alpha=1)
# plt.ylabel('Percentage', fontname='Arial', fontsize=13)
# plt.xlabel('Standard Deviation (SD)', fontname='Arial', fontsize=13)
# # plt.axis([0.9985, 1, 0, 0.3])
# plt.gca().yaxis.set_major_formatter(PercentFormatter(1))
# gradient = np.linspace(0, 0.1, 10).reshape(1, -1)
# grad1 = np.arange(0, 0.33, 0.001).reshape(1, -1)
# grad2 = np.arange(0.33, 0.67, 0.0005).reshape(1, -1)
# grad3 = np.arange(0.67, 1, 0.0008).reshape(1, -1)
# gradient = np.concatenate((grad1, grad2, grad3), axis=1)
# plt.imshow(gradient, extent=[0, 3, 0, 0.2], cmap='RdYlGn_r', aspect='auto')
# markerline, stemlines, baseline=plt.stem([1.8647], [0.15], markerfmt='ok', linefmt='--k')
# # plt.setp(stemlines, 'linewidth', 2)

# arrowprops2 = dict(arrowstyle = "->", connectionstyle = "angle,angleA=0,angleB=60,rad=5")
# bbox = dict(boxstyle='round',fc='w')
# plt.annotate('Observation', xy=(1.8647,0.15),xytext=(2, 0.16),bbox=bbox,arrowprops=arrowprops2)

# plt.axis([0, 3, -0.0, 0.2])
# plt.gca().yaxis.set_major_formatter(PercentFormatter(1))
```

```
# gradient = np.linspace(0, 0.1, 10).reshape(1, -1)
# grad1 = np.arange(0, 0.33, 0.001).reshape(1, -1)
# grad2 = np.arange(0.33, 0.67, 0.0005).reshape(1, -1)
# grad3 = np.arange(0.67, 1, 0.002).reshape(1, -1)
# gradient = np.concatenate((grad1, grad2, grad3), axis=1)
# plt.imshow(gradient, extent=[0.9985, 1, -0.5, 2], cmap='RdYlGn', aspect='auto')
# plt.savefig('Boundaries_SD_case1.png',bbox_inches='tight')
# plt.show()


#%%

# for i in range(N_si):
#     mat_si = mat_data[:,:,i]           # data for this indictor
#     mat_cur = mat_si.reshape((N_sample * N_res, 1)) # data in vector form (N_total x 1)
#     mat_global[:,i:i+1] = mat_cur
#     bound_cur = bound[i,:]             # boundaries for this indicator
#     # labeling the data
#     if bound_cur[0] > bound_cur[1]:
#         green = mat_cur >= bound_cur[0]
#         r1 = mat_cur < bound_cur[0]
#         r2 = mat_cur >= bound_cur[1]
#         yellow = np.logical_and(r1,r2)
#         red = mat_cur < bound_cur[1]
#         lab_arr[:,i:i+1] = 0 * green + 1 * yellow + 2 * red
#     else:
#         green = mat_cur <= bound_cur[0]
#         r1 = mat_cur > bound_cur[0]
#         r2 = mat_cur <= bound_cur[1]
#         yellow = np.logical_and(r1,r2)
#         red = mat_cur > bound_cur[1]
#         lab_arr[:,i:i+1] = 0 * green + 1 * yellow + 2 * red

# #aaa = lab_arr.reshape((N_sample*N_res,N_si))    # labels of the samples
# confidence = np.zeros((N_sample*N_res,3,N_si))
# st_global = np.zeros((N_si,3))
# d_total = np.zeros((N_si,3))

# for i in range(N_si):
#     mat_si = mat_data[:,:,i]           # data for i-th indicator
#     mat_cur = mat_si.reshape((N_sample * N_res, 1))

#     # estimating true mean distance
#     d_est = true_mean_distance(mat_cur, lab_arr[:,i:i+1],3)
#     d_total[i,:] = d_est
#     alpha = 0.674                    # correction factor for 1-dimensional case
#     st_dev = d_est / alpha             # bandwidth
#     st_global[i,:] = st_dev            # saving sigma in matrix

#     bound_cur = bound[i,:]             # boundaries for this indicator
#     if bound_cur[0] > bound_cur[1]:
#         # green boundary is higher than yellow boundary
#         for j in range(N_sample*N_res):
#             x_cur = mat_cur[j,:]       # current sample
#             y_cur = int(lab_arr[j,i])  # current label
#             st_cur = st_dev[:,y_cur]    # standard deviation for this sample
```

```
#             confidence[j,0,i] = integral(x_cur, st_cur, bound_cur[0], limits[i,1])
#             confidence[j,1,i] = integral(x_cur, st_cur, bound_cur[1], bound_cur[0])
#             confidence[j,2,i] = integral(x_cur, st_cur, limits[i,0], bound_cur[1])
#     else:
#         # green boundary is lower than yellow boundary
#         for j in range(N_sample*N_res):
#             x_cur = mat_cur[j,:]        # current sample
#             y_cur = int(lab_arr[j,i])   # current label
#             st_cur = st_dev[:,y_cur]    # standard deviation for this sample
#             confidence[j,0,i] = integral(x_cur, st_cur, limits[i,0], bound_cur[0])
#             confidence[j,1,i] = integral(x_cur, st_cur, bound_cur[0], bound_cur[1])
#             confidence[j,2,i] = integral(x_cur, st_cur, bound_cur[1], limits[i,1])

# # sum confidence in one row
# conf_sum = np.sum(confidence, axis=1)
# # confidence that sums to 1
# conf_true = np.zeros((N_sample*N_res,3,N_si))
# for k in range(3):
#     conf_true[:,k,:] = np.divide(confidence[:,k,:],conf_sum)


# ind_value = lab_arr / 2                # class values
# coh_mat, coh = coherence(ind_value)     # coherence calculation
# coh_mean = np.mean(coh,axis=0)          # calculating the average of coherences

# x_coh = np.zeros((11,12))
# for j in range(11):
#     x_coh[j,:] = np.arange(1,13,1)

# plt.figure(figsize=(6,3),dpi=300)
# plt.plot(np.transpose(x_coh),np.transpose(coh),'x',color='black')
# mark1, = plt.plot(np.arange(1,13,1),coh_mean,'bo',label='Mean')
# plt.ylabel('Coherence',fontsize=13,fontname='Arial')
# plt.xlabel('Indicator',fontsize=13,fontname='Arial')
# plt.xticks(np.arange(0,(N_si+1),1))
# plt.axis([0.5, 12.5, 0.898, 1.002])
#                 plt.xticks(np.arange(1,13,1),               ('CC',              'SD',              'SSE',              'ASLE',
'DABS','RMSE','ED','CSD','MM','SSRE','SSMMRE','$\\rho$'),rotation=20,fontsize='medium')
# plt.legend(handles=[mark1],loc='upper right', bbox_to_anchor=(1, 0.9),fontsize='small')
# plt.savefig('Coh.png', bbox_inches='tight')
# plt.show()


# # 1 KVA
# lab_1kva = int(lab_arr[243,0])
# conf_1kva = np.transpose(conf_true[243,:,0])
# mat_1kva = mat_global[243,0]

# plt.figure(figsize=(6,3),dpi=300)
# x, y = f_Gauss(mat_1kva, st_global[0,lab_1kva], 0.9984, 1)
# plt.plot(x, y)
# xgfill,ygfill = f_Gauss(mat_1kva,st_global[0,lab_1kva],bound[0,0],1)
# plt.fill_between(xgfill,ygfill,facecolor='green',alpha=0.5)
# xyfill,yyfill = f_Gauss(mat_1kva,st_global[0,lab_1kva],bound[0,1],bound[0,0])
# plt.fill_between(xyfill,yyfill,facecolor='gold',alpha=0.5)
# xrfill,yrfill = f_Gauss(mat_1kva,st_global[0,lab_1kva],0.9984,bound[0,1])
```

```
# plt.fill_between(xrfill,yrfill,facecolor='red',alpha=0.5)
# plt.ylabel('Density function',fontsize=13,fontname='Arial')
# plt.xlabel('Correlation coefficient',fontsize=13,fontname='Arial')
# # boundaries
# for j in range(2):
#     plt.axvline(x=bound[0,j],color='black',linewidth=1.5)
# # stemline
# ymax = max(y)
# plt.vlines(mat_1kva,0,ymax,linestyle='dashdot',color='black')
# # sample point
# plt.plot(mat_1kva,0.0,color='gold',marker='o',markeredgecolor='black',markersize=6,mew=1.5)

# arrowprops1 = dict(arrowstyle = "->", connectionstyle = "angle,angleA=0,angleB=60,rad=5")
# arrowprops2 = dict(arrowstyle = "->", connectionstyle = "angle,angleA=0,angleB=120,rad=5")
# arrowprops3 = dict(arrowstyle = "->")
# arrowprops4 = dict(arrowstyle = "->", connectionstyle = "angle,angleA=0,angleB=80,rad=5")
# arrowprops5 = dict(arrowstyle = "->", connectionstyle = "angle,angleA=0,angleB=110,rad=5")

# bbox = dict(boxstyle='round',fc='w')
# # annotation for red region
#                             plt.annotate('{:0.2f}%'.format(conf_1kva[2]*100),xy=(0.99895,300),xytext=(0.9986,
500),bbox=bbox,arrowprops=arrowprops2)
# # annotation for yellow region
#                           plt.annotate('{:0.2f}%'.format(conf_1kva[1]*100),xy=(0.9993,1200),xytext=(0.99948,
1400),bbox=bbox,arrowprops=arrowprops1)
# # annotation for green region
#                             plt.annotate('{:0.2f}%'.format(conf_1kva[0]*100),xy=(0.9998,-50),xytext=(0.99988,
200),bbox=bbox,arrowprops=arrowprops4)

# # annotate boundary green
#     plt.annotate('green-yellow\nboundary',multialignment='center',xy=(bound[0,0],2400),xytext=(0.99937,
2400),arrowprops=arrowprops3,verticalalignment='center',fontname='Arial')
# # annotate boundary yellow
#         plt.annotate('yellow-red\nboundary',multialignment='center',xy=(bound[0,1],2400),xytext=(0.99865,
2400),arrowprops=arrowprops3,verticalalignment='center',fontname='Arial')


# plt.savefig('1kva.png',bbox_inches='tight')
# plt.show()

# # 20KVA
# lab_20kva = int(lab_arr[376,0])
# conf_20kva = np.transpose(conf_true[376,:,0])
# mat_20kva = mat_global[376,0]

# plt.figure(figsize=(6,3),dpi=300)
# x, y = f_Gauss(mat_20kva, st_global[0,lab_20kva], 0.9984, 1)
# plt.plot(x, y)
# xgfill,ygfill = f_Gauss(mat_20kva,st_global[0,lab_20kva],bound[0,0],1)
# plt.fill_between(xgfill,ygfill,facecolor='green',alpha=0.5)
# xyfill,yyfill = f_Gauss(mat_20kva,st_global[0,lab_20kva],bound[0,1],bound[0,0])
# plt.fill_between(xyfill,yyfill,facecolor='gold',alpha=0.5)
# xrfill,yrfill = f_Gauss(mat_20kva,st_global[0,lab_20kva],0.9984,bound[0,1])
# plt.fill_between(xrfill,yrfill,facecolor='red',alpha=0.5)
# plt.ylabel('Density function',fontsize=13,fontname='Arial')
# plt.xlabel('Correlation coefficient',fontsize=13,fontname='Arial')
```

```
# # boundaries
# for j in range(2):
#     plt.axvline(x=bound[0,j],color='black',linewidth=1.5)
# # stemline
# ymax = max(y)
# plt.vlines(mat_20kva,0,ymax,linestyle='dashdot',color='black')
# # sample point
# plt.plot(mat_20kva,0.0,color='gold',marker='o',markeredgecolor='black',markersize=6,mew=1.5)

# # annotation for red region
#                         plt.annotate('{:0.2f}%'.format(conf_20kva[2]*100),xy=(0.9989,1000),xytext=(0.9985,
1200),bbox=bbox,arrowprops=arrowprops2)
# # annotation for yellow region
#                         plt.annotate('{:0.2f}%'.format(conf_20kva[1]*100),xy=(0.9991,1000),xytext=(0.9993,
1200),bbox=bbox,arrowprops=arrowprops1)
# # annotation for green region
#                          plt.annotate('{:0.2f}%'.format(conf_20kva[0]*100),xy=(0.9998,-50),xytext=(0.99988,
200),bbox=bbox,arrowprops=arrowprops4)

# # annotate boundary green
#     plt.annotate('green-yellow\nboundary',multialignment='center',xy=(bound[0,0],2400),xytext=(0.99935,
2400),arrowprops=arrowprops3,verticalalignment='center',fontname='Arial')
# # annotate boundary yellow
#         plt.annotate('yellow-red\nboundary',multialignment='center',xy=(bound[0,1],2400),xytext=(0.9986,
2400),arrowprops=arrowprops3,verticalalignment='center',fontname='Arial')


# plt.savefig('20kva.png',bbox_inches='tight')
# plt.show()

# # 40 MVA
# lab_40mva = int(lab_arr[406,0])
# conf_40mva = np.transpose(conf_true[406,:,0])
# mat_40mva = mat_global[406,0]

# plt.figure(figsize=(6,3),dpi=300)
# x, y = f_Gauss(mat_40mva, st_global[0,lab_40mva], 0.988, 1)
# plt.plot(x, y)
# xgfill,ygfill = f_Gauss(mat_40mva,st_global[0,lab_40mva],bound[0,0],1)
# plt.fill_between(xgfill,ygfill,facecolor='green',alpha=0.5)
# xyfill,yyfill = f_Gauss(mat_40mva,st_global[0,lab_40mva],bound[0,1],bound[0,0])
# plt.fill_between(xyfill,yyfill,facecolor='gold',alpha=0.5)
# xrfill,yrfill = f_Gauss(mat_40mva,st_global[0,lab_40mva],0.988,bound[0,1])
# plt.fill_between(xrfill,yrfill,facecolor='red',alpha=0.5)
# plt.ylabel('Density function',fontsize=13,fontname='Arial')
# plt.xlabel('Correlation coefficient',fontsize=13,fontname='Arial')

# # boundaries
# for j in range(2):
#     plt.axvline(x=bound[0,j],color='black',linewidth=1.5)
# # stemline
# ymax = max(y)
# plt.vlines(mat_40mva,0,ymax,linestyle='dashdot',color='black')
# # sample point
# plt.plot(mat_40mva,0.0,color='red',marker='o',markeredgecolor='black',markersize=6,mew=1.5)
```

```
# # annotation for red region
#                                 plt.annotate('{:0.2f}%'.format(conf_40mva[2]*100),xy=(0.993,100),xytext=(0.99,
120),bbox=bbox,arrowprops=arrowprops2)
# # annotation for yellow region
#                               plt.annotate('{:0.2f}%'.format(conf_40mva[1]*100),xy=(0.9996,-5),xytext=(0.9975,
25),bbox=bbox,arrowprops=arrowprops5)
# # annotation for green region
# plt.annotate('0%',xy=(1,-5),xytext=(0.998, 75),bbox=bbox,arrowprops=arrowprops5)

# # annotate boundary green
#           plt.annotate('green-yellow\nboundary',multialignment='center',xy=(bound[0,0],200),xytext=(0.996,
200),arrowprops=arrowprops3,verticalalignment='center',fontname='Arial')
# # annotate boundary yellow
#            plt.annotate('yellow-red\nboundary',multialignment='center',xy=(bound[0,1],260),xytext=(0.9962,
260),arrowprops=arrowprops3,verticalalignment='center',fontname='Arial')


# plt.savefig('40mva.png',bbox_inches='tight')
# plt.show()

# with open('coherence.txt','w') as nt:
#     for i in range(np.size(coh,0)):
#         for j in range(np.size(coh,1)):
#             nt.write("%0.4f\t" % coh[i,j])
#         nt.write("\n")

# with open('st_dev.txt','w') as nt:
#     for i in range(np.size(d_total,0)):
#         for j in range(np.size(d_total,1)):
#             nt.write("%0.4e\t" % d_total[i,j])
#         nt.write("\n")
#     nt.write("\n")
#     for i in range(np.size(d_total,0)):
#         for j in range(np.size(d_total,1)):
#             nt.write("%0.4e\t" % st_global[i,j])
#         nt.write("\n")

# # confidence of 1 kva
# conf_1kva = np.transpose(conf_true[243,:,:])
# # confidence of 20 kva
# conf_20kva = np.transpose(conf_true[376,:,:])
# # confidence of 40 mva
# conf_40mva = np.transpose(conf_true[406,:,:])

"""
mat_all = mat_data.reshape((396,12))

workbook = xlsxwriter.Workbook('classification.xlsx')
worksheet = workbook.add_worksheet()
for j in range(N_res):
    for i in range(N_sample*N_res):
        worksheet.write(i+1, j+1, lab_arr[i,j])
worksheet2 = workbook.add_worksheet()
for i in range(N_sample*N_res):
    for j in range(N_si):
        worksheet.write(i+1, j+1, mat_all[i,j])
```

```
    for k in range(3):
        worksheet.write(i+1, k+2+N_si, confidence[i,k,0])


workbook.close()
"""
```

Appendix J. Area under the kernel calculation

```
import numpy as np
# 1 kVA 4kOhm
conf_243=confidence[243,:,:]
# 20 kVA
conf_376=confidence[376,:,:]
# 40 MVA
conf_406=confidence[406,:,:]

index_mat = np.load('index_mat.npy')
mult=np.ones((len(index_mat),1))

for j in range(len(index_mat)):
    ind = index_mat[j,:]
    for i in range(12):
        mult[j,:] *= conf_243[ind[i],i]

[x, y] = np.nonzero(mult)
true_ind = index_mat[x,:]
true_mult = mult[x,:]
```